

Development of a within-host mathematical model of urethral gonorrhoea infection and application to treatment

Author:

Jayasundara, Pavithra

Publication Date:

2022

DOI:

<https://doi.org/10.26190/unsworks/1948>

License:

<https://creativecommons.org/licenses/by/4.0/>

Link to license to see what you are allowed to do with this resource.

Downloaded from <http://hdl.handle.net/1959.4/100039> in <https://unsworks.unsw.edu.au> on 2024-04-18

Development of a within-host mathematical model of urethral gonorrhoea infection and application to treatment

Samarage Dona Pavithra Jayasundara

A thesis in fulfilment of the requirements for the degree of
Doctor of Philosophy



School of Population Health
Faculty of Medicine

January 2022

Thesis Title

Development of a within-host mathematical model of urethral gonorrhoea infection and application to treatment

Thesis Abstract

Background

To understand the emergence and spread of drug resistance in the context of *Neisseria gonorrhoeae* (NG) it is first important to characterise the within-host dynamics that influence these events. However, in the context of NG, the within-host infection process is not well understood, with little investigation into the role of intracellular NG on the progression of natural infection and the dynamics of infection under treatment. This thesis aims to address this gap through the use of novel within-host mathematical models to describe symptomatic male urethral NG infection.

Methods

Initially, we developed a model to describe the progression of natural infection by considering the interaction between extracellular and intracellular NG with immune response through PMN. This initial model was then adopted to incorporate treatment of NG infection through pharmacokinetic (PK) and pharmacodynamic (PD) approaches for several antibiotics, examining both extracellular and intracellular dynamics after treatment. While this relatively simple treatment model with conventional approaches was successful in explaining the infection dynamics for the non- β -lactam drugs we test, using β -lactams the model struggled to describe infection dynamics consistent with the literature, leading to a revised approach applied to cefixime and ceftriaxone. This new approach incorporated a transition between bacteriostatic and bactericidal effects determined through threshold effects applied to the fraction of drug bound penicillin-binding-proteins. Parameter values were estimated by fitting to existing empirical data where sub-models to reflect different *in vitro* experimental conditions were adopted.

Results

Using the natural infection model, we successfully reproduced known phenomena on bacterial load and infection duration and found that the simulated natural infection was mainly driven by intracellular NG with ~80% of the total NG population internalised from day 5 on. In addition, we achieved realistic infection clearance times for each drug considered and simulations showed treatment failure to be largely driven by unsuccessful clearance of intracellular NG. We also identified relevant PK indices at the intracellular level that differentiated treatment success and failure. Although we investigated multiple dose strategies for orally administered drugs (gepofidacin, azithromycin and cefixime), we found little difference in treatment success for a fixed total dose.

Discussion

In this study we contribute new theoretical results tied to available observations in an area that has had limited experimental attention. In particular, this has involved development of a new mechanistic model of NG infection within-host and incorporation of realistic features of treatment. The study findings mainly emphasise the importance of the role of intracellular NG in prolonging natural infection and determining treatment success. The treatment model facilitates exploration of differing treatment regimens, the link between PK/PD indices and treatment success and where relevant incorporates mechanistic effects of drug-target binding. This work suggests the importance of intracellular infection in both persistence of infection and drug clearance, and presents an opportunity to investigate these predictions in future experiments. The approach taken here is flexible and has the potential to be expanded in various ways, including to other anatomical sites, consider the role of vaccines in clearance and to address the motivating questions around the emergence of drug resistance within-host.

ORIGINALITY STATEMENT

☒ I hereby declare that this submission is my own work and to the best of my knowledge it contains no materials previously published or written by another person, or substantial proportions of material which have been accepted for the award of any other degree or diploma at UNSW or any other educational institution, except where due acknowledgement is made in the thesis. Any contribution made to the research by others, with whom I have worked at UNSW or elsewhere, is explicitly acknowledged in the thesis. I also declare that the intellectual content of this thesis is the product of my own work, except to the extent that assistance from others in the project's design and conception or in style, presentation and linguistic expression is acknowledged.

COPYRIGHT STATEMENT

☒ I hereby grant the University of New South Wales or its agents a non-exclusive licence to archive and to make available (including to members of the public) my thesis or dissertation in whole or part in the University libraries in all forms of media, now or here after known. I acknowledge that I retain all intellectual property rights which subsist in my thesis or dissertation, such as copyright and patent rights, subject to applicable law. I also retain the right to use all or part of my thesis or dissertation in future works (such as articles or books).

For any substantial portions of copyright material used in this thesis, written permission for use has been obtained, or the copyright material is removed from the final public version of the thesis.

AUTHENTICITY STATEMENT

☒ I certify that the Library deposit digital copy is a direct equivalent of the final officially approved version of my thesis.

UNSW is supportive of candidates publishing their research results during their candidature as detailed in the UNSW Thesis Examination Procedure.

Publications can be used in the candidate's thesis in lieu of a Chapter provided:

- The candidate contributed **greater than 50%** of the content in the publication and are the "primary author", i.e. they were responsible primarily for the planning, execution and preparation of the work for publication.
- The candidate has obtained approval to include the publication in their thesis in lieu of a Chapter from their Supervisor and Postgraduate Coordinator.
- The publication is not subject to any obligations or contractual agreements with a third party that would constrain its inclusion in the thesis.

☒ The candidate has declared that **their thesis has publications - either published or submitted for publication - incorporated into it in lieu of a Chapter/s. Details of these publications are provided below..**

Publication Details #1

Full Title:	Modelling the in-host dynamics of Neisseria gonorrhoeae infection
Authors:	Pavithra Jayasundara , David G Regan , Kate L Seib , Duleepa Jayasundara , James G Wood
Journal or Book Name:	Journal of Pathogens and Disease
Volume/Page Numbers:	77
Date Accepted/Published:	Feb 1, 2019
Status:	published
The Candidate's Contribution to the Work:	I conceived the study design in collaboration with my supervisors and Prof. Kate Seib from Griffith University. I was also responsible for model development and conducted the relevant analysis and simulation work and I drafted and revised the manuscript.

Location of the work in the thesis and/or how the work is incorporated in the thesis:	This is the first modelling project in the thesis and is included in Chapter 3. This describes the basic framework of the untreated natural infection and is used in the subsequent chapters (4 -6) when including treatment effects.
--	---

Candidate's Declaration



I confirm that where I have used a publication in lieu of a chapter, the listed publication(s) above meet(s) the requirements to be included in the thesis. I also declare that I have complied with the Thesis Examination Procedure.

Content

Content	i
List of abbreviations	ix
List of Figures	xi
List of Tables	xiii
Acknowledgements	xv
Chapter 1 Introduction	1
1.1 Introduction and thesis motivation	1
1.2 Thesis overview	4
Chapter 2 Literature review	7
2.1 Clinical manifestation and sequelae	7
2.2 Natural history of NG infection	8
2.2.1 Natural history of symptomatic male urethral NG infection	9
2.3 Within-host dynamics of NG infection	11
2.3.1 NG interaction with epithelial cells	12
2.4 The immune response to NG infection	13
2.5 Antibiotic treatment for gonorrhoea	17
2.5.1 Novel treatment options for gonorrhoea	20
2.5.2 Mechanisms of drug action and entry into cells	21
2.6 Susceptibility breakpoints in the literature	23
2.7 Pharmacokinetics and pharmacodynamics (PK/PD) of antibiotics	26

2.7.1	Pharmacokinetics	26
2.7.2	Modelling pharmacokinetics	28
2.7.3	PK indices	30
2.7.4	Drug binding to plasma proteins	31
2.7.5	Pharmacodynamics	32
2.7.6	Mechanistic pharmacodynamic models and drug-target binding kinetics	34
2.7.7	Drug interactions in combination therapy	35
2.7.8	Effects of antibiotics on intracellular bacteria	37
2.8	Mathematical models for between-host and within-host infectious disease dynamics.....	39
2.8.1	Applications of mathematical models in the context of gonorrhoea	41
Chapter 3 Modelling the in-host dynamics of <i>Neisseria gonorrhoeae</i> infection.....		44
3.1	Introduction	44
3.2	Materials and Methods	47
3.2.1	Model structure and formulation to describe human urethral NG infection...	47
3.2.2	Model parameters	58
3.2.3	Initial conditions	61
3.2.4	Multivariate sensitivity analysis	63
3.2.5	Fitting to mouse model data	64
3.3	Results	65
3.3.1	Parameter estimation for the human model	65
3.3.2	Human infection model results based on point estimates.....	67

3.3.3 Multivariate sensitivity analysis	69
3.3.4 Validation against mouse model data	70
3.4 Discussion	73
3.5 Conclusion.....	77
Chapter 4 Modelling treatment effects for gonorrhoea.....	79
4.1 Introduction	79
4.2 Materials and Methods	80
4.2.1 Mathematical model of antibiotic treatment.....	80
4.2.2 Modelling pharmacodynamics.....	83
4.2.3 Modelling pharmacokinetics	85
4.2.4 Incorporation of parametric uncertainty	92
4.2.5 Calibrating PK/PD parameters using susceptibility breakpoints.....	92
4.2.6 Extracellular vs intracellular susceptibility breakpoints.....	94
4.2.7 Sensitivity analysis for ceftriaxone and cefixime	95
4.3 Results	95
4.3.1 Estimates of pharmacodynamic parameters	95
4.3.2 Drug concentration profiles	98
4.3.3 Modelled infection clearance times under monotreatment.....	100
4.3.4 Calibration of PK/PD parameters	102
4.3.5 Extracellular vs intracellular susceptibility breakpoint	102
4.3.6 Sensitivity analysis on model-derived susceptibility breakpoints for ceftriaxone and cefixime.....	105

4.4 Discussion	108
4.5 Conclusions	111
Chapter 5 Effectiveness of different treatment regimens for gonorrhoea.....	112
5.1 Introduction	112
5.2 Methods	113
5.2.1 Testing different treatment strategies	114
5.2.2 Modelling dual antibiotic treatment.....	116
5.2.3 PK indices	116
5.2.4 Sensitivity of monotreatment and dual treatment options to changes in the MIC	117
5.3 Results	118
5.3.1 Gepotidacin monotreatment.....	118
5.3.2 Dual treatment with gentamicin + azithromycin	124
5.4 Discussion	127
5.5 Conclusions	130
Chapter 6 Evaluation of ceftriaxone and cefixime treatment strategies using a model that incorporates drug-target binding	131
6.1 Introduction	131
6.2 Materials and Methods.	133
6.2.1 Mathematical Model.....	133
6.2.2 Additional model details and parameter estimation	136
6.2.3 MIC expression.....	148

6.2.4 Converting number of molecules to drug concentration	148
6.2.5 Incorporation of parametric uncertainty	148
6.2.6 Calibrating PK/PD parameters using empirical susceptibility breakpoints..	149
6.2.7 Different treatment strategies	150
6.2.8 Comparison of infection clearance with Chapter 4	151
6.3 Results	151
6.3.1 Parameter estimation	151
6.3.2 Simulated drug concentration profiles	155
6.3.3 General model behaviour	155
6.3.4 Model-derived susceptibility breakpoints.....	157
6.3.5 Testing infection clearance for different MIC	160
6.3.6 Different cefixime treatment strategies	161
6.3.7 Comparison of infection clearance with the model described in Chapter 4 .	164
6.4 Discussion	166
6.5 Conclusions	170
Chapter 7 Conclusions and future work.....	171
Appendix A Supplementary material pertaining to Chapter 3.....	183
A.1 Parameter estimation	183
A.1.1 Replication rate of <i>Bs</i> (<i>r3</i>).....	183
A.1.2 Parameter estimation through model fitting	183
A.2 Sensitivity Analysis	188

A.2.1 Multivariate sensitivity analysis	188
A.2.2 In vitro credible intervals around point estimates.....	194
A.2.3 Expanded sensitivity analysis around in vitro estimates on epithelial internalisation	195
A.3 Model with PMN delay in activation	197
A.4 Comparison of the model NG load with the study by Craig, <i>et al.</i> (2015).....	199
A.5. Fitting to mouse model data	200
A.5.1 Mouse parameters k_1 and N_{\max}	200
A.5.2 Fixing the parameters p and η across mice	200
A.5.3 Estimated mouse parameters	202
Appendix A2 Additional details on Chapter 3	206
A2.1 Further clarifications to figure captions in Chapter 3.....	206
A2.2 Simplifying model assumptions	209
A2.3 Additional model limitations	211
A2.4 Additional sensitivity analysis.....	212
Appendix B Supplementary material pertaining to Chapter 4	215
B.1 Hill function parameter estimation	215
B.1.1 The Hill function	215
B.1.2 Data used to estimate Hill function parameter estimates.	216
B.1.3 Fitting procedure	217
B.2 PK/PD parameter calibration	221

B.3 Model equations.....	227
B.3.1 Antibiotic concentration modelled as a one-compartment (ceftriaxone, cefixime and gepotidacin).....	227
B.3.2 Model equations when antibiotic concentration modelled as a two-compartment model (azithromycin and gentamicin).	228
B.4 Drug concentration profiles	230
B.5 NG load behaviour around cut-off MIC	231
Appendix C Supplementary material pertaining to Chapter 5	233
C.1 Dual treatment	233
C.1.1 Loewe additivity	233
C.2 Gepotidacin monotreatment.....	235
C.2.1 Association between model-derived breakpoint MIC and drug dose.	235
C.2.2 PK indices to explain effectiveness of different treatment strategies	237
C.2.3 Threshold gepotidacin concentration required for treatment success	237
C.2.4 Testing higher doses of gepotidacin monotreatment	240
C.3 Gentamicin treatment.....	242
C.3.1 Impact on patient non-compliance on multiple-dose strategies of gentamicin	242
C.4 The Difference in bacterial killing rates elicited by the monotreatment and dual treatment options.	244
Appendix D Supplementary material pertaining to Chapter 6.....	245
D.1 Model equations	245

D.2 Concentration-dependent protein binding of ceftriaxone	248
D.3 Estimating parameter values related to drug-mediated killing and dormancy ...	248
D.3.1 Estimating the point estimates of the Hill function parameters	250
D.4 PK parameter estimation	251
D.5 Estimation of the fraction of administered drug molecules that reaches the urethra (<i>fs</i>)	254
D.6 PK/PD parameter calibration	255
D.7 MIC expression	257
D.8 Different cefixime treatment strategies	259
D.8.1 Effectiveness of different multiple dose strategies of cefixime	260
D.8.2 Patient non-adherence with multiple dose strategies	261
References	263

List of abbreviations

AGSP	Australian Gonococcal Surveillance Program
AST	Antimicrobial Susceptibility Testing
AUC	Area under the curve
AZM	Azithromycin
CDC	Centers for Disease Control and Prevention
CFM	Cefixime
CFO	Ceftriaxone
CFU	Colony-forming Units
CLSI	Clinical and Laboratory Standards Institute
EUCAST	European Committee on Antimicrobial Susceptibility Testing
GEN	Gentamicin
GEP	Gepotidacin
HIV	Human Immunodeficiency Virus
LHS	Latin Hypercube Sampling
MIC	Minimum Inhibitory Concentrations
NAAT	Nucleic Acid Amplification Test
NG	<i>Neisseria gonorrhoeae</i>
Opa	Opacity associated proteins
PAE	Post-antibiotic effect
PBP	Penicillin Binding Proteins
PBPK	Physiologically Based Pharmacokinetic Modelling
PD	Pharmacodynamic

PK	Pharmacokinetic
PMN	Polymorphonuclear Neutrophils
PRCC	Partial rank correlation coefficients
STI	Sexually Transmitted Infection
UK	United Kingdom
US	United States
WHO	World Health Organisation

List of Figures

Figure 2.1: Simplified illustration of some of the main elements of NG pathogenesis..	12
Figure 2.2: Timeline of antibiotic treatments for gonorrhoea and resistance..	18
Figure 3.1: Schematic illustration of the within-host model of NG infection..	49
Figure 3.2: Flow diagram summarising the sub-models and data used to estimate the human infection model point-estimate parameters.	62
Figure 3.3: Model fit to in vitro studies to estimate parameters..	66
Figure 3.4: Changes in the four bacterial populations as well as the neutrophil population are shown along with the total bacterial load.....	68
Figure 3.5: Log-scale time course for all model states using the point estimates in Table 3.2 as parameter values.	69
Figure 3.6: Model fits to mouse NG data.....	71
Figure 3.7: Estimated parameter values of the ratio $d_c, r_1, \mu \times N_{max}, d, r_3$, and p obtained across the mouse models compared with the human estimates.....	72
Figure 4.1: Schematic illustration of the within-host NG infection model including antibiotic treatment.....	82
Figure 4.2: Net growth rates obtained from the estimated PD values	98
Figure 4.3: Extracellular and intracellular drug concentration of (a) ceftriaxone (CFO) 1000mg; (b) gepotidacin (GEP) 3000mg; (c) cefixime (CFM) 400mg; (d) gentamicin (GEN) 240mg; and (e) azithromycin (AZM) 1g.....	100
Figure 4.4: Change in total NG (a), extracellular NG (b) and intracellular NG (c) after initiation of single-drug treatment of wild-type infection.....	101

Figure 4.5: Change in the extracellular and intracellular drug concentration over time for the simulations that result in model-derived susceptibility breakpoint below and above the empirical susceptibility breakpoints.	105
Figure 5.1: Effect of gepotidacin dose spacing of 8,12 and 24h in a 500mg \times 6 schedule on (a) intracellular drug concentration and (b) total NG load.....	120
Figure 5.2: Comparison of PK/PD indices to differentiate treatment success and failure..	123
Figure 6.1: Schematic diagram of the infection model with the addition of treatment..	147
Figure 6.2: Change in (a) extracellular (ex) drug concentration over time and; (b) the change in the net bacterial growth rate to the changes in the antibiotic concentration shown for Chapters 4 and 6.....	153
Figure 6.3: Model behaviour as a function of the rate constant for cefixime binding to PBP.....	157
Figure 6.4: Time the extracellular drug concentration remains above the MIC and the number of intracellular drug molecules at the time of reaching the extracellular drug-bound PBP threshold for single and multiple cefixime dosing strategies.....	164
Figure 6.5: Comparison of the infection dynamics between Chapters 4 and 6.....	166

List of Tables

Table 2.1: Empirical susceptibility breakpoints (mg/L) defined by CLSI and EUCAST for NG.	25
Table 3.1: Human infection model initial conditions	50
Table 3.2: Model parameter values and the parameter ranges based on the sensitivity analysis.....	51
Table 3.3: Main data sources used for parameter estimation.....	55
Table 4.1: Model parameter values for the five antibiotics ceftriaxone (CFO), cefixime (CFM), gepotidacin (GEP), gentamicin (GEN) and azithromycin (AZM).....	88
Table 4.2: Estimated Hill function parameter values for ceftriaxone, cefixime, gepotidacin, gentamicin and azithromycin.	97
Table 4.3: Susceptibility breakpoints (mg/L) derived from the three sub-models and the full model and comparison with empirical breakpoints.....	103
Table 4.4: Parameter values that result in simulations achieving a model-derived susceptibility breakpoint of 0.125mg/L (EUCAST defined susceptibility breakpoint) for ceftriaxone (CFO) and cefixime (CFM)).	107
Table 5.1: Percentage of simulations using LHS samples (out of 5402) that clear infection in ≤ 7 days when using single and multiple dose gepotidacin treatment strategies.....	119
Table 5.2: Percentage of simulations that clear the infection (out of 5402 LHS samples) at various MIC values when using dual treatment gentamicin (GEN) and azithromycin (AZM) strategies.	126
Table 6.1: Model variables and initial conditions.....	137

Table 6.2: Model parameter values relating to the model of treatment with ceftriaxone (CFO) and cefixime (CFM).	139
Table 6.3: Parameter estimates obtained through model fitting to data on ceftriaxone (CFO) and cefixime (CFM).	154
Table 6.4: Percentage of simulations that clear the infection in ≤ 7 days when treated using the standard doses of ceftriaxone (CFO) and cefixime (CFM).	159
Table 6.5: Infection clearance behaviour in relation to intracellular and extracellular thresholds for model simulations using LHS samples.	161
Table 6.6: Percentage of simulations that clear the infection in ≤ 7 days when treated using different dosing strategies of cefixime ^a	162

Acknowledgements

My PhD journey would not be successful if not for the immense help, support and guidance I received from many people.

It is with immense gratitude that I express my sincere appreciation to all my supervisors, Associate Professor James Wood, Associate Professor David Regan, Professor Matthew Law and Dr. Duleepa Jayasundara, for being extremely supportive throughout my research project. I am grateful for their continuous support, guidance, and tutelage on both my research work and career paths.

I would also like to thank my research collaborators, Professor Kate Seib and Professor Philip Kuchel for sharing their profound expertise. Their suggestions and feedback have led me to produce impactful work during my PhD candidature.

I would also like to remind my research progress review panel members, Professor Basil Donovan, Dr. Richard Grey and Dr. Deborah Cromer.

I also like to acknowledge the funding and resources received for my PhD through the scholarships provided by the University of New South Wales, PRISM² National Health and Medical Research Council Centre for Research Excellence and the Australian Government Research Training Program Scholarship.

Finally, I would like to express my heartfelt thanks to my parents, family and partner for their continuous support, encouragement and blessings.

Chapter 1

Introduction

1.1 Introduction and thesis motivation

Gonorrhoea is a sexually transmitted infection (STI) caused by bacteria of the species *Neisseria gonorrhoeae* (NG). NG is a gram-negative bacterium for which humans are the only natural host (Unemo, *et al.* 2019). Since the 1930s when the first antibiotic, penicillin, became available gonorrhoea has been successfully treated using antibiotics. However, since the beginning of antibiotic usage, NG has progressively developed resistance to all classes of drugs that have been used to treat gonorrhoea, and current treatments are now under threat with few alternatives of proven safety and efficacy (Terreni, *et al.* 2021; Unemo, *et al.* 2016). Drug resistant NG has become a major public health concern (Centers for Disease Control and Prevention 2019a; World Health Organization 2012) and the development of new treatment options and prophylactic vaccines are seen as increasingly important in population control of gonorrhoea.

Population-level and within-host mathematical models of transmissible diseases, while limited by existing knowledge and measurements in terms of their ability to capture the complexity of biological systems, can be useful in providing insights into infection transmission (e.g., Chan, *et al.* 2012; Keeling and Danon 2009) and underlying biological phenomena (e.g., Ho, *et al.* 1995; Perelson and Ribeiro 2013). Within-host infectious disease models, in particular, have several uses such as the ability to simulate an *in vivo* environment as for example in the model developed by Smith, *et al.* (2011) for pneumococcal infection which studied the impact of immune responses on clearance of

infection. Within-host models can also be used to explain and understand phenomena that are difficult to explore with existing experimental methods. For instance, in work on human immunodeficiency virus (HIV), Ho, *et al.* (1995) showed that the turnover of infected cells is a fast-paced process disproving earlier beliefs to the contrary. Similarly, in the epidemiological context, insights from infectious disease models have the potential to guide public health policy by evaluating the effects of relevant interventions on transmission, for instance in assessing the impact of a potential NG vaccine on the prevalence of gonorrhoea (Craig, *et al.* 2015).

Within-host and population-level processes may interact and these interactions have been studied through mathematical models to better understand the dynamics of infections such as HIV (e.g., Jie, *et al.* 2015; Martcheva and Li 2013), tuberculosis (e.g., Colijn and Cohen 2015) and malaria (e.g., Legros and Bonhoeffer 2016). For example, Martcheva and Li (2013) analysed the impact of within-host dynamics on the prevalence of HIV infection, by linking within-host viral load with between-host transmission and disease-related mortality at the population-level. In the context of NG, Craig, *et al.* (2015) carried out a similar study where a within-host parametric model of the bacterial load was used to determine the infectiousness of individuals in a population-level model that was used to assess the impact of a potential vaccine on the prevalence of gonorrhoea.

The ability to study details of within-host NG dynamics is somewhat challenged by the limitations in existing experimental studies. Several published studies provide useful information on the initial stages of within-host NG infection. Examples are *in vitro* studies (e.g. Chateau and Seifert 2016; Criss and Seifert 2006; Rest, *et al.* 1982) that explore intracellular NG survival and replication mechanisms, and human experimental studies (e.g., Schmidt, *et al.* 2000; Schneider, *et al.* 1991; Swanson, *et al.* 1988) that

provide information on the natural infection time-course in the first 5-7 days. However, most of these studies do not seek to quantify intracellular dynamics (NG survival and replication within polymorphonuclear leukocytes (PMN) and epithelial cells) and do not reflect longer-term infection dynamics including natural infection clearance. Ethical requirements for treatment early in the infection time-course mean that human experimental studies cannot be used to understand long-term infection dynamics. Furthermore, due to the human-specific intracellular survival mechanisms exhibited by NG (Jerse, *et al.* 2011; Sadarangani, *et al.* 2011), bacterial load data measured in mouse models cannot be directly extrapolated to infection within the human host.

The initial aim of this thesis was to develop a mathematical model to link within-host NG infection processes with population resistance patterns, such as in the theoretical study by Colijn and Cohen (2015). In this study, the authors attempted to establish whether an aggressive or moderate approach to antibiotic treatment is likely to drive drug resistance in the population. However, the lack of prior attention to quantitative descriptions of the within-host dynamics of NG infection led me to deviate from this path, in order to focus on exploring intracellular NG infection dynamics and clearance with and without treatment. The limited existing body of evidence led me to first develop a model to gain an understanding of the underlying within-host processes relating to infection with NG, focusing on symptomatic male urethral NG infection, for which the limited *in vivo* data available primarily concern. In order to test the model against known outcomes I then used this within-host model to evaluate treatment effectiveness for a variety of antibiotics that are either currently in use or being considered for use in the future.

Given the lack of experimental studies, especially in regard to intracellular NG dynamics, it is perhaps not surprising that I could not identify any prior studies exploring antibiotic treatment effects on intracellular NG. As intracellular NG has the potential to

evade host immune responses (Simons, *et al.* 2006; Unemo, *et al.* 2019), the antibiotic mediated killing of these intracellular NG can play a vital role in infection clearance. Differences in the effectiveness in drug mediated killing of extracellular and intracellular bacteria have also been observed for various pathogens such as *S. aureus* (Barcia-Macay, *et al.* 2006; Evans, *et al.* 2020; Peyrusson, *et al.* 2018), but to the best of my knowledge, such analyses have not been conducted in the context of NG. A recent study by Sena, *et al.* (2020) has emphasised the importance of using mathematical models “to understand the interactions and dynamic effects of ceftriaxone and azithromycin as dual therapy and in monotherapies, their gonococcal and *M genitalium* kill rates, antimicrobial resistance suppression, and optimal dosing” (Sena, *et al.* 2020) and several of these ideas align with my thesis aims.

Motivated by the above observations I identify three aims to be pursued in this thesis.

1. To develop a mechanistic within-host mathematical model of untreated male urethral NG infection that encapsulates the relevant extracellular and intracellular NG dynamics and immune response.
2. To quantify extracellular and intracellular antibiotic effects and their influence on treatment effectiveness for NG.
3. To investigate the effectiveness of alternative treatment regimens and combinations for clearance of NG infection.

1.2 Thesis overview

In pursuing these research aims, I first needed to understand the underlying NG infection and antibiotic treatment processes to guide the development of my within-host

mathematical models. Therefore, in Chapter 2 (Literature review), I review the literature pertaining to gonorrhoea infection dynamics, antibiotic treatment for gonorrhoea, the extracellular and intracellular activity of antibiotics, drug protein binding effects and PK/PD of antibiotics.

In Chapter 3 (Modelling the in-host dynamics of *Neisseria gonorrhoeae* infection), I develop a deterministic compartmental within-host mathematical model to describe untreated urethral infection in men. To capture the within-host infection processes, I consider the interactions between bacteria, host cells (epithelial cells) and the immune response mediated by PMN. Here, parameter values are estimated by fitting the model to existing data and, through model calibration to known infection outcomes. Using this model, I attempt to understand factors associated with clearance of infection without treatment and the role of intracellular NG in prolonging infection. This model then forms the basis for subsequent analyses carried out in this thesis.

In Chapter 4 (Modelling treatment effects for gonorrhoea), I extend the model developed in Chapter 3 to integrate treatment dynamics for gonorrhoea by accounting for key PK/PD features. This extended model is used to explore treatment using drugs that are currently in-use (ceftriaxone, cefixime and azithromycin) and potential treatment options (gepotidacin, gentamicin). In this chapter I analyse how intracellular NG and PK/PD variables affect infection clearance and show that the model successfully produces infection clearance times that align with those reported in the literature for gepotidacin, gentamicin and azithromycin. In this chapter, I also discuss the limitations of the model in regard to capturing treatment effects for ceftriaxone and cefixime.

In Chapter 5 (Effectiveness of different treatment regimens for gonorrhoea), I use the model developed in Chapter 4 to investigate different treatment regimens for two potential treatment options (monotreatment with gepotidacin and dual treatment with

gentamicin and azithromycin). Here, I test single and multiple dose strategies for both mono and dual treatment options. I also attempt to quantify effective drug concentrations through appropriate PK indices calculated using extracellular and intracellular drug concentrations.

In Chapter 6 (Evaluation of ceftriaxone and cefixime treatment strategies using a model that incorporates drug-target binding), I hypothesise that my previous model failed to accurately describe ceftriaxone and cefixime treatment due to inadequate description of the transition to bacteriostatic and bactericidal effects as well as post-antibiotic effects. Here, I develop a mechanistic model that explicitly captures drug-binding to penicillin binding proteins (PBP), building on previous approaches used for the pathogens *V. cholerae* and *E. coli* (Abel zur Wiesch, *et al.* 2015). To the best of my knowledge, this is the first model to incorporate a mechanistic representation of ceftriaxone and cefixime drug binding interactions in the context of modelling treatment of NG infection.

Finally, in Chapter 7 (Conclusions and future work), I discuss the main findings from these studies, limitations and future research directions.

In regards to the results chapters, while significant contributions were made by my supervisors in terms of the design and review of the studies and in relation to chapters 4-6, by Professor Phillip Kuchel of University of Sydney, I was solely responsible for writing the manuscripts, deriving model equations and implementing simulations and producing the results described in these chapters.

Chapter 2

Literature review

2.1 Clinical manifestation and sequelae

In 2016, it was estimated that there were 86.9 million new gonorrhoea cases worldwide among males and females aged 15-49 years (Rowley, *et al.* 2019). The global prevalence of gonorrhoea in 2016 was estimated to be 0.9% in females and 0.7% in males, corresponding to a total of 30.6 million prevalent cases of gonorrhoea worldwide (Rowley, *et al.* 2019). Gonorrhoea remains a common infection with a significant disease burden due to the associated risk of infection and potential complications. NG can infect various anatomical sites, in particular urethral, anorectal, conjunctival, pharyngeal and ovarian infections. When it ascends to the upper reproductive tract, gonorrhoea can lead to serious sequelae in women including epididymitis or pelvic inflammatory disease, which in turn can lead to infertility and ectopic pregnancy (Unemo, *et al.* 2019). Maternal gonorrhoea can also lead to various complications such as pre-term birth and neonatal blindness. Gonorrhoea also increases the risk of human immunodeficiency virus (HIV) acquisition (Guvenc, *et al.* 2020; Holmes, *et al.* 2008; Miller 2006; Unemo, *et al.* 2019; Unemo and Shafer 2014). In rare cases, gonorrhoea infection can lead to disseminated infection, with clinical symptoms including arthritis and skin lesions (Holmes, *et al.* 2008; Lohani, *et al.* 2016; Unemo, *et al.* 2019).

In both men and women, gonorrhoea can be symptomatic or asymptomatic, with the symptomatic fraction varying by anatomical site. The endocervical canal is the primary infection site in women (Edwards and Apicella 2004) and such infections are

often asymptomatic and can act as a reservoir for onward transmission of infection in the community (Miller 2006). Urethral infection in men is primarily symptomatic but it is estimated that 10-25% of cases can be asymptomatic (Fairley, *et al.* 2019; Lovett and Duncan 2019). Around 90% and 85% of pharyngeal and rectal infections, respectively, are asymptomatic (Kent, *et al.* 2005; Morris, *et al.* 2006). Accurate estimates of the true symptomatic proportion are challenging to compile, with published studies subject to limitations in diagnostic sensitivity and specificity in testing methods (culture vs nucleic acid amplification test (NAAT)) and recall bias (Fairley, *et al.* 2019).

2.2 Natural history of NG infection

Clinical studies of the natural history of NG infection provide evidence about untreated NG infection such as the changes in the bacterial load over time, the nature and timing of symptoms and the duration of infection. For instance, experimental NG infection studies with male volunteers (Hobbs, *et al.* 2011; Hook and Holmes 1985; Isbey, *et al.* 1997; Ramsey, *et al.* 1995; Schmidt, *et al.* 2001) show similar clinical features to natural infection and have provided insights into characteristics of untreated symptomatic male urethral NG infection.

There are substantial differences between infections at different anatomical sites, with for instance lower bacterial loads (approximately 2×10^5 bacteria (Chow, *et al.* 2016)) and a shorter duration of untreated infection observed at the pharynx (5 – 20 weeks (Barbee, *et al.* 2021)) in comparison to the urethral NG infection (discussed in Section 2.2.1). However, natural history studies at non-urethral sites are limited, with no human experimental studies to my knowledge. In addition, due to the potential risk of reproductive complications associated with vaginal/cervical female NG infection (see Section 2.1) human experimental studies have not been conducted in women at this site.

I am also only aware of repeat measures of bacterial load over time being taken from urethral exudates, with only single observations conducted for other anatomical sites. For example, in a clinical study in men who have sex with men with untreated pharyngeal gonorrhoea, Chow, *et al.* (2016) report bacterial counts only at the time of starting treatment. Due to the lack of natural history data regarding female NG infection or non-urethral NG infection in men, I focus in what follows on symptomatic urethral NG infection in men.

2.2.1 Natural history of symptomatic male urethral NG infection

Human experimental studies of NG infection using male volunteers report the bacterial counts in urine or semen collected over a period of time, usually 2h from the start of the infection and every 12 or 24h after that up to 5-7 days. In these studies, an ‘eclipse’ period is observed about 2h after inoculation, where few or no gonococci are observed in urine (Hobbs, *et al.* 2011). Although no clear explanation has been offered for this phenomenon, it is thought that this may be due to NG internalisation within the urethral epithelium which provides NG with the opportunity to survive and replicate intracellularly (Edwards and Apicella 2004). While this has been observed in experimental infection, it is unknown as to whether an eclipse period occurs after sexual transmission. After this eclipse period an increasing number of NG is detected in urine (Hobbs, *et al.* 2011).

The incubation period (time from infection to the onset of symptoms) of urethral NG infection in men is reported to vary in the range of 1-14 days (Holmes, *et al.* 2008), with a majority of human experimental studies reporting a range of 2-6 days (Hobbs, *et al.* 2011; Hook and Holmes 1985; Schmidt, *et al.* 2001). Human experimental studies report a peak bacterial load of $10^6 - 10^8$ bacteria (Ramsey, *et al.* 1995; Schmidt, *et al.*

2001; Schneider, *et al.* 1995; Schneider, *et al.* 1991; Schneider, *et al.* 1996), with symptoms typified by purulent discharge and dysuria (Cohen, *et al.* 1994; Swanson, *et al.* 1988; Swanson, *et al.* 1987). A major limitation in these studies is the absence of data on bacterial counts of NG surviving intracellularly (within polymorphonuclear neutrophils (PMN) or epithelial cells).

Although several studies report natural resolution of extragenital infection (primarily pharyngeal infection), it is difficult to find information on clearance of male urethral NG infection without treatment (Mensforth and Ross 2018). Due to ethical considerations, data from human experimental studies are restricted to the initial stages of the urethral infection, with no observations on the duration of untreated infection. Therefore, evidence regarding untreated infection of longer duration comes primarily from pre-antibiotic era studies or clinical studies of asymptomatic infection where treatment was withheld. Pre-antibiotic era studies (Hill 1943; Pelouze 1939) suggest a urethral infection duration of 1-2 months. In a clinical study where treatment was ineffective for sulphonamide resistant cases, Herrell, *et al.* (1943) concluded that male urethral NG infections persist for 1-4 months, while Korenromp, *et al.* (2002) estimated a mean duration of 4 months using data from the clinical study by Handsfield, *et al.* (1974).

However, the infection durations reported in the above-mentioned studies are subject to uncertainty due to limitations associated with these experiments. The early pre-antibiotic era studies are inconsistent in regard to the size of the bacterial load of the inoculum, inoculation technique and are not directly comparable to modern human experimental studies. During the period when treatment of asymptomatic men was not standard practice, Handsfield, *et al.* (1974) conducted a prospective study of the natural history of male urethral asymptomatic infection. In this study, some individuals remained

asymptomatic throughout the study period (165 days) while some became symptomatic or resulted in spontaneous infection clearance. In the theoretical study by Korenromp, *et al.* (2002), the infection duration was estimated using data from Handsfield, *et al.* (1974), but when generating these estimates additional simplifying assumptions are made such as exponentially distributed clearance times and equivalence in infection duration by symptom status. However, Korenromp, *et al.* (2002) made adjustments to capture some of the limitations in Handsfield, *et al.* (1974) data as for example with weekly follow-up via culture to determine infection status, re-infections occurring after spontaneous cure cannot be excluded from Handsfield, *et al.* (1974) data. Furthermore with culture being less sensitive than NAAT (Meyer and Buder 2020), there was potential to underestimate infection duration due to false-negative results. On the other hand, more recent studies using NAAT can produce positive results even with non-viable bacteria (Barbee, *et al.* 2021).

2.3 Within-host dynamics of NG infection

NG is a facultative intracellular bacterium meaning that it can survive and replicate both outside and inside host cells (Hill, *et al.* 2016). During infection, NG primarily interacts with host epithelial cells and PMN and NG have adapted mechanisms to survive and replicate within these host cells (referred hereinafter to as intracellular NG). NG express several virulence factors on their surface including pili, opacity-associated proteins (Opa) and porin proteins (Edwards and Apicella 2004; Holmes, *et al.* 2008; Unemo, *et al.* 2019), which play a critical role during infection. I have summarised NG pathogenesis in Fig.2.1 and described this in detail in the following sections.

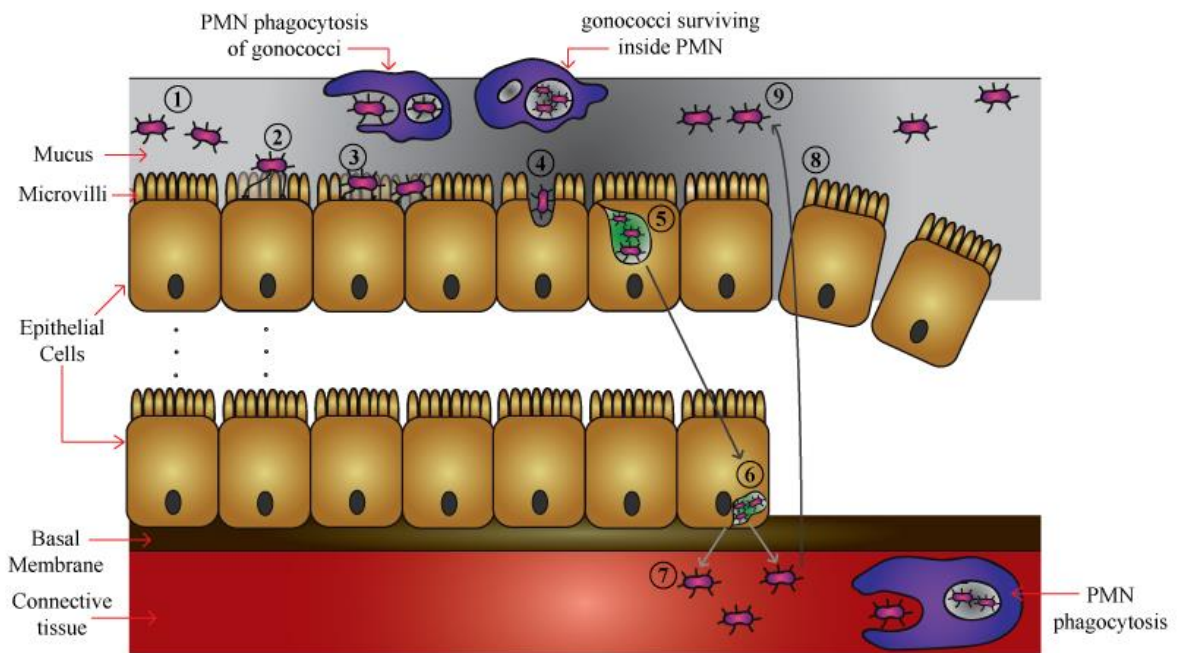


Figure 2.1: Simplified illustration of some of the main elements of NG pathogenesis.

Descriptions of the numbered components are as follows: 1) extracellular NG; 2) NG attachment to epithelial cells through pili; 3) increased adherence through Opacity associated proteins; 4) NG internalisation within epithelial cells; 5) NG within vacuoles; 6) transport of vacuole with gonococci to the basal surface; 7) release of NG into the basal layers and bloodstream; 8) exfoliation of epithelial cells and; 9) released gonococci infecting adjacent cells.

2.3.1 NG interaction with epithelial cells

The epithelial layer is the first-line of defence against NG (Sadarangani, *et al.* 2011) as NG attachment to epithelial cells is required for infection (Ward and Watt 1972). Pili (a thin hair-like appendage expressed on the surface of NG composed of pilin protein) mediate the initial attachment to epithelial cells (Rudel, *et al.* 1992; Swanson 1973) and enhanced adherence is mediated by Opa proteins (an NG outer membrane protein) (Merz

and So 2000). Attached NG can be internalised within epithelial cells where they can replicate and evade immune response attacks (Criss and Seifert 2006; Shaw and Falkow 1988) and delay apoptosis of epithelial cells as a survival mechanism (Binnicker, *et al.* 2003; Follows, *et al.* 2009). Internalised NG are enclosed in vacuoles which can transport NG to the lateral and basal surfaces of the epithelium (Harvey, *et al.* 1997). NG are released from these vacuoles through lysis of the vacuole membrane and the infected epithelial cells are shed resulting in a thinning of the epithelium (Apicella, *et al.* 1996; Mosleh, *et al.* 1997). These released NG can further infect adjacent and deeper layers within the epithelium which may result in prolonged infection and, in rare cases, cause disseminated infection (McGee, *et al.* 1981; McGee, *et al.* 1983; Mosleh, *et al.* 1997).

As discussed above although intracellular survival and replication of NG is well recognised and has been extensively studied through *in vitro* cell culture models (e.g., Criss and Seifert 2012; Edwards and Apicella 2004; Mosleh, *et al.* 1997), the extent of NG internalisation and its impact on the course of infection have not been quantitatively described in most experimental studies. In human experimental studies, although the number of gonococci that is recovered from the urine is measured (Schmidt, *et al.* 2000; Schmidt, *et al.* 2001; Schneider, *et al.* 1995), these studies do not quantify the number of intracellular NG. The study by Veale, *et al.* (1979) is the only study I could identify that has measured the proportion of the overall NG population in different cellular states (extracellular, NG within PMN and epithelial cells). However, the results of this study are presented for only a single fixed time-point (the precise timing of collection is not reported) and thus the dynamical changes in intracellular bacterial populations are not captured.

2.4 The immune response to NG infection

The immune system consists of two fundamental components: the innate and adaptive immune systems. The innate immune system provides the first line of defence which is elicited rapidly and triggered through a limited set of receptors that can detect invading pathogens (Chaplin 2010). Elements of the innate immune response include various cells including neutrophils and macrophages (Turvey and Broide 2010). Neutrophils are polymorphonuclear lymphocytes that are short-lived and are one of the first inflammatory cells to be present at the site of inflammation (Döhrmann, *et al.* 2016). They are the most abundant cell type in the blood and more than 10^{11} cells are produced per day from the bone marrow. Antimicrobial mechanisms adopted by neutrophils include phagocytosis, degranulation, oxidative burst and neutrophil extracellular traps (Döhrmann, *et al.* 2016). Once neutrophils reach the end of their life-cycle they are phagocytosed primarily by macrophages (Rosales 2018), which carry out various functions including phagocytosis of pathogens and engulfment of apoptotic cells. Macrophages (and to an extent PMN) are also responsible for producing cytokines, which are molecules that are responsible for integrating functions to generate a robust immune response and ensuring the immune response subsides after an adequate period (Lacy and Stow 2011). The innate immune response also plays an important role in activating the adaptive immune response which targets disease causing antigens using a diverse repertoire of receptors expressed by T and B cells and is generally triggered more slowly than the innate immune response (Turvey and Broide 2010). The adaptive immune response also generates immunologic memory to the pathogen so that in the case of re-infection it can respond rapidly (Chaplin 2010).

During infection with NG, an elevated cytokine response is observed (Ramsey, *et al.* 1995) which stimulates the innate immune system primarily through the recruitment of PMN to the infection site. Purulent exudate observed in experimentally infected males

is a result of this elicited inflammatory response (Edwards and Apicella 2004; Shafer and Rest 1989). PMN can kill NG by phagocytic engulfment (Ramsey, *et al.* 1995; Rest, *et al.* 1982). However, *in vitro* studies have shown that approximately 50% of NG within PMN remain viable (Veale, *et al.* 1979) and these surviving NG are capable of replicating within PMN (Parsons, *et al.* 1985; Parsons, *et al.* 1986; Simons, *et al.* 2005; Veale, *et al.* 1979; Watt 1970), delaying PMN apoptosis (Simons, *et al.* 2006), suppressing oxidative burst (Gunderson and Seifert 2015) and delaying phagosome maturation (Johnson and Criss 2013).

Human-specific infection and survival mechanisms of NG make it challenging to develop a successful animal model that reflects certain features of human infection and immune response such as intracellular NG survival and replication (Rice, *et al.* 2017). With 17β -estradiol treatment to cause prolonged infection (Jerse, *et al.* 2011; Rice, *et al.* 2017) female mouse infection models have been used to understand NG pathogenesis including the elicited PMN response. Mice are most susceptible to infection with NG when they are at their proestrus stage as with the influx of increased levels of PMN during postovulatory stages, mice start to show resistance to NG (Francis, *et al.* 2018; Rice, *et al.* 2017). Therefore, in the mouse models in order to achieve a longer infection duration (lasting for ~10-12 days), estradiol is required as it can prolong the duration of the NG favourable estrous-like environment, by suppressing the natural PMN influx in mice.

When interpreting results from mouse models, the time-varying impact of estradiol needs to be taken into consideration (Jerse 1999; Packiam, *et al.* 2010). Typically, estradiol is administered to both test and control mice via slow-release pellet or subcutaneous administration on days -2, 0 and 2 relative to inoculation with NG or phosphate-buffered saline in test and control mice, respectively. PMN influx in response to NG infection has been observed in several mouse models at 4-9 days after inoculation

(Jerse 1999; Packiam, *et al.* 2010; Soler-Garcia and Jerse 2007). Around 9 days post-inoculation, as estradiol wears off, mice reach postovulatory stages where even uninfected mice treated with estradiol show an increase in PMN response (Jerse 1999; Jerse, *et al.* 2011) following the resumption of the estrous cycle.

Although PMN are considered to be the main immune response to infection with NG, macrophages are also believed to play an important role by phagocytosing NG and recruiting PMN to the infection site (Château and Seifert 2016; Escobar, *et al.* 2018). NG has adapted to survive and replicate within macrophages as well and is capable of delaying macrophage apoptosis (Château and Seifert 2016; Escobar, *et al.* 2018). However, there remains limited literature on the role of macrophages during NG infection.

Despite immune-mediated clearance of infection, individuals do not appear to be protected from re-infections through acquired immunity. The detailed diary of James Boswell (1740-1795), which relates the story of having urethritis nineteen times, including at least twelve apparent re-infections, is generally presented as anecdotal evidence of lack of acquisition of protective immunity following infection (Ober 1970). From human experimental studies, it is also evident that individuals can be infected multiple times with closely related strains (Schmidt, *et al.* 2001; Stupiansky, *et al.* 2011), with re-infection with the same strain also demonstrated in mouse models (Song, *et al.* 2008). Therefore, the adaptive immune response against infection with NG is considered to have a limited effect with relatively weak and short-lived antibody responses (Holmes, *et al.* 2008). However, with the apparent partial protection against NG observed in New Zealand conferred by vaccination against meningococcal B disease (Petousis-Harris, *et al.* 2017; Seib 2017; Semchenko, *et al.* 2019), interest in protection via vaccine-induced

adaptive immune responses has been reinvigorated (Leduc, *et al.* 2020; Semchenko, *et al.* 2019).

2.5 Antibiotic treatment for gonorrhoea

Since the introduction of antimicrobials in the 1930s, gonorrhoea has remained a readily treated infection with several classes of antibiotics having been successfully used to treat gonorrhoea. These include sulphonamides (e.g., sulfathiazole), β -lactams (e.g., penicillin and third-generation cephalosporins such as ceftriaxone and cefixime), aminoglycosides (e.g., streptomycin), tetracyclines (e.g., aureomycin), macrolides (e.g., azithromycin) and quinolones (e.g., ciprofloxacin). However, due to the propensity of NG to acquire resistance to antimicrobials, available treatment options have greatly diminished and most of the above-mentioned treatment options are now removed from treatment recommendations (see Fig. 2.2 for a summary).

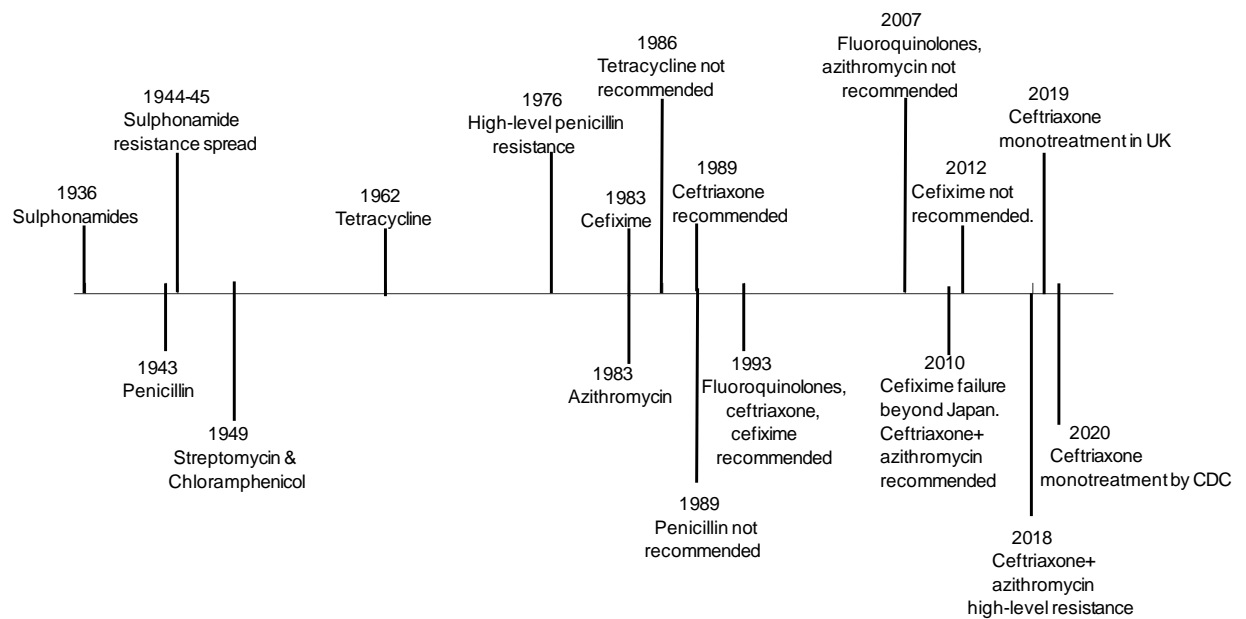


Figure 2.2: Timeline of antibiotic treatments for gonorrhoea and resistance. The figure is based on reports in the published literature (Eyre, *et al.* 2018; Fifer H, *et al.* 2019; St. Cyr, *et al.* 2020; Unemo and Shafer 2011; Unemo and Shafer 2014).

Cefixime and ceftriaxone are both third-generation cephalosporins that are currently used to treat NG infection, with the former in limited use. In around 2012, there were frequent cases of NG strains showing increased minimum inhibitory concentration (MIC, the lowest drug concentration that is required to inhibit bacterial growth) for cefixime. Due to these resistance concerns, cefixime was removed as a first-line treatment option in the United States (US) in 2012 (Centers for Disease Control and Prevention 2012) and was also removed from the recommendations in the European guidelines (Bignell and Unemo 2013). If cefixime is used as an alternative option, the US Centers for Disease Control and Prevention (CDC) recommends a test of cure at the site of infection (Centers for Disease Control and Prevention 2015).

Ceftriaxone is considered to be the last remaining treatment option for gonorrhoea with proven safety and efficacy for routine use but strains of ceftriaxone resistance or

decreased susceptibility are reported from several countries. Resistance to ceftriaxone in NG is chromosomally mediated and in recent isolates this is related to the presence of a mosaic *penA* allele that encodes altered forms of penicillin binding protein (PBP) 2 which shows a substantial decrease in acylation by ceftriaxone (Nakayama, *et al.* 2016; Tomberg, *et al.* 2013; Unemo, *et al.* 2011). Mosaic *penA* alleles appear to have arisen from recombination events between NG and commensal *Neisseria* species commonly found in the nasopharynx (Ito, *et al.* 2005). The first ceftriaxone resistant strain (H041) with concerning levels of resistance was reported in Japan with an elevated MIC of 2-4 mg/L (Ohnishi, *et al.* 2011). This strain was also resistant to other drugs and classes including cefixime, penicillin, azithromycin and fluoroquinolones. Since then, multidrug resistant strains with resistance to ceftriaxone have been reported from several countries including the F89 strain in France (Unemo, *et al.* 2012) and Spain (Camara, *et al.* 2012) and A8806 in Australia (Lahra, *et al.* 2014). In 2017, the strain FC428, which was initially found in Japan (Nakayama, *et al.* 2016) was independently reported in Denmark (Terkelsen, *et al.* 2017) and Canada (Lefebvre, *et al.* 2018) and a strain with similar characteristics was later found in Australia (Lahra, *et al.* 2018), with further reports internationally described by Eyre, *et al.* (2019). Sustained transmission of FC428 was recently reported in China (Chen, *et al.* 2020; Yan, *et al.* 2021) and Japan (Lee, *et al.* 2019).

Between 2010 and 2012 the treatment guidelines in the United Kingdom (UK) and the US were changed to dual treatment with intramuscular ceftriaxone and oral azithromycin in an attempt to reduce the threat of resistance for ceftriaxone (Workowski and Berman 2010). However, there have been recent reports of strains showing resistance to both ceftriaxone (MIC of 0.5mg/L) and azithromycin (MIC>256mg/L) (Eyre, *et al.* 2018; Whiley, *et al.* 2018). NG can readily acquire high-level azithromycin resistance

through point mutations (Chisholm, *et al.* 2010a) and with a moderate prevalence of azithromycin resistance but low levels of ceftriaxone resistance observed in both the UK (Public Health England 2018; Whittles, *et al.* 2018) and the US (Centers for Disease Control and Prevention 2018), dual therapy has been abandoned in those countries. Instead, the UK (Fifer H, *et al.* 2019) and the US (St. Cyr, *et al.* 2020) now recommend monotherapy with ceftriaxone but at elevated doses of 1g and 0.5g, respectively.

2.5.1 Novel treatment options for gonorrhoea

In response to the concerns about resistance described above, there is also considerable interest in new treatments, with several novel antimicrobials undergoing clinical trials as potential treatment options for gonorrhoea such as solithromycin (a fourth-generation macrolide), gepotidacin (a novel triazaacenaphthylene bacterial type II topoisomerase inhibitor) and zoliflodacin (first-in-class spiropyrimidinetrione that inhibits bacterial type II topoisomerase). Solithromycin, gepotidacin and zoliflodacin have, respectively, shown 92% (Chen, *et al.* 2019), >95% (Scangarella-Oman, *et al.* 2018; Taylor, *et al.* 2018b) and >95% (Taylor, *et al.* 2018a) treatment success against genital infections. However, all these drugs show poor efficacy against the limited number of samples tested from extragenital sites (rectal and pharyngeal), with lower NG treatment efficacy at the pharynx for other drugs previously associated with poor antibiotic penetration at that site (Barbee 2014; Moran 1995).

Due to the unique binding mechanism of gepotidacin that distinguishes this class from quinolones (also a bacterial topoisomerase inhibitor), it has shown *in vitro* success against NG strains which show resistance for ciprofloxacin (a quinolone) (Biedenbach, *et al.* 2016; Farrell, *et al.* 2017). However, concerningly, in the phase two clinical trial, the emergence of resistant NG strains under single dose gepotidacin therapy has already been observed (Scangarella-Oman, *et al.* 2018). Using an *in vitro* infection model, VanScoy,

et al. (2020) showed that the use of single or multiple dose regimens of gepotidacin that accumulate to 4.5g or higher prevented resistance from developing during treatment.

Existing antibiotics such as gentamicin have also been tested as new treatment options for gonorrhoea. Since 1993, gentamicin has been used successfully to treat gonorrhoea infection in Malawi (Brown, *et al.* 2010). In particular, combination therapy with gentamicin and azithromycin has been a recent focus of study but in clinical trial settings, the effectiveness of this combination against extragenital infections was found to be poor (Barbee, *et al.* 2019; Kirkcaldy, *et al.* 2014; Ross, *et al.* 2019).

There are several other drugs that are currently under investigation at *in vitro* and clinical trial stages including delafloxacin (Hook, *et al.* 2019), methyldopa and carbamazepine (Poole, *et al.* 2020), gold-containing auranofin (Elkashif and Seleem 2020), small-molecule antimicrobial SMT-571 (Jacobsson, *et al.* 2019) and DIS-73285 (Jacobsson, *et al.* 2020). Further studies on these novel treatment options need to be performed to better understand their pharmacokinetics, the potential for the emergence of drug resistance, suitable dosage and effective concentration required at the target site (Chen, *et al.* 2019), possible multidrug combination options (Taylor, *et al.* 2018b) and their effectiveness for extragenital infections.

2.5.2 Mechanisms of drug action and entry into cells

Different drugs have different mechanisms of action and targets depending on their drug class. Here I focus on the antibiotics that are discussed in this thesis, these being ceftriaxone and cefixime (β -lactams), gepotidacin (triazacacenaphthylene bacterial type II topoisomerase inhibitor), azithromycin (macrolide) and gentamicin (aminoglycoside). The β -lactam class works by inhibiting bacterial cell wall synthesis through binding of the β -lactam ring to membrane-bound PBP, which are enzymes that catalyse cell wall

synthesis. NG has four distinct PBP (PBP 1,2, 3 and 4), with differing drug binding affinities (Barbour 1981; Dougherty, *et al.* 1980; Stefanova, *et al.* 2004) where PBP2 has been identified as the main lethal target (Powell, *et al.* 2009; Ropp, *et al.* 2002; Unemo and Nicholas 2012). Azithromycin and gentamicin interfere with the process of protein synthesis through binding to the bacterial 50s (Ross, *et al.* 2019) and 30s (Mensforth and Ross 2019) ribosomal subunits, respectively. Gepotidacin has a unique mechanism of action that impairs DNA replication (Peyrusson, *et al.* 2018). Drug resistance and mechanisms of action are relevant during therapy and when deciding on possible drug combinations. However, full investigation into drug resistance is beyond the scope of this thesis. Various mechanisms of drug resistance adopted by NG is extensively reviewed in several studies for example by Unemo and Shafer (2014).

Depending on the level of antibacterial activity against a particular pathogen, antibiotics are mainly categorised as bactericidal or bacteriostatic. An antibiotic that kills 99.9% of a bacterial population is defined as bactericidal while an antibiotic that only inhibits the growth of the bacterial population is defined as bacteriostatic (Drusano 2004; Pankey and Sabath 2004). Generally, this categorisation of bactericidal or bacteriostatic can depend on several factors such as the size of the bacterial population (Levison 1995), pathogen (Delgado, *et al.* 2000; Lamb, *et al.* 1999) and growing conditions (Pankey and Sabath 2004). For example, azithromycin is bactericidal against *Staphylococcus aureus*, *Streptococcus pneumoniae* and *Haemophilus influenzae* (Dorfman, *et al.* 2008) but bacteriostatic against *Pseudomonas aeruginosa* (Imamura, *et al.* 2005). The time the drug concentration remains above the MIC and the drug concentration are also important variables in determining bactericidal and bacteriostatic effects of drugs. For example, β -lactam class of drugs require free drug to be above the MIC for differing fractions of the

dosing interval to achieve bacteriostatic and bactericidal effects. These factors are discussed in detail in Section 2.7.3.

The β -lactam class of drugs and macrolides are believed to enter cells through the mechanism of passive diffusion. Diffusion is the most common process of entering cells for small molecule drugs and the rate of diffusion vary with the environmental pH. For example, azithromycin due to their weak basic character are able to show high intracellular accumulation (Amsden 2001) while β -lactams as they are weak acids, show poor intracellular accumulation (Chanteux, *et al.* 2003; Laufen, *et al.* 1985). Aminoglycosides (e.g., gentamicin) enter cells through the process of endocytosis (Hashino and Shero 1995) which is a non-specific mechanism that drives poorly diffusible molecules to within cells.

2.6 Susceptibility breakpoints in the literature

Antimicrobial susceptibility tests (AST) are important for the clinical management of infection and surveillance of antimicrobial resistance. In order to interpret the results of AST, interpretive criteria that define clinical breakpoint values are required (Humphries, *et al.* 2019; Mercer, *et al.* 2020). The two main organisations responsible for setting breakpoint categories (susceptible, intermediate, resistant; see Table 2.1 below) are the Clinical and Laboratory Standards Institute (CLSI) and the European Union Committee on Antimicrobial Susceptibility Testing (EUCAST). Apart from these two organisations, the U.S. Food and Drug Administration Centre for Drug Evaluation and Research also sets breakpoints at the time of approval of new drugs (Weinstein and Lewis 2020). When setting these breakpoints, pharmacokinetic and pharmacodynamic data (discussed in Section 2.7), *in vitro* microbiological data (e.g., time-kill experiments) and clinical treatment success and failure rates are considered (Clinical and Laboratory

Standards Institute 2018; European Committee on Antimicrobial Susceptibility Testing 2019).

The two main categories used to define breakpoints are susceptible (S) and resistant (R) strains. A microorganism is defined as susceptible if there is a high likelihood of therapeutic success using a standard dosing regimen, and resistant if there is a high likelihood of therapeutic failure even when there is increased drug exposure (European Committee on Antimicrobial Susceptibility Testing 2019). A third category of “intermediate” or “increased exposure” (I) is used when there is uncertainty around categorisation but where a high likelihood of therapeutic success is obtained by increasing the dosing regimen or concentration at the site of infection (European Committee on Antimicrobial Susceptibility Testing 2019).

The NG breakpoints for ceftriaxone, cefixime and azithromycin are summarised in Table 2.1. For gentamicin and gepotidacin there are as yet no EUCAST or CLSI defined breakpoints. Based on epidemiological and clinical observations in Malawi, Brown, *et al.* (2010) defines susceptibility for gentamicin as $MIC \leq 4\text{mg/L}$, intermediate susceptibility as $8\text{-}16\text{mg/L}$ and resistance as $MIC \geq 32\text{mg/L}$.

Table 2.1: Empirical susceptibility breakpoints (mg/L) defined by CLSI and EUCAST for NG.

Drug ^a	S		R	
	CLSI	EUCAST	CLSI	EUCAST
Ceftriaxone	≤0.25	≤0.125	-	>0.25
Cefixime	≤0.25	≤0.125	-	>0.25
Azithromycin	≤1	≤0.25	-	>0.5 ^b

^a No intermediate category defined by CLSI or EUCAST.

^bBased on the 2018 guidelines (European Committee on Antimicrobial Susceptibility Testing 2018). In the 2019 guidelines, only an epidemiological cut-off (ECOFF) is defined (1mg/L). ECOFF is the highest MIC for the wild-type isolate (isolates with no detectable resistance or reduced susceptibility for the antimicrobial being evaluated). Only ECOFF is defined due to the poor correlation between MIC and clinical outcome.

2.7 Pharmacokinetics and pharmacodynamics (PK/PD) of antibiotics

Pharmacokinetic (PK)/pharmacodynamic (PD) data collected through experimental settings such as clinical trials (e.g., Barbee, *et al.* (2018)) and mouse models (e.g., Connolly, *et al.* (2019)) can be integrated with compartmental mathematical models (e.g., Chisholm, *et al.* (2010b)) to provide useful information on the relationship between drug exposure and treatment efficacy. The movement of the drug in the body after administration is referred to as a PK process while the bacteria's response to a given drug is referred to as a PD process (Holford and Sheiner 1982). Analysis of PK/PD for antibiotics is useful when attempting to optimise treatment strategies and minimise the development of resistance for existing and novel treatment options. The insights from PK/PD analysis can be used to design clinical trials (VanScoy, *et al.* 2020) and assist in making changes to existing treatment recommendations (St. Cyr, *et al.* 2020) and susceptibility breakpoints (Clinical and Laboratory Standards Institute 2018). When developing treatment regimens both PK and PD aspects are taken into consideration since PK properties influence the dose, dosing frequency and the route of administration while PD elements determine the relationship between drug concentration and the drug's effect on the net bacterial growth at the infection site.

2.7.1 Pharmacokinetics

PK properties govern drug absorption, metabolism, elimination and distribution. Absorption is the process by which a drug reaches the blood from its site of administration. Intravascular drugs are administered directly into the blood, either intravenously or intra-arterially and hence there is no absorption phase involved. Extravascularly administered drugs (e.g., oral, subcutaneous, or intramuscular) need to be first absorbed from the injection site to enter blood (Rowland and Tozer 1995). The

rate of drug absorption (k_a) and bioavailability (F) are the main determinants of absorption of an extravascularly administered drug. Bioavailability is defined as the fraction of the administered dose of the drug that reaches systemic circulation (Levison and Levison 2009). Once absorbed a drug is delivered by the blood to various organs and tissues in the body.

Clearance (CL) is a PK property that represents the capacity of different organs in removing drug and is defined as the volume of plasma that is completely cleared of drug per unit time (Rowland and Tozer 1995). As clearance is associated with drug removal from circulation, it is related to the elimination rate constant (k_{el}) and volume of distribution (V_d) as, $CL = V_d \times k_{el}$.

The volume of distribution is defined as the apparent volume into which a drug distributes in the body at equilibrium (Levison and Levison 2009). Consequently, the volume of distribution is the volume of plasma at the drug concentration, C , required to account for all drug in the body, A , so that $V_d = \frac{A}{C}$. For drugs represented through a single compartment (described in the next Section 2.7.2) (e.g., intravascularly administered), the volume of distribution is simply calculated as, $V_d = \frac{D}{C_o}$, where D is the dose amount of that reaches systemic circulation and C_o is the plasma drug concentration at time 0. Drugs represented through multiple compartments (described in Section 2.7.2), have separate volume of distribution values calculated in the elimination phase (V_β) which depends on drug clearance and at steady state (V_{ss}) (Smith, *et al.* 2015), where the net flux between the central and peripheral compartments is zero.

The elimination rate constant (k_{el}) describes the rate at which plasma drug concentration declines in the elimination phase, where elimination is defined as the

irreversible removal of the drug from the body (Rowland and Tozer 1995). For a drug with a constant rate of elimination (first-order kinetics), the drug concentration at any given time t (C_t) is given by, $C_t = C_0 \times e^{-k_{el} t}$. It follows that the half-life ($t_{1/2}$) of a drug is $t_{1/2} = \frac{\ln(2)}{k_{el}}$, where drug half-life is defined as the time taken to reduce the drug concentration by one-half (Rowland and Tozer 1995). The volume of distribution and drug clearance are related to the drug half-life as, $t_{1/2} = \frac{\ln(2) \times V_d}{CL}$. Therefore, the drug half-life is linearly proportional to V_d and inversely proportional to the rate of clearance.

2.7.2 *Modelling pharmacokinetics*

Conducting clinical trials is expensive and time-consuming, and recruiting a sufficient number of patients for large trials is often difficult (Hook, *et al.* 2020; Theuretzbacher, *et al.* 2020). Pharmacokinetic models are therefore a useful adjunct to clinical trials for estimating the optimum dosing regimens, establishing susceptibility breakpoints, informing the design of clinical trials and gaining insights on the PK data collected from clinical trials (Bulitta, *et al.* 2019).

PK models are used to simulate the change in the drug concentration within the body and the most classic uses of these are the one and two-compartment models. The compartments of a PK model do not necessarily reflect a specific physical space (Rowland and Tozer 1995). In the one-compartment model, the entire body is assumed to function as a single unit and hence is portrayed as one central compartment. Here, it is assumed that drug equilibration between tissues and blood occurs instantaneously (Rowland and Tozer 1995). For some drugs (e.g., azithromycin), drug distribution is not instantaneous and when the plasma concentrations are plotted on a log-linear scale a bi-exponential decline can be observed with a rapid distribution observed among well-perfused tissues while a slow distribution phase is observed in less-well perfused tissues

(Ripa, *et al.* 1996; Rowland and Tozer 1995). These PK profiles can be described using a two-compartment PK model. In this representation, the two compartments are generally referred to as central and peripheral compartments, where the central compartment includes blood and the highly perfused tissues and organs while the peripheral compartment includes less well-perfused tissues into which drug distributes more slowly. If indicated by the distribution of the plasma concentration profile, further compartments can also be included (Cascone, *et al.* 2013; Pene Dumitrescu, *et al.* 2013).

In addition to these classic compartmental models, recent advances have been made in physiologically-based pharmacokinetic modelling (PBPK), which unlike classical PK models represent actual organs and tissue spaces (e.g., heart, lung, brain, kidney, spleen) and their physical volumes (Aarons 2005). This approach can be used to quantify the drug concentration profiles at these individual organs/tissues rather than relying on plasma concentrations alone (Kuepfer, *et al.* 2016). However, these models involve a large number of parameters which can lead to issues of parameter identifiability (the ability to uniquely determine parameter values from available data) unless sufficient data is available for estimation (Tan, *et al.* 2018; Yates 2006). These PBPK models can also be combined with pharmacodynamic effects (PBPK/PD models) (Gordji, *et al.* 2005) to quantify the elicited drug response at the target sites.

Data to inform PK models can be obtained from *in vitro* and *in vivo* experimental studies. *In vivo* studies typically include measurements of plasma drug concentration from healthy volunteers (Barbee, *et al.* 2018; Patel, *et al.* 1981) and mouse models (Connolly, *et al.* 2019). The plasma concentrations measured in healthy volunteers (Barbee, *et al.* 2018; Patel, *et al.* 1981) are useful to inform PK parameters for simulation studies (Chisholm, *et al.* 2011), which can assess the effectiveness of different drug doses in achieving relevant PK targets (discussed in Section 2.7.3). In the context of NG, mouse

models have shown the potential to be used to determine appropriate dose amounts for treating human infection. The mouse model by Connolly, *et al.* (2019) resulted in time above the MIC (discussed in Section 2.7.3) calculations for ceftriaxone and cefixime consistent with those observed for human infections in the study by Chisholm, *et al.* (2011). However, there are some limitations in translating results from mouse models to human infection as some PK properties such as drug half-life differ from humans (Bulitta, *et al.* 2019).

Dynamic *in vitro* models such as chemostat and hollow fibre infection models (described in detail in Bulitta, *et al.* (2019)) allow the experimental setup to match the drug concentration profiles observed in humans. These models can also be used to explore both PK and PD effects together (Bulitta, *et al.* 2019). Recently, VanScoy, *et al.* (2020) developed a hollow fibre model with NG grown over a 7-day period and assessed treatment efficacies for gepotidacin, ceftriaxone and cefixime along with the risk of *de novo* resistance emerging. The findings of this study were used to inform the dosing regimens of a phase three clinical trial for gepotidacin (ClinicalTrials.gov Identifier: NCT04010539), expected to be completed in 2023. However, this hollow fibre infection model has not yet been validated against clinical outcomes (Theuretzbacher, *et al.* 2020) and as yet, such dynamic *in vitro* models do not include intracellular NG infection and treatment effects.

2.7.3 PK indices

The indices used to describe the effectiveness of a dosing regimen can vary depending on the antimicrobial class. The three main indices used are the time in which the drug concentration remains above the MIC (t_{MIC}), the area under the concentration curve (AUC) and the peak drug concentration, C_{max} .

Drugs in the β -lactam class display time-dependent activity as it has been experimentally confirmed that the elicited microbiological effect (the rate of pathogen killing) depends directly upon t_{MIC} (Craig 1995; Craig, *et al.* 1991; Eagle, *et al.* 1953). Once the time the drug concentration remains above the MIC exceeds a certain t_{MIC} , the rate of pathogen killing does not appear to be further increased by increasing the drug concentration. The relevance of t_{MIC} for β -lactams is clearly shown in a mouse-model study by Flückiger, *et al.* (1991), where for two treatment strategies that achieve the same AUC, the strategy that achieves a higher t_{MIC} elicits a greater biological effect. For concentration-dependent antibiotics such as fluoroquinolones, macrolides and aminoglycosides, the rate of pathogen killing is dependent on the magnitude of the drug exposure and hence AUC and/or C_{max} are observed to best correlate with antibacterial activity for these drugs (Andes and Craig 2002; Forrest, *et al.* 1993).

2.7.4 Drug binding to plasma proteins

Protein binding is the rapid and reversible reaction of a drug with plasma proteins such as human serum albumin and glycoprotein (Wise 1986). The extent of protein binding varies greatly between antimicrobials with gentamicin ~0% bound, while ceftriaxone is ~95% bound (Popick, *et al.* 1987; Rowland and Tozer 1995). With protein binding, the total drug concentration is typically divided into the free drug concentration and the protein-bound drug concentration. Typically, the total drug concentration is measured in pharmacokinetic studies with the free drug concentration calculated as the unbound fraction of the total concentration (Chisholm, *et al.* 2010b). Only the free drug molecules are considered to be microbiologically active (Van Bambeke, *et al.* 2006; Wise 1986). A comparison of drug penetration into human lymph nodes using 13 antibiotics with varying protein binding values (0% to 96%) by Bergan, *et al.* (1987) showed a clear

relationship between the level of protein binding and drug penetration indicating that only the free drug can penetrate tissues.

The free drug concentration can change over time due to factors such as disassociation from plasma proteins and drug elimination and this can alter the free drug fraction and PK parameters such as the drug half-life and volume of distribution. However, protein binding is not always clinically relevant as for drugs with a low hepatic extraction ratio (fraction of the drug removed from blood by the liver) it is considered that the drug concentration a patient is exposed to is independent of the amount of protein binding and therefore drug doses do not need adjustment to account for differing free fraction (Benet and Hoener 2002).

Protein binding can also slow the elimination of drugs that are primarily eliminated via glomerular filtration in the kidneys as only the free drug can be filtered by the pores in the glomerulus (Craig 2000). For such drugs, a high protein bound fraction may be desirable as it is associated with increased half-life and time the drug concentration remains above the MIC (Craig 2000). For example, ceftriaxone, which is ~95% protein bound and is primarily eliminated through glomerular filtration, has the longest half-life among cephalosporins (~7- 8h) (Craig 2000; Wise 1986) as high protein binding reduces renal clearance. Drugs eliminated through tubular secretion in the kidneys are unaffected by protein binding (Craig 2000).

2.7.5 Pharmacodynamics

Pharmacodynamics describes the relationship between the drug concentration at the target site and the drug's impact on bacterial growth or decline. When a drug interacts with a binding target a pharmacological effect is elicited which describes the drug exposure-efficacy relationship. A simple drug-target binding reaction assuming a single

binding site on target can be described as the interaction between the drug molecules (A) and drug targets (T), which form the drug-target complexes (AT) as:



Here, k_{on} is the rate constant for drug molecules binding to the targets and k_{off} is the rate constant of disassociation of the drug molecules from the targets.

Based on the drug-target interaction described in Eq. 2.1, the rate of change of drug-target complexes (AT) can be described as:

$$\frac{d AT}{dt} = k_{on}(T_0 - AT(t))A - k_{off} AT(t) \quad (2.2)$$

Here, T_0 is the initial number of targets. At equilibrium Eq. 2.2 simplifies to,

$$AT = \frac{T_0 A}{K_D + A} \quad (2.3)$$

where $K_D = \frac{k_{off}}{k_{on}}$ is the disassociation rate constant.

At equilibrium, if I then assume that the magnitude of the elicited dose-response effect ($E(A)$) is directly proportional to the concentration of the drug-target complex AT and that the free drug concentration remains constant (Clark 1926), the dose-response effect can be expressed as the following Hill function:

$$E(A) = \frac{E_{max} A}{K_D + A} \quad (2.4)$$

This form involving the maximum effect (E_{max}) is derived by noting that in the limit as A tends to infinity (all targets are occupied by drug), the expression $\frac{A}{K_D + A} = 1$. A

more general form of the Hill function can be expressed as, $E(A) = \frac{E_{max} A^\alpha}{EC_{50}^\alpha + A^\alpha}$. Here, EC_{50} is the antibiotic concentration at which the bacterial killing rate is at half of its maximum, α refers to the Hill coefficient which is a measure of the steepness of the sigmoidal function and other parameters are as described above.

The use of Hill function to explain empirical dose-response effects are described in several studies (reviewed by Goutelle, *et al.* (2008)). The data to inform these Hill function models can be obtained through *in vitro* time-kill experiments such as Foerster, *et al.* (2016) and Regoes, *et al.* (2004).

2.7.6 Mechanistic pharmacodynamic models and drug-target binding kinetics

As described in Eq.2.4, the Hill function is a simple representation used to describe the dose-response relationship, which I here refer to as a “traditional PD model”. In these traditional PD models, the underlying mechanisms of drug binding kinetics to their targets are not explicitly captured due to the use of simplifying assumptions such as those discussed in the above Section 2.7.5. Mechanistic models that capture the dynamics of drug-target interactions in more detail (Abel zur Wiesch, *et al.* 2015; Abel zur Wiesch, *et al.* 2017) can be used to relax these assumptions underlying traditional PD models. These approaches are described in detail by Clarelli, *et al.* (2020a).

Directly capturing drug-target interactions has been shown to be helpful in explaining the underlying mechanisms of various phenomena including post-antibiotic effects (PAE), where bacterial growth remains suppressed after the drug concentration falls below MIC. Abel zur Wiesch, *et al.* (2015) showed that in the treatment of *E.coli* with tetracycline, a delay in the disassociation of drug-target complexes along with slow drug diffusion across the cell membrane and the release of non-specifically bound drug (bound not specifically to the target) can explain the mechanisms underlying PAE effects.

These mechanistic models have further applications for drug optimisation (Clarelli, *et al.* 2020b), analysing the impact of initial bacterial load (inoculum effect) on antibacterial efficacy (Abel zur Wiesch, *et al.* 2015) and providing mechanistic explanations of the relationships between drug classes and relevant PK indices (Abel zur Wiesch, *et al.* 2017).

While capturing additional features of drug effects, these mechanistic models are more complex and require additional data (e.g., rate constants of drug-target binding and disassociation and threshold levels for bacteriostatic and bactericidal effects) to guarantee parameter identifiability (Alahmadi, *et al.* 2020; De Angelis, *et al.* 2015).

2.7.7 Drug interactions in combination therapy

Combination therapy involves interactions of two or more drugs, with the potential for synergistic, antagonistic or additive effects to occur. When the effect of a combination of drugs exhibits theoretically expected effects (not more or less effective than expected), this is defined as an additive effect (Berenbaum 1977; Greco, *et al.* 1995). When the combined effect is greater than what is predicted through an additive model, the effect is described as synergistic and conversely, a combined effect below that of the additive model is described as antagonistic (Berenbaum 1977). These drug interactions are typically described in the scientific literature using the concepts of Loewe additivity (Loewe 1928) or Bliss independence (Bliss 1939), which define reference models for determining synergistic or antagonistic effects.

Loewe additivity assumes that the interacting drugs have the same mechanisms of action and/or targets and act as if they are different dilutions of the same compound (Greco, *et al.* 1990; Tallarida 2006). The action of these drugs in combination is then assumed to be that of a single drug with relevant adjustments of PD parameters in the Hill function (mathematical details provided in Appendix C, Section C.1.1).

Bliss independence (Bliss 1939) is used when the interacting drugs have different mechanisms of action and/or targets and is a generalisation of the concept of probabilistic independence. For example, considering a two-drug combination, if f_α is the fraction of bacteria killed by drug α within a unit time step and if f_β is the fraction of bacteria killed by drug β within that time period, then the fraction of bacteria that survive their independent action over a unit time step is given by $(1 - f_\alpha)(1 - f_\beta)$. Converting to rate constants of killing I can define $E_\alpha = -\log(1 - f_\alpha)$ and $E_\beta = -\log(1 - f_\beta)$ with the associated net killing rate $= -\log((1 - f_\alpha)(1 - f_\beta)) = E_\alpha + E_\beta$. While this example describes additive effects of the two drugs, Bliss independence is defined more generally with an interaction term that accounts for synergistic or antagonistic effects:

$$E_{Bliss} = E_\alpha + E_\beta + \gamma E_\alpha E_\beta \quad (2.5)$$

Here, E_{Bliss} denotes the rate constant of bacterial killing by the combination of the two drugs, while E_α and E_β denote the rate constants of bacterial killing from the individual drugs α and β , respectively, which can be calculated according to the Hill function given by Eq. 2.4. The interaction parameter (γ) distinguishes between synergy and antagonism (Ankomah and Levin 2012), whereby $\gamma = 0$ for additive effects, $\gamma < 0$ for antagonistic effects, and $\gamma > 0$ for synergistic effects.

In empirical studies, synergistic or antagonistic effects of drug combinations can be estimated using these reference models. For example, Lee, *et al.* (2007) use Loewe additivity to find synergistic drug combinations to improve the therapeutic effect on precancerous cells while Ankomah and Levin (2012) apply Bliss independence to determine concentration-dependent synergistic and antagonistic effects in several drug combinations against *M. marinum*. The use of these two reference models can lead to conflicting results when both models are applied to the same data, as Bliss independence

will typically produce a larger effect of the two drugs in the absence of interactions. As such, an antagonistic effect under assumed Bliss independence can appear as synergistic under the assumption of Loewe additivity (Baeder, *et al.* 2016; Rao, *et al.* 2018).

Multidrug treatment regimens are used with the objective of increasing treatment efficacy and decreasing the probability of the emergence of drug resistance (Michel, *et al.* 2008). Although synergistic reactions are preferred with the objective of enhancing treatment efficacy because they increase the killing potency, in terms of minimising the risk of drug resistance synergistic combinations are not always ideal. Using drug pairs with different characteristics such as different frequencies of resistance to single drugs against *S. aureus*, Michel, *et al.* (2008) found synergistic drug pairs to favour the evolution of drug resistance. Torella, *et al.* (2010) further found that synergistic drug combinations can increase the risk of developing drug resistance in settings with strong competition for resources within-host. Antagonistic drug combinations can reduce the probability of emergence of drug resistance (Michel, *et al.* 2008).

Understanding synergistic or antagonistic reactions help to identify the cellular functions the drugs attack. Using two classes of drugs that inhibits DNA replication (ciprofloxacin) and that inhibits protein synthesis (tetracycline), the drug combination effects on *E. coli* was analysed by Bollenbach, *et al.* (2009). Due to suppressive drug interactions, they found this particular combination to in fact support improved bacterial survival and growth. Therefore, better understanding of drug interactions can provide insights on new ways to reduce bacterial growth and the emergence of drug resistance.

2.7.8 Effects of antibiotics on intracellular bacteria

As well as being protected from the immune system, intracellular bacteria are also afforded some protection from antibiotics, which must first penetrate the cell membrane

of host cells harbouring the bacteria (Kamaruzzaman, *et al.* 2017). Antibiotics can be effective against both extracellular and intracellular bacterial infections (Barcia-Macay, *et al.* 2006; Carryn, *et al.* 2002), but the levels of antibiotic penetration, accumulation and effectiveness differ between host cell types and drugs (Barcia-Macay, *et al.* 2006; Buyck, *et al.* 2013; Phanucharas and Gorby 1997; Prokesch and Hand 1982; Veale, *et al.* 1976).

Intracellular drug penetration, accumulation and effectiveness vary for different drug classes. Macrolides due to their weak basic character, accumulate well inside cells (Bosnar, *et al.* 2005; Kobuchi, *et al.* 2020). Although aminoglycosides are generally considered to be effective only in the extracellular environment (Shaw and Falkow 1988), they can enter cells through endocytosis (Van Bambeke, *et al.* 2006) and show slow accumulation within cells (Tulkens and Trouet 1974; Tulkens and Trouet 1978). While β -lactam antibiotics can penetrate host cells, they do not accumulate well within cells possibly due to their acidic nature (Renard, *et al.* 1987; Van Bambeke, *et al.* 2006). However, β -lactams can show intracellular efficacy if intracellular concentrations exceed the MIC sufficiently. For instance, in an *in vitro* time-kill experiment Barcia-Macay, *et al.* (2006) observed intracellular bactericidal effects using oxacillin (a β -lactam).

I am not aware of any specific experimental studies of intracellular PK/PD effects in the context of NG. However, this has been studied for other infections such as *S. aureus* (Barcia-Macay, *et al.* 2006; Evans, *et al.* 2020; Peyrusson, *et al.* 2018) and *L. monocytogenes* (Grayo, *et al.* 2008; Imbuluzqueta, *et al.* 2012) and intracellular activity has been observed to vary between drugs and across pathogens. For example, in an *in vitro* time-kill experiment, Barcia-Macay, *et al.* (2006) compared antibiotic effectiveness for several drug classes against *S. aureus* in the extracellular and intracellular (within human THP-1 macrophages) environments. In this study, at relatively low drug concentrations of $1 \times \text{MIC}$ and $10 \times \text{MIC}$, all drugs showed bactericidal effects in the

extracellular environment but none in the intracellular environment, where a 2-log decrease in bacterial load from baseline was used as the criteria for bactericidal effects. At a concentration equivalent to the peak drug concentration achieved within humans, some drugs including the β -lactam, oxacillin (at a concentration of $60 \times \text{MIC}$) showed intracellular bactericidal effects while other drugs did not. Despite evidence of intracellular bactericidal effects, such effects in the extracellular environment were observed more quickly (6h vs 24h), with the net killing effect using oxacillin after 24h being 5 and 2-log declines in bacterial load from baseline in the extracellular and intracellular environments, respectively.

2.8 Mathematical models for between-host and within-host infectious disease dynamics

One of the earliest historical uses of mathematical modelling to describe infectious diseases was the work by Daniel Bernoulli in 1760, where he illustrated the importance of inoculation with live smallpox virus to reduce the mortality from infection (Bernoulli and Blower 2004). Later, in 1927, Kermack and McKendrick introduced the Susceptible (S)-Infected (I)-Recovered (R) model which described the progression of infection through a population from which individuals recovered to gain complete immunity (Kermack, *et al.* 1927). This was the foundation of epidemic models and different variations and complexities were later incorporated into this such as age structures, spatial aspects and risk groups (Keeling and Danon 2009).

Analysis of similar models in the context of malaria later led to the important concept of the basic reproduction number (R_0) (Macdonald 1952), which is defined as the average number of secondary infectious persons resulting from one infectious person following their introduction into a totally susceptible population (Diekmann, *et al.* 1990). Applications of R_0 , include its use as a threshold parameter for determining whether an

infection can become established in a given population or setting requirements for intervention strategies that could lead to local elimination of infection (Austin, *et al.* 1999; McLean 1992).

Models with a similar structure can also be applied to describe within-host infection dynamics. The most notable historical use of within-host models (Nowak and May 2000) was to describe the dynamics of HIV infection under treatment (Ho, *et al.* 1995). In this study, using data on an antiretroviral treatment that inhibits viral replication, the half-life of infected cells, which was initially considered to be a slow-paced process (Nowak, *et al.* 1990), was estimated to be around 2-3 days indicating a rapid turnover of infected cells. This work illustrates the value of mathematical models in establishing evidence for dynamic behaviour that can be difficult to observe directly through experiments.

The basic viral dynamic model describes the host-pathogen interaction through uninfected cells (x), free virus (v) and infected cells (y) as:

$$\begin{aligned}\frac{dx}{dt} &= \lambda - dx - \beta xv \\ \frac{dy}{dt} &= \beta xv - ay \\ \frac{dv}{dt} &= ky - uv\end{aligned}\tag{2.6}$$

Here, uninfected cells and free virus particles interact at a rate β to produce infected cells. From the infected cells, free virions are produced at rate k and the death rates of the x , y , and v populations are d , a and u , respectively.

This viral dynamic model has formed the basis for more detailed and complex models of HIV that are now used to capture many features of infection such as HIV

persistence and drug resistance (Hill 2018; Perelson and Ribeiro 2013). Although within-host models were initially used primarily to describe HIV infection, their use has now become more widespread extending to other viral infections such as influenza (e.g., Koelle, *et al.* 2019), hepatitis B (e.g., Nowak, *et al.* 1996) and vector-borne diseases such as dengue (e.g., Clapham, *et al.* 2016), and bacterial infections such as chlamydia (e.g., Wilson 2004). Further extensions have enabled many other phenomena to be captured such as antigenic variation, differences in immune response and strain diversity (Nowak and Bangham 1996; Nowak and May 2000) and different bacterial states including intracellular populations (e.g., Ankomah and Levin 2014; Brown, *et al.* 2006; Helaine, *et al.* 2010; Wilson 2004).

2.8.1 Applications of mathematical models in the context of gonorrhoea

Several population-level mathematical models have been developed to describe the dynamics of gonorrhoea transmission and the emergence of resistance. Hethcote and Yorke laid the foundation for these epidemiological models in showing the importance of core groups (a group with a high turnover of sexual partners) in describing gonorrhoea epidemiology (Hethcote and Yorke 1984). Since then a variety of population-level mathematical models have been applied to questions including identifying target groups for effective infection control (Chan, *et al.* 2012) and factors contributing to disease prevalence in high burden communities (Ghani and Aral 2005; Hui, *et al.* 2015; Hui, *et al.* 2013). Furthermore, applications in the context of gonorrhoea include analysis of the association between treatment rates and resistance dissemination (Fingerhuth, *et al.* 2016; Xiridou, *et al.* 2015), the fitness cost of resistance and the possibility of re-using old antibiotics (Whittles, *et al.* 2017) and effects of a potential vaccine (Craig, *et al.* 2015; Whittles, *et al.* 2020).

Within-host dynamics and population-level dynamics are usually studied separately. However, these processes are not independent as for example, transmission rates between hosts can be dependent on within-host pathogen loads (Grassly and Fraser 2008; Nguyet, *et al.* 2013). These links suggest it is of interest to explore this interdependency between epidemiological determinants (e.g., between-host infection transmission rate, disease-induced death rate, recovery rate) and within-host dynamics such as the pathogen load, pathogen evolution and characteristics of the immune response (Gog, *et al.* 2015; Mideo, *et al.* 2008).

Although models that integrate between-host and within-host scales have been developed for other infections such as HIV (Jie, *et al.* 2015; Martcheva and Li 2013), a very limited attention has been paid in the context of NG infection mainly due to the lack of previous within-host modelling work on NG infection. Craig, *et al.* (2015) is the only study to my knowledge that attempts to bridge these two scales, with an in-host parametric model of bacterial load used to determine the infectiousness of individuals in a population-level model. However, this study does not consider within-host cellular dynamics and instead uses a simple parametric function to capture the initial exponential growth, peak load, and exponential decline in NG load.

To the best of my knowledge, Mao and Lu (2016) and Fingerhuth (2017) are the only modelling studies that explicitly capture NG interactions within the host. By considering the interaction of NG with a genomic pool, Mao and Lu (2016) quantified the characteristics of horizontal gene transfer by natural transformation. Fingerhuth (2017) explored the probability of treatment failure using a compartment model that considers sensitive and resistant NG strains. However, neither Mao and Lu (2016) nor Fingerhuth (2017) explicitly captures the intracellular interactions of NG with host cells

and the immune response which, as discussed in Sections 2.3 and 2.4, are observed to be key features in defining NG infection dynamics.

In the next chapter, using the evidence described here on NG infection, I develop a within-host mathematical model to describe untreated urethral NG infection in men.

Chapter 3

Modelling the in-host dynamics of *Neisseria gonorrhoeae* infection

This chapter was written based on a peer-reviewed article Jayasundara, *et al.* (2019). I conceived the study design in collaboration with my supervisors and Prof. Kate Seib from Griffith University. I was also responsible for model development and conducted the relevant analysis and simulation work and I drafted and revised the manuscript. The work was published in the Journal of Pathogens and Disease. The Chapter contains all the content in the published version without any textual changes but the formatting (numbering of sections, tables, figures and appendix section numbering) was changed to be consistent with the thesis structure.

3.1 Introduction

Gonorrhoea is a sexually transmitted infection caused by the bacterial species *Neisseria gonorrhoeae* (NG). The incidence of gonorrhoea is increasing worldwide (Centers for Disease Control and Prevention 2017; The Kirby Institute 2018), and the World Health Organization estimated that in 2012, 78 million cases of infection occurred worldwide (Newman, *et al.* 2015). The male urethra and the lower female genital tract are the predominant sites of infection with NG (Edwards 2008; Miller 2006), which can result in serious sequelae including neonatal blindness, epididymitis, pelvic inflammatory disease, infertility and ectopic pregnancy (Holmes, *et al.* 2008; Stevens and Criss 2018; Unemo and Shafer 2014). Infection also commonly occurs at the pharynx and rectum through a diverse range of sexual practises (Fairley, *et al.* 2017). With the emergence of

multi-drug resistant NG strains being reported in several countries, including strains that exhibit high-level resistance to all extended-spectrum cephalosporins, our last remaining proven options for gonorrhoea monotherapy, there is increasing concern that NG may become untreatable in the near future (Eyre, *et al.* 2018; Golparian, *et al.* 2018; Poncin, *et al.* 2018; Regan, *et al.* 2018; Whiley, *et al.* 2018).

NG is highly adapted to establish infection and survive within the human host. In order to establish infection, NG must attach to mucosal epithelial cells. This process is facilitated by surface components, including pili and opacity associated proteins (Opa). Once attached, NG can be internalized within epithelial cells (Apicella, *et al.* 1996) where they can replicate (Criss and Seifert 2006; Shaw and Falkow 1988), evade the immune system, delay apoptosis of epithelial cells and infect cells deeper within the epithelium (Binnicker, *et al.* 2003; McGee, *et al.* 1983; Mosleh, *et al.* 1997). The innate immune system is triggered in response to NG infection by the elevation of pro-inflammatory cytokines and chemokines, which lead to the recruitment of polymorphonuclear leukocytes (PMN, or simply neutrophils) to the infection site. Despite rapid recruitment of PMN, NG are able to resist killing by PMN (Criss and Seifert 2012; Simons, *et al.* 2005; Simons, *et al.* 2006) to the extent that viable NG are commonly found within PMN in exudates examined from natural human infections (Casey, *et al.* 1980; Veale, *et al.* 1979). Furthermore, NG has evolved to avoid and suppress the adaptive immune response (Edwards, *et al.* 2016; Liu, *et al.* 2014; Liu and Russell 2011). Although IgG, IgM and IgA antibodies have been found in human mucosa in response to NG infection (Ison, *et al.* 1986), these antibody response levels are relatively weak and short lived (Holmes, *et al.* 2008). As such, the adaptive immune response against infection with NG is considered to be, at best, only weakly effective and reinfection is common (Schmidt, *et al.* 2001; Stupiansky, *et al.* 2011).

Experimental NG infection models in humans have been limited to males, as infection in females can result in serious reproductive complications including pelvic inflammatory disease and infertility. Even in the case of experiments conducted in men, prolonged infection without provision of treatment is considered unethical and therefore treatment is provided when symptoms appear, typically 5-7 days post infection (Hobbs, *et al.* 2011; Schmidt, *et al.* 2001; Schneider, *et al.* 1995). These limitations have hampered our ability to study the natural course of infection *in vivo* and our current understanding is largely derived from *in vitro* studies and animal models of infection.

In particular, mouse models have been used to understand within-host dynamics to a certain extent (Francis, *et al.* 2018; Jerse 1999; Li, *et al.* 2011; Packiam, *et al.* 2010). These are typically models of vaginal infection in female mice, which require hormonal treatment with 17β -estradiol to allow prolonged infection (Jerse, *et al.* 2011; Rice, *et al.* 2017), and most closely resemble human asymptomatic vaginal infection (Francis, *et al.* 2018). However, there are limitations to the mouse model, due to the specificity of several gonococcal proteins for human specific targets, including receptors required for adherence and invasion of epithelial cells, as well as iron sources required by NG for survival (Jerse, *et al.* 2011; Rice, *et al.* 2017).

Although mathematical models have been developed to describe transmission of NG infection at a population level (for example, Chan, *et al.* 2012; Fingerhuth, *et al.* 2016; Hui, *et al.* 2015; Hui, *et al.* 2013), there has been very little focus on developing models capturing the course of NG infection at a within- host level. Such within-host models have been developed for other pathogens, describing the interaction between pathogen, host cells, and host immune response (for example, Colijn and Cohen 2015; Nowak and Bangham 1996; Smith, *et al.* 2011; Wilson, *et al.* 2003). However, the infection processes, immune responses and mechanisms describing the acquisition of

resistance related to infection described by these models differ from those that are essential for NG infection. To the best of our knowledge, the only published within-host model of NG infection is Mao and Lu (2016). In that study, horizontal gene transfer by natural transformation is modelled by considering the interaction of NG with a genomic pool without specific consideration of interaction with host cells. Although not specifically a within-host model, the theoretical NG vaccine study by Craig, *et al.* (2015) described infectiousness of individuals using a parametric function for the within-host NG load.

An improved understanding of the within-host dynamics of NG infection offers the potential to gain insights about the immune response, development of antibiotic resistance and potential mechanisms for vaccine action. However, the existing *in-vivo* or *in-vitro* studies are unable to fully capture the long-term infection dynamics of NG infection. To address this, we have developed a model that captures the natural course of untreated symptomatic urethral NG infection in men, which will assist in understanding the within-host factors that govern the ability of NG infection to persist and the ability of the immune system to clear infection. In concert with multivariate sensitivity analysis we have also sought to constrain plausible ranges for relevant biological parameters. In addition, due to the absence of time-course data on untreated human NG infection, we attempted to validate the modelling approach by fitting the model to time course data from a mouse model of NG infection described by Jerse (1999).

3.2 Materials and Methods

3.2.1 Model structure and formulation to describe human urethral NG infection

A compartmental mathematical model was developed to capture the time course of urethral NG infection in men by considering the interaction between bacteria (NG),

epithelial cells, and the PMN subset of the innate immune response. The model has five compartments. Four of the compartments describe interactions between NG and the host: NG unattached (B) or attached (B_a) to epithelial cells, NG internalized within epithelial cells (B_i) and NG surviving within PMN (B_s). The fifth compartment represents the activated PMN cells (N). Transitions between the five compartments are illustrated schematically in Fig. 3.1. An overview of the modelling approach follows with a complete and detailed description provided in Appendix A.

The model is formulated as a system of ordinary differential equations as follows:

$$\frac{dB}{dt} = \left(1 - \frac{B + B_a}{k_1}\right) (r_1 B + d_3 B_s + e B_i) - d \frac{B N}{c N + B} - d_2 B - a_1 B \left(1 - \frac{B_a}{k_1 a_2}\right)$$

$$\frac{dB_a}{dt} = r_1 B_a \left(1 - \frac{B + B_a}{k_1}\right) + a_1 B \left(1 - \frac{B_a}{k_1 a_2}\right) - d \frac{B_a N}{c N + B_a} - \eta B_a$$

$$\frac{dB_i}{dt} = \left(1 - \frac{B_i}{k_1 a_2}\right) (\eta B_a + r_2 B_i) - e B_i$$

$$\frac{dB_s}{dt} = \left(1 - \frac{B_s}{N k_2}\right) \left(p d \frac{B N}{c N + B} + p d \frac{B_a N}{c N + B_a} + r_3 B_s\right) - d_3 B_s$$

$$\frac{dN}{dt} = \mu (N_{max} - N) (B + B_a) - d_3 N$$

The model initial conditions are given in Table 3.1 and the model parameters, including transition rates are provided in Table 3.2. Key study sources that inform their assigned values are described in more detail in Table 3.3.

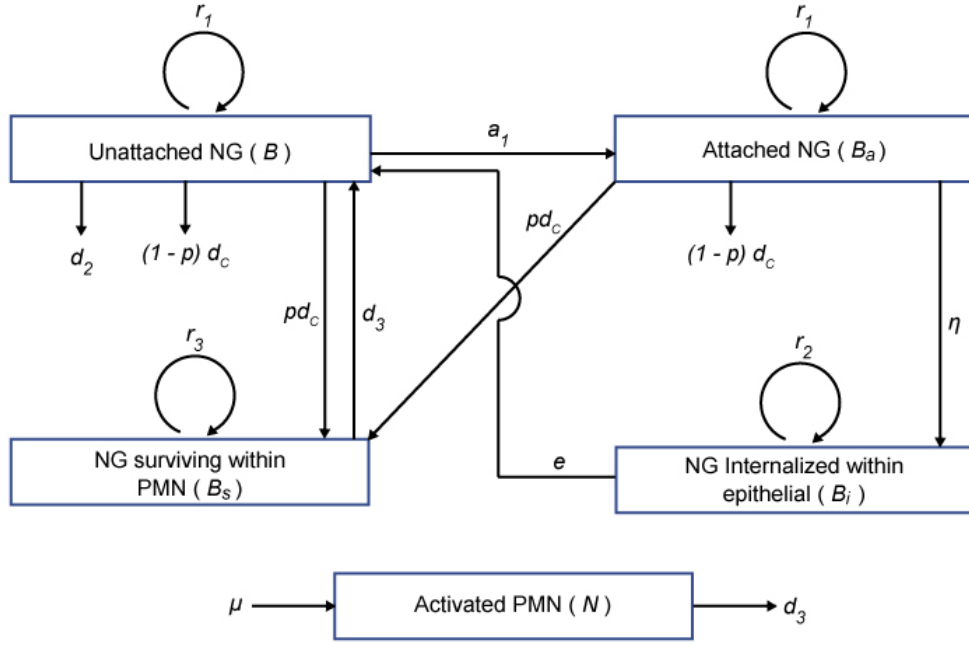


Figure 3.1: Schematic illustration of the within-host model of NG infection. The arrows indicate transitions between model states: unattached NG (B), attached NG (B_a), bacteria internalized within epithelial cells (B_i), NG surviving within PMN (B_s) and activated PMN (N). Model parameters and their assigned values are given in Table 3.2 (d_c refers to the engulfment rate of NG by PMN subject to the ratio dependent constant. When N is relatively low, $d_c \rightarrow d$ while when N is relatively high $d_c \rightarrow \frac{d}{c}$).

Table 3.1: Human infection model initial conditions

Symbol	Parameter	Value	Reference/ Comments
Initial Conditions			
B	Unattached bacteria population	1000 <i>bacteria</i>	(Schmidt, <i>et al.</i> 2001; Schneider, <i>et al.</i> 1996)
B_a	Attached bacteria	0 <i>bacteria</i>	Assumption
B_s	Bacteria surviving within PMN	0 <i>bacteria</i>	(Criss and Seifert 2012; Ramsey, <i>et al.</i> 1995)
B_i	Bacteria internalised within epithelial	0 <i>bacteria</i>	(Shaw and Falkow 1988)
N	Activated PMN	10^{-8} <i>cells</i>	(Criss and Seifert 2012; Ramsey, <i>et al.</i> 1995)

Table 3.2: Model parameter values and the parameter ranges based on the sensitivity analysis.

Parameters		Point estimate	Parameter range used to generate LHS samples	Reference / Comments	95 % credible interval after outcome filtering
r_1	Replication rate of non-internalized bacteria	0.489 $hour^{-1}$	0.374 – 0.53	Point estimate was obtained by fitting the model to total NG load data generated based on qualitative features of the time course of infection. Range based on estimates by Craig, <i>et al.</i> (2015), using the individual variation in human experimental studies Schmidt, <i>et al.</i> (2001) and Schneider, <i>et al.</i> (1996). The study-derived range 0.13 - 0.53 $hour^{-1}$ was refined after initial LHS to this range as values outside of this were inconsistent with the outcome ranges.	0.386 – 0.527
r_2	Replication rate of internalized NG	0.533 $hour^{-1}$	0.27 – 1.06	Four-fold range around point estimate from Shaw and Falkow (1988).	0.289 – 1.014
r_3	Replication rate of NG surviving within PMN	0.340 $hour^{-1}$	0.31 – 0.41	Based on the variation of measured values in Simons, <i>et al.</i> (2005).	0.312 – 0.408

a_1	NG attachment rate to epithelial cells	0.340 $hour^{-1}$	0.3 – 0.43	Based on fitting to data regarding pilated and non-piliated NG strains in Gubish, <i>et al.</i> (1979)	0.303 – 0.427
a_2	Maximal NG attachment capacity per epithelial cell	12	6 – 12	Based on fitting to data regarding pilated and non-piliated NG strains in Gubish, <i>et al.</i> (1979)	6 – 12
d	NG engulfment rate by PMN	2.586 $bacteria$ $hour^{-1} cell^{-1}$	$d \sim b \times c + a$	Point estimate was obtained by fitting the model to total NG load data generated based on qualitative features of the time course of infection. Initial LHS analysis showed that in samples that met outcome criteria d and c were strongly correlated, satisfying a regression line of the form $d \sim b \times c + a$. For revised LHS samples, using this relationship we generated d from c , with $b \in (0.207, 0.497)$ and $a \in (0.816, 1.95)$.	1.174 – 3.85
d_2	Wash out rate of unattached bacteria	10^{-3} $hour^{-1}$	$5 \times 10^{-4} - 2 \times 10^{-3}$	Assumption, with four-fold range around the point estimate.	$5.4 \times 10^{-4} - 0.002$
d_3	Death rate of activated PMN	1/24 $hour^{-1}$	0.02 – 0.045	Point estimate derived from Simons, <i>et al.</i> (2005). Four-fold range around the point estimate reduced through initial LHS comparison to outcome ranges.	0.02 – 0.043
e	Exit rate of internalized NG	0.650 $hour^{-1}$	0.55 – 1.3	Assumption, with four-fold range around the point estimate reduced through initial LHS comparison to outcome ranges.	0.587 – 1.287

μ	PMN activation rate	5.72×10^{-13} <i>hour⁻¹</i> <i>bacteria⁻¹</i>	$2.82 \times 10^{-13} - 8.76 \times 10^{-13}$	Point estimate was obtained by fitting the model to total NG load data generated based on qualitative features of the time course of infection. For LHS, four-fold range around the point estimate reduced through initial LHS comparison to outcome ranges.	$2.962 \times 10^{-13} - 8.530 \times 10^{-13}$
c	Ratio dependent constant	3.135 <i>bacteria</i> <i>cell⁻¹</i>	$10^{-3} - 6.27$	Point estimate was obtained by fitting the model to total NG load data generated based on qualitative features of the time course of infection. Lower limit set to include range from <i>in vitro</i> estimates derived from Rest, et al. (1982) and upper limit $2 \times$ point estimate.	0.487 – 6.092
η	Rate of internalization into epithelial cells	0.28 <i>hour⁻¹</i>	0.14 – 0.37	Point estimate derived from Shaw and Falkow (1988), with four-fold range. For LHS, four-fold range around the point estimate reduced through initial LHS comparison to outcome ranges.	0.143 – 0.367
p	Proportion of NG surviving within PMN	0.25	0.01 – 0.5	Point estimate was obtained by fitting the model to total NG load data generated based on qualitative features of the time course of infection. Lower limit set to include range from <i>in vitro</i> estimates derived from Rest, et al. (1982) and upper limit $2 \times$ point estimate.	0.022 – 0.488
k_1	Urethral carrying capacity	10^7 <i>bacteria</i>	Kept fixed during the sensitivity analysis	explained in text.	Kept fixed during the sensitivity analysis

k_2	Survival capacity of NG per PMN	8 <i>bacteria cell</i> ⁻¹	4 – 16	Point estimate derived from Simons, <i>et al.</i> (2005), with four-fold range.	5 - 16
N_{max}	Total number of PMN in the body	2.50×10^{10} <i>cell</i>	Kept fixed during the sensitivity analysis	explained in text.	Kept fixed during the sensitivity analysis

Table 3.3: Main data sources used for parameter estimation.

Study	Related parameters	Study description
Gubish, <i>et al.</i> (1979)	Bacterial attachment rate (a_1) and maximal NG attachment capacity of an epithelial cell (a_2).	NG attachment to HeLa cells was measured over a period of 4 hours using two types of NG; piliated and non-piliated (<i>in vitro</i> study).
Shaw and Falkow (1988)	Rate of internalization of NG into epithelial cells (η) and the replication rate of internalized NG (r_2).	Number of NG that survived gentamicin exposure and invaded epithelial cells over the period of 12 hours (<i>in vitro</i> study).
Rest, <i>et al.</i> (1982)	Bacterial engulfment rate (d), the proportion of NG surviving within PMN (p) and the ratio dependent constant (c).	PMN phagocytosis of non-piliated NG in the absence of serum, measured over a period of 135 minutes (<i>in vitro</i> study).
Simons, <i>et al.</i> (2005)	Intracellular growth of NG within PMN (r_3).	Number of viable intracellular NG within PMN measured over 6 hours (<i>in vitro</i> study).
Jerse (1999)	NG load time-series in 8 mice that was used to as a validation exercise for the human infection model.	NG load recovered in vaginal swabs of 8 mice over the time course of 14 days is reported. However, as mentioned in section ‘Fitting to mouse model data’, only the first 9 days of bacterial data were used for fitting.

3.2.1.1 Bacteria

Growth of the NG population occurs through bacterial replication (Apicella, *et al.* 1996; Criss and Seifert 2006; Shaw and Falkow 1988; Simons, *et al.* 2005) at the rates r_1 for both unattached NG (B) and NG attached to epithelial cells (B_a), r_2 for NG internalized in epithelial cells (B_i) and r_3 for NG surviving in PMN (B_s). NG growth in unattached and attached NG states was bounded by a maximal urethral infection capacity (k_1) (based on the approximate surface area of the urethra and the cross-sectional area of NG). In addition, as several NG can attach to the surface of a single epithelial cell (Gubish, *et al.* 1979; Heckels, *et al.* 1976), the rate of attachment to epithelial cells was limited by the maximal attachment capacity ($k_1 a_2$), where a_2 was the maximal NG attachment capacity per epithelial cell. NG surviving within PMN can delay PMN apoptosis to provide NG with time for replication within PMN (Simons, *et al.* 2006). In the study by Simons, *et al.* (2005) it was observed that PMN with delayed apoptosis had less than 10 associated NG per PMN and based on this we limited the maximum number of NG that can survive within PMN to delay apoptosis (k_2).

Engulfment of non-internalised NG (unattached NG and NG attached to epithelial cells) by PMN (at rate d) was modelled in a manner corresponding to a ratio-dependent predator-prey interaction (Arditi and Ginzburg 1989; Getz 1984). When the number of NG is small relative to the number of PMN, the engulfment rate per NG approaches a maximum constant level $\frac{d}{c}$, while when the NG population is large, the engulfment rate of bacteria is directly proportional to the number of PMN. The ratio dependent constant c reflects the reduction in NG engulfment by PMN as the NG population decreases (Getz 1984; Getz 1998). NG in the internalised (B_i) state were considered to be inaccessible to killing by PMN.

Unattached NG were assumed to be washed away (e.g., by passive efflux from the urethra and through urination) at the rate d_2 (Burgess 1971; Pelouze 1939; Schneider, *et al.* 1995). NG in the internalized state (B_i) exit from epithelial cells at rate e (Criss and Seifert 2006; Mosleh, *et al.* 1997) and are then available again to further infect epithelial cells. NG that survive within PMN (B_s) were assumed to exit that state at the same rate as for PMN death (d_3). However, the number of NG that can exit from the B_i and B_s states and move onto the unattached state is constrained through the urethral carrying capacity term (k_1). NG that could not move into the unattached state due to this capacity restriction were assumed to be washed away.

When referring to the NG load we use the term “bacteria” throughout, which refers to modelled numbers of bacteria and also to empirical data reported as number of colony-forming units (CFU).

3.2.1.2 Immune response: PMN

The total number of PMN (N_{max}) was assumed to remain constant over time, with the immune response assumed to be triggered by their activation. Inactivated PMN were assumed to be activated at a rate μ multiplied by the number of non-internalized NG. During infection, engulfed NG have been observed to prolong the lifespan of PMN and, based on Simons, *et al.* (2006), it was assumed that PMN were apoptotic at 24 hours (d_3).

In studies of infection in humans, cytokines were observed to be elevated two hours following inoculation (Ramsey, *et al.* 1995; Ramsey, *et al.* 1994), and the PMN response was therefore assumed to be initiated early in the infection. However, it was not established whether this early cytokine response in experimental models was a result of the inoculation procedure itself or occurred in response to gonococcal infection (Ramsey, *et al.* 1995) as several studies had indicated a 2-3 day delay in PMN response (Cohen, *et*

al. 1994; Criss and Seifert 2012; Seifert, *et al.* 1994). We focus on the model without a PMN delay term in our main analysis but present results including a delay in Appendix A, Fig. A.8 in Section A.3.

3.2.2 Model parameters

Initial conditions for model states are listed in Table 3.1, while the parameters used in this study and their assigned values are listed in Table 3.2. Where possible, parameter values were based on estimates found in the published literature. Where parameter values could not be informed directly by the literature, they were estimated by fitting simplified versions of the model (sub-models) to relevant *in vitro* data (Further details provided in Appendix A, 2.1.2). These sub-models reflect the fact that the *in vitro* studies used for parameter estimation do not consider NG interactions with both epithelial cells and PMN simultaneously and hence, some model states and interaction terms were set to 0 as part of these parameter estimation exercises. There is a lack of published empirical data to inform the values for the two parameters, wash out rate of unattached NG (d_2) and exit rate of internalized NG (e). For d_2 , we assigned a value around the median of the retained samples in the multivariate sensitivity analysis (described below), and for e a value near the mode, to ensure point estimate values that are consistent with an infection duration of 75 days. Finally, the bacterial engulfment rate (d), proportion of NG surviving within PMN (p), ratio dependent constant (c), the replication rate of non-internalised NG (r_1) and the PMN activation rate (μ) were estimated by fitting the model to simulated data sets that were generated based on the known qualitative features of the infection. These qualitative features used to generate data are described below in the section ‘*Qualitative features of the time-course of infection*’.

3.2.2.1 Parameters derived from published literature

The replication rate of NG surviving within PMN (r_3) was based on the intracellular replication of NG within PMN that was measured in the *in vitro* study by Simons, *et al.* (2005) over a time period of 5 hours. The urethral carrying capacity (k_1) was estimated based on the approximate surface area of the urethra and the cross-sectional area of NG (NG has a diameter of 0.5 - 1 μm (Herz, *et al.* 1996; Westling-Haggstrom, *et al.* 1977); the length of the entire male urethra is around 20 cm (Moore 2006) with a diameter of 8-9 mm (Talati 1989)). The total number of PMN in the body (N_{max}) was based on estimates of the normal range of PMN in the body ($2.5\text{-}7.5 \times 10^9/L$) from the study by von Vietinghoff and Ley (2008), and an average blood volume in adults of approximately 5L (Wei, *et al.* 1995).

3.2.2.2 Parameter estimation through model fitting

In this section, we summarise parameter estimation via fitting of sub-models to data from *in vitro* studies using the MATLAB (MathWorks, Natick, MA) nonlinear least squares solver '*lsqcurvefit*'. Further details of the study data and sub-models are provided in Appendix A, Section A.1.2 and summarised in Fig. 3.2.

The *in vitro* data used to estimate these parameters are summarised in Table 3.3. A function of the form $a_2(1 - e^{-a_1 t})$ was fitted to data in Gubish, *et al.* (1979) to estimate the bacterial attachment rate (a_1) and maximal NG attachment capacity of an epithelial cell (a_2). In order to estimate the replication rate of internalized NG (r_2) and the rate of internalization (η), the sub-model described in Appendix A, Section A.1.2.2 was fitted to data from Shaw and Falkow (1988). Data in the *in vitro* study by Rest, *et al.* (1982) were used to obtain estimates of the bacteria engulfment rate (d), the proportion of NG surviving within PMN (p) and the ratio dependent constant (c) by fitting the sub-model described in Appendix A, A.1.2.3. Uncertainty intervals around both sets of *in*

vitro estimates were developed by varying the fixed parameters within specified ranges. In the case of r_2 and η , this involved varying the urethral carrying capacity (k_1) and maximal NG attachment capacity of an epithelial cell (a_2) (details in Appendix A, Section A.2.2.1). For d, c and p this involved varying r_1, r_3 and k_2 (described in Appendix A, Section A.2.2.2).

3.2.2.3 Model fitting to estimate bacterial engulfment rate (d), proportion of NG

surviving within PMN (p), ratio dependent constant (c), PMN activation rate (μ) and replication rate of non-internalized bacteria (r_1).

When the values for d, p and c obtained from least squares minimization by fitting sub-models to the data in the study by Rest, *et al.* (1982) were used as parameters in the full model, the duration of untreated infection obtained was well below the desired range (Fig. 3.5(b)). We investigated whether adjustment of epithelial internalisation parameters might resolve this issue but the results did not match other observations (see Appendix A, Section A.2.3). Additional sensitivity analyses around *in vitro* estimates are described in Section A.2.2.2 of Appendix A but did not support use of the *in vitro* estimates in the full model.

As we lacked other experimental evidence on which to base these parameters and to obtain a point estimate for the parameters μ and r_1 , we fitted the total NG load ($B + B_a + B_i + B_s$) obtained from our human infection model to 1000 simulated data sets, consisting of total bacterial load values at 5 time points. These were generated based on the qualitative features of the time-course of infection described in the next paragraph, while the data generation and fitting procedure is described in detail in Appendix A, Section A.1.2.4. The median of the 1000 estimates of each parameter was used as the respective point estimate of d, c, p, μ and r_1 .

3.2.2.4 Qualitative features of the time-course of infection

Human experimental studies suggested a peak NG load of 10^6 - 10^8 bacteria reached at around 2-5 days into infection (Ramsey, *et al.* 1995; Schmidt, *et al.* 2001; Schneider, *et al.* 1995; Schneider, *et al.* 1991; Schneider, *et al.* 1996). In these studies, it was observed that the bacterial load reached a plateau level of above 10^6 bacteria from around day 1-2 to the initiation of treatment usually at around days 5-7. Based on pre-antibiotic era empirical studies (Hill 1943; Pelouze 1939) and theoretical estimates (Johnson, *et al.* 2010; Korenromp, *et al.* 2002), the expected duration of untreated male symptomatic infection is considered to be in the range of 1-6 months. The infection is considered to be cleared once the NG load falls below 10 bacteria (Schneider, *et al.* 1995).

3.2.3 Initial conditions

The number of unattached NG at time 0 ($B(0) = 1000$) was taken from the study by Schmidt, *et al.* (2001) and Schneider, *et al.* (1996). We assumed that initially there were no attached NG ($B_a(0) = 0$) or internalised NG ($B_i(0) = 0$). The latter assumption is supported by Shaw and Falkow (1988), where internalized NG were not observed until > 6 hours after the start of the experiment. We also assumed no initial NG internalised in PMN ($B_s(0) = 0$), supported by the cytokine response being elevated at > 2 hours after inoculation (Criss and Seifert 2012; Ramsey, *et al.* 1995). The ratio-dependent term in our equations does not allow solution when the activated PMN value is exactly 0 and hence we assumed a small positive initial PMN value ($N(0) = 10^{-8}$ cells).

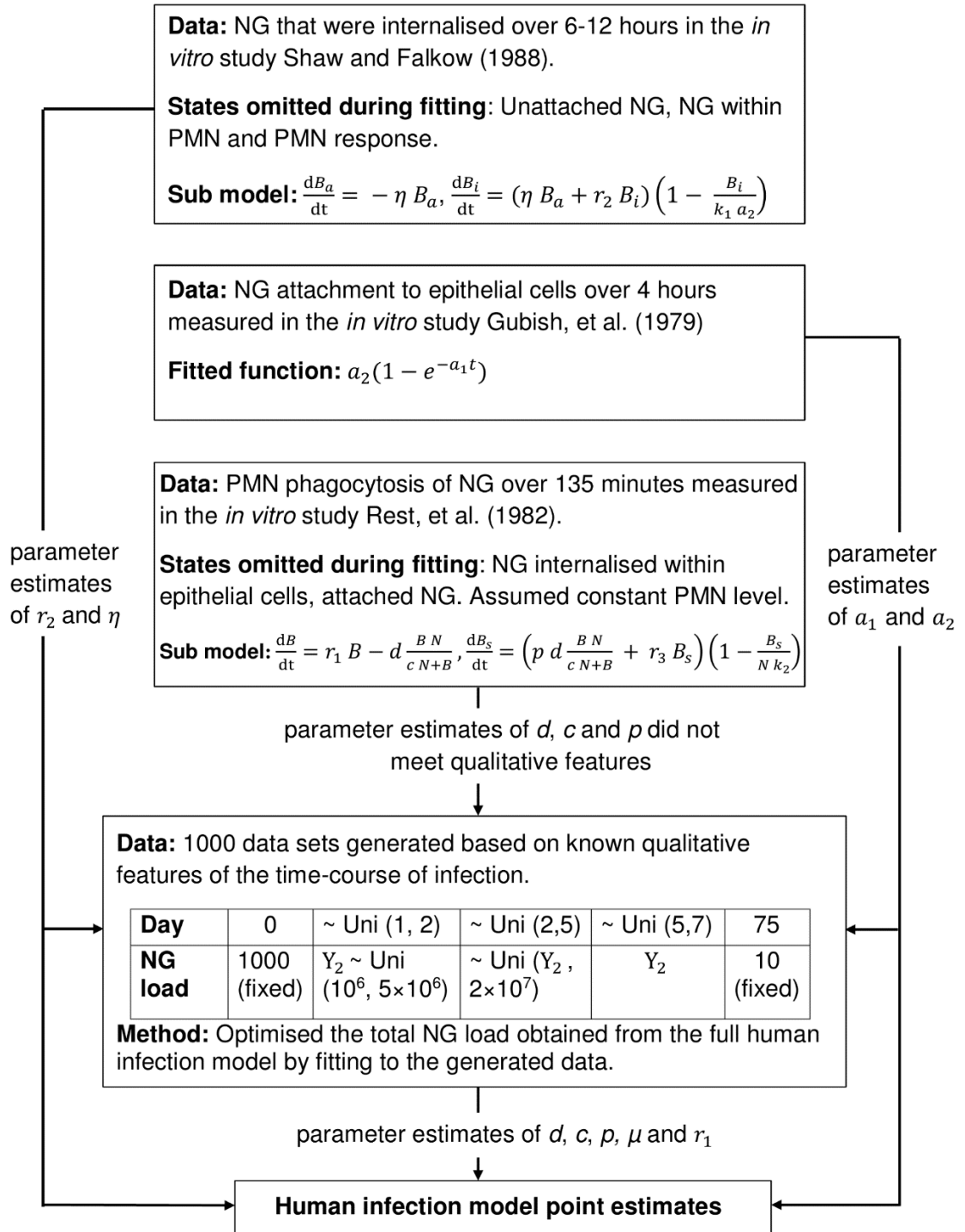


Figure 3.2: Flow diagram summarising the sub-models and data used to estimate the human infection model point-estimate parameters, and illustrating how the estimates feed into the final model.

3.2.4 Multivariate sensitivity analysis

We conducted a multivariate sensitivity analysis of the full human model in order to capture uncertainty around model outcomes and to refine plausible ranges for model parameters. All parameters were included except the urethral carrying capacity (k_1) and the total PMN count (N_{max}) as these parameters define more global constraints on model behaviour and interact strongly with the NG growth and survival parameters. For most parameters a factor of 2 above and below the point estimate (4-fold range) was used (shown in Table 3.2). Using Latin Hypercube Sampling (LHS) (Blower and Dowlatabadi 1994), 100,000 parameter samples were generated assuming uniform distributions for all parameters within the defined ranges. The software package SaSAT was used to generate the LHS samples and carry out the multivariate sensitivity analysis (Hoare, *et al.* 2008). When the model was run using these parameter sets, only those samples that met the desired broad criteria around the peak NG load, peak time and the infection duration (described below) were retained for the subsequent analysis. These retained parameter sets were then analysed for pairwise correlations, with correlations between the parameters d and c used to inform a revised LHS analysis. The parameter ranges associated with this revised analysis are reported in Table 3.2. More details on the multivariate sensitivity analysis are provided on Appendix A, Section A.2.1.

Outcome criteria: We retained only the parameter sets which were consistent with peak NG load of $10^6 - 10^8$ bacteria occurring 1-7 days after infection (Ramsey, *et al.* 1995; Schmidt, *et al.* 2001; Schneider, *et al.* 1995; Schneider, *et al.* 1991; Schneider, *et al.* 1996), with clearance of infection (<10 NG, as in Schneider, *et al.* (1995)) between 1 and 6 months (Based on pre-antibiotic era empirical studies (Hill 1943; Pelouze 1939) and theoretical estimates (Johnson, *et al.* 2010; Korenromp, *et al.* 2002)). We also

conducted a sub-analysis of the samples that met the above criteria and cleared infection in the more restricted window of 2-6 months.

3.2.5 Fitting to mouse model data

As an exercise in validation of the model structure and qualitative behaviour, and due to the unavailability of human data on prolonged untreated NG infection, we fitted our model to time course data from a mouse model of NG infection. The main purpose of this fitting exercise was to assess whether the model could describe the quantitative time course data in a related animal model. In addition, we were interested in what features of the human model were required to describe mouse infection and to obtain a comparison of parameters between the two hosts.

NG load data on eight mice were obtained from the study by Jerse (1999) where mice were treated with estradiol to facilitate prolonged infection. As the effects of estradiol declined after around 9 days, we included only the first 9 days of NG data for each mouse in this fitting exercise. The total NG load ($B + B_a + B_i + B_s$) was fitted to the data for the full model described above and then model fitting was repeated for 3 progressively simpler models where first the epithelial internalisation state (B_i) was removed, then both attachment (B_a) and epithelial internalisation states were removed, and finally a model where in addition neutrophil internalisation (B_s) was removed. The parameters that were estimated and kept fixed at each stage of the fitting are summarised in Table A.3 in Appendix A, Section A.5.3.

As there were only 9 NG data points per mouse, we had to limit the number of parameters estimated in the fitting process. We kept several parameters ($a_1, a_2, d_3, d_2, e, r_2$ and k_2) at the same values as assigned for the human model point estimates (Table 3.2) as discussed in Appendix A, Section A.5.3. The capacity related

parameters k_1 and N_{max} were adjusted to take into account the smaller relevant cell counts for mice. Hence, for mice, N_{max} was taken as 8.32×10^6 cells and the carrying capacity (k_1) was taken as 3×10^6 bacteria (details provided in Appendix A, Section A.5.1). This left us with the need to estimate the parameters d , c , μ , p , η , r_3 and r_1 through the fitting process. After experimenting with individual model fits (see Appendix A, Section A.5.2 for details), we were able to fix the values of p and η at 5.4×10^{-5} and $5 \times 10^{-6} \text{ hour}^{-1}$, respectively, across all mice. Finally, the five parameters that govern the growth (r_3 and r_1) and decline (d , c , μ) of the NG load were estimated per mouse using least squares optimisation (in the model where neutrophil internalisation was removed, r_3 is not relevant). For the optimisation procedure, the MATLAB (MathWorks, Natick, MA) function ‘*fmincon*’ was used with the potential for multiple local minima investigated through the use of the ‘*multistart*’ function by using 1000 different initial starting points for the parameter values for each mouse. Initial conditions for unattached bacteria and PMN were based on the first data point for each mouse.

3.3 Results

3.3.1 Parameter estimation for the human model

The parameter estimates obtained by fitting the sub-models to respective *in vitro* data are presented in this section and summarized in Table 3.2. The credible intervals around estimates of respective parameters derived from the *in vitro* sensitivity analyses described in Appendix A, Section A.2.2 are shown in the shaded region in Fig. 3.3(b) and 3.3(c). Fits to data on attachment of piliated and non-piliated NG to HeLa cells (Gubish, *et al.* 1979), are shown in Fig. 3.3(a) and were used to estimate the attachment rate (a_1) and the maximal NG attachment capacity of an epithelial cell (a_2). Estimates of the replication rate of internalized NG within epithelial cells (r_2) and rate of internalization (η) are shown in Fig. 3.3(b) (estimated values and credible intervals around *in vitro*

estimates are presented in Appendix A, Table A.1). Fig. 3.3(c) shows the best fit to *in vitro* data in the study by Rest, *et al.* (1982) compared to the curve based on estimates obtained by fitting to the simulated data based on the qualitative features of the untreated human infection. A comparison of estimates of d , p and c from the optimal fits to *in vitro* data as opposed to the simulated data informed by qualitative features, is provided in Appendix A, Table A.2 along with the 95% credible intervals around the *in vitro* estimates.

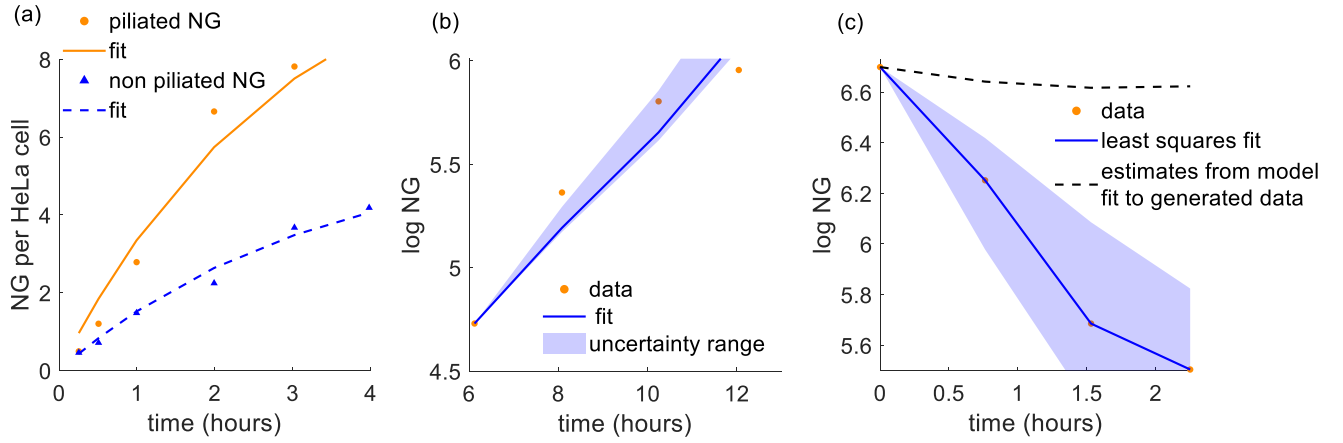


Figure 3.3: Model fit to *in vitro* studies to estimate parameters. (a) The *in vitro* data on NG attachment to HeLa cells by two types of NG (piliated and non-piliated) from the study by Gubish, et al. (1979) is shown with the fitted function described in Appendix A, Section A.1.2.1. (b) Data on NG internalization over the period of 6-12 hours as observed in the study by Shaw and Falkow (1988) is shown with the best fit curve obtained by fitting the sub-model on NG internalization to these data (sub-model explained in Appendix A, Section A.1.2.2). The optimal fit is shown by the solid line and the credible intervals obtained around the *in vitro* point estimates are shown by the shaded region. (c) NG killing by PMN as measured by the study by Rest, et al. (1982). The solid line represents the curve

obtained from least squares minimization by fitting to the sub model explained in Appendix A, Section A.1.2.3, while the dashed line is the equivalent curve for the base-case parameters, determined through fitting the full model to simulated data based on the qualitative features of the time course of infection. The credible intervals obtained around the *in vitro* point estimates are shown by the shaded region.

3.3.2 Human infection model results based on point estimates.

3.3.2.1 Time course of urethral infection in symptomatic men

The simulated cell populations for the first 40 days of infection are shown in Fig. 3.4(a) and for the full time-course of infection in Fig. 3.5(a). The total NG load, consisting of NG in all four states (B , B_a , B_s and B_i), reached a peak of 4.27×10^6 bacteria by 3.6 days. The PMN response followed a qualitatively similar pattern to the NG load. Peaks in PMN and NG curves were reached around the same time point with the peak PMN cell count reaching 2.8×10^5 cells. The NG load remained above 10^6 bacteria from days 2.3 to 7.5, after which it declined due to PMN killing. By 75 days, the NG load declined to <10 bacteria, which was our condition for clearance (Fig. 3.5(a)).

We also analysed the proportion of NG in the various states of attachment and internalisation over time (Fig. 3.4(b) and (c)). The initial NG load consisted of only unattached bacteria. However, two hours into infection, the modelled NG population had started to colonise the host and become attached to or internalized within epithelial cells (Fig. 3.4(c)). The two intracellular NG populations (NG surviving within PMN (B_s) and NG internalized within epithelial cells (B_i)) showed similar dynamics. The NG populations occupying these two states increased with continued entry and replication and showed a small decline as NG exited from these compartments. In the later stages of

infection, the non-internalized population (NG attached (B_a) and unattached (B) to epithelial cells) reached a stable value of $\sim 20\%$ of the total NG population. In the long term, NG that survived within PMN and NG internalized within epithelial cells comprised 56% and 24% of the total NG population, respectively (Fig. 3.4(b)).

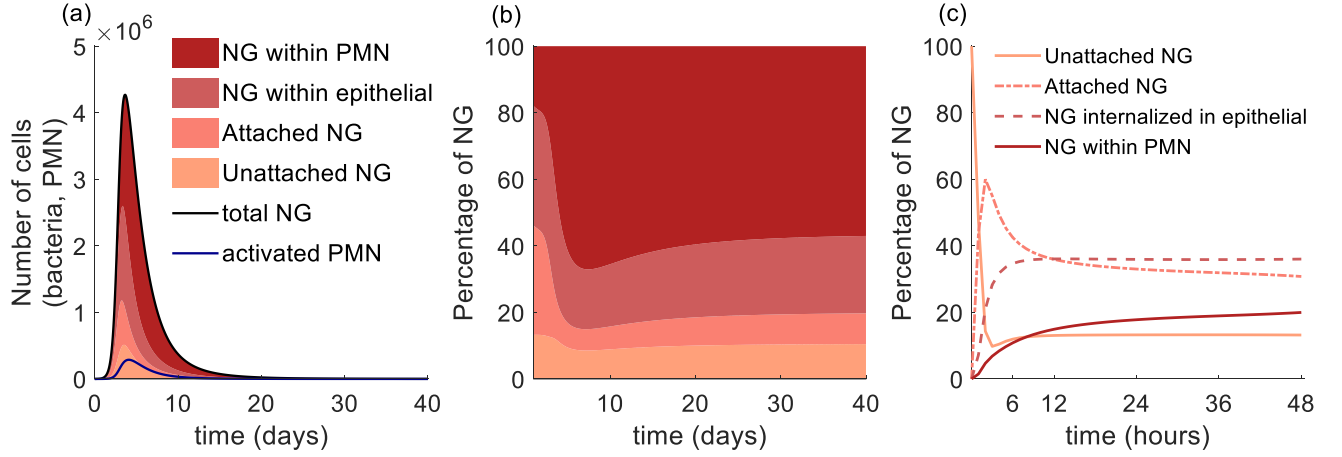


Figure 3.4: (a) Changes in the four bacterial populations as well as the neutrophil population are shown along with the total bacterial load ($B + B_a + B_s + B_i$) over the first 40 days of infection. (b) Proportions of NG across the bacterial states over 40 days. Colours in each panel relate to bacterial populations as defined in the panel (a) legend. (c) Changes in the relative proportions of NG in each bacterial state during the first 2 days of infection.

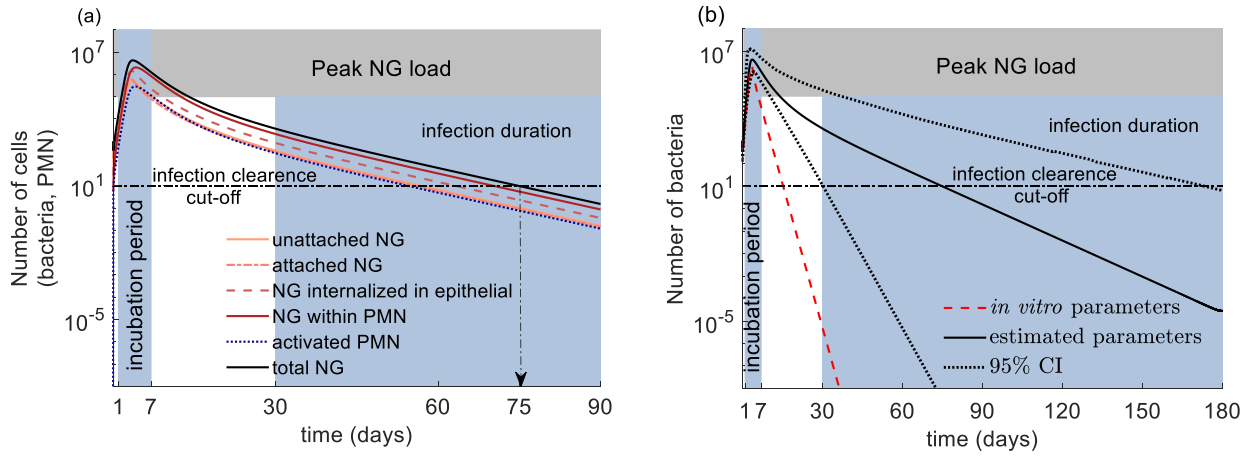


Figure 3.5: (a) Log-scale time course for all model states using the point estimates in Table 3.2 as parameter values, with shaded regions representing realistic intervals for incubation and clearance periods and the peak load. (b) Comparison of log-scale infection time course for overall bacteria obtained using point estimate values in Table 3.2, along with 95% credible interval from multivariate sensitivity analysis (clearance at 1-6 months) and bacterial curve when using *in-vitro* parameter estimates without adjustment.

3.3.3 Multivariate sensitivity analysis

3.3.3.1 Human infection model results based on simulations from LHS samples

The 95% credible intervals of model parameters, derived from model simulations that met the outcome criteria, are given in Table 3.2. The point-estimates for d , p , c , μ and r_1 were broadly consistent with the refined ranges derived from the multivariate sensitivity analysis as shown in Table 3.2.

The corresponding 95% range for total NG load obtained is shown in Fig. 3.5(b), while the distributions of these simulations in terms of the peak time, peak load, and infection duration are shown in Fig. A.4 (in Appendix A, Section A.2.1.2) and the

distribution of proportions of NG by state is shown in Fig. A.6 (in Appendix A, Section A.2.1.2).

Partial rank correlation coefficients (PRCC) were calculated to assess the relative contribution of each parameter's associated uncertainty to variability in the model outcomes. This analysis identified PMN activation rate (μ), replication rate of non-internalized NG (r_1) and internalisation rate into epithelial cells (η) as important contributors to variability in the peak time and the peak load. Parameters associated with NG killing (ratio dependent constant (c) and μ) as well as the capacity constraint on NG surviving within PMN (k_2) were identified as the most important contributors to variability in the infection duration. These results are presented in Fig. A.5 in Appendix A, Section A.2.1.2.

3.3.4 Validation against mouse model data

The results of the model fit to bacterial load data of the eight mice obtained from the study by Jerse (1999) are presented in this section. Fits of different versions of the re-parameterised model to mouse NG load data are shown in the panels of Fig. 3.6. The mouse data are broadly grouped to reflect similar load patterns over the 9 days. In general, based on the sums of squared errors (SSE) shown in Appendix A, Table A.4, the simplified models without the B_i state (internalisation within epithelial cells) or the B_i and B_a states (internalisation within and attachment to epithelial cells) fitted data in 7 of the 8 mice just as well as when using the full human infection model. However, further removal of the state where NG survive within PMN (B_s) led to poor fits, both in terms of qualitative behaviour and the SSE.

The estimated values for d, c, μ, r_3 and r_1 for the four model variants are summarized in Table A.4 and Fig. 3.7. In general, mouse-derived estimates of d, r_3 and p were substantially lower than those estimated for the human model (Fig. 3.7). However, the 95% range of the estimates of the ratio of $\frac{d}{c}$ and r_1 were similar in both mouse and human models. Although the PMN activation rate (μ) was substantially lower in the human model, when multiplied by the total PMN, the neutrophils recruited per unit time (μN) were consistent across human and mouse models. The high variation in the NG time course between mice is reflected in large ranges for resulting parameter estimates when summarised across the 8 mice (Fig. 3.7).

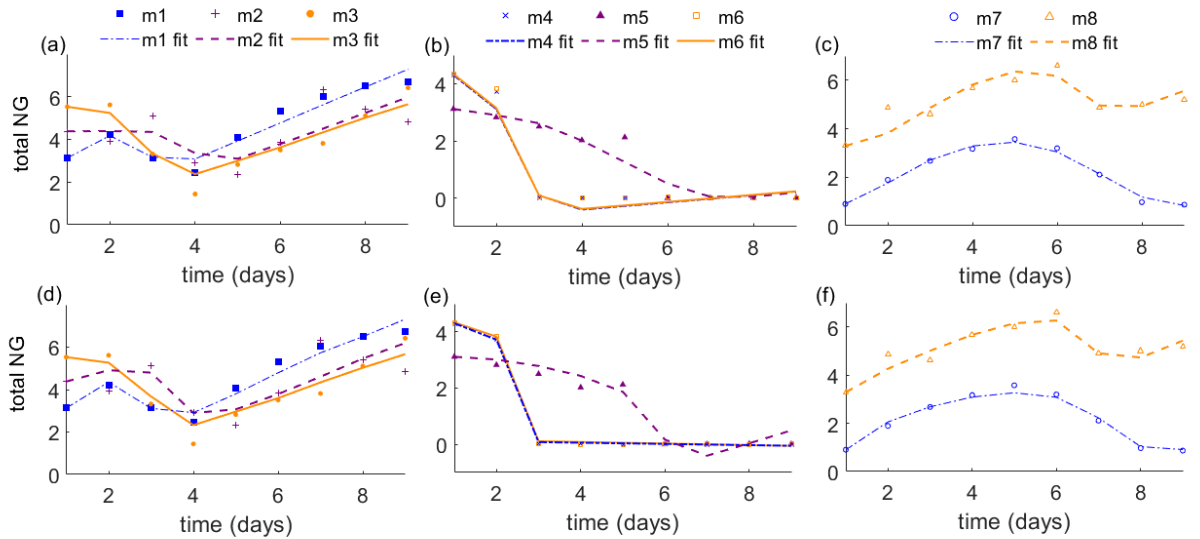


Figure 3.6: Model fits to mouse NG data. (a)-(c) NG data from mouse model described in Jerse (1999) and fits to each mouse for the 5-state model developed for human infection. (d)-(f) As above but using a 3-state model where epithelial internalisation (B_i) and attachment (B_a) states have been removed. Mice are labelled m1 to m8, with data represented by markers and fits by lines of the same colour.

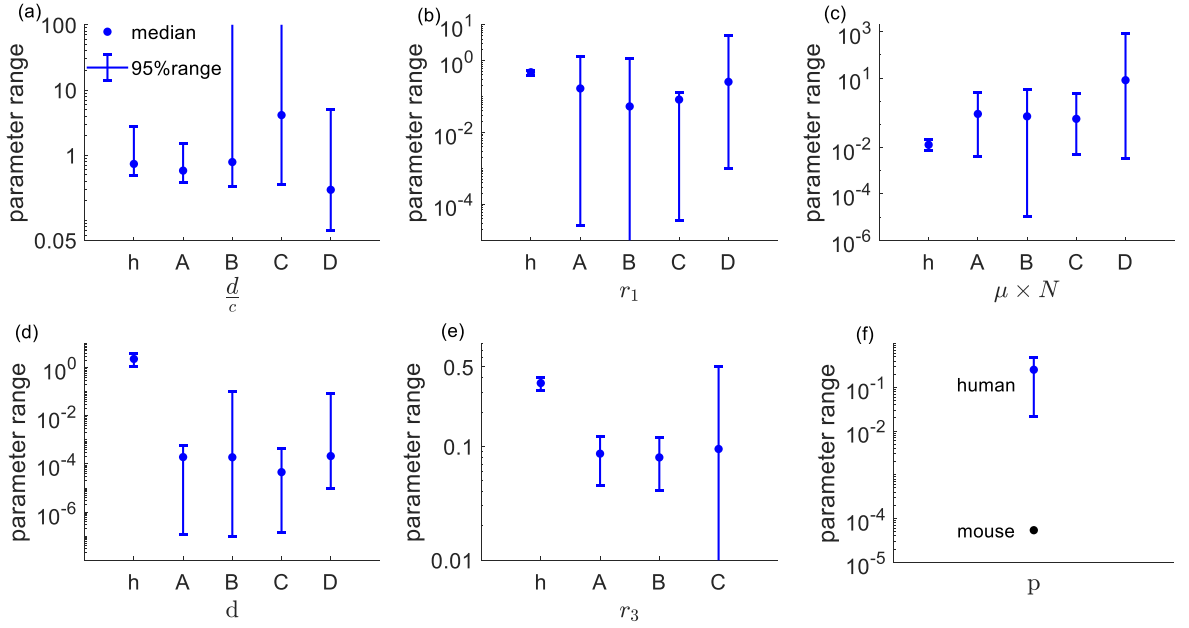


Figure 3.7: Estimated parameter values of the ratio $\frac{d}{c}$, r_1 , $\mu \times N_{max}$, d , r_3 , and p obtained

across the mouse models (labelled A to D) compared with the human estimates (labelled h) are shown in panels (a to f) respectively. Here, A represents the full 5-state model, B the model without an epithelial internalisation state (B_i), C the model without attachment (B_a) or epithelial internalisation states (B_i) and D the model without attachment (B_a), epithelial (B_i) and neutrophil (B_s) internalisation states. Ranges for mice are minimum and maximum values across the 8 mice while for the human estimates, the 95% credible intervals shown in Table 3.2 are displayed along with the median value. Note that in panel (f) no range is displayed because we fix the neutrophil internalisation proportion p in the relevant mouse models.

3.4 Discussion

In this study, we developed a within-host model to describe untreated symptomatic urethral NG infection in men. Assuming that the peak NG load is reached around the time period of symptom expression, the model using our default parameters produces a bacterial load and time course consistent with the known features from experimental infection (Schmidt, *et al.* 2001; Schneider, *et al.* 1995; Schneider, *et al.* 1996; Stupiansky, *et al.* 2011) and pre-antibiotic era studies of natural infection (Hill 1943; Pelouze 1939). In addition, when the model was validated using time course data on bacterial load from a study in mice by Jerse (1999), the model was able to closely match the course of infection in seven out of eight mice.

Model simulations produced NG load $> 10^6$ bacteria from days 2.3 to 7.5, with a similar plateau seen in the human experimental studies by Schneider, *et al.* (1995), Ramsey, *et al.* (1995) and Schmidt, *et al.* (2001), where the bacterial load remained high (NG $> 10^6$ bacteria) from around day 1-2 to the initiation of treatment at day 5-7. However, in these studies, as treatment was initiated shortly after reaching the peak load, it is not possible to know the exact duration of this high NG load around the peak.

In our model, the growth phase for NG is monotonic, without an “eclipse” period as has been observed in some human experimental studies. The “eclipse” period is the time period in which few NG could be recovered in the exudate. In the experimental studies this was observed 2 - 4 hours after inoculation (Cohen, *et al.* 1994; Hobbs, *et al.* 2011; Schmidt, *et al.* 2001; Schneider, *et al.* 1995). At the end of the eclipse period, the bacterial population was seen to expand exponentially from the few NG that were present in the inoculum (Hobbs, *et al.* 2011). While the underlying reason for this eclipse period has not been established (Cohen, *et al.* 1994; Schneider, *et al.* 1995), it is plausible that it

relates to the initial period of NG attachment and internalisation. Our aim, however, was to capture bacterial dynamics over a time-scale of days to weeks rather than hours.

To the best of our knowledge, Craig, *et al.* (2015) is the only previous mathematical modelling study that has described the NG load of an infected individual. In that study, the NG load was primarily used to determine the infectiousness of an individual and the potential impact of a vaccine. However, they describe the NG load through a parametric function without explicit consideration of the mechanisms of infection or the interaction of NG with host cells, in contrast to our explicit description of these processes. Comparisons between our predicted total NG curve and that from Craig, *et al.* (2015) show agreement in terms of the qualitative features of the time-course of infection (see Fig. A.9 in Appendix A, Section A.4). However, our model is able to make predictions related to intracellular NG growth and decline, including relative proportions over time of the bacterial population that are unattached, attached and internalised and the effectiveness of PMN in infection clearance.

Based on urethral exudates from 33 male patients, the *in vivo* study by Veale, *et al.* (1979) reported the relative extracellular, epithelial internalised and PMN internalised NG proportions as $35.1 \pm 3.6\%$, $15.7 \pm 3.1\%$ and $49.2 \pm 4.4\%$, respectively. Precise timing of these measurements is not reported but was likely during the incubation period 2-6 days after inoculation. By comparison, at 2-6 days post infection, our model produced relative bacterial proportions of 15% - 44% (extracellular), 19% - 36% (epithelial internalisation) and 20% - 65% (PMN internalisation). In the later stages of infection, our model indicated that the intracellular populations consisting of B_s and B_i comprised 80% of the total NG population, with the bacterial population within PMN (B_s) stabilising at 56% of the total NG population. This suggests that the model infection dynamics are mainly driven by the intracellular NG populations and these cell populations

are mainly responsible for prolonging the duration of infection. This finding is consistent with observations that in addition to killing a portion of NG, PMN provide a reservoir for bacterial survival and replication that prolongs infection (Criss and Seifert 2012; Quillin and Seifert 2018).

A full multivariate sensitivity analysis was also conducted, with parameters relating to PMN availability and PMN engulfment of NG (through the ratio dependent constant) being most influential in terms of clearance time, further supporting the importance of PMNs in the infection dynamics. In addition, after filtering the parameter sets generated through the analysis according to qualitative outcome criteria around peak load, timing and clearance, the retained parameter sets showed good agreement with our default parameters but departures from values estimated purely from *in vitro* data.

The absence of human bacterial load data over longer timeframes led us to attempt further validation of the model against mouse model data (Jerse (1999)). The single mouse (mouse 2) for which the model could not describe the data well showed weak correlation between NG load and measured PMN levels found in Jerse (1999) whereas the other mice showed stronger association as the bacterial load declined at high PMN levels. We note that internalisation within mouse epithelial cells and survival within mouse PMN are impaired as some of the mechanisms that NG uses for internalization and survival are explicitly human host restricted (Edwards, *et al.* 2016; Jerse, *et al.* 2011; Sadarangani, *et al.* 2011). In line with these observations, our estimates for the proportion of NG surviving within PMN (p) was 3-5 orders of magnitude lower than estimated for the human model. The ineffectiveness of NG internalisation and attachment to mouse epithelial cells was made evident by equivalent fits to the mouse data of simplified models that excluded attachment and epithelial internalisation. This supports the observed

differences in infection durations between human and mouse infection, as in humans the intracellular compartments were vital in prolonging infection durations. However, when internalisation within PMN was also excluded it resulted in poor fits to mouse data, suggesting that although NG survival within PMN is limited in mice, it is still needed to explain the dynamics of mouse infection.

Limitations of our model design mainly arise from simplifications in the representation of the immune response. We only considered the immune response mediated by PMN and did not consider the contribution from macrophages or the possibility of an adaptive immune response. During infection with NG, the PMN response is considered to be the primary immune response that is initiated, evidenced by the fact that purulent discharge in symptomatic infection occurs as a result of PMN influx (Edwards and Apicella 2004; Handsfield, *et al.* 1974). However, it is believed that macrophages also play a role by phagocytosing NG and recruiting PMN to the infection site (Chateau and Seifert 2016). Furthermore, as with PMN, NG has acquired mechanisms to replicate and survive within macrophages providing NG with an additional reservoir to facilitate prolonged infection (Chateau and Seifert 2016). Therefore, macrophages may play a role in defining infection dynamics. We also did not include immune responses mediated by the adaptive immune response as while its role in controlling and eliminating infection is not clearly understood, it is generally considered to be only weakly effective (Schmidt, *et al.* 2001; Stupiansky, *et al.* 2011). Furthermore, the characteristic antigenic and phase variations exhibited by surface proteins (e.g., Opacity associated proteins (Opa) and pili (Alcorn and Cohen 1994; Dehio, *et al.* 1998; Virji 2009)) were not considered in the model and these may be important in determining within-host behaviour.

Parameter estimation and model validation were limited by the paucity of data on human infection, and the limited applicability of mouse model data and *in vitro* studies

to *in vivo* infection. In particular, the absence of more sophisticated *in vitro* experiments capturing the simultaneous interaction of NG, epithelial cells and PMN made it difficult to further constrain model parameters. This was addressed in our study to some extent through the multivariate sensitivity analysis, which provided ranges for parameter values and intervals around outcomes that might potentially be tested through future experiments. Improved data on within-host NG interactions would likely reduce parameter uncertainty and facilitate refinements to model structure and assumptions.

3.5 Conclusion

In this study, we developed a mathematical model of in-host gonorrhoea infection that broadly reproduces features of untreated symptomatic male infection as described in experimental, pre-antibiotic and *in vitro* studies. Untreated NG infection dynamics are poorly understood as it is not possible to obtain experimental human infection data over prolonged time periods, and *in vitro* experiments involving multiple cell types (e.g., both PMN and epithelial cells) are very difficult to conduct. Our model goes some way to filling this knowledge gap by providing a means of understanding how NG interacts with and occupies host cells in the later stages of the infection and points to the importance of the intracellular compartments (NG surviving within PMN and NG internalised within epithelial cells) in determining the course of human infection. Validation of the mathematical model on human infection using mouse model data demonstrated that the model can closely replicate the course of untreated infection in a related animal model using differing parameter values that account for biological differences between the two species.

This model should provide a foundation for extensions in several directions, including the interaction of multiple NG strains and emergence of resistance under selective pressure from antibiotics. Other potential developments include extension to

asymptomatic infection and infection at different anatomical sites, and consideration of potential vaccine conferred immunity such as recently reported for meningococcal vaccines (Petousis-Harris, *et al.* 2017; Seib 2017).

Chapter 4

Modelling treatment effects for gonorrhoea

4.1 Introduction

In Chapter 3, we observed that intracellularly surviving and replicating *Neisseria gonorrhoeae* (NG) are a key determinant in prolonging natural infection duration in simulations and therefore it is of interest to consider how treatment resolves infection while accounting for intracellular NG states. Quantitative predictions of the drug movement in the body (pharmacokinetics (PK)) and the drug's effect on the body (pharmacodynamics (PD)) are especially important in accurately capturing the treatment effects, especially against high minimum inhibitory concentration (MIC) values. However, as outlined in Chapter 2, Section 2.7.2, some of these existing experimental studies to determine the extracellular PK/PD effects for NG infection are subject to several limitations and in relation to intracellular PK/PD effects, we were unable to find any studies that explored these in the context of NG infection.

Generally, within-host mathematical models are useful in providing insights on phenomena that are difficult to be explored empirically, such as the modelling study by Ho, *et al.* (1995) on the human immunodeficiency virus which indicated a rapid turnover of infected cells which was initially considered as a slow-paced process. In the context of NG, a within-host model has the potential to explore intracellular treatment effects for which there is little experimental evidence. However, to the best of our knowledge, only the thesis by Fingerhuth (2017), which analyses the probability of treatment failure using

different antibiotic classes, applies a mechanistic within-host model integrated with PK/PD effects in the context of NG. This study, however, does not consider drug-specific PK differences, the role of immune responses or differentiate between extracellular and intracellular NG states.

In this chapter, we extend the model developed in Chapter 3 to include antibiotic treatment effects. Here, the main focus is on model development, parameter estimation and calibration, and understanding model behaviour, while in Chapter 5, we apply the model to assess the effectiveness of different treatment strategies and combinations. In regard to model behaviour, we investigate the impact of intracellular NG in determining MIC for treatment regimens in current use (ceftriaxone (CFO), cefixime (CFM) and azithromycin (AZM)) and for alternative treatments that have been evaluated in recent trials (gepofidacin (GEP) and gentamicin (GEN)). Finally, we outline limitations of the model in relation to describing treatment dynamics using the β -lactam antibiotics, ceftriaxone and cefixime.

4.2 Materials and Methods

4.2.1 Mathematical model of antibiotic treatment

In Chapter 3, we developed a deterministic compartmental model to describe untreated male urethral infection with NG. In that model, four NG states (unattached NG (B), NG attached to epithelial cells (B_a), NG internalised within epithelial cells (B_i) and NG surviving within PMN (B_s)) and the innate immune response through PMN are used to describe the infection process. In this chapter, we extend this model to include treatment effects by PK/PD principles. Treatment effects are incorporated to both the extracellular (B and B_a) and intracellular NG states (B_i and B_s) using drug-specific Hill functions, with differing concentrations of drug in the extracellular and intracellular

environments. Fig. 4.1 provides a schematic illustration of the natural infection model with the added treatment effects. Treatment is initiated at the peak NG load as identified in the model of untreated infection (at 3.6 days post-infection in the base case), at which point we assume symptoms to be apparent.

The full treatment model equations are given in Appendix B, Section B.3 with the treatment model specific parameter values given in Tables 4.1 and 4.2 and the natural infection model related parameters described in detail in Table 3.2 of Chapter 3.

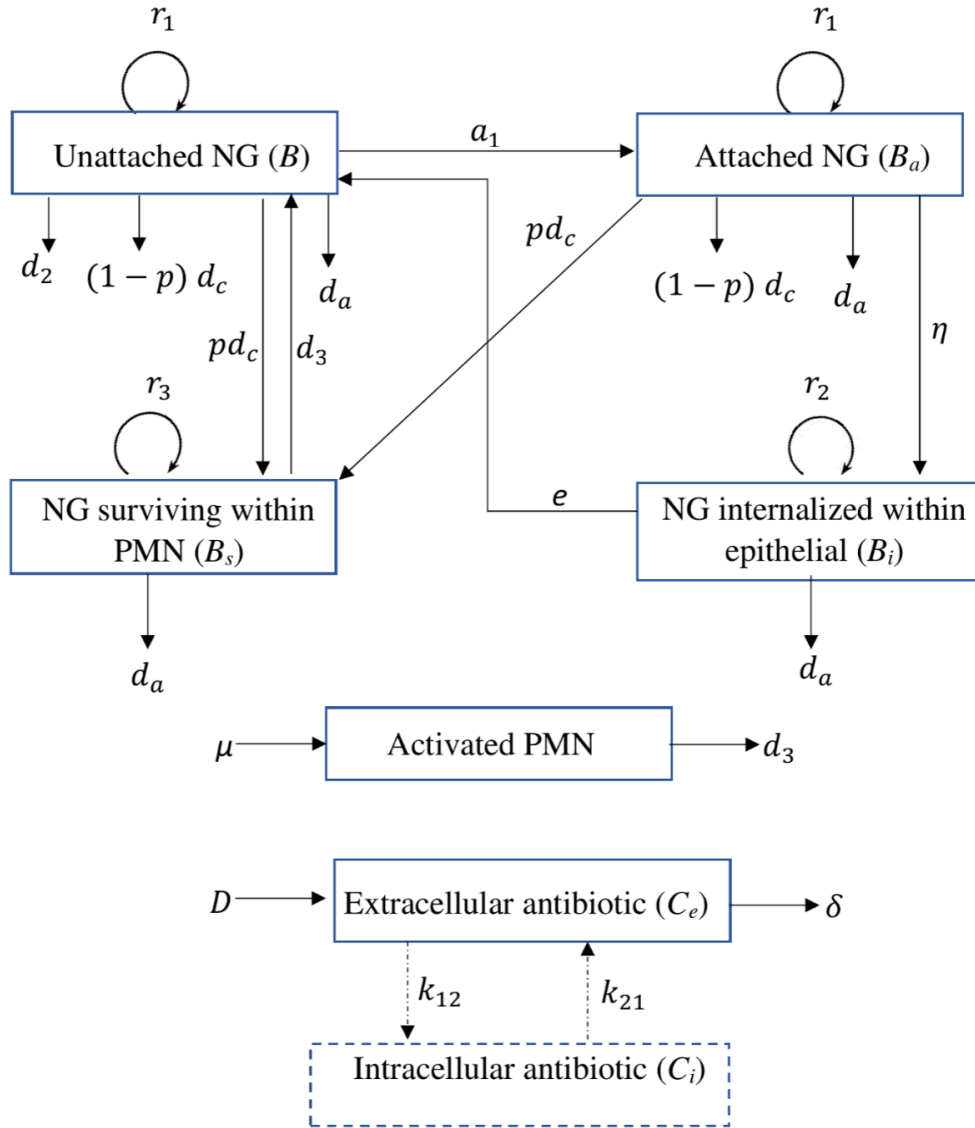


Figure 4.1: Schematic illustration of the within-host NG infection model including antibiotic treatment. The arrows indicate transitions between model states, which are indicated as boxes. Antibiotic- and PMN-mediated killing of NG are denoted as d_a and d_c , respectively (for killing by PMN see Chapter 3, Section 3.2.1). An explicit intracellular antibiotic compartment is included for gentamicin and azithromycin (see Section 4.2.3) and transitions between extra and intracellular drug concentrations (denoted as dashed lines) apply only for these two drugs.

4.2.2 Modelling pharmacodynamics.

Drug effects on the NG population are modelled using a Hill function as in Regoes, *et al.* (2004), where the authors used the Hill function to describe the relationship between the growth rates of *E.coli* and the concentrations of antibiotics (C) of different classes that are measured through *in vitro* time-kill experiments. The Hill function (described in detail in Appendix B Section B.1.1) is determined by four parameters: the maximum (φ_{max}) and minimum (φ_{min}) bacterial growth rates in the absence and presence of the antibiotic, respectively; the MIC; and the Hill coefficient (k_H), which reflects the sensitivity of the change in the net bacterial growth rate to the changes in the antibiotic concentration $\varphi(C)$. Under this parameterisation, $\varphi(C)$ is then described by Eq. 4.1:

$$\varphi(C) = \varphi_{max} - \frac{(\varphi_{max} - \varphi_{min}) \left(\frac{C}{MIC}\right)^{k_H}}{\left(\frac{C}{MIC}\right)^{k_H} - \frac{\varphi_{min}}{\varphi_{max}}}. \quad (4.1)$$

4.2.2.1 Estimation of the Hill function parameters

The Hill function parameters are estimated using the NG growth data reported in the time-kill experiments for ceftriaxone, cefixime, gentamicin and azithromycin in the study by Foerster, *et al.* (2016) and for gepotidacin in the study by Farrell, *et al.* (2017). In Foerster, *et al.* (2016), NG growth is measured hourly from 0-6 hours inclusive and in Farrell, *et al.* (2017) it is measured at 0, 2, 4, 8 and 24 hour time points. These studies compare NG growth in the absence and presence of the antibiotic at a stable concentration. The antibiotic concentrations that are used in Foerster, *et al.* (2016) range from $0.016 \times MIC$ to $16 \times MIC$, while in Farrell, *et al.* (2017) these range from $0.25 \times MIC$ to $10 \times MIC$. Further details on the data are provided in Appendix B, Section B.1.2.

Fitting is carried out as a two-step process. As φ_{max} can be independently estimated from the rest of the Hill function in the absence of treatment, this parameter was first estimated using time-kill experiment data without treatment. Then, using this estimated φ_{max} value, the remaining Hill function parameters φ_{min} , MIC and k_H are estimated by fitting Eq. 4.2 to the NG load data that are measured at different drug concentrations.

$$\frac{dB}{dt} = \varphi(C) B = \varphi_{max} B - \frac{(\varphi_{max} - \varphi_{min}) \left(\frac{C}{MIC}\right)^{k_H}}{\left(\frac{C}{MIC}\right)^{k_H} - \frac{\varphi_{min}}{\varphi_{max}}} B. \quad (4.2)$$

Here, B represents the bacterial load. Eq. 4.2 assumes simple exponential growth or decline with no lag phase.

Parameters are estimated by simultaneously fitting to the NG growth data on all antibiotic concentrations and minimising the objective function given by Eq. 4.3:

$$\sum_{j=1}^{n_a} \sum_{i=0}^t (\log(B_{aij}) - \log(\widehat{B_{aij}}))^2. \quad (4.3)$$

Here, B_{aij} represents the number of bacteria (as measured in time-kill experiments) at a particular time point (i) and antibiotic concentration (j) for the antibiotic (a), while $\widehat{B_{aij}}$ represents the bacterial load that is estimated from the model. The number of drug dilutions (n_a) and the specific drug concentration values vary by the antibiotic (details provided in Appendix B, Section B.1.2).

As Foerster, *et al.* (2016) carried out two independent sets of time-kill experiments, the Hill function parameter values are estimated using the above method applied independently to the experimental data sets for each specific drug. To account for substantial differences in estimated values between the experiments, we fit Eq. 4.1 to the mean Hill function effect that is obtained from the fits to the two individual experiments.

We take this approach rather than taking the average of the parameter estimates from the two individual experiments because of the dependencies between parameters of the Hill function induced through fits to the individual experiments. When estimating the Hill function parameters Foerster, *et al.* (2016) adopt a different approach to ours. They first use linear regression to estimate the net bacterial growth rates at each drug concentration and then fit the Hill function (Eq. 4.1) to these estimated net growth rates. This two-step process caused some information loss as the initial stage did not describe the NG load data over time particularly well. Goodness of fit statistics are used to compare the errors between our approach and the approach of Foerster, *et al.* (2016). Our estimation procedure for the Hill function parameters is described in detail in Appendix B, Section B.1.3 along with the approach in obtaining uncertainty ranges around parameter estimates.

4.2.3 Modelling pharmacokinetics

4.2.3.1 Ceftriaxone, cefixime and gepotidacin

When modelling drug concentrations, we adopt a one-compartment model (Rowland and Tozer 1995) as has been applied by Meyers, *et al.* (1983), Brittain, *et al.* (1985) and So, *et al.* (2015), for ceftriaxone, cefixime and gepotidacin, respectively. A one-compartment model can be used when the drug concentration time-dependence profile can be explained by a single exponential function such as with intravascular drug administration or for drugs with relatively poor accumulation within host cells (Rowland and Tozer 1995). Here we assume that drug concentrations decline exponentially on a time-scale determined by the half-life ($t_{1/2}$) of the drug. Specifically, extracellular drug concentrations are modelled as $\frac{dC_e}{dt} = -\delta C_e$, where δ is the rate of decline of drug concentration and C_e is the extracellular drug concentration. The initial extracellular drug

concentration level, $C_e(0)$, is obtained using the drug dose (D), drug bioavailability (b_d), fraction unbound (not bound to plasma proteins) (f_u), and volume of distribution (V_d) as, $C_e(0) = \frac{D \times b_d \times f_u}{V_d}$. See Chapter 2, Section 2.7.1 for definitions of these terms.

In model simulations described in Chapter 3, we found that ~80% of the total NG population are intracellular beyond 5 days of infection. This suggests the need for considering drug-specific intracellular kinetics when including treatment effects in the model. Ceftriaxone, cefixime and gepotidacin show relatively low intracellular accumulation compared with drugs such as azithromycin (Jacobs, *et al.* 1986; Peyrusson, *et al.* 2018). As such, for these drugs, we assume the intracellular concentration to be proportional to the extracellular concentration with proportionality constant $\alpha \approx 0.4$ for ceftriaxone and cefixime (Jacobs, *et al.* 1986) and $\alpha \approx 1.5$ for gepotidacin (Peyrusson, *et al.* 2018). In Jacobs, *et al.* (1986) and Peyrusson, *et al.* (2018) α is estimated through measurements of cellular uptake of radiolabelled gepotidacin and β -lactams into human PMN and THP-1 monocytes, respectively.

4.2.3.2 Modelling gentamicin and azithromycin pharmacokinetics.

The assumption of exponential decay of drug concentration implies instantaneous drug distribution and equilibration throughout relevant tissue (Austin, *et al.* 1998). However, data from studies involving azithromycin and gentamicin are inconsistent with this assumption (Foulds, *et al.* 1990; Tulkens 1991). Azithromycin shows rapid entry into host cells and high intracellular accumulation followed by slow release into the extracellular environment (Foulds, *et al.* 1990; Wildfeuer, *et al.* 1996). In the case of gentamicin, while it has been considered to principally kill extracellular NG due to its poor intracellular penetration (Shaw and Falkow 1988), other studies have observed a slow increase in intracellular drug concentration that plateaus after about 3-4 days.

(Tulkens and Trouet 1978; Tulkens 1991). To capture these differences in drug distribution the antibiotic concentrations of gentamicin and azithromycin are captured through a two-compartment model where the extracellular (C_e) and intracellular (C_i) antibiotic concentrations are modelled separately according to Eq. 4.4 and 4.5:

$$\frac{dC_e}{dt} = -\delta C_e - k_{12} C_e + k_{21} C_i \frac{V_i}{V_e}. \quad (4.4)$$

$$\frac{dC_i}{dt} = k_{12} C_e \frac{V_e}{V_i} - k_{21} C_i. \quad (4.5)$$

Here, δ is the drug elimination rate constant, k_{12} and k_{21} are respectively the rate constants of drug movement from and to the extracellular compartment, V_e and V_i are respectively the extracellular and intracellular volumes of distribution. The parameter values and sources for these are described in Table 4.1.

Table 4.1: Model parameter values for the five antibiotics ceftriaxone (CFO), cefixime (CFM), gepotidacin (GEP), gentamicin (GEN) and azithromycin (AZM).

Symbol	Parameter (units)	Drug	Point Estimate ^a (LHS range)	References/Comments
D	Initial antibiotic dose (mg)	CFO	1000	Monotreatment recommendation in UK (Fifer H, <i>et al.</i> 2019)
		CFM	400	CDC Recommended dose prior to 2012 (Centers for Disease Control and Prevention 2012).
		GEP	1500 / 3000	Trial doses. (Scangarella-Oman, <i>et al.</i> 2018; Taylor, <i>et al.</i> 2018b)
		GEN	240	Trial doses. (Brittain, <i>et al.</i> 2016; Hira, <i>et al.</i> 1985)
		AZM	1000	CDC recommended dose for dual treatment (Centers for Disease Control and Prevention 2015).
b_a	Bioavailability	CFO	1	(Zhou, <i>et al.</i> 1985). Given intramuscularly.
		CFM	0.45 (0.40 – 0.50)	(Faulkner, <i>et al.</i> 1988; Levison and Levison 2009)
		GEP	0.44 (0.38 – 0.5)	(Negash, <i>et al.</i> 2016; Tiffany, <i>et al.</i> 2014)
		GEN	1	Given intramuscularly (Katzung 2018).
		AZM	0.37	(Foulds, <i>et al.</i> 1990)
V_d	Volume of distribution (L)	CFO	9.37 (7.80 – 9.53)	Point estimate from Patel, <i>et al.</i> (1982), range refined via calibration with susceptibility breakpoint.
		CFM	16.95 (16.9 – 19)	(Duverne, <i>et al.</i> 1992)
		GEP	188.7	(Negash, <i>et al.</i> 2016)
		GEN	16.8 (10 – 20)	(Al-Lanqawi, <i>et al.</i> 2009)
		AZM	3219 (1593 – 5475)	(Ripa, <i>et al.</i> 1996)

f_u	Fraction unbound	CFO	0.05 (0.04 – 0.17)	(Popick, <i>et al.</i> 1987; Stoeckel, <i>et al.</i> 1981)
		CFM	0.35	(Faulkner, <i>et al.</i> 1987b)
		GEN	0.85 – 1	(Bailey and Briggs 2004)
		AZM	0.88	(Singlas 1995)
		GEP	0.76	(Bulik, <i>et al.</i> 2017)
α	The ratio of intracellular to extracellular drug concentration	CFO	0.55 (0.49 – 0.61)	Point estimate from Jacobs, <i>et al.</i> (1986) for ceftriaxone, range refined via calibration with susceptibility breakpoint.
		CFM	0.55 (0.49 – 0.61)	Point estimate from Jacobs, <i>et al.</i> (1986) for ceftriaxone, range refined range for ceftriaxone.
		GEP	1.8 (1.5 – 2.5)	(Peyrusson, <i>et al.</i> 2018)
$C_e(0)$	Initial extracellular drug concentration level (mg/L)	CFO	5.34 (5.25 – 6.41)	<p>Computed using the formula (Austin, <i>et al.</i> 1998)</p> $\frac{D \times b_d \times f_u}{V_d}$
		CFM	3.72 (2.95 – 4.14)	
		GEP	2.64 (2.43 – 3.04)	
		GEN	14.29 (10.21 – 23.76)	
		AZM	10.85 (9.31 – 13.02)	
$C_i(0)$	Initial intracellular drug concentration level (mg/L).	CFO	2.03 (2.00 – 3.21)	<p>Computed using the formula (Chisholm, <i>et al.</i> 2010b)</p> $\alpha \times C_e(0)$
		CFM	1.41 (1.12 – 2.53)	
		GEP	4.75 (3.65 – 7.6)	
		GEN	0	Drug enters from the extracellular compartment.
		AZM	0	

k_{12}	Transfer rate from the extracellular to intracellular compartment (h^{-1})	GEN	0.04 (0.03 – 0.04)	Point estimate from Schentag, <i>et al.</i> (1977), range refined via calibration with susceptibility breakpoint.
		AZM	0.12 (0.10 – 0.18)	Point estimate from Ripa, <i>et al.</i> (1996), range refined via calibration with susceptibility breakpoint.
k_{21}	Transfer rate from the intracellular to extracellular compartment (h^{-1})	GEN	0.01 (0.008 – 0.016)	(Schentag, <i>et al.</i> 1977)
		AZM	0.04 (0.03 – 0.06)	Point estimate from Ripa, <i>et al.</i> (1996), range refined via calibration with susceptibility breakpoint.
V_e	Volume of the extracellular compartment (L)	AZM	569 (485 – 779)	Point estimate from Ripa, <i>et al.</i> (1996), range refined via calibration with susceptibility breakpoint.
		GEN	0.95 (0.60 – 1.29)	Point estimate from Schentag, <i>et al.</i> (1977), range refined via calibration with susceptibility breakpoint.
V_i	Volume of the intracellular compartment (L)	AZM	1779 (981–1916)	Point estimate from Ripa, <i>et al.</i> (1996), range refined via calibration with susceptibility breakpoint.
		GEN	0.23 (0.18 – 0.27)	(Schentag, <i>et al.</i> 1977)
δ	Rate of drug elimination (h^{-1})	CFO	0.085 (0.08 – 0.09)	estimated as $\frac{\log(2)}{t_{1/2}}$. (Patel, <i>et al.</i> 1982; Scully, <i>et al.</i> 1984)
		CFM	0.20 (0.17 – 0.23)	estimated as $\frac{\log(2)}{t_{1/2}}$. (Faulkner, <i>et al.</i> 1988; Faulkner, <i>et al.</i> 1987a)
		GEP	0.06 (0.05 – 0.07)	Point estimate as $\frac{\log(2)}{\text{half-life}}$ using, Negash, <i>et al.</i> (2016). The lower and upper limit of the LHS samples are based on Hossain, <i>et al.</i> (2014) and Tiffany, <i>et al.</i> (2014) respectively.
		GEN	0.14 (0.11 – 0.18)	Elimination rate in Schentag, <i>et al.</i> (1977)

		AZM	0.08 (0.05 – 0.10)	Elimination rate in Ripa, <i>et al.</i> (1996)
--	--	-----	--------------------	--

^a Point estimates and the parameter ranges for the LHS samples (explained in Section 4.2.4) of the natural infection model are given in Table 3.2 of Chapter 3.

4.2.4 Incorporation of parametric uncertainty

In Chapter 3, to account for parametric uncertainty across the natural infection model, we generated 5402 parameter sets using Latin hypercube sampling (LHS), which met the relevant outcome criteria for the natural time-course of infection (here we index these LHS parameter sets as $i = 1, 2, \dots, 5402$). To incorporate parameter uncertainty that is related to treatment, we extend this previous LHS analysis by also simulating from the ranges that are associated with the treatment parameters. We achieve this by first generating 5402 uniform LHS samples (indexed as $j = 1, 2, \dots, 5402$) for the PK/PD parameters using the parameter ranges derived from relevant literature and summarised in Table 4.1 and Appendix B, Table B.2. Then to incorporate both natural infection and treatment-related parametric uncertainty, the LHS parameter sets that satisfy the indexing $i = j$ are combined to result in 5402 sets of parameter values. Using these 5402 samples, we assess the modelled infection clearance times.

We classify simulations in which infection is cleared in ≤ 7 days as treatment success, based on most studies indicating this timeframe in regards to successful infection clearance (Ayinde and Ross 2020; Scangarella-Oman, *et al.* 2018; Sultan, *et al.* 2020). Simulated infections are assumed to be cleared, when the total bacterial load ($B + B_a + B_i + B_s$) falls below 10 bacteria, as used in Chapter 3.

4.2.5 Calibrating PK/PD parameters using susceptibility breakpoints.

In this study, we do not directly model processes relating to antibiotic resistance, instead varying the MIC as a proxy for changes in the susceptibility to a given treatment (Kjellander and Finland 1963; Martin, *et al.* 1970). To capture the notion of decreased susceptibility (or increased resistance) to treatment, we explore the effect of treatment via the MIC parameter in the Hill function (from here on referred to simply as the ‘MIC’),

which we increase gradually from the antibiotic-specific MIC values estimated as described in Section 4.2.2 for a susceptible NG strain. To this end, we determine a ‘model-derived susceptibility breakpoint’ such that for MIC below and above the breakpoint, the infection clears in ≤ 7 days and > 7 days, respectively.

When the model-derived susceptibility breakpoints are evaluated using the LHS samples derived from the above section (Section 4.2.4), in some cases the proportion of simulations that achieved clearance when the Hill function MIC parameter was set at ‘empirical breakpoints’ was lower than the expected 95% clearance rate. Here we define the term ‘empirical breakpoints’ to refer to susceptibility breakpoints published by the Clinical and Laboratory Standards Institute (CLSI) and the European Committee on Antimicrobial Susceptibility Testing (EUCAST) or in relation to new candidate drugs from relevant published studies (hereafter in the thesis ‘empirical breakpoints’ refer to these breakpoint values defined in the literature). In order to align the model-derived breakpoints with empirical breakpoints, we then decided to calibrate the model to these empirical breakpoints and thereby refine the ranges of the parameters that are influential in determining the model-derived susceptibility breakpoints. We identify these influential parameters through a multivariate sensitivity analysis (see Appendix B, Section B.2 for details) and use partial rank correlation coefficients to determine the importance of each parameter's uncertainty in contributing to the variability of the model-derived susceptibility breakpoints. For each drug, the most influential parameters for determining model-derived breakpoints are treatment related and do not include any parameters introduced in the natural infection model in Chapter 3 (Appendix B, Fig. B.4).

For these influential parameters, the initial parameter ranges based on published literature are refined, where possible, such that the relevant model-derived and empirical breakpoints match. Further details on the calibration process are provided in Appendix B,

Section B.2 and a comparison between the original parameter values (before model calibration) and the refined parameter ranges (after calibration) is shown in Appendix B, Table B.2. Using these refined treatment parameter ranges, a new set of LHS samples are generated for the treatment parameters (PK/PD related) and are then combined with the LHS samples from the natural infection model as described previously in Section 4.2.4.

4.2.6 Extracellular vs intracellular susceptibility breakpoints

To understand potential differences between *in vitro* and *in vivo* clearance behaviour, we compare the susceptibility breakpoints derived from sub-models of increasing complexity starting with only extracellular states and progressing to the full model involving epithelial cells and neutrophils.

Model A reflects an *in vitro* time-kill study, in which extracellular NG but no host cells (epithelial cells or PMN) are present. In simulations, NG are allowed to grow exponentially and the drug concentration is kept constant (no drug decay), similar to the experimental design used in the *in vitro* study by Foerster, *et al.* (2016). In Model B, epithelial cells are added, leading to the inclusion of unattached NG, NG attached to epithelial cells and NG internalised within epithelial cells. In model C, NG interaction with epithelial cells is removed but the PMN response and NG survival within PMN are included in the simulations. In models B and C and the full-treatment model, logistic constraints on growth are applied as described previously on Chapter 3, Section 3.2.1.1 and the drug concentration varies over time as described in Section 4.2.3. Comparisons of the derived susceptibility breakpoints are then made between the sub-models and the full model for the same initial extracellular drug concentration.

We further use a parametric approach to validate the results on the differences in derived MIC in extracellular and intracellular settings. In the full treatment model, we

vary the parameter values of the intracellular growth rates (r_2 and r_3) over the range of $0.1 - 0.6h^{-1}$ and determine the model-derived susceptibility breakpoint as described above.

4.2.7 Sensitivity analysis for ceftriaxone and cefixime

We also conduct an additional univariate sensitivity analysis using wider ranges for the PK/PD parameters to assess whether the model can match empirical susceptibility breakpoints for ceftriaxone and cefixime. As described in Section 4.2.5, only the PK/PD parameters are influential for infection clearance times under treatment and therefore only the ratio of intracellular to extracellular drug concentration (α), the minimum bacterial growth rate in the presence of antibiotics (φ_{min}), the rate of drug elimination (δ) and the Hill coefficient (k_H) are varied in this analysis.

4.3 Results

4.3.1 Estimates of pharmacodynamic parameters

The estimates of pharmacodynamic (Hill function) parameters are given in Table 4.2. and the fits to data in Foerster, *et al.* (2016) and Farrell, *et al.* (2017) to estimate these parameter values are shown in Fig.4.2. Both studies used wild-type NG strains that do not express resistance against the tested antibiotics and these strains are used to estimate MIC values for all drugs. The Hill function estimates that are obtained using our approach of directly fitting the model to NG load data improve the fits (with reduced SSE) compared with those we obtain using the estimates in Foerster, *et al.* (2016) (Appendix B, Table B.1) as we reduce the intermediate smoothing errors. Among the tested antibiotics, gentamicin induces the strongest bactericidal effects ($\varphi_{min} = -8.2h^{-1}$), while for azithromycin this is lower at $\varphi_{min} = -1.5h^{-1}$ but still higher than for cefixime, ceftriaxone and gepotidacin which have similar estimates of $\varphi_{min} \approx -0.5h^{-1}$. The net growth rates at

the highest drug concentrations in Fig. 4.2 approach the estimated φ_{min} values. For all drugs, the point estimates of Hill coefficients vary between 0.9-2.5, with gepotidacin featuring the steepest decline and azithromycin the least steep. In general, the PD parameter estimates are similar for the two β -lactams, ceftriaxone and cefixime. Variation in the maximal NG growth rate in the absence of drug (φ_{max}) is also seen but in model simulations φ_{max} values are replaced with the natural growth rates estimated in Chapter 3, Table 3.2, which are slower than in the *in vitro* environment.

Table 4.2: Estimated Hill function parameter values for ceftriaxone, cefixime, gepotidacin, gentamicin and azithromycin.

Parameter	Point estimate (range)				
	Ceftriaxone	Cefixime	Gepotidacin	Gentamicin	Azithromycin
φ_{min} (h ⁻¹)	-0.45 (-0.54, -0.36)	-0.51 (-0.76, -0.52)	-0.53 (-0.64, -0.46)	-8.18 (-10.00, -6.35)	-1.50 (-2.06, -0.99)
k_H	1.75 (1.08, 2.64)	1.89 (0.87, 1.82)	2.47 (1.78, 3.64)	1.70 (1.14, 2.64)	0.91 (0.70, 1.32)
MIC (mg/L)	2.97×10^{-4} (2.81×10^{-4} , 3.96×10^{-4})	2.13×10^{-4} (1.23×10^{-4} , 4.63×10^{-4})	0.26 (0.20, 0.32)	0.24 (0.17, 0.32)	0.03 (0.02, 0.33)
φ_{max} (h ⁻¹)	0.75 (0.68 – 0.77)	0.73 (0.67 – 0.78)	0.79 (0.76 – 0.84)	0.89 (0.82 – 0.91)	0.63 (0.61 – 0.69)

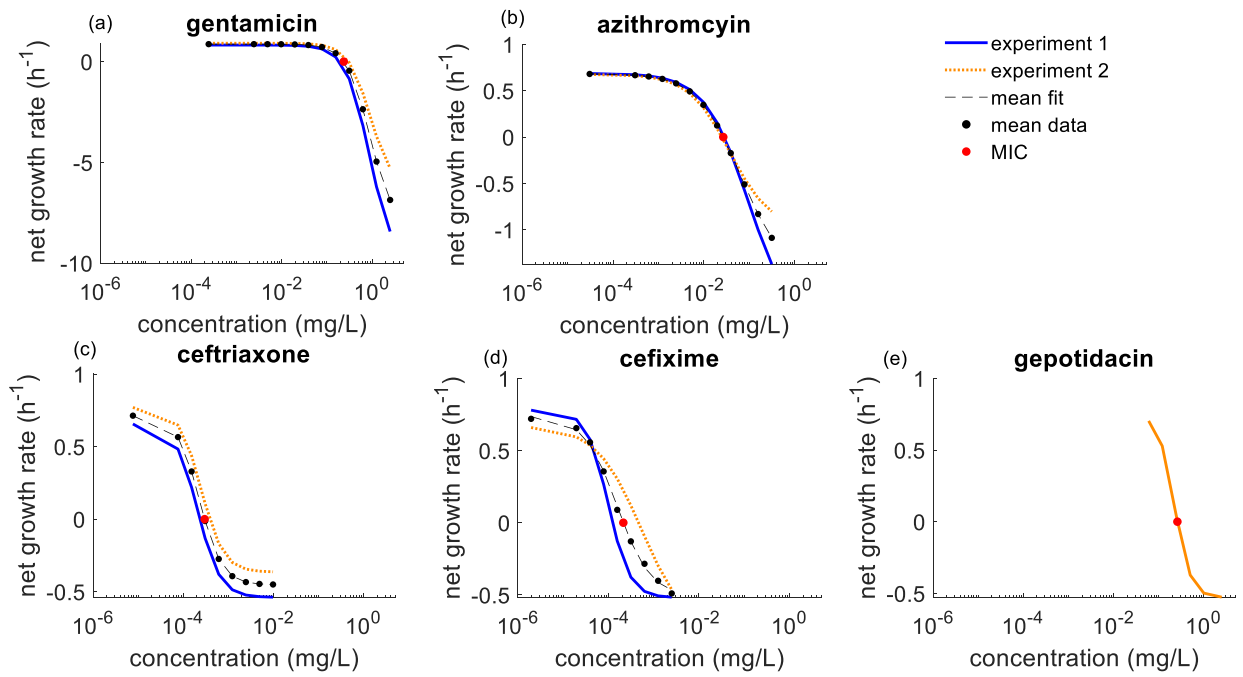


Figure 4.2: Net growth rates obtained from the estimated PD values through fits to the two individual experiments in Foerster, *et al.* (2016), along with the mean net growth rates, are shown for (a) gentamicin, (b) azithromycin, (c) ceftriaxone and (d) cefixime. The net growth rate for gepotidacin (panel e) is obtained through fitting to data generated in a single experiment by Farrell, *et al.* (2017). The black dots are the data points of the mean net growth rates at each drug concentration value. The red dot represents the estimated MIC value for the NG strain used in the relevant *in vitro* experiments.

4.3.2 Drug concentration profiles

The change in drug concentration over time is shown in Fig. 4.3 for the five tested drugs using the default dose values listed in Table 4.1. For ceftriaxone and cefixime, the median extracellular concentrations remain above empirical susceptibility breakpoints for 31.9 and 13.1 hours, respectively, but exceed this for shorter periods of 24.1 and 8.6 hours, respectively, in the intracellular environments. This pattern is reversed for

gentamicin and azithromycin with the relevant extracellular periods of 21.8 and 24.1h, respectively, compared to 26.1 and 43.9h, respectively in the intracellular environment. For these latter two drugs, which are modelled using two compartments, the intracellular effects are achieved at delays of 21.8h and 3.8h. For the drugs that are modelled through a one-compartment model, the gepotidacin intracellular concentration is higher than the extracellular concentration whereas for cefixime and ceftriaxone intracellular concentration is lower. This is due to the difference in the ratio of intracellular to extracellular drug concentration α , which is <1 for ceftriaxone and cefixime and >1 for gepotidacin. The median intracellular to extracellular concentration ratio (C_i/C_e) for gentamicin gradually plateaus at 3 in approximately 4 days but plateaus more rapidly at 1.4 in approximately 27h for azithromycin. This difference in intracellular drug accumulation of gentamicin and azithromycin is associated with the rates of drug transfer to (k_{12}) and from (k_{21}) the intracellular compartment (Appendix B, Fig. B.9). An increase in k_{12} results in an increase in C_i/C_e which plateaus rapidly while the increase in k_{21} results in a decrease in the ratio of C_i/C_e (Appendix B, Fig. B.9).

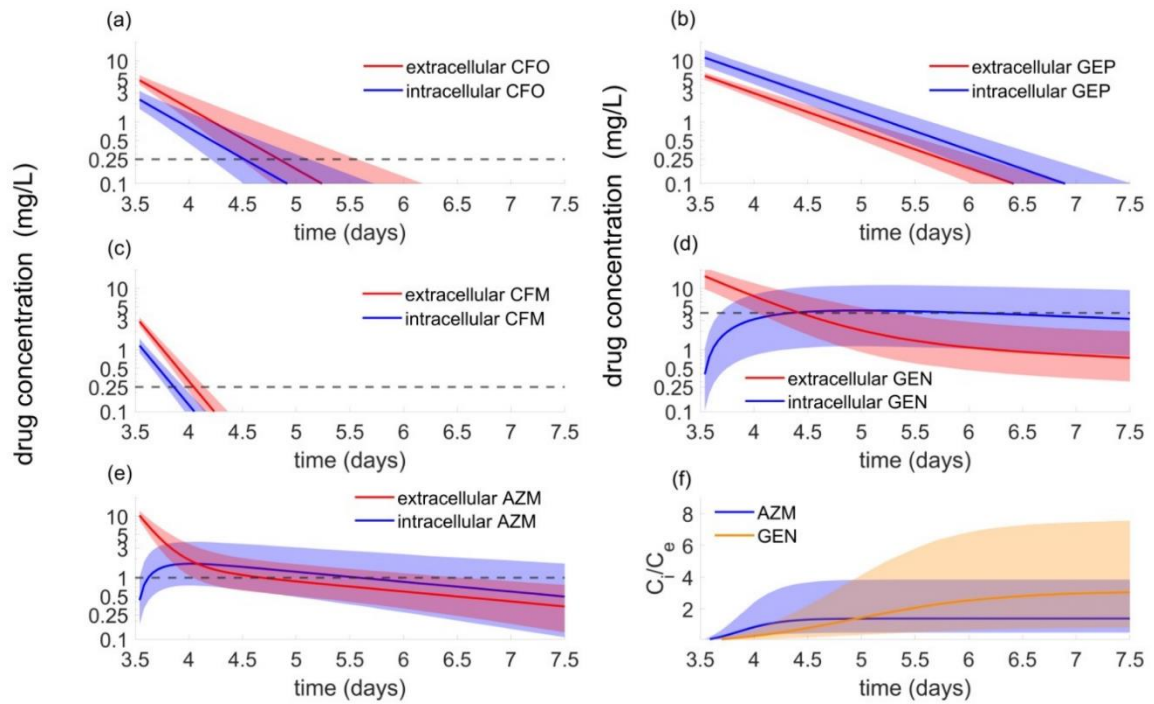


Figure 4.3: Extracellular and intracellular drug concentration of (a) ceftriaxone (CFO) 1000mg; (b) gepotidacin (GEP) 3000mg; (c) cefixime (CFM) 400mg; (d) gentamicin (GEN) 240mg; and (e) azithromycin (AZM) 1g. The change in intracellular to extracellular drug concentration ratio (C_i/C_e) over time is shown in panel (f) for azithromycin and gentamicin, for which a two-compartment model is used. Solid lines denote medians and shaded areas indicate the 95% ranges. The black dashed lines in (a), (c), (d) and (e) represent the empirical susceptibility breakpoints for each drug, while for gepotidacin (panel (b)), an empirical breakpoint yet to be defined.

4.3.3 Modelled infection clearance times under monotherapy

The infection clearance times that are estimated from the model using the PD estimates in Table 4.2 are shown in Fig. 4.4. The MIC values used in this analysis are given in Table 4.2 and are estimated for a wild-type strain that does not show resistance

against the tested drugs. Simulations using these MIC and point estimates for parameter values show successful clearance for each drug (Fig. 4.4). At the time of adding treatment, we note from Fig. 4.4 that the intracellular bacterial load (2.9×10^6) is higher than the extracellular (1×10^6) bacterial load and the infection clearance time coincides with the time taken to clear intracellular NG. For example, using point estimates for parameter values, overall clearance occurs 27.6h following treatment with ceftriaxone which is when intracellular NG fall below 10 bacteria.

In simulations assuming infection with a wild-type strain (MIC as in Table 4.2) and performed using the full set of LHS samples for parameters, 100% of simulations show infection clearance in <7 days (range 0.08 – 2.06 days) for all drugs except cefixime. For cefixime, 2.6% (141/5402) of simulations fail to clear within 7 days (clearance times from 26 to 66 days), with clearance times of 0.77 – 1.82 days for the 97.4% samples that successfully clear infection.

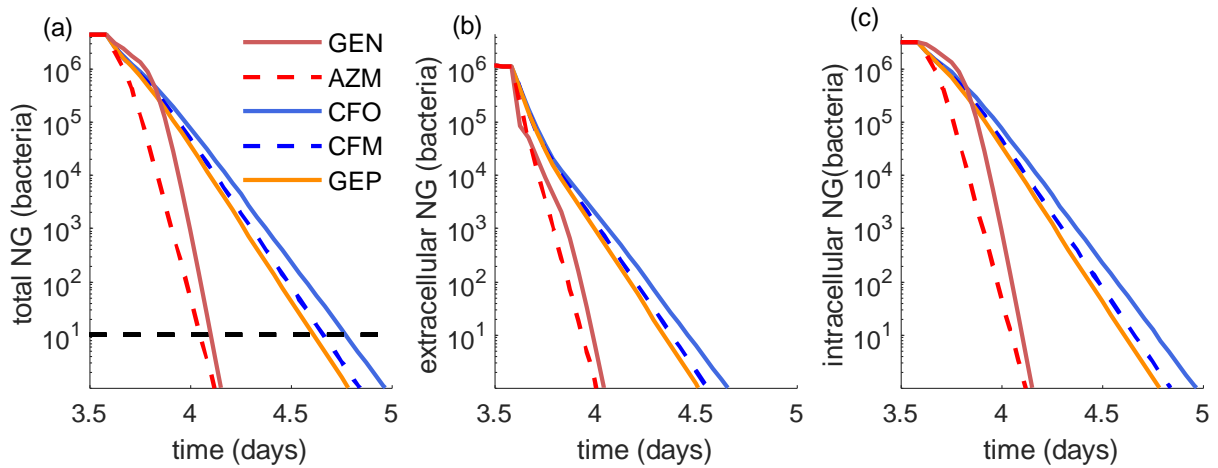


Figure 4.4: Change in total NG (a), extracellular NG (b) and intracellular NG (c) after initiation of single-drug treatment of wild-type infection at 3.6 days for gentamicin (GEN), azithromycin (AZM), ceftriaxone (CFO), cefixime (CFM) and

gepotidacin (GEP). The infection clearance cut-off of 10 bacteria is denoted by a dashed black line in (a).

4.3.4 Calibration of PK/PD parameters

Results for clearance and model-derived breakpoints presented in this chapter are generated using parameter ranges that were refined through calibration to empirical susceptibility breakpoints as described in Section 4.2.5. These refined ranges are compared to pre-calibration ranges in Appendix B, Table B.2. No empirical breakpoint was available for gepotidacin and calibration proved impossible for cefixime. For other drugs, calibration primarily influenced the ranges for the volume of distribution and parameters that define intracellular accumulation. For gentamicin, calibration led to 2-fold and 3-fold increases in the lower bound of the range for the volume of distribution (V_e) and the rate of drug transfer from the extracellular compartment (k_{12}), respectively. For ceftriaxone, there is a small decrease in the upper limit of the volume of distribution but approximately 3-fold increase in the lower bound for the ratio of intracellular to extracellular drug concentration (α). As the same range for α is used for both cefixime and ceftriaxone in simulations, this refined range is applied for both drugs.

4.3.5 Extracellular vs intracellular susceptibility breakpoint

For each of the sub-models described in Section 4.2.6 we determine drug-specific model-derived susceptibility breakpoints, with simulation results based on point estimates for each model parameter summarised together with those from the full treatment model in Table 4.3. In addition, breakpoint ranges derived from simulations using all LHS parameters are provided for the full model and compared with empirical breakpoints where available.

Table 4.3: Susceptibility breakpoints (mg/L) derived from the three sub-models and the full model and comparison with empirical breakpoints.

Drug	Susceptibility breakpoints (mg/L)				
	Model A (extracellular NG only)	Model B (NG interaction with epithelial cells only)	Model C (NG interaction with PMN)	Full model point estimate (LHS range)	Empirical
CFO	4.15	0.12	0.08	0.06 (1×10^{-3} , 0.19)	0.25 ^a , 0.125 ^b
CFM	3.00	0.007	0.006	0.004 (1×10^{-5} , 0.09)	0.25 ^a , 0.125 ^b
GEP	2.55	0.79	0.73	0.64 (0.48 – 1.1)	Not available ^c
AZM	9.35	0.89	0.70	0.69 (0.55 – 1.29)	0.5 ^d , 1 ^e
GEN	12.75	1.94	1.74	1.60 (1.51 – 5.54)	4 ^f (Brown, <i>et al.</i> 2010)

^a Susceptibility breakpoint as defined by the Clinical and Laboratory Standards Institute (2018).

^b Susceptibility breakpoint as defined by the European Committee on Antimicrobial Susceptibility Testing (2019).

^c Currently there is no established susceptibility breakpoint MIC with gepotidacin still at the clinical trial stage.

^d Azithromycin susceptibility breakpoint as defined by EUCAST (European Committee on Antimicrobial Susceptibility Testing 2018).

^e Susceptibility breakpoint defined by Clinical and Laboratory Standards Institute (2018).

^f No CLSI or EUCAST defined susceptibility breakpoints. Based on epidemiological and clinical observations in Malawi, Brown, *et al.* (2010) have defined a susceptibility breakpoint of 4mg/L.

We observe that with the addition of intracellular compartments the model-derived susceptibility breakpoint reduces from the value that is derived for model A (model with only unattached NG). For ceftriaxone and cefixime, the full model-derived susceptibility breakpoint is >50-fold lower than the comparable breakpoint for model A. For azithromycin and gentamicin, the susceptibility breakpoint is, respectively, 8-fold and 14-fold lower and 4-fold lower for gepotidacin. Susceptibility breakpoints derived from models B (consisting of unattached and attached NG and NG within epithelial cells) and C (consisting of unattached and NG within PMN) are similar to that of the full model, indicating that this large change in model-derived susceptibility thresholds is associated with the unsuccessful clearance of intracellular NG in simulations. The increase of cut-off MIC with the addition of intracellular NG states is further validated with our parametric analysis. As the intracellular NG replication rates increase the cut-off MIC decreased and the results are shown in Appendix B, Fig. B.11.

From Table 4.3 we note that for ceftriaxone, gentamicin and cefixime, the susceptibility breakpoints that are derived from our full treatment model deviate from the empirical estimates. For cefixime, no simulations are compatible with empirical susceptibility breakpoints. For ceftriaxone, despite calibration, only 15% of the simulations using the LHS samples for parameters result in a model-derived susceptibility breakpoint $\geq 0.125\text{mg/L}$ (the EUCAST breakpoint) and none result in a susceptibility breakpoint $\geq 0.25\text{mg/L}$ (the CLSI breakpoint). For gentamicin, only 57% of the simulations using the LHS samples for parameters result in a model-derived susceptibility breakpoint $\geq 4\text{mg/L}$, which is the susceptibility breakpoint defined in the literature using epidemiological and clinical observations in Malawi (Brown, *et al.* 2010). CLSI or EUCAST have not defined susceptibility breakpoints for this drug. For ceftriaxone and gentamicin, the simulations with model-derived susceptibility breakpoints below the

empirical breakpoints have relatively low intracellular drug concentrations (Fig. 4.5) and further, this appears to be driven by lower values of volume of distribution and parameters defining intracellular accumulation (Appendix B, Fig. B.6 and B.8).

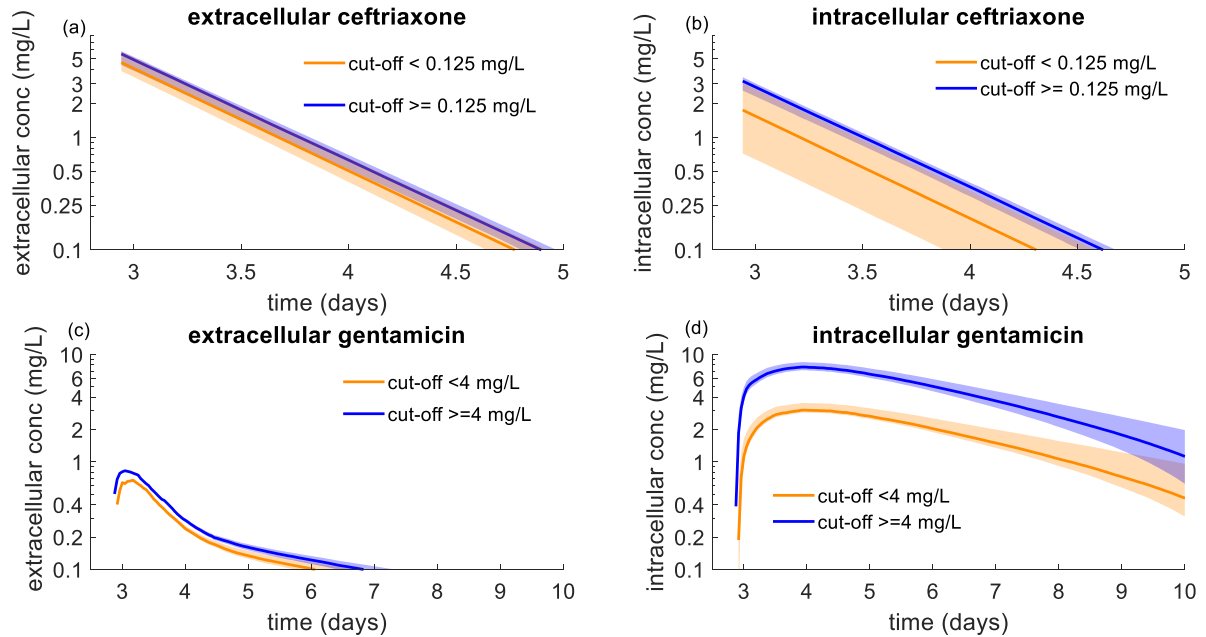


Figure 4.5: Change in the extracellular and intracellular drug concentration over time for the simulations that result in model-derived susceptibility breakpoint below and above the empirical susceptibility breakpoints: extracellular (a, c) and intracellular (b, d) drug concentration for ceftriaxone and gentamicin, respectively. The solid lines denote the median and the shaded areas indicate the 95% range of the drug concentration obtained from the simulations using LHS samples.

4.3.6 Sensitivity analysis on model-derived susceptibility breakpoints for ceftriaxone and cefixime

To further understand the model behaviour underpinning the low model-derived breakpoints for ceftriaxone and cefixime, we examine wider ranges for PK/PD parameters

in order to see what values would be consistent with empirical breakpoints. For this, we conduct a sensitivity analysis as described in Section 4.2.7.

We observe that to obtain model-derived susceptibility breakpoints for ceftriaxone and cefixime consistent with empirical susceptibility breakpoints, the ranges of PK/PD parameters need to be altered to values that are outside of those reported in the literature (Table 4.4). The parameter specifying the ratio of intracellular to extracellular drug concentration (α) has to be 4- to 8-fold above the upper end of our literature derived range for ceftriaxone and cefixime, respectively. To meet the empirical susceptibility breakpoints the values of φ_{min} need to be consistent with more bactericidal drugs at -3.1 and -3.3h^{-1} for ceftriaxone and cefixime, respectively, or respective drug half-lives need to be approximately twice the estimates from PK studies. It is not possible to meet the empirical susceptibility breakpoints when using a 2-fold range around the literature estimates of the Hill coefficient parameter (k_H).

Table 4.4: Parameter values that result in simulations achieving a model-derived susceptibility breakpoint of 0.125mg/L (EUCAST defined susceptibility breakpoint) for ceftriaxone (CFO) and cefixime (CFM)).

Drug	Parameter	Change in the parameter value to achieve a model-derived susceptibility breakpoint of 0.125mg/L.	Literature value of the parameter
CFO	Intracellular: extracellular concentration ratio (α)	>2.5	0.15-0.61 ^a
CFM		>5	0.15-0.61 ^a
CFO	Minimum net growth rate of the bacteria (φ_{min})	< -3.1	-0.8 to -0.4 ^b
CFM		< -3.3	-1 to -0.6 ^b
CFO	Rate of drug elimination (δ)	<0.04	0.08-0.09 ^c
CFM		<0.08	0.17-0.22 ^d
CFO	Hill coefficient (k_H)	Could not meet the breakpoint for changes between 0.5-.5. Chosen range is 2-fold range around the literature estimates.	1.5-1.7 ^b
CFM			1.2-2.2 ^b

^a (Jacobs, *et al.* 1986)

^b (Foerster, *et al.* 2016)

^c (Patel, *et al.* 1982; Scully, *et al.* 1984)

^d (Faulkner, *et al.* 1988; Faulkner, *et al.* 1987a)

4.4 Discussion

In this study, we develop a within-host mathematical model to describe antibiotic treatment effects while considering NG interaction with host cells. The PD parameter values are estimated by fitting to bacterial load data from published *in vitro* time-kill studies and these estimates, together with PK parameters derived from the published literature, are then further refined through calibration of the model to empirical susceptibility breakpoints. The influence of intracellular states is assessed via comparison of model-derived susceptibility breakpoints using sub-models of increasing complexity starting with extracellular NG only and progressively adding intracellular states. Using these models, we observe that the addition of intracellular NG substantially reduces the model-derived susceptibility breakpoints. We further observe that our model-derived susceptibility breakpoints for ceftriaxone and cefixime are substantially lower than published empirical susceptibility breakpoints, with these differences not able to be resolved using realistic PK/PD parameter values.

Our simulations of drug concentration profiles for all tested drugs closely align with those that have been reported in the literature. The concentration profiles that we simulate for ceftriaxone (Patel, *et al.* 1982; Scully, *et al.* 1984), cefixime (Brittain, *et al.* 1985; Faulkner, *et al.* 1988) and gepotidacin (Taylor, *et al.* 2018b) align with plasma drug concentration measurements in the respective studies. The ratio of intracellular to extracellular drug concentration (C_i/C_e) for azithromycin (Fig. 4.3) is comparable with the drug accumulation that has been measured within uterine and cervical tissues (Foulds and Johnson 1993). We note that the level of drug accumulation can be dependent on the tissue type with high C_i/C_e ratios (range of 0.5 – 342) being observed for example in rectal tissues (Kong, *et al.* 2017). The C_i/C_e ratio for gentamicin resulting from model

simulations (Fig. 4.3) is also consistent with literature observations where a C_i/C_e ratio of around 2–5 was observed after around 3–4 days (Tulkens and Trouet 1974; Tulkens and Trouet 1978; Tulkens 1990).

We observe that the inclusion of intracellular NG model compartments leads to a large reduction in the model-derived susceptibility breakpoint from what is obtained from a model that only accounts for extracellular NG (Table 4.3). This is especially clear for ceftriaxone and cefixime, which fail to match the empirical susceptibility breakpoints using the full treatment model (consisting of extra and intracellular NG) but are able to match these breakpoints with the sub-model consisting of only extracellular NG. While we are unable to find studies that directly compare MIC values from *in vitro* and *in vivo* settings, there are clinical studies that report treatment failure despite predicting susceptibility based on breakpoint values. For instance, clinical treatment failures are reported for azithromycin (Tapsall, *et al.* 1998) and gentamicin (Ross, *et al.* 2019) at MIC of 0.125 – 0.25mg/L and 4mg/L, respectively. These MIC values are categorised as susceptible according to the empirical susceptibility breakpoints (see Table 4.3 for empirical susceptibility breakpoints).

In Chapter 3, we showed the importance of intracellular NG in prolonging natural infection duration and here we show the importance of intracellular antibiotic mediated killing in determining treatment success in our model. The relevance of different intracellular NG states (NG within PMN and epithelial cells) in determining treatment success is still debated by experts in the field (Theuretzbacher, *et al.* 2020). The difficulty in reaching a consensus on this issue is likely due to limited experimental evidence of the impact of intracellular antibiotic-mediated killing on treatment outcomes. Although *in vitro* models such as those developed using immortal cell lines (e.g., HeLa cells) (Gubish,

et al. 1979) have been used to explore the intracellular behaviour of NG, we are not aware of any study that considers antibiotic interactions with intracellular NG. Here, our findings on the model-derived susceptibility breakpoints in the presence of intracellular NG, suggest further experiments assessing the role of intracellular NG in determining treatment success could be valuable.

In estimating parameter values, we have had to rely extensively on *in vitro* data. While most PK parameters (e.g., volume of distribution, drug half-life) are based on plasma drug concentration profiles measured in patients, the PD parameters and some PK parameters rely on *in vitro* estimates. The experimental limitations of these *in vitro* studies, such as the use of constant drug concentrations and lack of intracellular bacteria, do not reflect the true *in vivo* environment and add potential for error in these parameters. While in some cases we are able to adjust these to reflect *in vivo* environment, such as replacing φ_{max} estimates from *in vitro* time-kill data with replication rates we estimate in Chapter 3 (see Table 3.2), for most parameters we could not account for this potential translational error. These natural growth rates estimated in Chapter 3 are used instead of φ_{max} estimates when modelling treatment effects in Chapters 4,5 and 6. We also adopt a parsimonious approach in relation to intracellular PK effects for PMN and epithelial cells, assuming these are the same, as although drug accumulation and penetration can depend on the host cell and tissue type (Kong, *et al.* (2017) and Van Bambeke, *et al.* (2006)) we lacked relevant data to support different estimates.

In Chapter 5, we further utilize this model to analyse differing treatment regimens with gepotidacin, gentamicin and azithromycin, for which the current model successfully matches empirical treatment outcomes. Further, we address the limitations of this model in regard to ceftriaxone and cefixime in Chapter 6 through a revised model that

incorporates the underlying drug-target binding kinetics of the two β -lactam antibiotics, ceftriaxone and cefixime.

4.5 Conclusions

In this chapter, we have developed a PK/PD analysis approach to study antibiotic interaction with NG in different cellular states and to compare the differences in MIC values derived from *in vitro* and *in vivo* settings. To the best of our knowledge, this is the first within-host mathematical modelling study that explores the intracellular antibiotic killing of NG. Our findings suggest the importance of considering intracellular dynamics when deciding on treatment regimens as the model-derived susceptibility breakpoints are observed to be substantially impacted by the killing of NG within PMN and epithelial cells. This also draws attention to the potential importance of further experimental studies that capture intracellular PK/PD effects in regard to gonorrhoea treatment. Such investigation into the intracellular antibiotic effects may be useful when developing novel antibiotics for gonorrhoea.

Chapter 5

Effectiveness of different treatment regimens for gonorrhoea

5.1 Introduction

In Chapter 4 we showed that in simulations, the antibiotic mediated killing of intracellular *Neisseria gonorrhoeae* (NG) is the primary determinant of successful infection clearance. Here we use this model to evaluate the effectiveness of two treatment regimens that are being trialled as future options; monotreatment with gepotidacin (GEP) and dual treatment with gentamicin (GEN) + azithromycin (AZM). In clinical trial settings both gepotidacin (Scangarella-Oman, *et al.* 2018; Taylor, *et al.* 2018b) and gentamicin + azithromycin (Kirkcaldy, *et al.* 2014; Rob, *et al.* 2020; Ross, *et al.* 2019) have shown potential for treating urethral NG infection. Clinical trials report much higher treatment effectiveness using dual therapy with gentamicin + azithromycin (100% cure rate) (Kirkcaldy, *et al.* 2014) than with gentamicin monotherapy (68-98% cure rate) (Dowell and Kirkcaldy 2013). This combination option is recommended as an alternative treatment option for patients who cannot be treated with the recommended treatment option of ceftriaxone, due to infection with ceftriaxone resistant strains, allergy or unavailability of ceftriaxone.

As clinical trials have limitations in terms of expense, duration and ethical constraints they are not ideal for optimising doses, regimens and drug combinations (Hook, *et al.* 2020). In this case, simulations through compartment PK models such as in Chisholm, *et al.* (2010b) are useful in determining the effective dosing regimens. With

the use of the model developed in Chapter 4, we can simulate a range of different treatment regimens and drug combinations to assess their effectiveness at various values of the minimum inhibitory concentration (MIC) which can potentially be used to guide future clinical trial design.

In this study, we use the model developed in Chapter 4 to assess the effectiveness of single dose strategies that have been tested in clinical trials of urethral treatment with GEP or GEN+AZM, as well as multiple dose strategies that are yet to be tested in clinical trials. We also analyse the importance of intracellular PK/PD dynamics in achieving successful infection clearance and find the intracellular drug concentration levels that are needed to achieve treatment success.

5.2 Methods

Treatment effects are evaluated using the model developed in Chapter 4 and here only a brief overview of the model is provided. The model considers the interaction of different bacterial states including extracellular (unattached and attached NG to epithelial cells) and intracellular NG (NG within polymorphonuclear leukocytes (PMN) and epithelial cells). The pharmacokinetics are modelled based on the characteristics of the individual drugs and pharmacodynamic effects are captured through the Hill function (see Chapter 4, Sections 4.2.2 and 4.2.3). Only the free drug (drug unbound to albumin) is considered in the analysis as only the free drug molecules are considered to be microbiologically active (Van Bambeke, *et al.* 2006; Wise 1986). As described in Chapter 4, Section 4.2.4, treatment is initiated on the day of the infection at the peak NG load (3.6th day for the point estimate), with infection viewed as being successfully cleared if total NG falls below 10 bacteria in ≤ 7 days. Parametric uncertainty is captured through Latin hypercube sampling (LHS) as described in Chapter 4, Section 4.2.4.

The associated PK/PD parameter values are given in Tables 4.1 and 4.2 (Chapter 4) and the natural infection model-related parameter values are given in Table 3.2 (Chapter 3). The model equations for monotreatment with gepotidacin are given in Appendix B, Section B.3.1 and for dual treatment (gentamicin + azithromycin) in Appendix C, Section C.1

5.2.1 Testing different treatment strategies

In this study, we look at the effectiveness of several possible treatment strategies by simulating the dosing regimens that are summarised in Tables 5.1 and 5.2. Both single and multiple dose strategies are tested for the monotreatment (using gepotidacin) and dual treatment (using gentamicin + azithromycin) options. As a validation process, we assess treatment strategies that are tested in clinical trials as well as some possible novel strategies. For gepotidacin, we test single dose treatments of 1.5g and 3g as tested in clinical trials (Scangarella-Oman, *et al.* 2018; Taylor, *et al.* 2018b) and higher single doses of 4.5g and 6g which have only been previously tested *in vitro* (VanScoy, *et al.* 2020). As novel gepotidacin treatment regimens, we also test multiple dose regimens including alternative spacing of doses. For the combination of gentamicin + azithromycin, we test the single dose options of 240mg gentamicin and 1g azithromycin (Ross, *et al.* 2019) or 2g azithromycin (Kirkcaldy, *et al.* 2014) which have been previously tested in the respective clinical trials. We also consider several multiple dose regimens for the gentamicin + azithromycin combination that have not been previously tested in clinical trials. Here, for our multiple dose regimens using gentamicin, we choose a daily administration of 240mg which is the dose amount that has been tested in clinical trials (Daly, *et al.* 1997; Kirkcaldy, *et al.* 2014; Ross, *et al.* 2019), and limit the duration of dosing to 3 days basing on medical advice relating to toxicity concerns (Queensland Health 2018).

For multiple dose strategies of gentamicin which extend over 3 days, we also test the impact of limited non-adherence by the patient. Specifically, we consider a uniformly distributed delay of between 0 and 24h to the 2nd dose in comparison to the recommended schedule, with subsequent doses then taken at the correct spacing from the previous dose. Treatment efficacy is analysed when 15%, 25%, 50%, 75% and 100% of the simulations deriving from the LHS samples are assumed to be subject to non-adherence.

Any regimen that is approved for the treatment of gonorrhoea should have $\geq 95\%$ treatment efficacy (Moran and Levine 1995; World Health Organization 2003). Here, we adopt an analogous definition in terms of our simulations whereby for a given MIC value if $\geq 95\%$ of simulations that are generated from our LHS samples achieve treatment success we consider that particular treatment strategy to be effective. Throughout the remaining chapters we define simulated 'treatment effectiveness' as the proportion of model simulations that result in successful infection clearance. We note that the sources of variation present in our model are not directly comparable to the variability observed during the treatment of natural human infection and these percentages cannot be directly interpreted as estimates of treatment effectiveness.

In this chapter, by MIC we refer to the value of the Hill function MIC parameter. We test treatment strategies at MIC values that are reported in epidemiological studies which cover values associated with reduced susceptibility: for gepotidacin at MIC of 0.05, 0.125, 0.25, 0.5 and 1mg/L (Scangarella-Oman, *et al.* 2018), for gentamicin at MIC of 4, 8 and 16mg/L (Chisholm, *et al.* 2011; Kirkcaldy, *et al.* 2014; Ross, *et al.* 2019) and for azithromycin at MIC of 0.5 and 1mg/L (Clinical and Laboratory Standards Institute 2018; European Committee on Antimicrobial Susceptibility Testing 2019). As observed in Chapter 4, as the value of the MIC increases, we reach a cut-off that differentiates between $\geq 95\%$ treatment success and $< 95\%$ treatment success. We refer to this cut-off (the largest

value of the MIC where $\geq 95\%$ treatment success is achieved) as the ‘model-derived susceptibility breakpoint’ as any increase from this breakpoint results in this strategy being unsuccessful under our definition. These model-derived susceptibility breakpoints are compared with what we term ‘empirical susceptibility breakpoints’ (see Chapter 4, Section 4.2.5 for definition).

5.2.2 Modelling dual antibiotic treatment.

Drug interactions are commonly modelled using Loewe additivity (Loewe 1928) when their mechanisms of action or targets are similar, or Bliss independence (Bliss 1939) when these differ. In simple terms, Loewe additivity combines the effects of both drugs into a single drug of higher potency, while Bliss independence assumes independent multiplicative effects of the two drugs on bacterial survival. As gentamicin and azithromycin have similar targets and mechanisms of action (see Chapter 2, Section 2.5.2), we use the concept of Loewe additivity to model dual treatment effects, according to the method described in Dini, *et al.* (2018). Further details on the approach, including dual treatment model equations, are given in Appendix C, Section C.1.

With combination therapy, drugs can exhibit additive, synergistic or antagonistic effects. As *in vitro* studies have not demonstrated synergistic or antagonistic effects for the gentamicin + azithromycin combination (Furuya, *et al.* 2006; Pereira, *et al.* 2012; Singh, *et al.* 2018) we conduct our analysis assuming additive effects for this combination.

5.2.3 PK indices

To compare the effectiveness of different treatment regimens of gepotidacin monotreatment, we evaluate three PK indices: time above the MIC (t_{MIC}); the ratio of

area under the drug concentration curve to the MIC (AUC/MIC); and the ratio of peak drug concentration to the MIC (C_{\max}/MIC). The area integrated over the total drug concentration curve ($\text{AUC}_{0-\infty}/\text{MIC}$) is used as the default AUC/MIC index but we also test the area under the curve above the MIC (removing the area below the MIC from the total area under the curve) and AUC over a fixed time period of 7 days ($\text{AUC}_{0-7}/\text{MIC}$) as alternative indices (see Appendix C, Section C.2.3). For multiple dose strategies, we also calculate the total time the drug concentration remains above the MIC (t_{MIC}) and this is used as the default index of t_{MIC} but we also consider some alternative definitions of t_{MIC} in Appendix C, Section C.2.3. We calculate the three PK indices for both intracellular and extracellular drug concentrations and they are differentiated, respectively, with subscripts ‘in’ and ‘ex’: $t_{\text{MIC}_{\text{in}}}$, $\text{AUC}/\text{MIC}_{\text{in}}$, $C_{\max}/\text{MIC}_{\text{in}}$ and $t_{\text{MIC}_{\text{ex}}}$, $\text{AUC}/\text{MIC}_{\text{ex}}$, $C_{\max}/\text{MIC}_{\text{ex}}$.

5.2.4 Sensitivity of monotreatment and dual treatment options to changes in the MIC

We also compared changes in treatment success with increasing MIC values between monotreatment with gepotidacin and dual treatment with gentamicin and azithromycin, where the combination was modelled using Loewe additivity. For this comparison, for monotreatment we assess the change in the bacterial growth rate as a function of MIC through the function,

$$\varphi(C) = \varphi_{\max} - \frac{(\varphi_{\max} - \varphi_{\min}) \left(\frac{C}{\text{MIC}} \right)^{k_H}}{\left(\frac{C}{\text{MIC}} \right)^{k_H} - \frac{\varphi_{\min}}{\varphi_{\max}}} \quad (5.1)$$

where $\varphi(C)$ is the net bacterial growth rate when exposed to an antibiotic concentration, C and the other parameters are as described in Chapter 4, Section 4.2.2. For dual treatment strategy modelled under the concept of Loewe additivity, the change

in net bacterial growth rate is assessed according to Appendix C, Eq. C.1. This analysis is conducted using the point estimates given in Chapter 4, Table 4.1.

5.3 Results

5.3.1 *Gepotidacin monotreatment.*

The results of model simulations for gepotidacin monotreatment are summarised in Table 5.1. Gepotidacin doses of 1500mg, irrespective of whether administered as single or multiple doses (accumulating to 1500mg), achieve treatment success for $\text{MIC} \leq 0.5\text{mg/L}$, while most of the tested strategies with a total dose of 3000mg (single and multiple) achieve success for $\text{MIC} \leq 1\text{mg/L}$. In our model, clearance behaviour is invariant when the MIC/dose ratio is held fixed (see Appendix C, Section C.2.1), with higher dose strategies of 4.5g and 6g gepotidacin being successful for $\text{MIC} \leq 1.5\text{mg/L}$ and $\text{MIC} \leq 2\text{mg/L}$, respectively (Appendix C, Table C.1).

We also examine multiple dose regimens for gepotidacin that have not yet been tested in clinical trials. In most of the strategies that we test, single and multiple dose strategies with the same total dose amount are successful (achieve $\geq 95\%$ clearance) for the same assigned value of the MIC parameter in the Hill function. However, for the $500\text{mg} \times 6, 24\text{h}$ apart strategy at $\text{MIC}=1\text{mg/L}$ infection is cleared in only $\sim 66\%$ of simulations from LHS samples, despite all other tested strategies with a total dose amount of 3000mg clearing $\geq 95\%$ of simulations at this MIC. We discuss this in detail in the next Section, 5.3.1.1.

Table 5.1: Percentage of simulations using LHS samples (out of 5402) that clear infection in ≤ 7 days when using single and multiple dose gepotidacin treatment strategies.

Treatment strategy	Percentage of simulations that clear infection				
	MIC (mg/L)				
	0.05	0.125	0.25	0.5	1
1500mg single dose	100.00	100.00	99.98	95.04	20.84
500mg \times 3, 8h apart	100.00	100.00	100.00	99.22	38.17
500mg \times 3, 12h apart	100.00	100.00	100.00	99.69	40.47
500mg \times 3, 24h apart	100.00	100.00	100.00	98.97	14.07
3000mg single dose	100.00	100.00	100.00	99.98	95.04
500mg \times 6, 8h apart	100.00	100.00	100.00	100.00	99.85
500mg \times 6, 12h apart	100.00	100.00	100.00	100.00	99.52
500mg \times 6, 24h apart	100.00	100.00	100.00	100.00	66.29
1500mg \times 2, 8h apart	100.00	100.00	100.00	100.00	95.72
1500mg \times 2, 12h apart	100.00	100.00	100.00	100.00	98.48
1500mg \times 2, 24h apart	100.00	100.00	100.00	100.00	99.33

5.3.1.1 Effectiveness of different dosing strategies of gepotidacin

We calculate different PK indices (as described in Section 5.2.3) to compare the effectiveness of single and multiple gepotidacin dosing strategies and different dosing intervals and present separate indices for extracellular and intracellular states. For the multiple dose regimens that we test using 500mg gepotidacin, a 24h time gap between doses is less effective than strategies with 8 or 12h gaps (Table 5.1) for a total drug dose of 1500mg or 3000mg. In particular, while other strategies accumulating to 3000mg are effective at a MIC of 1mg/L, the dosing strategy of 500mg \times 6, at 24h interval fails (only 66.29% of simulations achieve clearance). This failure can be explained by the intracellular drug concentration being maintained above the MIC ($t_{MIC_{in}}$) for only 47% of the dosing interval and corresponding spikes in the bacterial load (Fig. 5.1). By comparison, for 500mg \times 6 dosing regimens at intervals of 8 and 12h the intracellular drug concentration is above 1mg/L for 100% and 94% of the dosing interval, respectively.

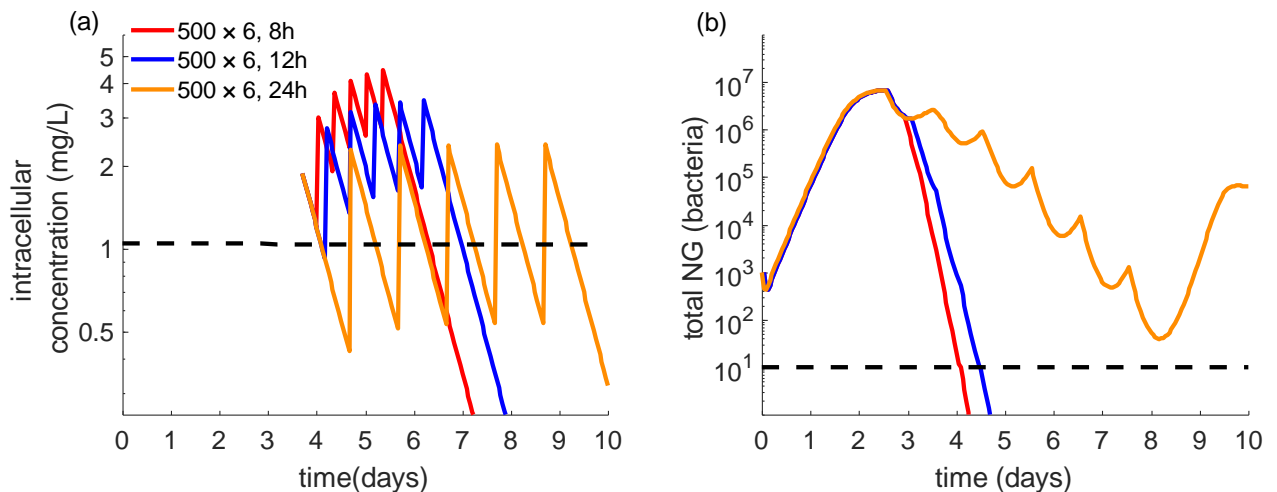


Figure 5.1: Effect of gepotidacin dose spacing of 8,12 and 24h in a 500mg \times 6 schedule on (a) intracellular drug concentration and (b) total NG load. Dashed lines

indicate MIC of 1mg/L (a) and infection clearance cut-off of 10 bacteria (b).

Parameter values are specified in Chapter 4, Table 4.1.

From the simulation results in Table 5.1, we also note that in most cases the multiple dose regimens with the same total dose amount clear infection in a higher number of simulations than a single dose strategy. For example, the 1500mg single dose strategy achieves clearance in 95.04% simulations while the 500mg \times 3 strategies that we test with dosing frequencies of 8, 12 and 24h clear infection in >98% simulations. Here, the multiple dose strategies achieve an increased $t_{MIC_{in}}$ in comparison to the single dose strategy (Appendix C, Fig.C.1). The highest value of this PK index also occurs with the most effective dosing interval (24h) when we considered a total dose of 3000mg split into two (1500mg \times 2 given 8, 12 or 24h apart) as shown in Appendix C, Fig. C.1.

5.3.1.2 Threshold gepotidacin concentration required for treatment success.

We also attempt to determine the drug concentrations that are required to be maintained for treatment success. Extracellular PK indices fail to sharply distinguish simulations in which treatment succeeds from those where it fails, as there are simulations with the same PK index value but opposite treatment outcomes (Fig. 5.2). The ratio of peak intracellular drug concentration: MIC (C_{max}/MIC_{in}) index is also unable to discriminate between success or failure to clear infection. In contrast, intracellular indices for the ratio of area under the total drug concentration curve to the MIC (AUC/MIC_{in}) and time above the MIC ($t_{MIC_{in}}$), clearly differentiate between treatment success and failure. However, the $t_{MIC_{in}}$ value that differentiates treatment success and failure, varies in our simulations as a function of the dosing schedule, whereas a common cut-off across all dosing schedules could be obtained with the AUC/MIC_{in} index (Fig.5.2). This behaviour

is preserved under the alternative definition whereby only the AUC above the MIC is considered (Appendix C, Fig. C.3). The observation of dose-dependence in regard to $t_{\text{MIC}_{\text{in}}}$ cut-off is also preserved with the alternative forms of $t_{\text{MIC}_{\text{in}}}$ calculations that we consider (Appendix C, Fig. C.2). We therefore focus on the AUC/MIC_{in} index for gepotidacin in regard to determination of a threshold parameter.

From the simulated concentration profiles, we observe that treatment success for gepotidacin occurs in simulations where AUC/MIC_{in} >150h (Fig.5.2 and Appendix C, Fig. C.3). We note that there are 6 simulations with AUC/MIC_{in} in the range of 147-150h that fail to clear the infection. The behaviours of these failed simulations are shown in Appendix C, Fig.C.4. In these unsuccessful simulations, although the total bacterial load declines close to the infection clearance threshold (to ~11 bacteria in some instances), the exact model criterion for infection clearance (total NG load <10 bacteria) is not achieved. Therefore AUC/MIC_{in} >150h, is a suitable threshold to differentiate between simulated treatment success and failure.

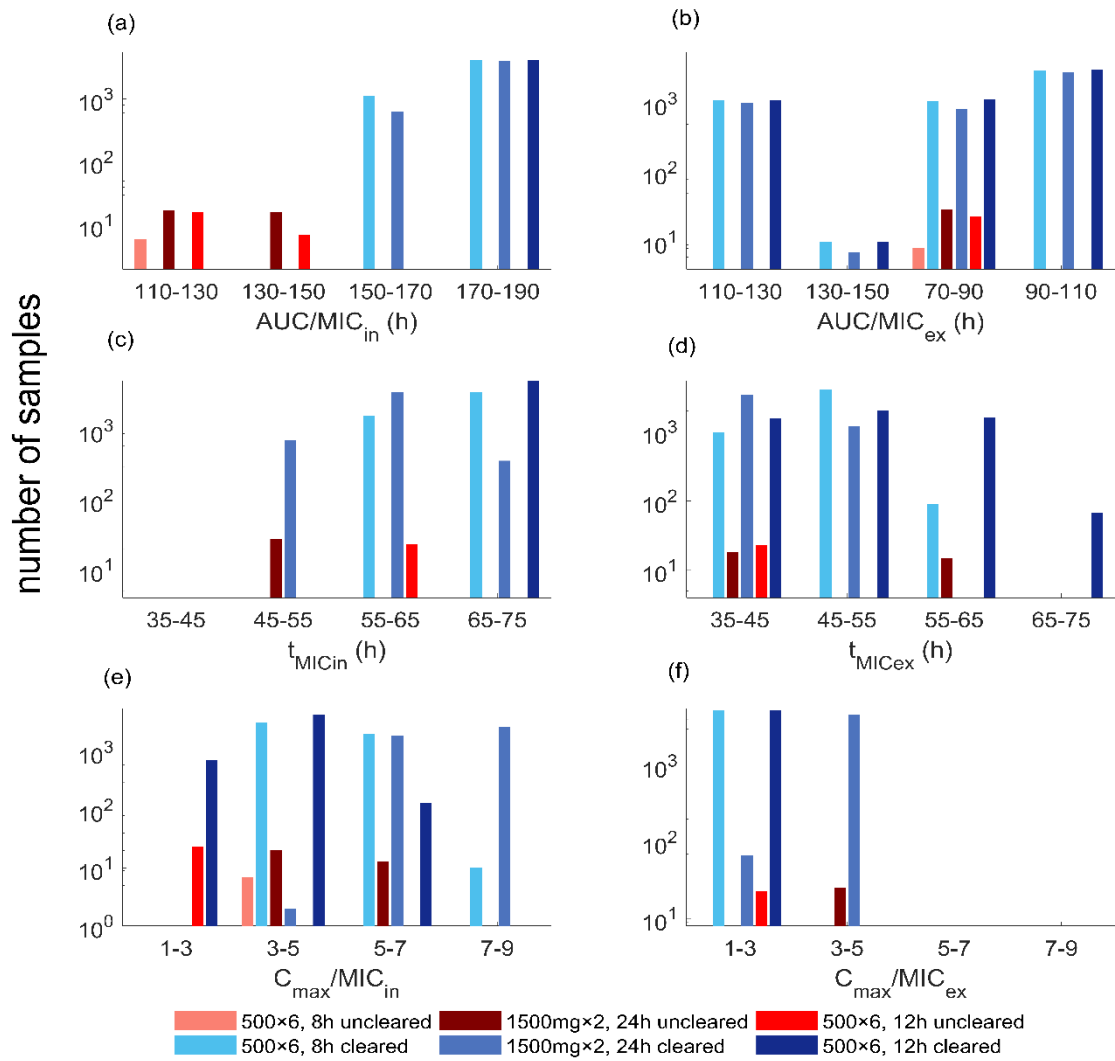


Figure 5.2: Comparison of PK/PD indices to differentiate treatment success and failure. The ratio of area under the curve to the MIC are shown for: (a) intracellular and (b) extracellular drug concentration; the time above the MIC calculated for intracellular (c) and extracellular (d) drug concentration; the ratio of peak drug concentration to the MIC for intracellular (e) and extracellular (f) drug concentration.

5.3.2 Dual treatment with gentamicin + azithromycin

5.3.2.1 Effectiveness of different dosing strategies of gentamicin + azithromycin

The effectiveness of dual treatment with gentamicin + azithromycin across single and multiple dose strategies is summarised in Table 5.2. For the same total dose amount, multiple doses of gentamicin and multiple doses of azithromycin result in similar effectiveness to the single dose strategy and the results do not differ substantially by dosing frequencies. Treatment failures are associated with reduced intracellular drug concentration as for both drugs, the parameters that are related to increasing the intracellular drug concentration (the rate of the drug moving to and from the intracellular compartment and volume of distribution) are associated with infection clearance (Appendix B, Fig. B.4).

Among the tested strategies, only $240\text{mg} \times 3$ gentamicin, given 24h apart in combination with 2g single dose of azithromycin is effective at high MIC for both gentamicin and azithromycin (16 mg/L and 1 mg/L, respectively, Table 5.2). As this is a multiple dose strategy, we evaluate the treatment efficacy reflecting a scenario of patient non-adherence where the second dose is assumed to be taken later (24-48h after the first dose) than the prescribed interval. For the 100% non-adherence scenario (in all LHS samples, the second dose is not taken at the correct time), 94.13% treatment success is observed at MIC for gentamicin and azithromycin of 16mg/L and 1 mg/L, respectively, showing similar effectiveness to the 100% adherent scenario (Appendix C, Table C.2).

5.3.2.2 Sensitivity of monotreatment and dual treatment options to changes in the MIC

The fraction of simulations clearing the infection is much more sensitive to a doubling of the MIC with monotreatment (Table 5.1) than in the dual therapy (Table 5.2). For example, with a 1500mg single dose of gepotidacin, as the MIC increases from 0.5

to 1mg/L, the percentage of simulations that successfully clears the infection declines from 95% to 21%. However, under dual treatment with 240mg gentamicin and 1g azithromycin and with a MIC for azithromycin of 0.5mg/L, the percentage of simulations that successfully clears the infection declines only marginally from 96% to 87% as the gentamicin MIC doubles from 4 to 8mg/L.

The above difference between monotreatment and dual treatment options can be more clearly seen when monotreatment with gentamicin and monotreatment with azithromycin are compared with the dual treatment option of gentamicin + azithromycin. As an example, when treated using gentamicin monotreatment, for a fixed gentamicin concentration of 6mg/L, as the MIC for gentamicin doubles from 4mg/L to 8mg/L, the net bacterial growth rate increase from -0.43h^{-1} to 0.18h^{-1} (Appendix C, Fig. C.5). However, for the same changes in the MIC for gentamicin and assuming the NG strain has a fixed MIC for azithromycin of 0.5mg/L, with dual treatment the net bacterial growth rate only increases from -1.09h^{-1} to -1.03h^{-1} . This difference between mono and dual therapy occurs in part due to using Loewe additivity to model the combination therapy between gentamicin and azithromycin because of their similar mechanisms of action. Loewe additivity combines both antibiotics into a single drug of higher effect and here, based on the parameter values used in this example azithromycin is the dominant drug in the interaction (see Appendix C, Fig. C.5). This means that even large changes in the gentamicin MIC have a relatively limited effect on bacterial killing rates and treatment effectiveness in this dual-therapy situation.

Table 5.2: Percentage of simulations that clear the infection (out of 5402 LHS samples) at various MIC values when using dual treatment gentamicin (GEN) and azithromycin (AZM) strategies.

Treatment strategy	Percentage of simulations that clear infection					
	(Gentamicin/azithromycin) MIC ^a (mg/L)					
	(4/0.5)	(4/1)	(8/0.5)	(8/1)	(16/0.5)	(16/ 1)
strategies with gentamicin total accumulation of 240 mg						
240mg GEN + 1g AZM	95.59	85.95	86.94	61.05	78.47	39.73
240mg GEN + 2g AZM	99.70	95.59	98.80	86.97	97.69	78.47
80mg GEN × 3, 8h apart + 1g AZM single dose ^b	95.59	86.02	86.97	61.09	78.52	39.75
120mg GEN × 2, 8h apart + 1g AZM single dose	95.61	86.17	86.98	61.96	78.86	39.80
strategies with gentamicin total accumulation of 480mg						
120mg GEN × 2, 12h apart for 2 days + 1g AZM single dose	99.78	99.32	97.91	93.71	92.50	76.21
240mg GEN × 2, 24h apart + 1g AZM single dose	99.78	99.22	97.83	93.10	92.08	74.84
strategies with gentamicin total accumulation of 720mg						
240mg GEN × 3, 24h apart + 1g AZM single dose	99.91	99.74	98.78	96.37	94.48	82.19
240mg GEN × 3, 24h apart + 2g AZM single dose	100.00	99.91	99.96	98.96	99.76	95.45
240mg GEN × 3, 24h apart + 1g AZM × 2, 24h apart	100.00	99.91	99.85	98.48	99.35	93.54

^a Tested MIC for gentamicin denotes susceptibility ($\leq 4\text{mg/L}$), intermediate susceptibility ($8\text{--}16\text{mg/L}$) and resistance ($\geq 32\text{mg/L}$) (Brown, *et al.* 2010) and tested MIC for azithromycin of 0.5 and 1mg/L are the empirical susceptibility breakpoints (Clinical and Laboratory Standards Institute 2018; European Committee on Antimicrobial Susceptibility Testing 2018).

^b Results are shown only for the 8h strategy as clearance did not differ for dosing intervals of 8,12 and 24h.

5.4 Discussion

In this chapter, we use the model developed in Chapter 4 to test different treatment strategies, drug combinations and dosing frequencies to better understand regimens that would be effective for a range of MIC values. We find that for gepotidacin, gentamicin and azithromycin, there are limited improvements in infection clearance using multiple dose regimens that have the same total drug dose as a single dose regimen. We also analyse the correlation of PK indices with treatment success and the level of intracellular drug concentration that must be maintained to achieve successful infection clearance. For gepotidacin monotreatment, we find that in our simulations an AUC/MIC index value of above 150h, calculated using the intracellular drug concentration, is correlated with treatment success. We also note that the proportion of simulations clearing infection is less sensitive to changes in individual drug MIC under dual treatment with gentamicin and azithromycin than monotreatment with gepotidacin.

For single doses of 1500mg and 3000mg gepotidacin at a MIC ≤ 0.5 mg/L the model results accord with the 100% treatment success that is observed in clinical trials (Scangarella-Oman, *et al.* 2018; Taylor, *et al.* 2018b). Results are less consistent at a MIC of 1mg/L, with our model achieving >95% treatment success for a 3000mg single dose compared with success with only 1 out of 3 isolates with MIC=1mg/L in the clinical trial conducted by Scangarella-Oman, *et al.* (2018). However, with only 3 such isolates in the study, it is difficult to draw any strong conclusions about the validity of our model results for this MIC. Further clinical assessment using a larger sample size would be useful in providing a more definitive estimate of efficacy for comparison with our results.

We are able to describe the treatment effectiveness of gepotidacin using the intracellular area under the curve index. Consistent with our findings, a strong correlation

between AUC/MIC index and bacterial killing of two gram-positive pathogens (*S.aures* and *S.pneumoniae*) is observed by Bulik, *et al.* (2017). While extracellular indices from our model align with calculations based on plasma drug concentrations (Negash, *et al.* 2016), treatment success and failure could only be clearly differentiated through intracellular indices. This is because, in our model implementation, a majority of NG reside intracellularly (Chapter 3, Section 3.3.2.1) and treatment success is observed to be mainly determined through the killing of intracellular NG (Chapter 4, Table 4.3).

Our analysis of dual treatment using single doses of gentamicin + azithromycin is comparable, to a certain extent, with the limited data available from clinical trials. The two clinical trials that have been conducted for this drug combination report an overall genital infection treatment success rate of 94% (Ross, *et al.* 2019) and 100% (Kirkcaldy, *et al.* 2014) using 240mg gentamicin combined with 1g and 2g azithromycin doses, respectively. In the clinical trial by Ross, *et al.* (2019), 97.7% and 95.7% of isolates had MIC for gentamicin $\leq 4\text{mg/L}$ and MIC for azithromycin $\leq 0.5\text{mg/L}$, respectively. However, in these studies treatment success is not disaggregated into MIC ranges and therefore, a clear comparison cannot be made with our model simulation results for MIC for gentamicin and azithromycin of 4mg/L and 0.5mg/L, respectively.

We test multiple dose gentamicin strategies in combination with azithromycin which have so far not been tested in clinical trials. Our results indicate that for the same total dose amount of gentamicin and for the same total dose amount of azithromycin, multiple doses of gentamicin and multiple doses of azithromycin result in similar effectiveness to single dose strategies (Table 5.2). When using multiple doses of gentamicin, the dose amounts need to be monitored carefully as it has a high risk of toxicity (Drusano, *et al.* 2007). From our simulations, we also found 2g azithromycin to be more effective than 1g dose, especially at high MIC for gentamicin such as 16mg/L.

However, there is also concern over the use of 2g azithromycin as in the clinical trial conducted by Kirkcaldy, *et al.* (2014), 2g azithromycin was not as well tolerated as the 1g dose. In contrast to this observation, Rob, *et al.* (2020) found that a 2g dose is tolerated well when administered with food. Our findings on the use of multiple doses and high azithromycin doses in improving treatment effectiveness suggest the need for further assessment of safety and tolerability of multiple doses of gentamicin and appropriate administration methods (with or without food) of azithromycin. Our results in regard to dual-therapy being less sensitive to increase in MIC may be associated with the use of Loewe additivity to model drug interaction. This choice was made due to the similarity in mechanisms of action but if the drugs act more independently than we assume, it is possible that there would be increased sensitivity to individual drug MIC. In the clinical trials, the efficacy of the individual drugs used in the gentamicin + azithromycin regimen is not assessed and the benefit of adding a second drug and the role of gentamicin are not investigated (Kirkcaldy, *et al.* 2014; Rob, *et al.* 2020; Ross, *et al.* 2019). With the similar mechanisms of action and targets used by both drugs it would be interesting conduct further experimentation on the probability of resistance development for this regimen.

In this study, we have only evaluated clearance and have not focused on the potential to suppress the development of resistance through multiple-dose regimens or dual treatment options. While it has been suggested that multiple dose regimens are better at suppressing the emergence of drug resistance (Theuretzbacher, *et al.* 2020), this idea has not been substantiated in the literature. For example, in the context of *M. genitalium*, Horner, *et al.* (2018) found multiple dose regimens of azithromycin to be better in suppressing the emergence of resistance while Read, *et al.* (2017) did not find such an association. The emergence of drug resistant NG strains under treatment was observed (Scangarella-Oman, *et al.* 2018) in a phase two clinical trial using single doses of

gepotidacin. In this case, it will be interesting to assess strategies that can minimise the emergence of resistance, including using gepotidacin in dual therapy and the possibility of multiple dose regimens in suppressing resistance. Extensions of the model to include resistance mechanisms might facilitate a more detailed exploration of these issues, with the potential for comparisons with a phase 3 clinical trial (ClinicalTrials.gov Identifier: NCT04010539) currently testing a two-dose regimen of gepotidacin (3000mg \times 2).

5.5 Conclusions

Our model provides a framework for assessing the effectiveness of novel treatment strategies over a range of MIC values, with model-produced cure rates aligning with observations from clinical trials for gepotidacin, gentamicin and azithromycin. Using this model, we are able to determine effective dosing intervals, dose amounts and assess the importance of intracellular PK/PD dynamics in determining NG infection clearance. Our work provides insight into the potential importance of intracellular antibiotic mediated killing in determining treatment success for gonorrhoea, which thus far has not been explored in experimental studies. In addition, our findings and the model more generally may have utility as a guide in identifying treatment regimens to explore further in clinical trials. In the next chapter, we return to the problem of accurately modelling treatment effects for NG using ceftriaxone and cefixime and address this using a revised model that captures drug-target interactions in greater detail.

Chapter 6

Evaluation of ceftriaxone and cefixime treatment strategies using a model that incorporates drug-target binding

6.1 Introduction

As discussed in Chapter 2, Section 2.5, ceftriaxone (CFO) and cefixime (CFM) are two β -lactam drugs that remain effective treatment options for gonorrhoea, although CFO is typically recommended in 1st-line treatment. The antibacterial activity of β -lactams involves inhibiting bacterial cell wall synthesis through binding of the β -lactam ring to the bacterial target, penicillin binding proteins (PBP). PBP are membrane-bound enzymes that catalyse cell wall synthesis. *Neisseria gonorrhoeae* (NG) has four types of PBP (PBP 1,2, 3 and 4), with differing drug binding affinities (Barbour 1981; Dougherty, *et al.* 1980; Stefanova, *et al.* 2004) but PBP 3 and 4 are not considered to be important for cell viability (Dougherty, *et al.* 1981). While high-levels of β -lactam binding to PBP1 on NG have been observed (Ropp, *et al.* 2002), PBP2 is considered to be the main lethal target for this pathogen (Powell, *et al.* 2009; Unemo and Nicholas 2012).

The model developed in Chapter 4 successfully reproduces infection clearance times and model-derived susceptibility breakpoints observed in the literature for the non β -lactam drugs considered. For ceftriaxone and cefixime this failure to meet empirical susceptibility breakpoints (see Chapter 4, Section 4.2.5 for definition) occurs when we include intracellular NG states, suggesting that some revision to our approach to incorporate treatment using β -lactams might be needed. When considering the

mechanism of action of β -lactams, Williamson and Tomasz (1985) showed that bacteriostasis occurs only when a large proportion of PBP are acylated with further increase in acylation leading to bactericidal effects. Apart from these transition features, this class of drugs also exhibit moderate levels of post antibiotic effect (PAE) against gram negative bacteria (Hanberger, *et al.* 1990; Hanberger, *et al.* 1991) such as NG. We hypothesised that the failure to adequately describe treatment with these drugs in Chapter 4 might be rectified by revising the underlying model to explicitly capture drug-target binding dynamics. This facilitates more direct incorporation of the transition to bacteriostatic and bactericidal states and PAE effects of ceftriaxone and cefixime as has been achieved for other drugs such as tetracycline (Abel zur Wiesch, *et al.* 2015).

Explicit drug-target interactions have been incorporated into within-host models for *V. cholerae* and *E. coli* (Abel zur Wiesch, *et al.* 2015), *P.aeruginosa* (Walkup, *et al.* 2015), and tumour cells (Singh, *et al.* 2019) but we are not aware of similar work for NG. In the approach used by Abel zur Wiesch, *et al.* (2015), drug-target binding is explicitly modelled, with effects on bacterial growth and death depending on the fraction of free target molecules. Here, we develop a similar model that incorporates β -lactam binding to PBP on NG but with simplifying assumptions due to the complex nature of within-host interactions of NG infection. In the study by Abel zur Wiesch, *et al.* (2015), each bacterium is assumed to have a fixed number of target molecules representing independent binding sites and an arbitrary number of these target molecules on a bacterium can be bound by drug molecules. With this approach bacteria are classified into compartments based on the number of bound target molecules and therefore explicitly captures the distribution in the number of bound target molecules across the bacterial population. In contrast, we assume that within a given state (intracellular/extracellular), at a specific point in time, each bacterium has the same number of bound target molecules.

In this study, we aim to test the ability of our model to reproduce known clearance behaviour for ceftriaxone and cefixime at epidemiologically observed minimum inhibitory concentrations (MIC). We explore how drug binding to PBP initiates bacteriostatic and bactericidal effects and identify possible factors contributing to the unsuccessful infection clearance in simulations. We also explore the effects of different dosing regimens and the PK characteristics of the simulations that clear infection.

6.2 Materials and Methods.

6.2.1 Mathematical Model

The starting point for the drug-target binding treatment model is the multi-cell natural infection model described in Chapter 3. Briefly, this involves four different NG states: unattached NG (B); NG attached to epithelial cells (B_a); NG within PMN (B_s); and NG within epithelial cells (B_i). We define the term ‘extracellular NG’ to denote unattached and attached NG while the term ‘intracellular NG’ denotes NG surviving and replicating within PMN and epithelial cells. Treatment effects are introduced to this base model as described below.

6.2.1.1 Description of β -lactam action

The antibiotic action of β -lactam drugs is mediated by binding of the drug’s β -lactam ring to the membrane-bound PBP molecules on NG. As described above, for these drugs, acylation of a large proportion of PBP is required to reach bacteriostasis, with further increases in acylation beyond this threshold leading to bactericidal effects (Williamson and Tomasz 1985). As PBP2 is considered to be the main lethal target (Powell, *et al.* 2009; Unemo and Nicholas 2012), we consider drug interactions with a single PBP type on NG, without including specific features to differentiate between PBP types.

6.2.1.2 Modelling drug-target binding kinetics

The reaction of antibiotics with PBP targets is defined by the formula $A + T \rightarrow T_b$, where the antibiotic molecules A react with the target molecules T with a rate constant k_{PBP} forming the drug-bound PBP complex, T_b . The binding of the drug to PBP targets is assumed to be an irreversible reaction (Frère 1995).

6.2.1.3 Modelling bacteriostatic and bactericidal effects

The initiation of bacteriostatic and bactericidal effects is considered to be dependent on the fraction of PBP molecules to which drug is bound (referred to henceforth as the drug-bound PBP fraction). We denote the drug-bound PBP fractions associated with extracellular and intracellular NG as f_{bound_e} and f_{bound_i} , respectively. Here, for simplicity, we do not differentiate between free and drug bound PBP targets on NG within epithelial cells and PMN, so the same f_{bound_i} fraction is associated with both intracellular NG populations.

We then introduce a threshold (f_c) for the drug-bound PBP fraction above which bacteriostatic and bactericidal effects occur. Data directly relating NG growth to drug-bound PBP fractions were not available and so we elected not to try to estimate separate thresholds differentiating bacteriostatic and bactericidal effects. We instead assume that both these effects are initiated once the drug-bound PBP fraction exceeds a threshold, which we denote by f_c , assuming the same threshold applies in both intracellular and extracellular states. At this point bacteria in the relevant state are transferred to a ‘dormant NG’ state with rate-constant $k_{dormant}$. In dormant NG states, we assume that bacteria no longer replicate and are subject to antibiotic mediated killing at rates defined via a modified Hill function, depending on the drug-bound PBP fraction in the relevant intracellular or extracellular environment. Dormant NG states are denoted by the addition

of a prime symbol (') to the relevant bacterial states: unattached dormant NG (B'); dormant NG attached to epithelial cells (B_a'); and dormant NG surviving and replicating within PMN (B_s') and epithelial cells (B_i').

6.2.1.4 Modelling the PBP target molecules

The numbers of free and drug-bound PBP molecules are dynamic quantities reflecting the underlying bacterial population model, available drug and the degree of saturation of PBP. We assume that the total number of PBP targets is proportional to the total bacteria with a constant number of PBP sites per bacterium (y). We estimate y using information on the number of PBP molecules per *E.coli* cell and the relevant surface areas of *E.coli* and NG. As the surface area of an *E.coli* cell ($3.8 - 6.28 \mu m^2$ (Prats and de Pedro 1989; Young 2006)) and of the gonococcus are similar (approximately $2.26 - 6.28 \mu m^2$, Chapter 3, Section 3.2.2.1), we assume the number of PBP molecules per gonococcus to be in the same range as reported for *E.coli* in Dougherty, *et al.* (1996) so that $y \approx 120 - 220$. With antibiotic and PMN mediated bacterial killing, both free and drug-bound PBP targets are removed from the system. There is also a shift of free and drug-bound PBP between intracellular and extracellular respective states due to NG entering and exiting cells (see Appendix D, Section D.1 for model equations).

6.2.1.5 Modelling the free drug molecules

As in Chapters 4 and 5, we consider only the free drug to be microbiologically active. The number of free drug molecules is calculated as the total number of drug molecules \times free drug fraction (f_u). We did not explicitly model drug binding to plasma proteins due to the low binding and high unbinding rates for drug to albumin (Stoeckel, *et al.* 1981; Stoeckel, *et al.* 1988), which lead to negligible differences in infection clearance times when this process is included in model simulations.

While the free drug fraction for cefixime is reported to be independent of drug concentration ($f_u \approx 0.31$) (Faulkner, *et al.* 1987b), for ceftriaxone, free drug fractions vary from $\sim 0.05 - 0.17$ as the drug concentration is varied from approximately $0.5 - 300\text{mg/L}$ (Popick, *et al.* 1987; Stoeckel, *et al.* 1981). From our model simulations, we observe that the infection clearance times are only sensitive to log changes in f_u (variation of ceftriaxone f_u between 0.05 and 0.1 is not important, Appendix D, Fig. D.1) and $f_u > 0.1$ requires initial ceftriaxone doses of 3g or greater, which are higher than the 1g dose examined in this study. Therefore, in our approach, when modelling free ceftriaxone molecules, we do not consider concentration-dependent effects and instead consider a fixed free fraction (f_u) of 0.05 (Chisholm, *et al.* 2010b).

6.2.2 Additional model details and parameter estimation

Where possible, parameter values are drawn from published empirical studies. When we could not estimate parameter values directly from the literature, they are estimated by fitting simplified versions of the model (sub-models) to relevant data, and the estimates obtained are summarised in Tables 6.2 and 6.3. The following section describes additional details relating to the Hill function (drug-mediated killing), dormancy ($k_{dormant}$), antibiotic transfer between extra and intracellular compartments (k_f and k_r), and the fraction of drug molecules that reach the urethra (f_s).

Table 6.1: Model variables and initial conditions

Variable	Symbol	Initial condition	Reference/ Comments
Unattached NG (number of bacteria)	B	1000	Based on bacterial load measurements in human experimental studies (Schmidt, <i>et al.</i> 2001; Schneider, <i>et al.</i> 1996)
Dormant unattached NG (number of bacteria)	B'	0	Before treatment initiation dormant NG do not exist.
Attached NG (number of bacteria)	B_a	0	Based on NG internalisation measured in the <i>in vitro</i> study by Shaw and Falkow (1988).
Dormant attached NG (number of bacteria)	B_a'	0	Before treatment initiation dormant NG do not exist.
NG within PMN (number of bacteria)	B_s	0	Described in Chapter 3, Table 3.1.
Dormant NG within PMN (number of bacteria)	B_s'	0	Before treatment initiation dormant NG do not exist.
NG within epithelial cells (number of bacteria)	B_i	0	Described in Chapter 3, Table 3.1.
Dormant NG within epithelial cells (number of bacteria)	B_i'	0	Before treatment initiation dormant NG do not exist.
Dose (mg)	D	1000 (CFO), 400 (CFM)	(Centers for Disease Control and Prevention 2012; Fifer H, <i>et al.</i> 2019)
Drug-bound PBP molecules on extracellular NG	T_{be}	0	Before treatment initiation bound PBP do not exist.

(number of molecules)			
Drug-bound PBP molecules on intracellular NG (number of molecules)	T_{bi}	0	Before treatment initiation bound PBP do not exist.
Free extracellular PBP molecules (number of molecules)	T_e	$B(0) \times y$	Assuming the number of targets per bacterium is the same and constant.
Free intracellular PBP molecules (number of molecules)	T_i	0	The initial intracellular bacterial population is 0
Free extracellular drug molecules (number of molecules)	A_e	$\frac{Dose \times f_u \times b_a}{1000 \times M_w} n_A \times s_f$	Treatment initiated at the time point of reaching the peak bacterial load.
Free intracellular drug molecules (number of molecules)	A_i	0	Treatment initiated at the time point of reaching the peak bacterial load.

Table 6.2: Model parameter values relating to the model of treatment with ceftriaxone (CFO) and cefixime (CFM).

Parameter	Symbol	Point estimate (Parameter range) ^a	Reference/Comments
Free drug fraction	f_u	0.05 (CFO), 0.35 (CFM)	Plasma drug concentration measured in healthy volunteers (Faulkner, <i>et al.</i> 1987b; Stoeckel, <i>et al.</i> 1981)
Molecular weight of drug (g/mol)	M_w	554.58 (CFO), 453.45 (CFM)	(National Center for Biotechnology Information 2020a; National Center for Biotechnology Information 2020b)
Number of PBP targets per bacterium	y	170 (120 - 220)	Described in text, Section 6.2.1.4.
Avogadro constant (mol ⁻¹)	n_A	6.02×10^{23}	Constant (number of particles in 1 mole)
Drug-bound PBP fraction on extracellular NG	f_{bound_e}	$\frac{T_{be}}{T_{be} + T_e}$	Calculated
Drug-bound PBP fraction on intracellular NG	f_{bound_i}	$\frac{T_{bi}}{T_{bi} + T_i}$	Calculated
Trigger of movement from non-dormant to dormant NG states	-	$H(f_{bound_e} - f_c)$ for extracellular states. $H(f_{bound_i} - f_c)$ for intracellular states.	Heaviside step function that initiates movement from non-dormant to dormant NG states.
Rate constant for binding of drug to PBP (h ⁻¹ M ⁻¹)	k_{PBP}	$\frac{k_{dormant} \times f_c \times M_w \times 1000}{MIC \times (1 - f_c)}$	Calculated as described in Section 6.2.5. $k_{dormant}$ is given in Table 6.3.
Rate constant for drug moving to intracellular	k_f	0.60 (0.41 – 0.85) (CFO), 0.35 (0.17 – 0.57) (CFM)	Original range from Section 6.2.2.2 refined through calibration. Lower bound 90% of

compartment (h ⁻¹)			the simulations with susceptibility breakpoint $\geq 0.125\text{mg/L}$.
Rate constant for drug moving from intracellular compartment (h ⁻¹)	k_r	1.77 (1.35 – 2.6) (CFO), 3.69 (3.14 – 4.7) (CFM)	Original range from Section 6.2.2.2 refined through calibration. Upper bound 90% of the simulations with susceptibility breakpoint $\geq 0.125\text{mg/L}$.
Rate constant for cefixime absorption (h ⁻¹)	k_a	no absorption phase for CFO, 0.76 (0.61 – 0.9) (CFM)	Obtained by fitting to free cefixime data in Faulkner, <i>et al.</i> (1988), Section 6.2.2.2.
Rate constant for drug elimination (h)	k_{el}	0.11 (0.09 – 0.12) (CFO), 0.20 (0.17 – 0.23) (CFM)	Based on plasma drug concentration measured in healthy volunteers (Brittain, <i>et al.</i> 1985; Faulkner, <i>et al.</i> 1988; Patel, <i>et al.</i> 1981; Patel, <i>et al.</i> 1982)
Bioavailability	b_a	1 (CFO), 0.45 (CFM)	Based on plasma drug concentration measured in healthy volunteers (Faulkner, <i>et al.</i> 1988; Faulkner, <i>et al.</i> 1987b; Zhou, <i>et al.</i> 1985)
Critical threshold for drug-bound PBP fraction at which NG become dormant	f_c	0.95 (0.9 – 0.99)	Point estimate threshold for ampicillin used in Abel zur Wiesch, <i>et al.</i> (2017)
Cellular urethral volume (L)	V_u	0.01	(Pomaroli and Schlogel 1978)
Volume of distribution (L)	V_d	9.37 (7.80 – 9.53) (CFO), 16.95 (16.9 – 19) (CFM)	Based on plasma drug concentration measured in healthy volunteers (Duverne, <i>et al.</i> 1992; Patel, <i>et al.</i> 1982)

^aPoint estimate and LHS parameter values are used when treatment effects are added to the natural infection (Chapter 3) simulated using the point estimates and the LHS parameter ranges, respectively. Point estimates presented in Table 6.2 are the median values unless otherwise specified.

6.2.2.1 Estimating parameter values related to drug-mediated killing and dormancy.

To estimate parameters for drug-mediated NG killing and the rate at which NG moves to the dormant states we would ideally use data on bacterial growth measured as a function of the drug-bound PBP fraction. However, as we were unable to identify studies reporting such data, we instead made use of the *in vitro* time-kill experiments of Foerster, *et al.* (2016) linking drug concentrations to NG growth rates, together with Dougherty, *et al.* (1981) that links drug concentrations to drug-bound PBP fractions. Dougherty, *et al.* (1981) measured drug binding of different β -lactam antibiotics to PBP on extracellular NG at fixed drug concentrations ranging from 10^{-4} to 1mg/L. The drug bound PBP fraction was measured after exposing NG to the antibiotics for 15 minutes (more details on data is given in Appendix D, Section D.3). The data in Foerster, *et al.* (2016) are described in detail in Chapter 4, Section 4.2.2.1. With these two studies we are then able to link NG growth rates with the drug-bound PBP fractions (f_{bound_e}).

In this chapter to measure the bacterial killing effect as a function of the drug-bound PBP fraction, we adopt a different parameterisation of the Hill function (see Regoes, *et al.* (2004) for a description on the connection between the two forms of the Hill functions). We adopt this approach because in this chapter our equations are in units of drug molecules and do not include a concentration parameter (model equations are in Appendix D, Section D.1). Here we parameterise the Hill function as $E_{max} \frac{(f_{bound_e})^m}{EC_{50}^m + (f_{bound_e})^m}$, where E_{max} is the maximum change in bacterial net growth rate associated with bound PBP, EC_{50} is the bound PBP fraction at which the killing effect is at half its maximal effect and m is the Hill coefficient.

Using this form of the Hill function, the following sub-model (Eq. 6.1 and 6.2) is simultaneously fitted to the NG growth data at different drug-bound PBP fractions to

estimate the rate constant for NG becoming dormant ($k_{dormant}$) and the Hill function parameters:

$$\frac{dB}{dt} = r_1 B - k_{dormant} H(f_{bound_e} - f_c) B \quad (6.1)$$

$$\frac{dB'}{dt} = k_{dormant} H(f_{bound_e} - f_c) B - E_{max} \frac{(f_{bound_e})^m}{EC_{50}^m + (f_{bound_e})^m} B' \quad (6.2)$$

Here, $H(x)$ is the Heaviside step function with value 0 for $x < 0$ and 1 for $x \geq 0$.

The sub-model describes the population of non-dormant (B) and dormant (B') extracellular NG in the absence of attachment or internalisation within host cells. Non-dormant NG are assumed to grow exponentially, while dormant NG do not grow and are instead subject to antibiotic killing at a rate determined by the Hill function. For treatment with ceftriaxone and cefixime, deviation from exponential bacterial growth begins to occur 2h and 1h after treatment initiation, respectively (Foerster, *et al.* 2016). We view these time-points as corresponding to the time at which the drug-bound PBP fraction (f_{bound_e}) exceeds f_c , triggering NG transfer to the dormant state at the rate constant $k_{dormant}$. Fitting is carried out using the MATLAB (MathWorks, Natick, MA), non-linear least squares solver ‘*lsqnonlin*’.

As in Chapter 4, Section 4.2.2, the point estimates for the Hill function parameters are derived from the mean of the Hill function fits to the two individual experiments in Foerster, *et al.* (2016) (further details in Appendix D, Section D.3.1). The Hill function parameters and dormancy rate parameter are defined above and the parameter values are given in Table 6.3. For estimation using equations 6.1 and 6.2, the drug-bound PBP threshold (f_c) is set at the point estimate value of 0.95 (Abel zur Wiesch, *et al.* 2017), while the bacterial replication rate is set at $r_1 = 0.68 \text{ h}^{-1}$ and 0.77 h^{-1} for the two experiments

in Foerster, *et al.* (2016) for ceftriaxone and $r_1 = 0.78\text{h}^{-1}$ and 0.67h^{-1} for the two experiments using cefixime (see Appendix B, Table B.1).

6.2.2.2 Rate constants for transfer of drug between extracellular and intracellular compartments.

To estimate the point estimates for the pharmacokinetic rate constants for drug transfer between the extracellular and intracellular drug compartments (k_f and k_r) and for drug absorption (k_a), we use plasma drug concentration data measured in healthy volunteers in Stoeckel, *et al.* (1988) and Faulkner, *et al.* (1988) using 1g intravascular ceftriaxone and 400mg oral cefixime, respectively. Stoeckel, *et al.* (1988) and Faulkner, *et al.* (1988) report drug concentrations measured at frequent intervals over periods of 48h and 24h, respectively. For both drugs, we convert plasma drug concentrations to numbers of molecules using an estimated plasma volume of $0.58 \times 5\text{L} = 2.9\text{L}$, assuming an average adult blood volume of 5L (Wei, *et al.* 1995) of which 58% is plasma (Feher 2012).

The sub-model below (Eq. 6.3-6.5) describes the absorption of an extravascularly administered drug from the gut to the bloodstream, drug penetration into the intracellular compartments and elimination from the extracellular compartment, with these processes governed by the rate constants described above. The absorption phase in Eq. 6.3 (described in Chapter 2, Section 2.7.1) is only required for orally administered drugs and therefore is included for cefixime but excluded for ceftriaxone which is administered intramuscularly.

$$\frac{dA_a}{dt} = -k_a A_a \quad (6.3)$$

$$\frac{dA_e}{dt} = k_a A_a - k_{el} A_e - k_f A_e + k_r A_i \quad (6.4)$$

$$\frac{dA_i}{dt} = k_f A_e - k_r A_i \quad (6.5)$$

Here, A_a , A_e and A_i describe the numbers of unabsorbed, extracellular and intracellular drug molecules respectively, and are defined in Table 6.1. The drug elimination rate (k_{el}) is calculated as $\frac{\log(2)}{\text{half-life}}$ using drug half-life estimates from plasma drug concentration measurements over time (Brittain, *et al.* 1985; Faulkner, *et al.* 1988; Patel, *et al.* 1981) and is fixed during the fitting process at the point estimate value given in Table 6.2.

To incorporate parametric uncertainty around our estimates (handling parametric uncertainty is described in detail in Section 6.2.5) we generate parameter ranges for k_a , k_f and k_r , by generating 100 data sets on the number of drug molecules over time. For this, 100 Poisson random numbers for each time point are generated using as the mean the corresponding number of drug molecules calculated from Stoeckel, *et al.* (1988) and Faulkner, *et al.* (1988). The sub-model in Eq. 6.3-6.5 is then fitted to each of these generated data sets individually to estimate 100 sets of parameter values for k_a , k_f and k_r . The model fits and more details on the data generation procedure are provided in Appendix D, Section D.4. The median and the 95% range of the parameter estimates that is obtained from fits to these simulated datasets are designated as the point estimate and range, respectively, for each of the parameters (Table 6.2).

6.2.2.3 Estimating the fraction of administered drug molecules that reaches the urethra (f_s)

When the drug is distributed from the blood to different tissues and organs, only a fraction of the initial dose reaches the infection site. Additionally, distribution can vary by tissue type due to factors such as tissue permeability (Kallings, *et al.* 1979; Kong, *et*

al. 2017). To estimate a plausible range for the fraction of drug molecules that reach the urethra a scaling factor (f_s) is introduced, which is used to calculate the initial number of drug molecules at the urethra.

There is limited data in the literature to inform the value of the scaling factor f_s . Hence, we took an approach based on bounding the relevant range, such that the lower bound of f_s is the lowest value at which a susceptible strain clears infection in ≤ 7 days and the upper bound of f_s is the largest value at which a resistant strain fails to clear infection in ≤ 7 days. Estimated rates of drug binding to PBP (k_{PBP}) as reported in Tomberg, *et al.* (2017) for susceptible ($k_{PBP} = 5 \times 10^9$ (CFM) or $6 \times 10^9 M^{-1}h^{-1}$ (CFO)), and resistant strains ($k_{PBP} = 9 \times 10^5$ (CFM) or $3 \times 10^6 M^{-1}h^{-1}$ (CFO)) were used in the simulations for cefixime and ceftriaxone. Here, all other parameters are held fixed at their point estimates given in Tables 6.2 and 6.3, and f_s is varied to determine the associated range.

A schematic diagram of the model is shown in Fig.6.1. The model equations are described in Appendix D, Section D.1 and the model parameters are described in Tables 6.2 and 6.3. Parameter values for natural infection are given in Chapter 3, Table 3.2.

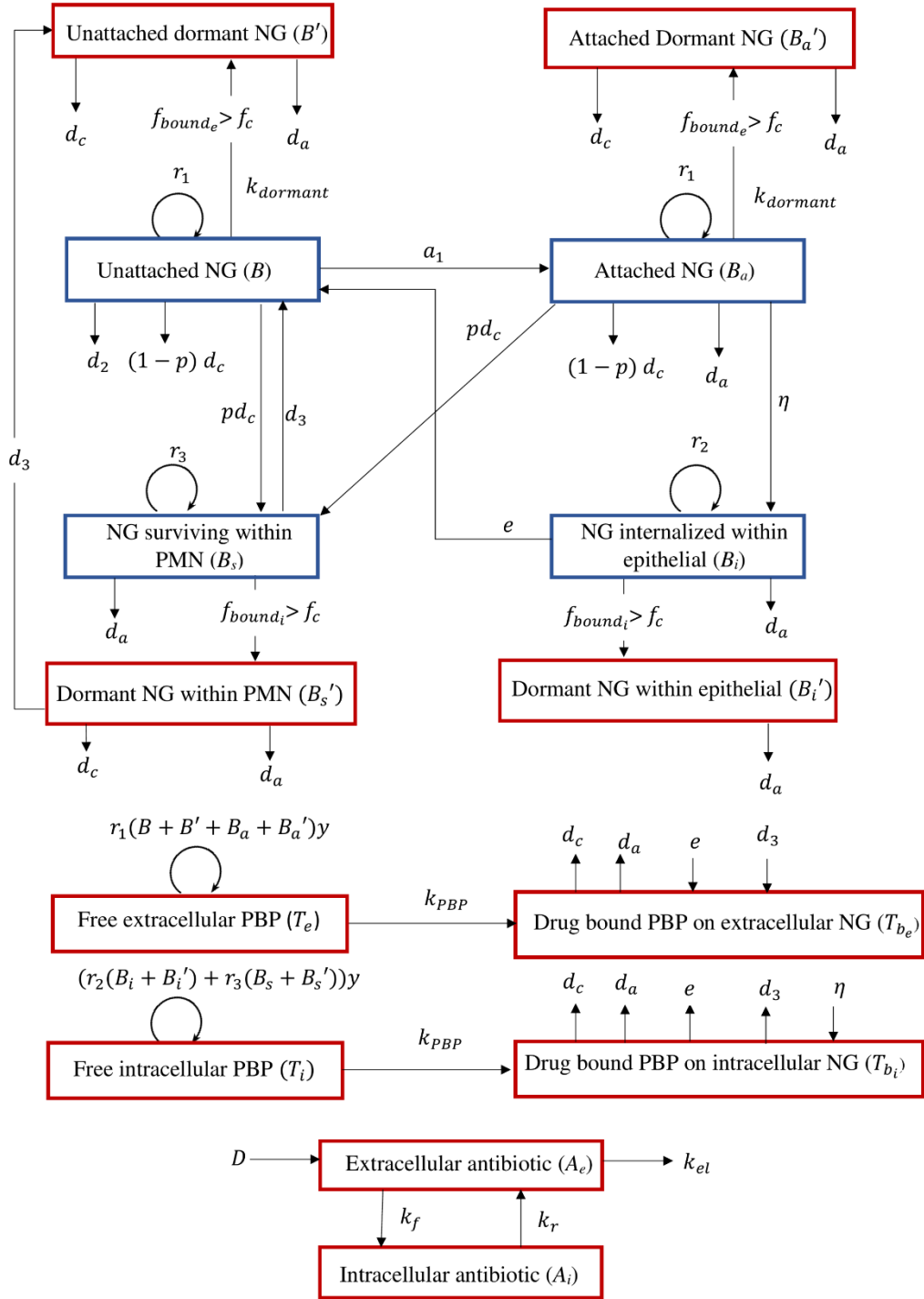


Figure 6.1: Schematic diagram of the infection model with the addition of treatment. Here,

d_a denotes antibiotic-mediated killing modelled as a Hill function of the form

$$E_{max} \frac{(f_{bound_e})^m}{EC_{50}^m + (f_{bound_e})^m}$$

and d_c denotes PMN-mediated NG killing (see Chapter 3,

Section 3.2.1.1). The blue and red outlined compartments represent the natural infection model states and additional treatment model states, respectively.

6.2.3 MIC expression

We derive an expression for the model-derived MIC (Eq. 6.6) using a sub-model reflecting an *in vitro* environment with unattached (B) and dormant (B') NG to reflect experimental techniques such as Etests that are used to measure the MIC. The details of the derivation are given in Appendix D, Section D.7.

$$MIC = \frac{k_{dormant} f_c M_w}{k_{PBP} (1 - f_c)} \quad (6.6)$$

Here, M_w is the molecular weight, with the other parameters defined previously and summarised along with relevant values in Tables 6.2 (f_c , M_w and k_{PBP}) and 6.3 ($k_{dormant}$).

6.2.4 Converting number of molecules to drug concentration

For comparison with existing literature, the number of drug molecules is converted to drug concentration as follows:

$$C_e = \frac{A_e \times M_w \times 1000}{V_d \times f_s \times n_A} \text{mg} / L \quad (6.7)$$

Here, C_e and A_e are the extracellular drug concentration and number of molecules, respectively. The parameter value of the fraction of the administered drug molecules that reach the urethra (f_s) is given in Table 6.3. The parameter values of the volume of distribution (V_d) and the Avogadro constant (n_A) are given in Table 6.2. The factor of 1000 is for unit conversion to represent concentration in the units of mg/L. As the intracellular (within PMN and epithelial cells) volume of distribution is not known, the conversion is only performed for the extracellular drug concentrations.

6.2.5 Incorporation of parametric uncertainty

In Chapter 3, to account for uncertainty associated with parameter values specifying the natural infection model, we use Latin hypercube sampling (LHS) to generate 5402 samples from the parameter ranges that we estimate. To incorporate parameter uncertainty related to treatment, we extend this previous LHS analysis by also simulating from the ranges that are associated with the treatment parameters. This extension to incorporate both natural history and treatment related parametric uncertainty is conducted using the same approach as described in Chapter 4, Section 4.2.4, but here, treatment uncertainty is incorporated using the parameter ranges given in Tables 6.2 and 6.3. As the MIC is not directly used in the Hill function in this chapter, in order to generate parameter combinations that are associated with a particular value of the MIC, Eq. 6.6 is solved for k_{BBP} when generating treatment related LHS parameters. The decision to solve the MIC expression for k_{BBP} is based on the clear differences in acylation rates that are associated with changes in MIC reported in the literature. With this approach we generate 5402 sets of parameter values that incorporate both natural history and treatment related parametric uncertainty which are then used to simulate infection clearance times.

6.2.6 Calibrating PK/PD parameters using empirical susceptibility breakpoints.

As described in Chapter 4, Section 4.2.5, we use the model to derive a susceptibility breakpoint such that above and below this breakpoint, respectively <95% and $\geq 95\%$ of simulations from LHS samples clear infection successfully and we refer to this as the ‘model-derived susceptibility breakpoint’. Here, when evaluating the susceptibility breakpoint for ceftriaxone and cefixime the model is tested for MIC of 0.06, 0.125, 0.25, 0.5 and 1mg/L which includes general MIC values for ceftriaxone and cefixime that are reported in epidemiological studies as for example in Chisholm, *et al.* (2010b) and Whittles, *et al.* (2018).

As described in Chapter 4, Section 4.2.5, the model-derived breakpoints using our primary doses of 1g ceftriaxone and 400mg cefixime are set, based on ‘empirical breakpoints’ and are used in calibration to refine ranges for parameters that are influential in determining model-derived breakpoints. The influential parameters are determined through a multivariate sensitivity analysis as described in Chapter 4, Section 4.2.5 and the parameters that we identify here as influential in determining breakpoints are shown in Appendix D, Fig. D.6. We then adopt the approach of Chapter 4, Section 4.2.5, for these influential parameters with original literature-defined parameter ranges replaced by refined parameter ranges (after calibration). A comparison between original and the refined parameter ranges is presented in Appendix D, Table D.2. A new set of LHS samples is then generated for the treatment parameters and combined with the LHS samples from the natural infection model as described previously in Section 6.2.5.

6.2.7 Different treatment strategies

When assessing different treatment strategies, we carry out two main sets of analyses in this chapter. The first analysis covers monotreatment with standard doses currently in use and the infection clearance times are evaluated from simulations using each LHS parameter set at a series of different MIC values. For this analysis, we consider 1g or 500mg doses of intramuscular ceftriaxone as currently recommended for monotreatment in the United Kingdom (UK) (Fifer H, *et al.* 2019) and United States (US) (St. Cyr, *et al.* 2020), respectively, and a single 400mg oral dose of cefixime as recommended prior to 2012 by the CDC (Centers for Disease Control and Prevention 2012).

The second analysis considers various single and multiple-dose cefixime regimens, while keeping the other aspects of simulations the same. As cefixime is orally

administered, multiple dose regimens are more feasible for outpatients than for ceftriaxone, which is administered by intramuscular injection. As in Chapter 5 Section 5.2.1, we consider treatment to be successful at a given MIC if $\geq 95\%$ of simulations clear infection within 7 days. For cefixime, we test multiple dose strategies having a total accumulation of 400mg (e.g., 200mg \times 2 given 12h apart), 800mg, 1200mg, 1600mg and 2400mg, with the higher doses of 800, 1200 and 2400mg previously tested in a phase 1 clinical trial of treatment of pharyngeal NG infection (Barbee, *et al.* 2018). We also assess the effect of dosing interval by evaluating treatment effectiveness when doses are administered at 4, 6 and 8h apart. In addition, we conduct a limited analysis of patient non-adherence, whereby the second dose is delayed by uniformly distributed time between 0 and 8 hours, with any subsequent doses then taken at the scheduled delay from the previous dose.

6.2.8 Comparison of infection clearance with Chapter 4

We also conduct a comparison of treatment dynamics in this model as opposed to those using the model described in Chapter 4. Here we use the same natural infection point estimates for both models and the point estimate treatment parameters described in each chapter. We then simulate infection dynamics under the two models for single doses of 1g ceftriaxone and 400mg cefixime for an NG strain with MIC of 0.125mg/L and compare simulated extra and intracellular bacterial loads and extracellular drug concentrations in the first 6 hours following treatment.

6.3 Results

6.3.1 Parameter estimation

The estimates of the Hill function parameter values, the rate constant for NG moving to the dormant state ($k_{dormant}$) and the fraction of the administered drug

molecules that reach the urethra (f_s) are given in Table 6.3 and are illustrated in Appendix D, Fig.D.3 and Appendix D, Fig. D.5, respectively. Although the parameter values and the Hill function formulations that we adopt in here and Chapter 4 differ, the resulting net growth rates are similar (Fig. 6.2). The ranges of the f_s estimates for ceftriaxone and cefixime are $7.9 \times 10^{-6} - 9.1 \times 10^{-5}$ and $9.1 \times 10^{-5} - 5.4 \times 10^{-4}$, respectively (Table 6.3) and differ between the drugs by approximately an order of magnitude.

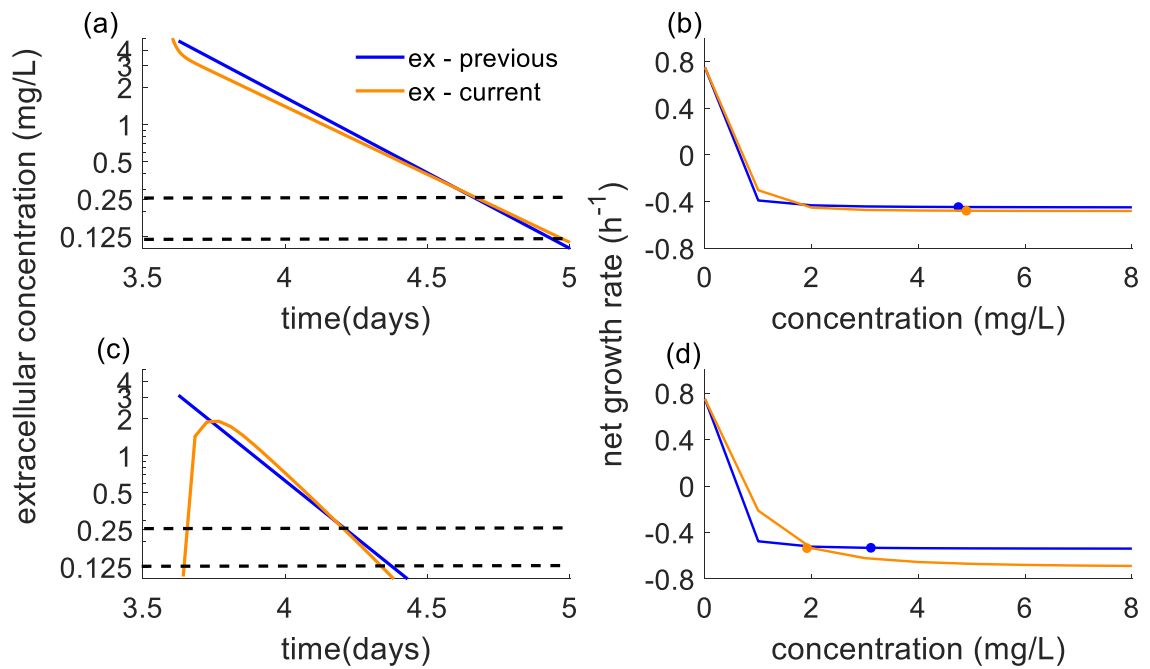


Figure 6.2: Change in (a) extracellular (ex) drug concentration over time and; (b) the change in the net bacterial growth rate to the changes in the antibiotic concentration shown for Chapters 4 (previous) and 6 (current). The upper row shows results for ceftriaxone and the bottom row for cefixime. The black dashed lines in (a) and (c) show the empirical susceptibility breakpoints of 0.125mg/L (EUCAST) and 0.25mg/L (CLSI). The dots in (b) and (d) denote the initial drug concentration for a 1g ceftriaxone and 400mg dose of cefixime, respectively. In panel (c), the current approach models an absorption phase so $C_e = 0$ while in the previous model no absorption phase was assumed and $C_e = 3.72mg/L$.

Table 6.3: Parameter estimates obtained through model fitting to data on ceftriaxone (CFO) and cefixime (CFM).

Parameter	Symbol	Point estimate (LHS range)
Maximum change in bacterial net growth rate associated with bound PBP (h^{-1})	E_{max}	CFO: 1.23 (0.49 – 1.69) CFM: 1.45 (0.87 – 1.98)
Bound PBP fraction at which the killing effect is at half its maximal effect.	EC_{50}	CFO: 0.53 (0.21 – 0.58) CFM: 0.71 (0.46 – 0.98)
Hill coefficient	m	CFO: 2.80 (2.21 – 4.61) CFM: 1.98 (1.42 – 4.74)
Rate constant for NG becoming dormant (h^{-1}) ^a	$k_{dormant}$	CFO: 4.95 – 6.05 CFM: 2.26 – 2.50
Fraction of the administered drug molecules that reach the urethra ^b	f_s	CFO: 7.9×10^{-6} – 7.1×10^{-5} CFM: 9.1×10^{-5} – 5.4×10^{-4}

^a Point estimates for the Hill function parameters are obtained by fitting the Hill function to the mean net growth rates that are obtained from the fits to the individual experiments in Foerster, *et al.* (2016). However, as $k_{dormant}$ is not a parameter in the Hill function, a point estimate could not be estimated.

^b Only a parameter range could be estimated based on the modelled infection clearance as described in Section 6.2.2.3.

6.3.2 Simulated drug concentration profiles

The simulated drug concentration profiles using 1g ceftriaxone and 400mg cefixime align with the simulated drug concentration profiles in Chapter 4 (Fig. 6.2). The median extracellular drug concentrations of ceftriaxone and cefixime remain above the empirical susceptibility breakpoint (0.25mg/L) for 32 and 13.9h, respectively, which aligns with the Chapter 4 results of 31.9 and 13.1h respectively, for ceftriaxone and cefixime.

6.3.3 General model behaviour

The model shows four distinct types of behaviours in regards to reaching the extracellular and intracellular drug-bound PBP threshold (f_c) (Fig. 6.3). Estimates of the rates of drug transfer between the extracellular and intracellular compartments (k_f and k_r) are such that the number of intracellular drug molecules is always less than in the extracellular state. Due to both lower number of intracellular drug molecules and higher numbers of intracellular NG in comparison to extracellular states at the time of adding treatment (Chapter 3, Section 3.3.2.1), $f_{bound_i} < f_{bound_e}$ for all simulations and if $f_{bound_i} > f_c$ then $f_{bound_e} > f_c$. The model only clears the infection in ≤ 7 days when both f_{bound_e} and f_{bound_i} reach and remain above f_c . When both f_{bound_e} and f_{bound_i} fail to reach f_c there is treatment failure. Treatment failure is also observed when f_{bound_e} reaches f_c but f_{bound_i} does not. For certain parameter values, we could generate simulations where both f_{bound_e} and f_{bound_i} reach f_c , but f_{bound_i} exceeds f_c only for a very brief period. For these simulations, the brief duration of antibiotic mediated killing of intracellular NG is insufficient for infection clearance within 7 days.

Examples of these four model behaviours are observed in Fig. 6.3 by varying the rate constant for binding of drug to PBP (k_{PBP}) which from Eq. 6.6 is inversely

proportional to the MIC. Here, other parameters are held fixed at their point estimate values. At low values of k_{PBP} ($1 \times 10^7 \text{ h}^{-1}\text{M}^{-1}$) neither f_{bound_e} or f_{bound_i} reach f_c and therefore NG are not subject to antibiotic-mediated killing. As k_{PBP} is gradually increased we note that at $k_{PBP} = 2 \times 10^7 \text{ h}^{-1}\text{M}^{-1}$, $f_{bound_e} > f_c$ but $f_{bound_i} < f_c$ and the infection is not successfully cleared within 7 days. At $k_{PBP} = 3.1 \times 10^7 \text{ h}^{-1}\text{M}^{-1}$, $f_{bound_e} > f_c$ while f_{bound_i} exceeds f_c only briefly ($\sim 6\text{h}$). Here, the total bacterial load declines to ~ 15 bacteria, before the bacterial load spikes again once intracellular NG killing ceases. At high values of k_{PBP} ($1 \times 10^9 \text{ h}^{-1}\text{M}^{-1}$), the drug-bound PBP threshold is reached in both extra and intracellular environments and the infection is cleared in $\sim 10\text{h}$. This suggests treatment success is determined by whether f_c is exceeded continuously in the intracellular environment and we explore this further in Section 6.3.5. Fig. 6.3 shows simulations for cefixime, but similar behaviour occurs for ceftriaxone.

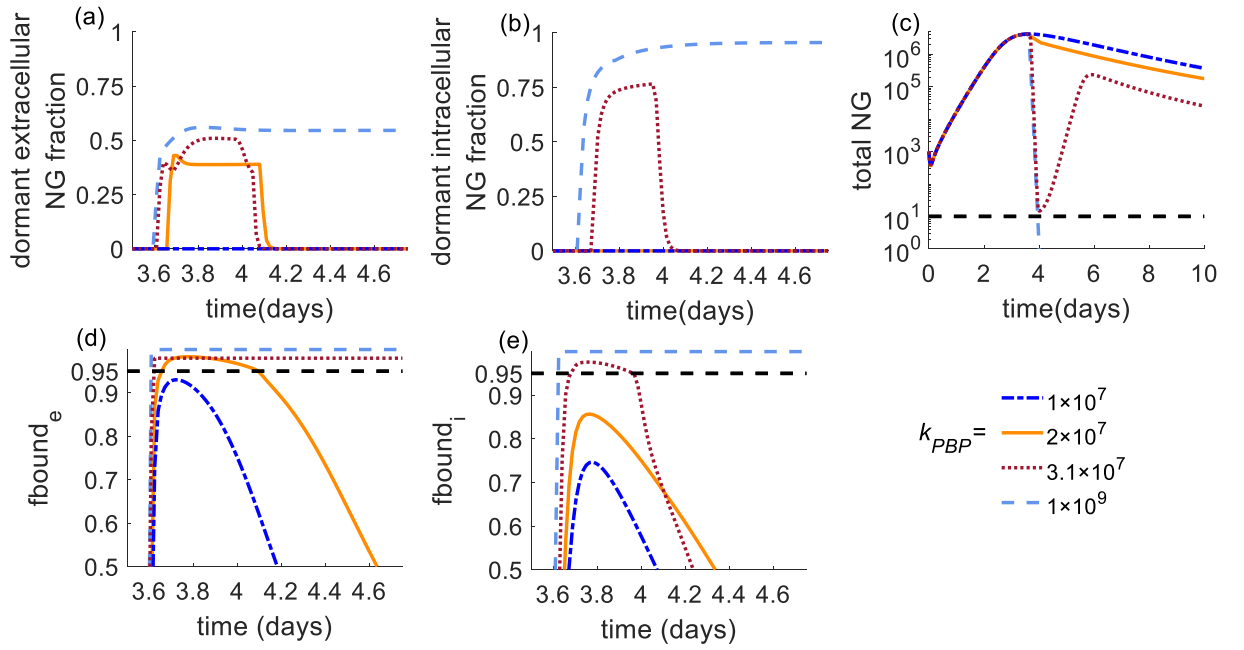


Figure 6.3: Model behaviour as a function of the rate constant for cefixime binding to PBP (k_{PBP} ($h^{-1}M^{-1}$)). Figure panels show: (a) fraction of dormant extracellular and (b) intracellular NG; (c) total NG load; (d) drug-bound PBP fraction on extracellular NG (f_{bound_e}) and (e) on intracellular NG (f_{bound_i}). In (a) and (d), when $f_{bound_e} < f_c$ or $f_{bound_i} < f_c$, respectively, no dormant NG are present. The black dashed lines in (d, e) indicate the drug-bound PBP threshold ($f_c = 0.95$), while in (c) this indicates the infection clearance cut-off of 10 bacteria. The k_{PBP} values shown in the legend apply to all panels.

6.3.4 Model-derived susceptibility breakpoints

In Table 6.4 we show the model-derived susceptibility breakpoints for the monotreatment strategies of ceftriaxone and cefixime that are currently in use. For ceftriaxone using 500mg and 1g doses the model-derived susceptibility breakpoints are, respectively, 0.125 and 0.25mg/L and for cefixime using a 400mg dose, the breakpoint is

0.125mg/L. At MIC for cefixime of 0.25mg/L, ~74% of simulations successfully clear infection but at higher MIC values the infection clearance is poorer (<31% simulations clear infection). At MIC for ceftriaxone of 0.5mg/L, using 1g and 500mg doses, respectively, 87% and 64% simulations clear infection and clearance is poor for both dose quantities at MIC of 1mg/L.

Table 6.4: Percentage of simulations that clear the infection in ≤ 7 days when treated using the standard doses of ceftriaxone (CFO) and cefixime (CFM).

Drug	Treatment Strategy	Percentage of simulations that clear infection				
		MIC (mg/L)				
		0.06	0.125	0.25	0.5	1
Strategies currently recommended						
CFO	500mg single ^a	100.00	97.54	86.72	64.35	37.85
	1g single ^b	100.00	100.00	97.65	87.21	64.91
CFM	400mg single ^c	99.97	94.93	73.95	30.27	6.37

^a Monotreatment strategy used in the US (St. Cyr, *et al.* 2020).

^b Monotreatment strategy used in the UK (Fifer H, *et al.* 2019).

^c Recommended dose before 2012 according to US CDC guidelines (Centers for Disease Control and Prevention 2012) and currently used as an alternative option.

6.3.5 Testing infection clearance for different MIC

We present in Table 6.5 the association between treatment success and the ability to reach the extra and intracellular drug-bound PBP thresholds for the simulations resulting from the same set of 5402 LHS samples used in Section 6.3.4 as the parameter values for each drug. Irrespective of whether f_c is reached in the extracellular environment, treatment failure occurs in all simulations where $f_{bound_i} < f_c$. We also note that in all situations where $f_{bound_i} > f_c$, there is successful infection clearance. In this analysis, there are no simulations with $f_{bound_i} > f_c$ only temporarily. Therefore, of the set of simulations where f_c is exceeded in the intracellular environment and which successfully clear the infection are identical (Table 6.5). This shows that treatment failure in simulations is driven by the unsuccessful clearance of intracellular NG.

Table 6.5: Infection clearance behaviour in relation to intracellular (f_{bound_i}) and extracellular (f_{bound_e}) thresholds for model simulations using LHS samples. Results are shown using 400mg single dose of cefixime and 1g single dose of ceftriaxone.

Percentage of simulations	Drug	MIC (mg/L)			
		0.125	0.25	0.5	1
Both f_{bound_e} and $f_{bound_i} > f_c$	CFM	94.93	73.95	30.27	6.37
	CFO	100.00	97.65	87.21	64.91
$f_{bound_e} > f_c > f_{bound_i}$	CFM	5.07	26.05	69.73	92.53
	CFO	0.00	2.35	12.79	33.50
Both f_{bound_e} and $f_{bound_i} < f_c$	CFM	0.00	0.00	0.00	1.10
	CFO	0.00	0.00	0.00	1.59
clear infection	CFM	94.93	73.95	30.27	6.37
	CFO	100.00	97.65	87.21	64.91

6.3.6 Different cefixime treatment strategies

We also test different cefixime dosing strategies over a range of MIC values (Table 6.6). The extracellular drug concentration profiles of these different tested strategies are shown in Appendix D, Fig D.7.

Table 6.6: Percentage of simulations that clear the infection in ≤ 7 days when treated using different dosing strategies of cefixime ^a.

Total accumulation	Treatment Strategy	Percentage of simulations that clear infection				
		MIC (mg/L)				
		0.06	0.125	0.25	0.5	1
400mg	400mg single ^b	99.97	94.93	73.95	30.27	6.37
	2 × 200mg, 4h apart	99.98	94.92	73.99	30.39	6.48
	2 × 200mg, 6h apart ^b	99.98	94.92	73.99	30.39	6.93
	2 × 200mg, 8h apart	99.98	94.92	73.99	30.41	6.98
800mg	800mg single ^c	100.00	100.00	95.15	74.01	30.95
	400mg ×2, 6h apart	100.00	100.00	95.22	74.14	30.98
1200mg	1200mg single dose ^c	100.00	100.00	99.72	89.72	60.64
	400mg ×3, 4h apart	100.00	100.00	99.72	89.89	60.65
	400mg ×3, 6h apart	100.00	100.00	99.72	89.91	60.69
	400mg ×3, 8h apart	100.00	100.00	99.72	89.95	60.76
	200mg 12h apart for 3 days ^d	99.98	99.89	98.79	87.45	55.28
1600mg	Single 1600mg	100.00	100.00	100.00	95.52	75.71
	800mg ×2, 6h apart	100.00	100.00	100.00	95.59	75.95
2400mg	800mg ×3, 4h apart	100.00	100.00	100.00	99.68	89.19
	800mg ×3, 6h apart	100.00	100.00	100.00	99.70	89.96
	800mg ×3, 8h apart ^c	100.00	100.00	100.00	99.70	90.06

^a The treatment success values represent simulation significance.

^b Tested in Chisholm, *et al.* (2010b).

^c Tested in Barbee, *et al.* (2018) for pharyngeal NG infection.

^d Treatment strategy used in Japan in 2004 for urethral NG infection (Japanese Society for Sexually Transmitted Diseases 2004).

In multiple dose strategies, we find that an 8h dosing interval performs best (Table 6.6) as it maximises t_{MIC} (Appendix D, Fig. D.9). For these strategies, increasing the dosing interval to 12h results in poorer treatment success (Table 6.6). However, the effectiveness of treatment strategies only marginally differs by dosing intervals and is unlikely to be clinically important. We also consider the impact of patient non-adherence (the impact of delaying the second dose as described in Section 6.2.7) on infection clearance when multiple dose strategies are used. With this form of non-adherence, treatment effectiveness is only marginally poorer than in simulations with full compliance with regimens (Appendix D, Table D.3).

Single and multiple dose treatment options that accumulate to the same total dose exhibit similar treatment effectiveness. This can be explained via a combination of two indices: 1) the number of intracellular drug molecules that is attained at the time of reaching f_c in the extracellular environment ($A_i^{critical}$); and 2) the time the extracellular drug concentration remains above the MIC (t_{MIC}). For example, we observe that strategies involving either a 1200mg single dose or doses of 400mg \times 3, at 8h intervals both achieve ~60% treatment success for a MIC of 1mg/L (Table 6.6). Here, the latter strategy achieves a longer t_{MIC} (Appendix D, Fig. D.8) but a lower number of intracellular drug molecules (Appendix D, Fig. D.8) than the former. Based on these observations, we investigated threshold indices differentiating treatment success and treatment failure for single and multiple dose cefixime strategies accumulating to 1200mg for MIC of 0.5mg/L and 1mg/L. In the context of this example, we find that simulations with extracellular $t_{MIC} > 22h$ are successful in clearing infection but if extracellular $t_{MIC} \leq 22h$ treatment success still occurs if $A_i^{critical} > 3 \times 10^{13}$ (Fig. 6.4).

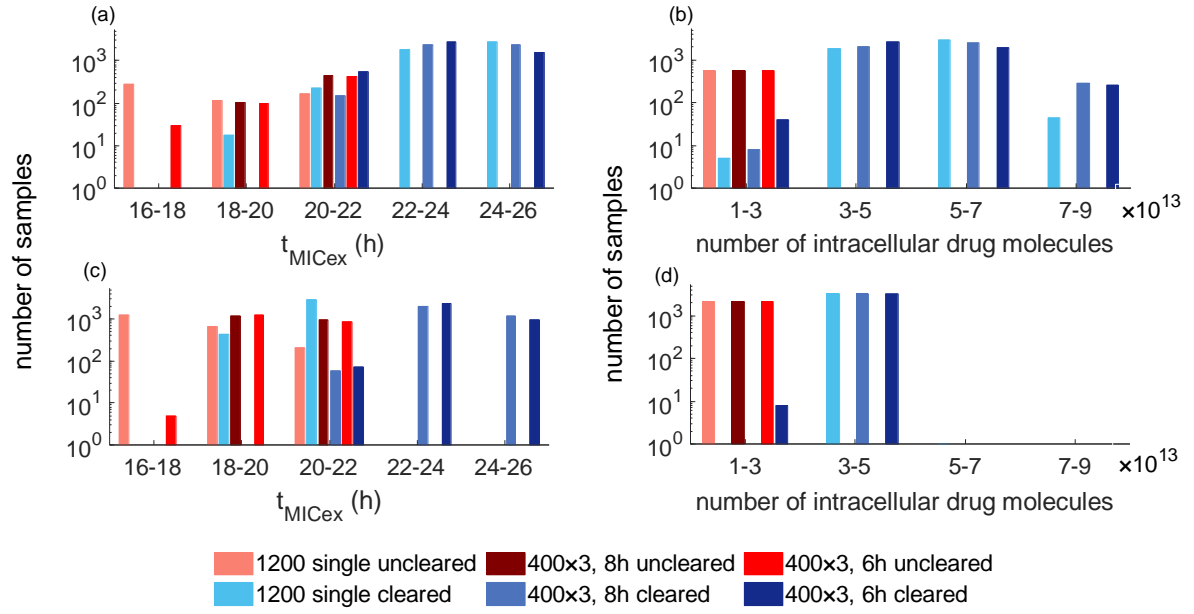


Figure 6.4: Time the extracellular drug concentration remains above the MIC (t_{MICex}) and the number of intracellular drug molecules at the time of reaching the extracellular drug-bound PBP threshold ($A_i^{critical}$) for single and multiple cefixime dosing strategies. Panels show MIC for cefixime of 0.5mg/L (a, b) and 1mg/L (c, d). The cefixime treatment strategies shown here are 1200mg single dose, 400mg \times 3, 8h apart and 400mg \times 3, 6h apart.

6.3.7 Comparison of infection clearance with the model described in Chapter 4

A comparison of extra and intracellular bacterial loads across the two models is shown in Fig.6.5 for the first 6 hours since treatment at MIC for ceftriaxone (1g dose) of 0.125mg/L. We note that the behaviour for cefixime is almost identical (results not shown). Extracellular ceftriaxone concentrations remain above the MIC for similar durations across the Chapter 4 and Chapter 6 models, at 41.4h and 41.6h, respectively (Fig. 6.2). From Fig. 6.2, we also note that bactericidal effects at the same drug concentration are similar in both models.

At 6h after initiation of ceftriaxone treatment, simulations using the Chapter 4 model have ~30-fold and ~145-fold higher extracellular and intracellular bacterial loads than in simulations using the model developed in this chapter (Fig. 6.5 (a)). The trajectories of the extracellular and intracellular bacterial loads simulated from the approaches in Chapters 4 and 6, start to diverge after around 2h from treatment initiation. In simulations using the model described in this chapter, by 6h after adding treatment, ~55% and ~90% NG reside in the dormant extracellular and intracellular states, respectively (Figure 6.5 (b)). With an increasing fraction of NG in the dormant state over time, a declining fraction of bacteria replicate, and therefore the number of new bacteria produced per unit time decreases. This resulting effect from bacteriostasis in Chapter 6 combined with the drug mediated killing (bactericidal) effects on dormant NG results in a much larger reduction in the NG population growth than in the model in Chapter 4, where the entire NG population are only subject to a relatively low bactericidal effects.

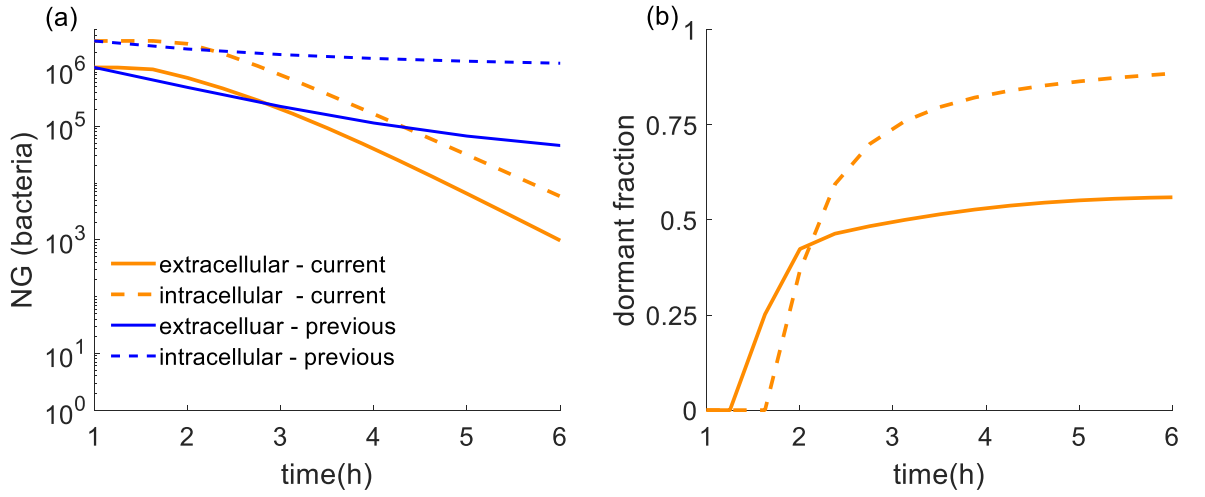


Figure 6.5: Comparison of the infection dynamics between Chapters 4 (previous) and 6 (current) showing the change of (a) total extracellular and intracellular NG and; (b) fraction of dormant NG over time for the first 6 hours since treatment using ceftriaxone. Total NG is stratified as dormant and non-dormant only in Chapter 6.

6.4 Discussion

In this study, we aimed to more accurately simulate urethral NG infection dynamics following treatment with the β -lactam antibiotics, ceftriaxone and cefixime. The use of a mechanistic drug-target binding model enables us to overcome the limitations faced with the approach taken in Chapter 4 and to generate infection clearance times and model-derived susceptibility breakpoints that align with empirical estimates. Consistent with the findings in the previous chapters, we again find treatment failure to be determined by insufficient antibiotic mediated killing effect on intracellular bacterial populations. Regarding cefixime, which is orally administered, simulations of multiple dose strategies with the same total dose are found to be similarly effective as a single dose strategy. We found the two indices, $t_{MIC_{ex}}$ and $A_i^{critical}$ to be effective in differentiating

between treatment success and failure, but this was in the specific context of dosing strategies with a total accumulation of 1200mg and requires further exploration over a wide range of treatment strategies.

We also attempt to highlight differences in model behaviour from earlier chapters that underpins the success of this model in explaining treatment dynamics using ceftriaxone and cefixime. Although the earlier model (Chapter 4) leads to antibiotic mediated killing in all states, in this chapter a larger net effect is achieved by the combination of bacteriostatic and bactericidal effects. This is because in addition to antibiotic mediated killing, dormant NG do not replicate and therefore new progeny are only generated from the small fraction of non-dormant NG which fail to sustain population growth in the presence of immune mediated and antibiotic mediated killing. In the Chapter 4 implementation, however, the relatively weak bactericidal effects of ceftriaxone and cefixime ($\varphi_{min} \approx -0.5 \text{ h}^{-1}$) combined with limited time above the MIC do not sufficiently suppress the generation of the new progeny from the entire surviving bacterial population.

The model produces infection clearance times that align with the limited data available in the literature. Using single doses of 1g ceftriaxone and 400mg cefixime, ~100% of simulations cleared infection within 7 days at MIC<0.125mg/L. This aligns with reports from empirical studies at MIC<0.125mg/L where ~99% treatment success using ceftriaxone (Ito, *et al.* 2016; Moran and Levine 1995) and 98.1% (Allen, *et al.* 2013) and 97.7% (Moran and Levine (1995) treatment success using cefixime is observed. There is limited information in the literature on treatment efficacy for urethral NG infection at high MIC values ($\geq 0.25\text{mg/L}$). This is because most of the studies that have evaluated clinical efficacy were conducted in the 1980s and 1990s (Kidd and Workowski 2015) when isolates with high MIC against 3rd generation cephalosporins were rare

(Deguchi, *et al.* 2016; Seike, *et al.* 2016) and lower doses such as 250mg for ceftriaxone were commonly used. We are not aware of any studies comparing the effectiveness of single vs multiple dose strategies of cefixime at different dosing frequencies. In this context, our results may provide some guidance for future clinical studies looking at multiple dosing strategies.

In 2019, the UK changed the recommendations in its treatment guidelines from dual treatment (1g azithromycin+ 500mg ceftriaxone) to monotreatment with 1g ceftriaxone (Fifer H, *et al.* 2019) due to the low prevalence of ceftriaxone resistance but frequent occurrences of high-level azithromycin resistance in the UK (Fifer H, *et al.* 2019). Due to similar observations of increasing azithromycin resistance in the US, dual treatment (1g azithromycin + 250mg ceftriaxone) has been replaced with monotherapy with an increased 500mg dose of ceftriaxone (St. Cyr, *et al.* 2020). In 2018, with only ~0.2% of isolates showing resistance ($\text{MIC} \geq 0.125\text{mg/L}$) to ceftriaxone in the UK (Public Health England 2019) and the US (Centers for Disease Control and Prevention 2019b), our model suggests this monotreatment strategy will be effective as treatment success for MIC of 0.125mg/L is observed in ~97% and 100% of simulations using 500mg and 1g doses, respectively.

The limitations of our modelling approach include simplifying assumptions around model structure such as the use of a single threshold to capture both bacteriostatic and bactericidal effects, reflecting limited data to inform model parameters and for validation of model outputs. To inform the drug-bound PBP threshold (f_c) for ceftriaxone and cefixime, we use the value reported for ampicillin ($f_c = 0.95$) in Abel zur Wiesch, *et al.* (2017). Considering the observed differences in PBP binding by different β -lactams (Dougherty, *et al.* 1981), it is possible that the drug-bound PBP thresholds for ceftriaxone and cefixime are different. We try to overcome this uncertainty to a certain extent through

sampling over the range 0.9-0.99 for f_c as bacteriostasis and bactericidal effects occur when a ‘high’ proportion of PBP are acylated (Williamson and Tomasz 1985) but, there is insufficient published data to precisely quantify this threshold for different drugs. When estimating the Hill function parameter values, we lacked direct observations on bacterial growth measured as a function of the drug-bound PBP fraction and therefore we used data from two studies Dougherty, *et al.* (1981) and Foerster, *et al.* (2016). Due to this limitation the estimation procedure that we have adopted here can introduce uncertainty into parameter estimates because of factors such as differences in the experimental settings and the differing antibiotics used in the two studies. Due to lack of data we also assume the same intracellular drug bound PBP fraction to act on both NG within PMN and epithelial cells. However, it is possible that the rates of drug binding to PBP on NG in these two environments are different.

Our decision to assume each bacterium has the same number of bound target molecules may have implications for the dichotomous behaviour observed when transitioning from infection clearance to non-clearance. With our approach, in situations where the drug bound PBP fraction is below the critical threshold (f_c), we may initially underestimate occupancy of the dormant state. This is because under a distributional approach, many bacteria will reach dormancy before the mean time of transition, which corresponds to our threshold. However, such an approach would result in further model complexity as bacteria require further classification based on the number of bound target molecules, with limited data to inform this process.

Although we only focus on ceftriaxone and cefixime dynamics in this study, we expect that the model can be generalised to other β -lactam drugs and potentially to represent other antibiotic classes. However, in some cases this would be non-trivial as drug classes that features reversible drug-target reactions and drug diffusion across the

bacterial cell envelope (Abel zur Wiesch, *et al.* 2017) might require revisions of the model. A more general model might be useful in guiding new drug development, with Clarelli, *et al.* (2020b) using a similar model in the context of *E. coli* to explain experimental findings that quinolones with fast binding to targets are more effective in inhibiting bacterial replication.

6.5 Conclusions

Our mechanistic model capturing threshold behaviour around binding of β -lactams to PBP resolves discrepancies between simulated and observed treatment outcomes in the presence of intracellular replication of NG that were observed in Chapter 4. The model provides a framework to evaluate treatment effectiveness using ceftriaxone and cefixime and with revision this model may offer the potential to more widely explore effective treatment options for NG.

Chapter 7

Conclusions and future work

Understanding the within-host dynamics of an infection can be useful for various purposes including designing treatment guidelines, developing new therapeutic options and interventions and managing the spread of infection in the population (Ciupe and Heffernan 2017; Jenner, *et al.* 2020; Vlazaki, *et al.* 2019). In the context of *Neisseria gonorrhoeae* (NG), our understanding of within-host infection processes is hindered by the limitations in experimental studies. In particular, there is poor understanding of the drivers of persistence of infection as it is difficult to sustain infection in animal models (Arko 1989; Rice, *et al.* 2017) and experiments using human volunteers (e.g., Ramsey, *et al.* 1995; Schmidt, *et al.* 2000; Schneider, *et al.* 1996) are limited to the initial stages of the infection due to ethical constraints.

The dynamics of intracellular NG populations (NG within polymorphonuclear neutrophils (PMN) and epithelial cells) and their role in sustaining infections are not well understood from published experimental studies (Theuretzbacher, *et al.* 2020). While *in vitro* cell culture models are used to understand NG replication and survival mechanisms within distinct host cells (Rest, *et al.* 1982; Shaw and Falkow 1988), they do not capture the simultaneous interactions between bacteria, PMN and epithelial cells that occur *in vivo*. In addition, to my knowledge these cell culture models have not been used to study the differential effects of antibiotics on extracellular (unattached and attached NG to epithelial cells) and intracellular NG.

In this regard, mathematical models are useful as they can encapsulate evidence from a variety of sources and experimental studies and provide a means to quantitatively

describe within-host phenomena currently unexplored in experimental studies. The initial objective of this thesis was to link within-host processes with population-level antibiotic resistance patterns but, due to the limited prior work on within-host dynamics in the context of NG, I had to deviate from this initial research path. This led me to first focus on modelling the within-host dynamics and antibiotic treatment effects of male urethral NG infection.

My attempt to mathematically model the within-host NG infection dynamics is a novel contribution to an area of study that has not been previously extensively studied. By collating information from various *in vitro* and *in vivo* experimental studies I have developed new mechanistic models of within-host NG infection that include relevant features of antibiotic treatment and attempt to align the simulated outcomes with antibiotic-treated and untreated infection. The main findings in this thesis suggest the importance of intracellular NG in prolonging the natural infection and in determining the effectiveness of antibiotic treatment regimens. These findings in some way contribute to filling the knowledge gap on the understanding of the long-term infection and intracellular NG dynamics that is difficult to be fulfilled using existing experimental methods. Using this modelling framework, I further simulate the effectiveness of different treatment regimens and identify the requirements of pharmacokinetic/pharmacodynamic (PK/PD) characteristics of drugs to attain successful infection clearance that can be useful when guiding the design of clinical trials.

As discussed in Chapter 2, there is very limited data describing the role of intracellular NG during infection or within-host infection beyond the first 5-7 days of infection. In an attempt to address this gap in understanding and to achieve the research aims outlined in Chapter 1 (Introduction), I first develop a novel within-host mathematical model that describes the dynamics of untreated urethral NG infection in

men (Chapter 3). This model captures NG interactions with epithelial cells and PMN, informed by *in vivo* and *in vitro* studies. Here, the focus is on male urethral infection as there are very limited data for infection at other anatomical sites (as described in Chapter 2, Section 2.2). The natural infection model is then used as a framework to study treatment effects. In subsequent chapters, the treatment effects of antibiotics that are currently in use, as well as potential new treatment options, are explored by including the relevant extracellular and intracellular PK/PD drug interactions and mechanisms of drug binding (for ceftriaxone and cefixime) to targets on NG.

Using the model developed in Chapter 3 (Modelling the in-host dynamics of *Neisseria gonorrhoeae* infection), I find that infection is prolonged by the intracellular NG populations, with ~80% of the total NG population internalised from day 5 onwards, consistent with the limited observations in urethral exudates described by Veale, *et al.* (1979). The importance of PMN in determining simulated NG infection dynamics is further established through the multivariate sensitivity analysis, the results of which suggest that parameters relating to PMN engulfment of NG and NG occupancy of PMN are most influential in terms of infection clearance time. I was also able to adapt the model to successfully describe mouse model data (Jerse 1999) through use of modified parameters for key variables associated with NG internalisation. This aligns with the known absence in mice of human host-specific internalisation and survival mechanisms used by NG (Edwards, *et al.* 2016; Jerse, *et al.* 2011; Sadarangani, *et al.* 2011).

In Chapter 4 (Modelling treatment effects for gonorrhoea), I extend the natural infection model developed in Chapter 3 to include antibiotic treatment with the main current treatments (ceftriaxone, cefixime, azithromycin) and two potential alternative treatment options (gepotidacin and gentamicin). Extracellular dynamics of NG under treatment are matched to *in vitro* time-kill studies (Farrell, *et al.* 2017; Foerster, *et al.*

2016), while simulated extracellular drug concentration profiles were designed to match observed plasma drug concentration measurements for ceftriaxone (Patel, *et al.* 1982; Scully, *et al.* 1984), cefixime (Brittain, *et al.* 1985; Faulkner, *et al.* 1988) and gepotidacin (Taylor, *et al.* 2018b) in the respective studies. For the two drugs that are modelled as two-compartment PK models, the simulated ratios of intracellular to extracellular drug concentration for azithromycin (Foulds and Johnson 1993) and gentamicin (Tulkens and Trouet 1974; Tulkens and Trouet 1978; Tulkens 1990) also align with the limited observations available in these respective studies.

In Chapter 4, I generate a ‘model-derived susceptibility breakpoint’ for each drug representing the largest MIC (Hill function parameter) resulting in successful infection clearance. The simulations suggest that if intracellular NG states are included, there are major reductions in these breakpoints. This suggests the importance of intracellular states in clearance behaviour but I have not been able to identify relevant data to compare this prediction against. However, I note that at MIC values that are categorised as susceptible according to the empirical susceptibility breakpoints, clinical treatment failures for NG infection have been reported for azithromycin (Tapsall, *et al.* 1998) and gentamicin (Ross, *et al.* 2019) at MIC of 0.125 – 0.25mg/L and 4mg/L, respectively.

The model developed in Chapter 4 successfully reproduces empirical breakpoints for gepotidacin, gentamicin and azithromycin, but did not succeed in this regard for ceftriaxone and cefixime. Therefore, the model developed in Chapter 4 is further used in Chapter 5 to evaluate treatment effectiveness of a monotreatment (gepotidacin) and dual treatment regimen (gentamicin + azithromycin) while treatment effects using these two β -lactams are addressed in a revised model in Chapter 6.

In Chapter 5 (Effectiveness of different treatment regimens for gonorrhoea), simulations of clearance behaviour using single dose gepotidacin regimens align with reported treatment success rates in clinical for NG strains with MIC ≤ 0.5 mg/L (Scangarella-Oman, *et al.* 2018; Taylor, *et al.* 2018b). Simulation results for dual therapy with gentamicin and azithromycin are broadly consistent with clinical observations (Kirkcaldy, *et al.* 2014; Ross, *et al.* 2019) but direct comparison by MIC strata are not possible. I find that a cut-off of 150h for the intracellular PK index, the ratio of area under the curve to MIC clearly discriminate between treatment success and failure using gepotidacin but no extracellular PK indices show this dichotomous behaviour. In the additional analysis presented in Chapter 5, I find that at increasing values of the MIC, the dual treatment regimen of gentamicin + azithromycin exhibits improved treatment effectiveness compared with the gepotidacin or gentamicin monotreatment options. This is because, under the assumption of Loewe additivity, the effects of both drugs are combined to effectively yield a single drug of higher antibacterial effectiveness (Dini, *et al.* 2018; Loewe 1928).

In Chapter 6 (Evaluation of ceftriaxone and cefixime treatment strategies using a model that incorporates drug-target binding), I revise the treatment model for ceftriaxone and cefixime to capture threshold effects for bacteriostatic and bactericidal effects associated with the drug-target binding dynamics observed in experimental studies (Williamson and Tomasz 1985). This model extends on the work by Abel zur Wiesch, *et al.* (2015) to explain *V. cholerae* and *E. coli* dynamics. This revised model allows a rapid transition of NG to a dormant, non-replicating state, where bactericidal effects are applied. As shown in the chapter this leads to substantially more rapid clearance of simulated bacteria despite maintaining similar concentration and killing profiles to the model used in Chapter 4.

Using this revised model for ceftriaxone and cefixime I am able to reproduce clinically observed behaviour while maintaining realistic parameter values. Consistent with the findings in Chapters 4 and 5, I find that insufficient killing of intracellular bacterial populations is the key determinant of treatment failure. Similar to the Chapter 5 findings using multiple doses of gepotidacin, gentamicin and azithromycin, here also multiple dose regimens of cefixime do not add any substantial benefit over a single dose regimen with a fixed total dose amount.

A common theme in these results is the apparent importance of intracellular NG in prolonging infection and determining the effectiveness of treatment regimens. The link between intracellular NG and prolonged infection established in Chapter 3, is broadly consistent with the observations from *in vitro* studies which suggest that PMN provide a reservoir for NG replication while evading the host immune responses (Criss and Seifert 2012; Quillin and Seifert 2018). In Chapters 4-6, a common feature of simulations is that antibiotic treatment failure is associated with failure to successfully clear intracellular NG. I also find that extracellular PK indices alone could not differentiate treatment success and failure. If additional data on antibiotic mediated killing of intracellular NG become available through future experimental studies (e.g., *in vitro* time-kill experiments), analogous for example to the study by Barcia-Macay, *et al.* (2006) that analysed drug mediated killing of extracellular and intracellular *S. aureus*, some of my findings on the rates of intracellular NG killing by antibiotics could then be compared with experimental data. Although such experimental studies on antibiotic activity against other intracellular pathogens can be a useful guide it is important to note that the magnitude of intracellular bacteriostatic/bactericidal effects depends on both the pathogen and the drug.

Throughout the thesis, I adopt a deterministic modelling framework rather than a stochastic one for modelling within-host NG infection. I make this decision primarily because for large population sizes the results from a stochastic model will generally converge with those derived from a deterministic model (Kurtz 1970; Kurtz 1972). In this thesis, as the NG loads peak at 10^6 - 10^8 bacteria and the number of drug molecules $\sim 10^{15}$, a deterministic model is appropriate. Furthermore, deterministic models are more tractable for analysis and computationally more efficient.

In the modelling work carried out in this thesis (Chapters 3- 6) several decisions around the model formulation are determined by the quantity and quality of the data and evidence available in the literature. For example, as discussed in Chapter 1, I only consider symptomatic male urethral NG infection, a decision driven by the lack of experimental studies on infection at other anatomical sites that investigate the dynamical changes of the bacterial load over time. Several simplifying assumptions are also made in regard to the way in which the immune response is modelled. For example, I only consider the PMN response which is considered to be the primary immune response triggered against NG infection (Unemo, *et al.* 2019). The possible contributions from macrophages or adaptive immune response are not considered due to the lack of strong evidence or extensive experimentation to assess the role of these immune components in describing infection dynamics.

A common limitation of the modelling approaches applied in this thesis is the use of dichotomous thresholds for defining resolution of infection in Chapters 3-6 and the drug-bound PBP threshold for shifting to bacteriostatic and bactericidal effects in Chapter 6. For example, as is observed in Chapter 5, Section 5.3.1.2, the use of strict thresholds in my definition of infection clearance leads to almost identical model trajectories being identified as having opposite treatment outcomes, i.e., successful versus unsuccessful

clearance. Here, a stochastic implementation of the model such as a continuous time Markov chain with discrete-valued outcome variables may better be suited to handle this uncertainty using stochastic extinction as the direct measure.

Wherever possible I attempt to validate simulated treatment effectiveness and infection clearance times by comparison with clinical observations. However, published data are limited, especially in regard to multiple dose regimens which made it impossible to validate the simulated treatment outcomes. In clinical trials of dual treatment regimens, it would be beneficial to report MIC values for both drugs relating to a particular isolate, as this would be informative as to whether treatment failure is related to resistance to just one drug or both involved. For example, in the clinical trial on dual treatment with gentamicin and azithromycin (Cole, *et al.* 2019) it is not clear what the value of MIC for azithromycin is in the samples with treatment failure that have MIC for gentamicin of 4mg/L. In clinical trials, it is also difficult to precisely determine the time taken for infection clearance as these studies only perform a test of cure at a selected time (Kirkcaldy, *et al.* 2014; Ross, *et al.* 2019) which lacks kinetic information and therefore cannot be directly comparable with.

My work can be extended to describe infection at other anatomical sites such as pharyngeal or rectal infection. However, the model will require substantial modification to capture anatomical site-specific differences such as differential drug penetration and accumulation in different sites (Kong, *et al.* 2017), and NG interaction with other *Neisseria* species (Weyand 2017). As described in Chapter 2, Section 2.2, a major challenge in adapting the model to describe other anatomical sites would be the lack of data to describe the dynamical changes in bacterial load over time at non-urethral sites.

In Chapters 4 and 6, when considering decreased susceptibility/resistance, resistant bacterial populations are not explicitly modelled. To the best of my knowledge,

Mao and Lu (2016) is the only study that considers a specific mechanism for NG resistance (horizontal gene transfer by natural transformation) in a within-host model. However, this model does not consider the infection process in detail as it lacks NG interactions with different host cells. When considering rare events such as the probability of within-host emergence of resistance with de-novo mutations, a stochastic model similar to that used in the work by Colijn, *et al.* (2011) on tuberculosis would be more appropriate. Here, the authors use a stochastic birth-death process to model the probability of within-host emergence of drug resistance in *M. tuberculosis* (Mtb).

A framework similar to Colijn, *et al.* (2011) could be used to extend the base model in Chapter 3 for modelling the within-host emergence of NG drug resistance, but the differences between the underlying mechanisms that confer resistance in the two bacteria Mtb and NG need to be considered. Horizontal transfer of resistant genes has not been reported in Mtb and the primary mode of acquiring drug resistance is through chromosomal mutation (Singh, *et al.* 2020; Smith, *et al.* 2013). In contrast, there are many ways that NG can acquire resistance including point mutations, uptake of exogenous DNA from commensal *Neisseria* species and plasmid conferred resistance (Unemo and Shafer 2014).

A within-host model to capture NG resistance may provide the opportunity to evaluate the probability of the emergence of resistance with dual treatment combinations, especially for combinations where the drugs used have the same mechanisms of action (e.g., gentamicin and azithromycin). Here, *in vitro* time-kill data that measure NG growth in the presence of both drugs are useful to determine differences in the drug mediated bacterial killing effects of sensitive and resistant strains

Generally, within-host and population-level dynamics are interrelated as, for example, an individual's susceptibility to infection can depend on immune memory and

the probability of transmission can be dependent on the individual's bacterial load (Grassly and Fraser 2008). In this case, my existing model can be used to capture within-host infection and bacterial load, with this potentially linked with infectiousness of individuals in a population-level model such as in Craig, *et al.* (2015). These kinds of models allow for consideration of how within-host resistance processes interact with population surveillance and control. A key question for NG control is how to sustain the use of ceftriaxone as effective therapy, and whether there are more effective approaches than population level switching of drugs when resistance to 1st-line therapy exceeds 5% (Moran and Levine 1995; World Health Organization 2012). There are several theoretical studies not specific to NG infection that integrate within-host and population-level scales to assess the optimal dosing regimens to reduce the emergence and spread of drug resistance in the population (e.g., Colijn and Cohen 2015; Davies, *et al.* 2019; Legros and Bonhoeffer 2016). For example, the theoretical study by Colijn and Cohen (2015) indicate that determination of whether the use of high or low dose treatment regimens will minimise the emergence of resistance depends on the within-host competition between drug-susceptible and drug-resistant strains.

Another possible future direction in which my work can be extended is to model vaccine effects. In a large retrospective case-control study that assessed the efficacy of an outer membrane meningococcal B vaccine (MeNZB) among people aged 15-30 years in New Zealand, 31% effectiveness against gonorrhoea was estimated (Petousis-Harris, *et al.* 2017). While the MeNZB vaccine was developed in response to a clonal meningococcal B epidemic, more recently the broadly protective meningococcal B vaccine Bexsero (GSK Inc.) has been developed. Epidemiological models have also shown that even a partially protective vaccine has the potential to substantially reduce

gonorrhoea prevalence (Craig, *et al.* 2015) even in high-risk populations such as men who have sex with men (Whittles, *et al.* 2020).

With a partially effective vaccine, it may be important to assess how a stimulated immune response affects bacterial growth, prevents symptoms or reduces infection duration. These aspects can be studied using a within-host vaccine model, based on the infection model developed in Chapter 3, but with added features to capture immune response stimulation. Here, the adaptive immune response would need to be captured specifically, and potentially some additional changes to the way the innate response through PMN is captured would need to be made. As human clinical trials of gonococcal vaccines are not yet completed, characteristics such as efficacy, duration of protective immunity and differences in efficacy by anatomical site remain unknown (Gottlieb, *et al.* 2020). The use of within-host models to simulate the effects of potential vaccines may be an interim way forward, with the potential to inform the design of clinical trials.

Understanding of the within-host NG infection dynamics is strongly limited by the paucity of current data and here I summarise several urgent data needs. From the sensitivity analysis conducted in Chapter 3, the rates of NG internalisation were identified as important variables in explaining infection duration. However, there is lack of data to inform the dynamical changes of the proportions of extracellular and intracellular NG which would be useful in validating the simulated cellular NG proportions and assist in better understanding the long-term time-course of natural infection dynamics. Throughout Chapters 4-6, parameters defining intracellular drug accumulation are identified as important in achieving treatment success. However, data on intracellular drug accumulation and penetration and intracellular antibiotic-mediated killing effects is lacking in the context of NG. Such intracellular PK/PD data would be further useful when optimising dosing regimens and determining effective drug combinations. When

measuring antibiotic mediated killing of intracellular NG, *in vitro* time-kill experiments such as conducted for *S. aureus* (e.g., Barcia-Macay, *et al.* 2006) would be useful. In Chapters 5 and 6, I simulated the effectiveness of different multiple dosing regimens using gepotidacin, cefixime, azithromycin and gentamicin. However, for validation of simulated treatment success rates, it would be useful for clinical trial results on multiple dosing regimens to be disaggregated by strain MIC. This would be a useful consideration during the proposed phase 3 clinical trial (ClinicalTrials.gov Identifier: NCT04010539) testing a two-dose regimen of gepotidacin (3000mg \times 2). Finally, when estimating the drug bound PBP thresholds to separate bacteriostatic from bactericidal effects, I lacked data directly linking NG growth to drug-bound PBP fractions. Availability of such data would enable more realistic representation of this transition behaviour within the model used in Chapter 6.

In summary, the main contribution of this thesis is to explore the influence of intracellular NG populations in describing within-host NG dynamics and relate intracellular antibiotic killing and PK/PD effects to clinical and experimental measures of treatment success. I hope these findings will promote future experimentation in this field on, for example, intracellular bacterial killing effects through immune response, the evaluation of intracellular PK/PD effects through the means of *in vitro* time-kill studies and reporting on the effectiveness of multiple dose regimens. The findings of this thesis may also have translational benefits in terms of potentially identifying characteristics of effective antibiotics and treatment regimens for NG.

Appendix A

Supplementary material pertaining to Chapter 3

A.1 Parameter estimation

A.1.1 Replication rate of B_s (r_3)

In the *in vitro* study of Simons, *et al.* (2005), NG survival within PMN and their replication was measured. It was seen that the number of intracellular NG increased from $83.12 \pm 12.15\%$ viable at 1 hour to $495.8 \pm 47.74\%$ viable at 6 hours. Therefore, the replication rate of NG in B_s was estimated to be around 0.308-0.408 per hour.

A.1.2 Parameter estimation through model fitting

In order to estimate the model parameters, the model was fitted to *in vitro* data. Data from the *in vitro* studies of Gubish, *et al.* (1979), Rest, *et al.* (1982) and Shaw and Falkow (1988) were extracted using the WebPlotDigitizer tool (Rohatgi 2018).

A.1.2.1 Bacterial attachment rate to epithelial cells (a_1) and maximal NG attachment capacity of an epithelial cell (a_2)

In the *in vitro* study by Gubish, *et al.* (1979) NG attachment to HeLa cells was measured over a period of 4 hours using various initial bacterium to cell ratios. In fitting to these data, a bacterium to cell ratio of 10:1 was used, as it was observed that this ratio yielded the most efficient binding. At higher ratios, saturation occurred and attachment was inhibited. The study had measured attachment on two NG types, piliated and non-piliated. A function of the form $a_2(1 - e^{-a_1 t})$ was fitted to both these NG types in Gubish, *et al.* (1979) to estimate a_1 and a_2 . The piliated NG type resulted in estimates of

0.34 $hour^{-1}$ and 12 *bacteria* for a_1 and a_2 respectively, while the non piliated NG type resulted in estimates of 0.31 $hour^{-1}$ and 6 *bacteria* for a_1 and a_2 respectively.

A.1.2.2 Replication rate of B_i (r_2) and rate of internalization (η)

In order to estimate r_2 and η , data from the study by Shaw and Falkow (1988) were used where the number of NG that survived gentamicin exposure was measured over 12 hours. However, for the first 6 hours of the experiment, gentamicin was not effective in killing attached NG due to some form of protection offered by the type of epithelial cell that was used. It was also observed that NG was not internalized during this period. Therefore, our model was fitted to NG that survived gentamicin exposure over a 6-12 hour time period as earlier time points included NG that were attached but not killed through gentamicin. Since gentamicin kills unattached and attached NG after 6 hours and the antibiotic was introduced every 2 hours, replication of unattached NG (r_1) was omitted from the fitting process. Furthermore, as exit of NG from epithelial cells was not measured and PMN were not involved in the experiment, those processes were not considered in the fitting.

Assuming that NG that have survived gentamicin exposure at the 6-hour time point reflect only attached NG (B_a), the following equations were fitted to estimate r_2 and η .

$$\frac{dB_a}{dt} = -\eta B_a$$

$$\frac{dB_i}{dt} = (\eta B_a + r_2 B_i) \left(1 - \frac{B_i}{k_1 a_2}\right)$$

Credible intervals around these point estimates were also obtained as discussed in more detail in Appendix A, Section A.2.2.

A.1.2.3 Bacteria engulfment rate (d), proportion of NG surviving within PMN (p) and ratio dependent constant (c) based on in vitro data

Data from the *in vitro* study by Rest, *et al.* (1982) on PMN phagocytosis of non piliated Opa expressing NG in the absence of serum, measured over a period of 135 minutes were used to obtain estimates of the bacterial engulfment rate (d), the proportion of NG surviving within PMN (p) and the ratio-dependent constant (c). In this experiment, epithelial cells were not involved and therefore when fitting the model to these data, the contribution of attached bacteria and internalized NG were not taken into consideration. Also, as the experiment was only conducted over a period of 135 minutes and the lifespan of PMN during gonococcal infection (d_3) is about 24 hours (Simons, *et al.* 2005), the PMN count was assumed to remain constant in the fitting process. This short duration also suggest that NG would not exit from PMN during the experiment. We further simplified the fitted model by noting that bacterial growth in this *in vitro* setting would not be limited by capacity constraints over this timeframe. Based on these assumptions, a simplified sub-model described by the following equations was fitted to the data reported in the study by Rest, *et al.* (1982):

$$\frac{dB}{dt} = r_1 B - d \frac{B N}{c N + B}$$

$$\frac{dB_s}{dt} = \left(p d \frac{B N}{c N + B} + r_3 B_s \right) \left(1 - \frac{B_s}{N k_2} \right)$$

Credible intervals around these point estimates were also obtained as discussed in more detail in Appendix A, Section A.2.2.

A.1.2.4 Model fitting to estimate bacteria engulfment rate (d), proportion of NG surviving within PMN (p), ratio dependent constant (c) and estimation of the PMN activation rate (μ) and replication rate of non-internalized bacteria (r_1).

Data for the fitting procedure to estimate d , c , p , μ and r_1 were generated based on the known qualitative features of the time-course of infection that are described in the Chapter 3 section ‘*Qualitative features of the time-course of infection*’. 1000 data samples, each consisting of five generated data points (denoted as (X_i, Y_i) , $i=1, 2 \dots 5$ below) were created. Total NG load obtained from the full five-state human infection model was fitted to these five data points in each sample to estimate the parameters d , c , p , μ and r_1 using the MATLAB (MathWorks, Natick, MA) optimisation function ‘*fmincon*’.

The five data points for each sample was generated as follows. The initial NG load at time 0 and the NG load at infection clearance (at 75 days) were held fixed at 1000 bacteria (Schmidt, *et al.* 2001; Schneider, *et al.* 1996) and 10 bacteria (Schneider, *et al.* 1995), respectively. The other three NG load data points based on plateau level and peak NG load and their respective time points were randomly generated from a uniform distribution. Based on the plateau level in bacterial load observed in the time-course of infection during days 1-2, we generated uniformly distributed pairs ($X_2 \sim \text{Uniform}(1, 2)$ days, $Y_2 \sim \text{Uniform}(10^6, 5 \times 10^6)$ bacteria). Observations of the peak load suggest this occurs between day 2 and 5, and we generated corresponding simulated pairs ($X_3 \sim \text{Uniform}(2, 5)$ days, $Y_3 \sim \text{Uniform}(Y_2, 10^7)$ bacteria). The NG load Y_2 was also used as the total NG load at the later time point $X_4 \sim \text{Uniform}(5, 7)$ days.

Estimates for the parameters d , c , p , μ and r_1 were produced by fitting the human infection model to the data described above using the ‘*fmincon*’ function in MATLAB

(MathWorks, Natick, MA). Model initial conditions were as in Chapter 3, Table 3.1, with all other parameters values fixed at the point estimates shown in Chapter 3, Table 3.2. Fitting involved minimising the objective function

$$\sum_{i=1}^5 (\log (X_i) - \log (\hat{X}_i))^2$$

where, X_i represents the simulated bacterial load data at time Y_i of a particular data sample and, \hat{X}_i represents the total bacterial load ($B + B_a + B_i + B_s$) at time Y_i predicted from the human infection model. In the objective function, the logarithmic differences between the data and the fitted values were used to account for large order of magnitude variations in the NG data (10^1 - 10^7). Across the 1000 fits, the median SSE 1.29 (95% range 0.009 – 4.45). Three example fits are shown in Fig. A.1. The medians of the ranges for each parameter across the 1000 fits were used as the respective point estimate of d , c , p , μ and r_1 (shown in Chapter 3, Table 3.2). The distributions of parameter estimates are shown in Fig. A.2.

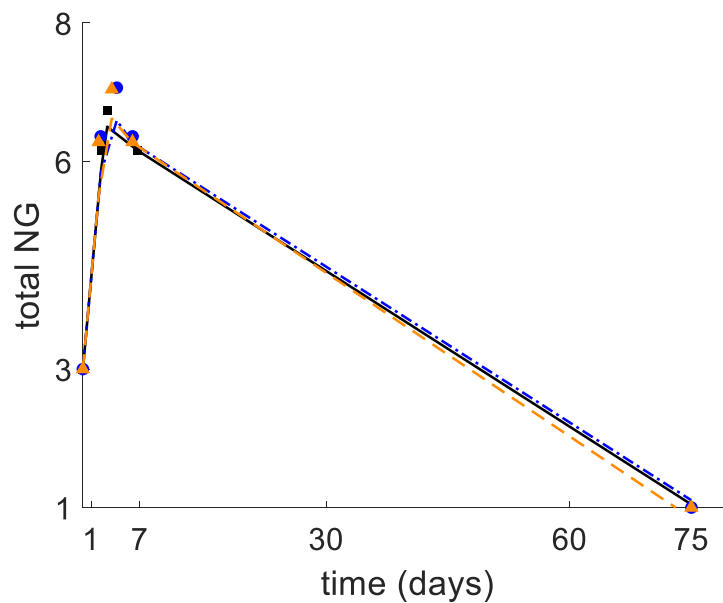


Figure A.1: Three instances of the model fits to three simulated data samples. Scatter points indicate the generated data on bacterial load at respective time points and the lines indicate the total bacterial load obtained from the human infection model using the estimated parameter values of d , c , p , μ and r_1 obtained for each data sample.

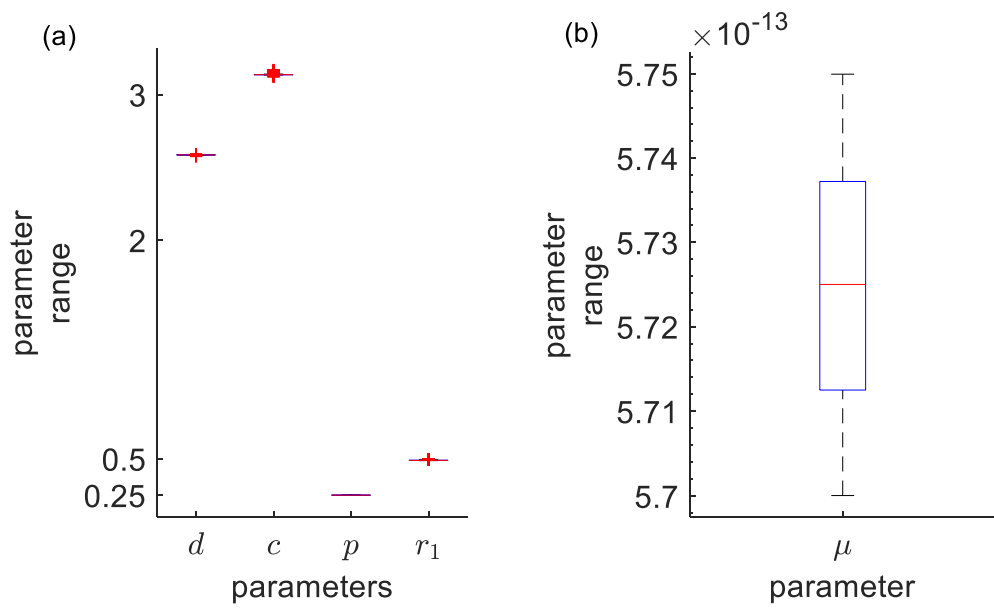


Figure A.2: Distribution of the estimated parameter values obtained by fitting to the 1000 simulated data samples. (a) Distribution of the parameter estimates of d , c , p and r_1 . (b) Distribution of the parameter estimates for μ .

A.2 Sensitivity Analysis

A.2.1 Multivariate sensitivity analysis

We analysed the samples that met the outcome criteria (described in the Section ‘*Multivariate sensitivity analysis*’ in Chapter 3) of the 100,000 initial Latin Hypercube (LHS) samples that were generated using the parameter ranges in Chapter3,

Table 3.2. When these retained samples were analysed in pairs to identify any associations between them, the only strong correlation that was observed was between the two parameters d and c . This was analysed both visually using scatter plots (Fig. A.3) and using Spearman's correlation coefficient ($\rho = 0.71$). When a regression line of the form $d \sim b \times c + a$ was fitted, the estimated slope with 95% confidence bounds was $b = 0.321$ (0.310, 0.331) and the intercept with 95% confidence bounds was $a = 1.262$ (1.224, 1.3). This relationship between d and c was used to re-run the multivariate sensitivity analysis with the distribution of d being determined with expanded three-fold ranges for b and a given by $b \in (0.207, 0.497)$ and $a \in (0.816, 1.95)$. The other parameters were varied in the ranges given in Chapter 3, Table 3.2. In this second run, from 100,000 LHS samples, 5.4% of the samples met the outcome criteria. In 60.49% of samples, infection cleared but did not meet those outcome criteria and the remainder (34.11 %) resulted in persistent infection. Out of those 5.4% of the samples that met the stricter outcome criteria there were 442 samples that met the stricter clearance criteria of 2-6 months, which were compared with the main sensitivity analysis results.

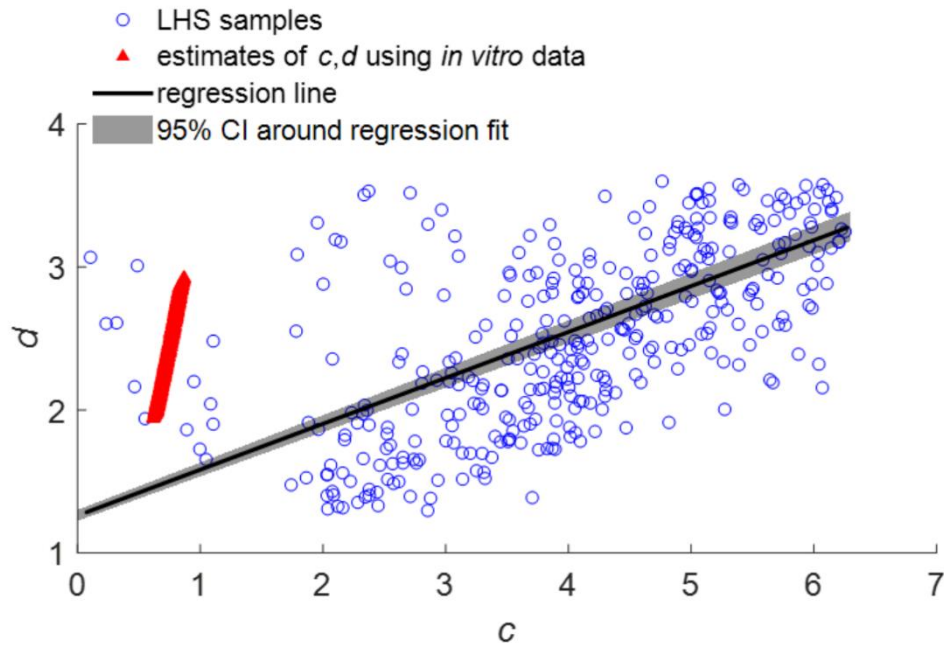


Figure A.3: Relationship between the two parameters d and c obtained from the samples that met the outcome criteria of the LHS parameter sets that were generated using the parameter ranges as described in Chapter 3, Table 3.2 (the range of d was in this instance varied from 1.295 – 5.178). A regression line is fitted of the form $d \sim b \times c + a$. Estimated d and c values by fitting the sub-model to the data in the *in vitro* study Rest, *et al.* (1982) are also shown in red.

A.2.1.2 Human infection model results based on simulations from LHS samples

The distribution of the outcome variables (peak time, peak NG load and infection duration) are shown in Fig. A.4 for all the LHS samples that met the features with an infection duration of 1-3 months and with a duration of 2-6 months. The infection duration of the samples that met the features is highly concentrated around 30 - 45 days.

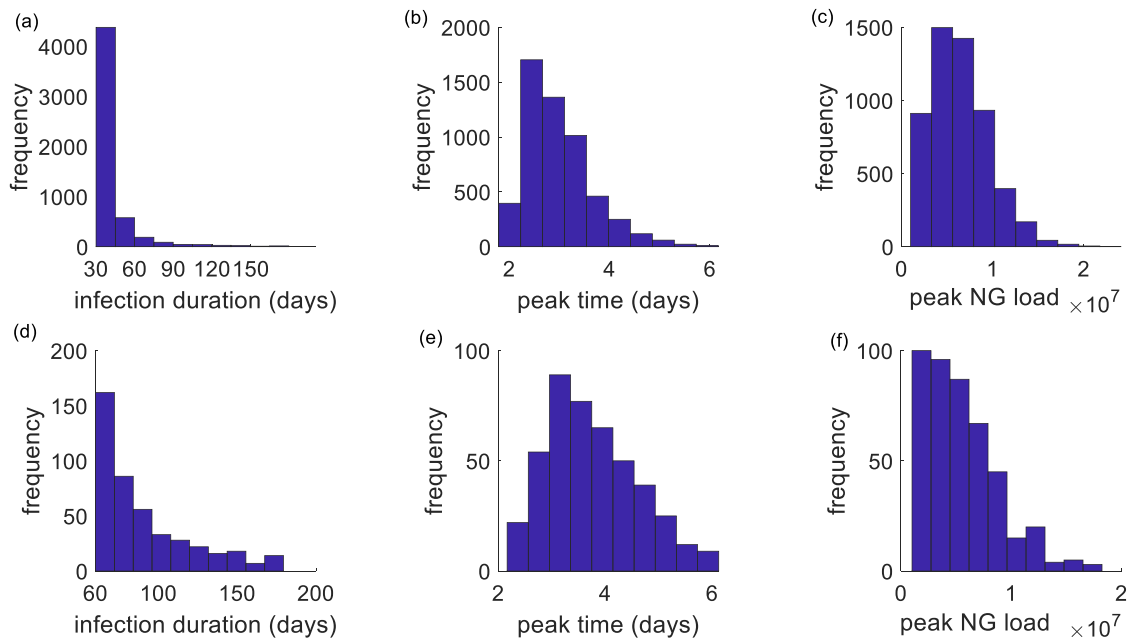


Figure A.4: Distribution of the outcomes of the samples that met the features. (a) – (c) represent the infection duration, peak time and peak NG load respectively of all the samples that met the features. (d) – (f) represent the infection duration, peak time and peak NG load respectively of the samples that met the features with infection duration of 2-6 months.

Using partial rank correlation coefficients (PRCC), we analysed the importance of each parameter's uncertainty in contributing to the variability of the model outcomes (Fig. A.5). Analysis was carried out using all the samples that met the features with an infection duration of 1-6 months.

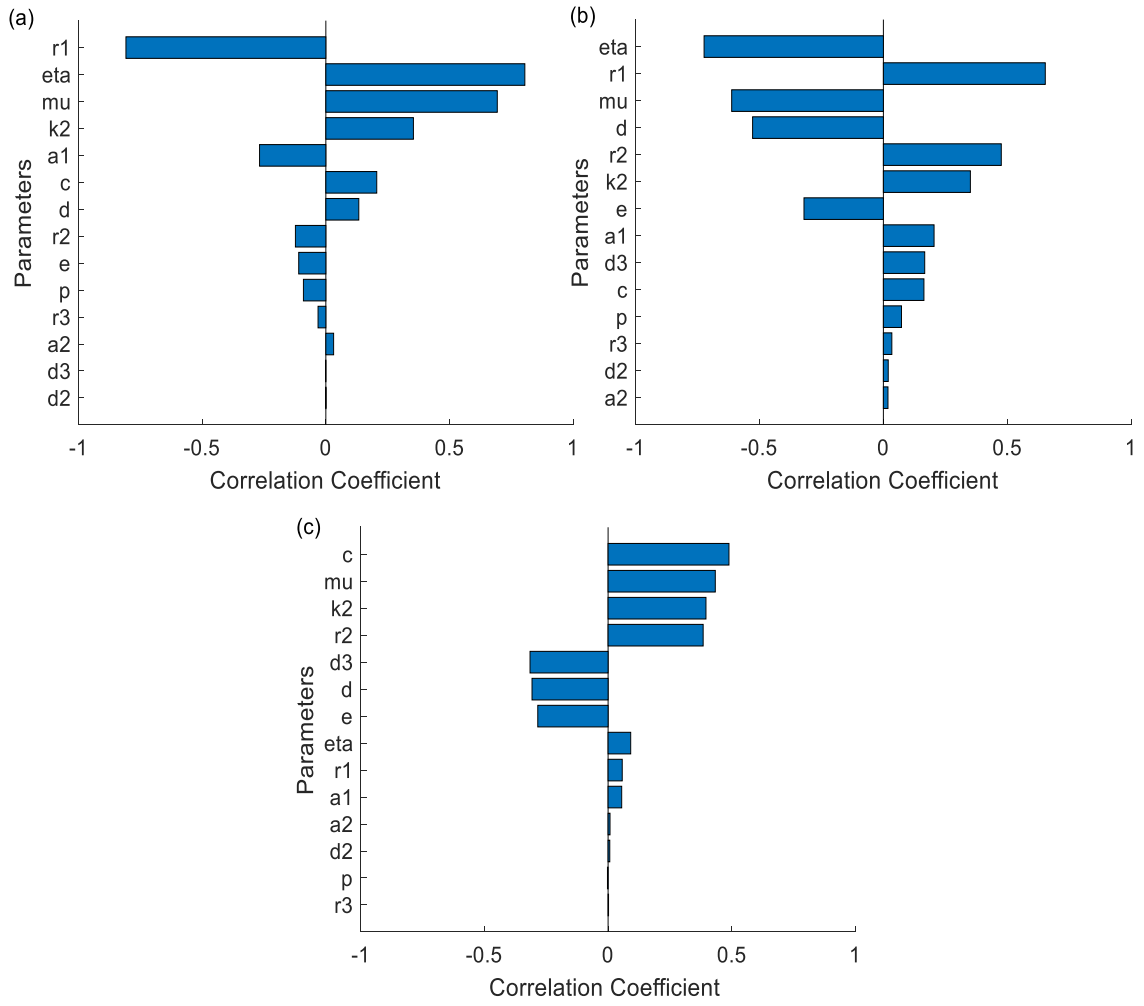


Figure A.5: Tornado plots of partial rank correlation coefficients, indicating the importance of each parameter's uncertainty in contributing to the variability in the model outcomes; (a) Peak time, (b) peak load and (c) infection duration. Results are based on the LHS samples that met the outcome criteria.

The percentage of NG in each state for all the samples that met the features with a clearance time from 1-6 months and 2-6 months is shown in Fig. A.6. In these LHS samples, the percentage of cells surviving within PMN (B_s) was substantially higher than

what was obtained using the point estimate parameter values in Chapter 3, Table 3.2 (cell percentages using the point estimates are shown in Chapter 3, Fig. 3.4).

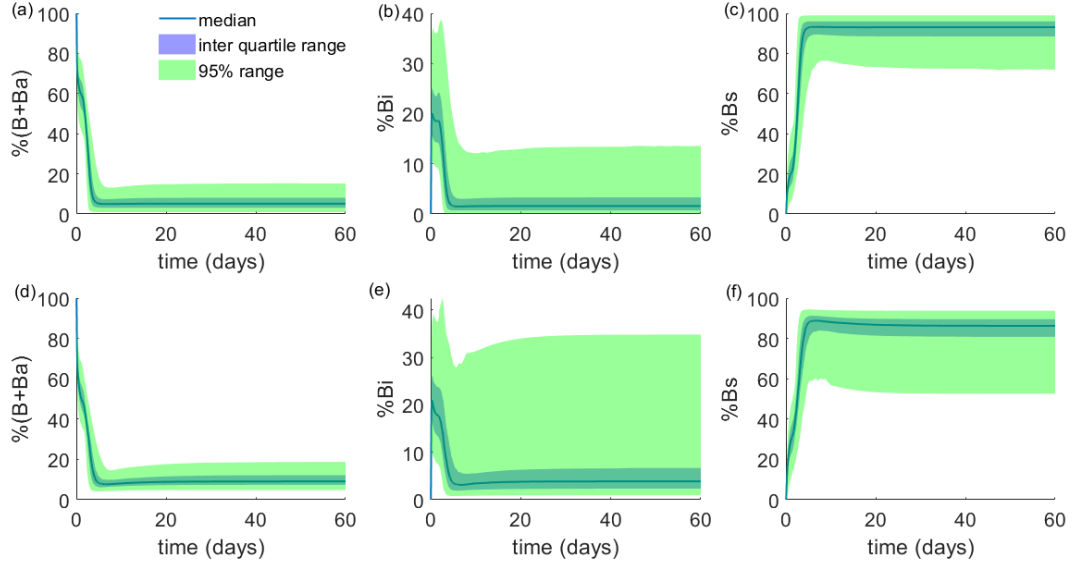


Figure A.6: Proportion of NG in each of the states over time during the first 60 days summarised across the LHS samples that met the features and had an infection duration of 1-3 months (a)-(c) and (d)-(f) an infection duration of 2-6 months. The median of the cell percentages, the interquartile range and the range in which 95% of the cell proportions fell is shown. (a) The proportion of NG at extracellular state ($B+B_a$). (b) Proportion of NG internalised within epithelial cells (B_i). (c) Proportion of NG that survive within PMN (B_s). (d) - (f) represents the same cell states as (a)-(c) for the infection duration of 2-6 months.

A.2.2 *In vitro* credible intervals around point estimates

A.2.2.1 *In vitro* credible intervals around replication rate of B_i (r_2) and rate of internalization (η)

In order to determine approximate credible intervals around the point estimates of r_2 and η obtained using the method described in Appendix A, Section A.1.2.2, we varied the urethral carrying capacity (k_1) and maximal NG attachment capacity of an epithelial cell (a_2) in the ranges $5 \times 10^6 - 2 \times 10^7$ (four-fold range around the point estimate) and 6-12 (as described in Appendix A, Section A.1.2.1), respectively, and generated 1000 LHS samples. Then the sub-model in Section A.1.2.2 was fitted to these generated samples. The resultant 95% credible intervals around the point estimates for r_2 and η are summarised in Table A.1.

Table A.1: Point estimates and 95% *in vitro* credible intervals for r_2 and η

Parameter	Point estimate	95% <i>in vitro</i> credible interval
r_2	0.533 $hour^{-1}$	0.51 - 0.65 $hour^{-1}$
η	0.28 $hour^{-1}$	0.27- 0.36 $hour^{-1}$

A.2.2.2 *In vitro* credible intervals around Bacteria engulfment rate (d), proportion of NG surviving within PMN (p) and ratio dependent constant (c)

In order to obtain credible intervals around our point estimates for d , c and p , we first looked for relevant measures in the experimental study Rest, *et al.* (1982) but none were provided. Instead, we varied the parameters that were held fixed during the estimation procedure described in Appendix A, Section A.1.2.3. These fixed parameters were varied in the ranges of: $r_1 \in (0.13 - 0.53)$ (Craig, *et al.* 2015), using the experimental studies by Schmidt, *et al.* (2001) and Schneider, *et al.* (1996)), $r_3 \in (0.3 -$

0.4) (Variation of measured values in Simons, *et al.* (2005)) and $k_2 \in (4 - 16)$ (four fold range from the point estimate). We then generated 1000 LHS samples from these ranges and re-estimated the d , p and c values for each sample parameter set. The resultant 95% credible intervals around the point estimates for d , c and p are summarised in Table A.2.

Table A.2: Point estimates, *in vitro* credible intervals for d , c and p compared to estimated values by fitting the full model to generated data based on the time course of infection.

Parameter	Value estimated from least squares fit	Estimated 95% credible interval around the <i>in vitro</i> fit	Estimates by fitting the full model to generated data based on time course of infection
d	2.783	1.94 – 2.93	2.586
c	0.821	0.61– 0.87	3.135
p	0.025	0.02 – 0.03	0.25

A.2.3 Expanded sensitivity analysis around *in vitro* estimates on epithelial internalisation

Since the *in vitro* study by Rest, *et al.* (1982) is carried out in the absence of epithelial cells, it is possible that the *in vitro* estimates of d , c , and p values are correct but are compensated by changes in internalisation parameters relating to epithelial cells. To check whether modified internalisation parameters could prolong infection while using *in vitro* estimates of d , p and c values, we first generated 100, 000 LHS samples with d , p and c being varied at the credible intervals found in Appendix A, Section A.2.2. The replication rate of internalised NG (r_2), rate of internalization (η) and exit rate of internalised NG (e) were varied over wider ranges ($r_2 \in (0.03 - 1.2)$, $\eta \in (0.1-1)$, $e \in (0.04 - 1.3)$) to look for potential solutions with longer internalisation. Other parameter values

were held at the base level in Chapter 3, Table 3.2. The model was run for these generated parameter samples and the parameter sets that met the outcome criteria were retained.

Although we were able to identify solutions with longer internalisation times that met the outcome criteria while retaining *in vitro* estimates of d , c and p , these parameter sets did not compare well to the other *in vitro* data that we had used to inform our estimates of r_2 , e and η . These data from Shaw and Falkow (1988) in particular suggest an r_2 estimate that is much higher than is consistent with longer internalisation times (Fig. A.7). We note that this higher growth rate is also more consistent with reported doubling times for NG from other *in vitro* studies (e.g., Foerster, *et al.* (2016) reported a NG doubling time of 54 minutes, which corresponds to a replication rate of 0.77 hour^{-1}).

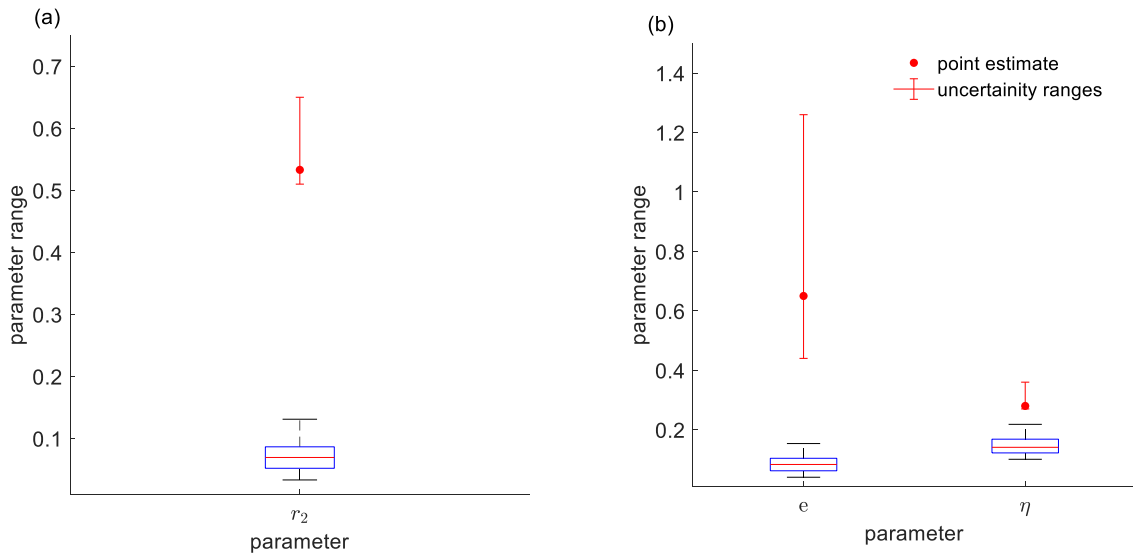


Figure A.7: Comparison of credible intervals for r_2 , e and η , calculated from the Shaw and Falkow (1988) *in vitro* data (point estimate and 95% range) and those generated from the *in vitro* sensitivity analysis described in Appendix A, Section A.2.3 (box plots, with median, interquartile range and 95% credible

intervals). (a) The credible intervals for internalised replication rate r_2 (b) Credible intervals for internalised proportion η and exit rate e .

Furthermore, these parameter values resulted in a very high proportion of NG internalised within epithelial cells (B_i). The B_i population of these samples comprised (out of the total NG population): 34 – 55% on day 2, 60 – 82% on day 3 and 68 – 93% on day 6. These results were substantially higher than what was observed from the *in vivo* study by Veale, *et al.* (1979) which, based on the urethral exudates from 33 male patients, reported the percentage of the B_i population as $15.7 \pm 3.1\%$ of the total NG population (We have assumed the cell proportion in Veale, *et al.* (1979) represents early infection in the range 2-6 days as this was a human experimental study).

Therefore, when the *in vitro* estimates for d , p and c are used in the model with longer epithelial internalisation times, we are unable to match other directly observed features of NG infection. As such, the manually adjusted values (which are consistent with samples for the multivariate sensitivity analysis) were preferred in our base-case to meet the desired qualitative features of the time course of infection.

A.3 Model with PMN delay in activation

The model in Chapter 3 (described under the Section ‘Model structure and formulation’) was changed to include a 3 days delay in PMN recruitment.

$$\frac{dB}{dt} = \left(1 - \frac{B + B_a}{k_1}\right) (r_1 B + d_3 B_s + e B_i) - d \frac{B N}{c N + B} - d_2 B - a_1 B \left(1 - \frac{B_a}{k_1 a_2}\right)$$

$$\frac{dB_a}{dt} = r_1 B_a \left(1 - \frac{B + B_a}{k_1}\right) + a_1 B \left(1 - \frac{B_a}{k_1 a_2}\right) - d \frac{B_a N}{c N + B_a} - \eta B_a$$

$$\frac{dB_i}{dt} = \left(1 - \frac{B_i}{k_1 a_2}\right) (\eta B_a + r_2 B_i) - e B_i$$

$$\frac{dB_s}{dt} = \left(1 - \frac{B_s}{N k_2}\right) \left(p d \frac{B N}{c N + B} + p d \frac{B_a N}{c N + B_a} + r_3 B_s\right) - d_3 B_s$$

$$\frac{dN}{dt} = \begin{cases} \mu (N_{max} - N)(B + B_a) - d_3 N & ; \text{if time} > 3 \text{ days} \\ 10^{-8} & ; \text{otherwise} \end{cases}$$

With this delay term, the qualitatively desired time course of infection can be achieved even when the optimal parameters from least squares estimation are used (Fig. A.8). With this model the peak NG load of 2.45×10^7 bacteria was reached in 4.17 days and the NG load fell below 10 bacteria by 75 days. The initial drop in NG load corresponds to the PMN activation.

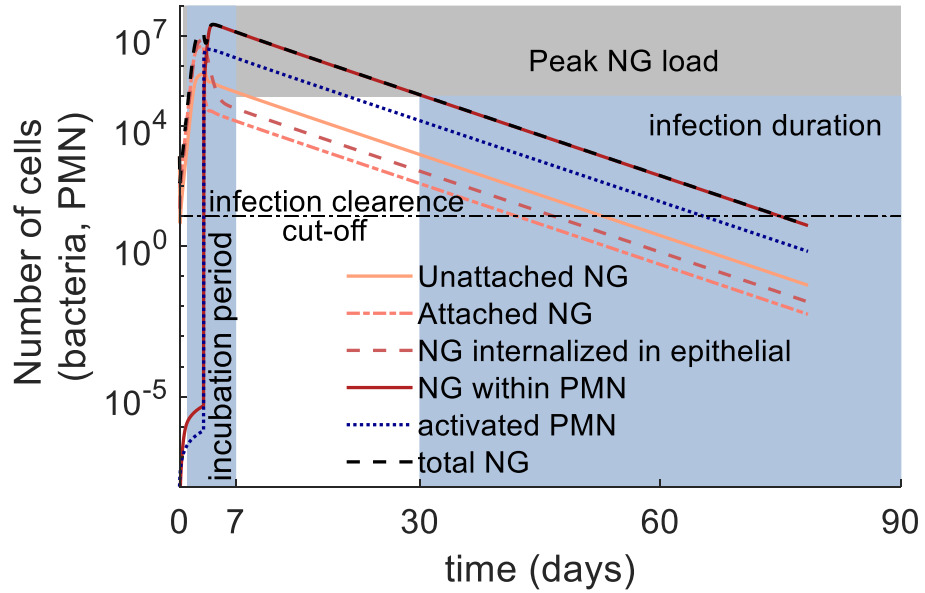


Figure A.8: Model with time delay in PMN activation. Model parameters took values $d = 2.783$, $c = 0.821$, $p = 0.025$ and $\mu = 1.605 \times 10^{-11}$. The other parameter values are the same as in Chapter 3, Table 3.2. The shaded areas represent the peak NG load, incubation period and infection duration reported from human experimental models and pre-antibiotic era studies.

A.4 Comparison of the model NG load with the study by Craig, *et al.* (2015)

The functional form that is used to describe the NG load in the study by Craig, *et al.* (2015) is given as: $l(t) = \frac{k l_0 e^{(r_e - r_h)t}}{(k - l_0) + l_0 e^{r_e t}}$ where, k refers to the peak NG load, l_0 is the initial NG load, $r_e = \frac{\ln 2}{t_e}$ is the replication rate of NG with t_e referring to the doubling time, $r_h = \frac{\ln 2}{t_h}$ is the decay rate with t_h referring to the half-life of NG. The NG load derived from this functional form was compared with the NG load of our model and the results are shown in Fig. A.9.

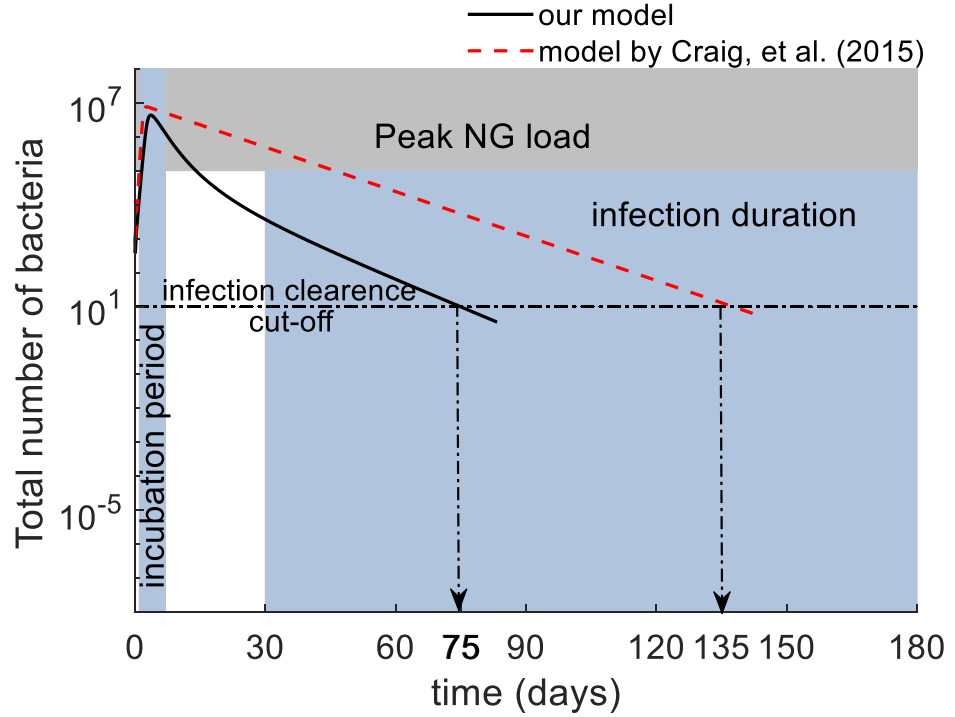


Figure A.9: The total NG load produced by our model and the functional form in Craig, *et al.* (2015). The parameters used to generate the curve of the study Craig, *et al.* (2015) are the base parameters in that study with $l_0 = 1000$, $k = 10^7$, $t_e = 3.4$ and $t_h = 6.9 \times 24$

A.5. Fitting to mouse model data

A.5.1 Mouse parameters k_1 and N_{max}

For mice, N_{max} was taken as 8.32×10^6 cells based on a mean PMN count in a mouse of approximately 4.1×10^3 per μl (von Vietinghoff & Ley, 2008, O'Connell *et al.*, 2015) and average blood volume of mL (O'Connell *et al.*, 2015). Carrying capacity (k_1) was taken as 3×10^6 bacteria based on the surface area of NG and surface area of the mouse urethra, which has a diameter of approximately 4 mm and length of 11 mm (Reis *et al.*, 2011).

A.5.2 Fixing the parameters p and η across mice

In order to analyse which parameters can be kept fixed across mice and also to account for the uncertainty associated with extraction of these NG data from the study by Jerse (1999), we added Poisson noise to the mouse data and refitted the model many times to examine the parameter variation between samples and mice. Specifically, 100 resampled NG load datasets were generated by using the observed NG data at each time point for each mouse as the mean for independently sampled Poisson random variables. In the study by Jerse (1999), NG data for mice are presented graphically and exact values are not reported. We therefore used the digitising tool WebPlotDigitizer (Rohatgi 2018) to extract the numerical values from the graphs and these generated samples allowed us to account for the uncertainty associated in data extraction. The model was fitted to these generated samples and d , c , μ , p , η , r_3 and r_1 were estimated. The results are summarised for each mouse in Fig. A.10, with the parameter p shown to be tightly constrained across mice. In addition, while the parameter values of η varied over the range of 2.244×10^{-4} to 1.033×10^{-6} , model fits were not sensitive to the specific value (Fig. A.11). Therefore, these two parameters were kept fixed across mice at the median values of p (5.4×10^{-5}) and η ($5 \times 10^{-6} \text{ hour}^{-1}$) across the 8 mice when fitting to the original mouse NG data.

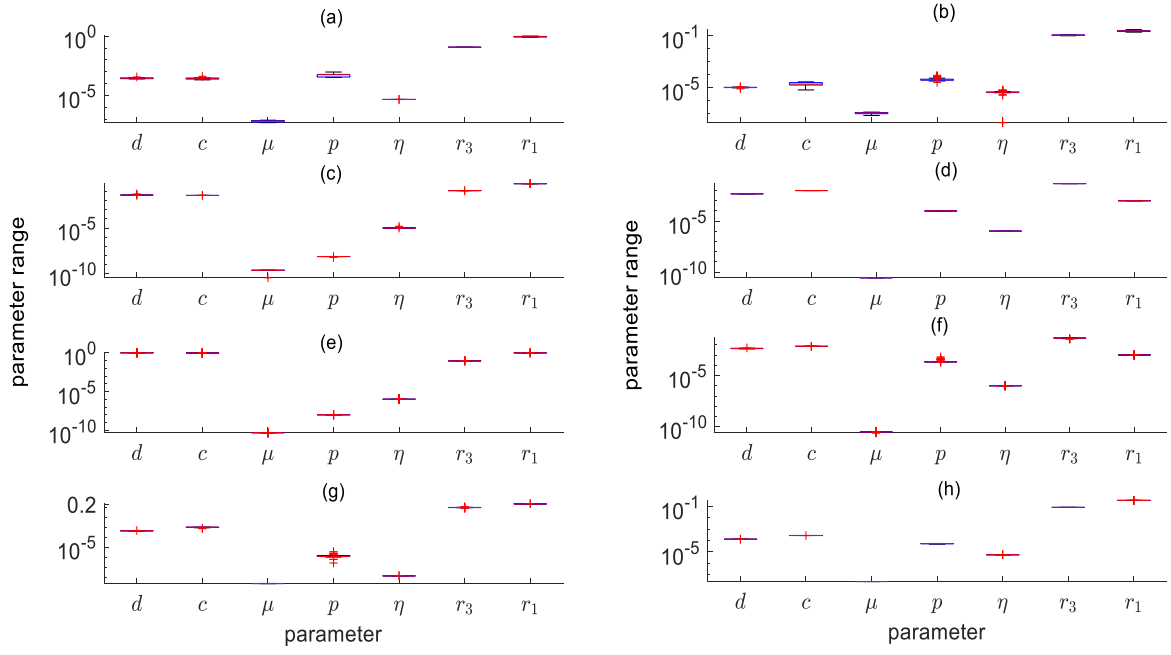


Figure A.10: Parameter ranges of each mouse when the model is fitted to the generated bootstrap samples. The sub plots (a) – (h) corresponds to each mouse from 1-8.

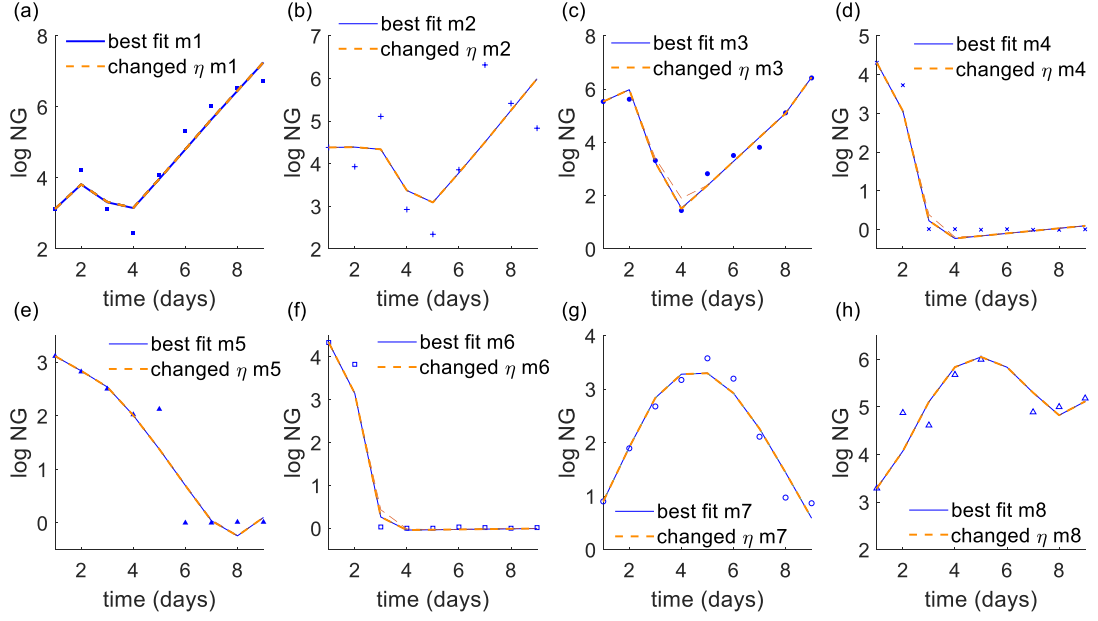


Figure A.11: Changing the parameter values of η over the range of 2.244×10^{-4} to 1.033×10^{-6} while keeping the other parameter values at the optimal value estimated from least square estimation for each mouse. The sub plots (a) – (h) corresponds to each mouse from 1-8. The fits do not deviate from the optimal fit as the parameter value for η is changed.

A.5.3 Estimated mouse parameters

We summarise the fixed parameters and those estimating by fitting to the mouse data in Table A.3, for the full human model and each of the reduced sub models (the 4-state model with B_i removed, the 3-state model with both B_i and B_a removed and the 2-state model with B_s removed as well).

Table A.3: Estimated and fixed parameters in mouse fitting to various models.

Model	Number of parameters in the model	Parameters held fixed	Estimated parameters
4 state	13	$k_1, d_2, d_3, p, N_{max}, a_1, a_2$ and k_2	d, c, μ, r_1 and r_3
3 state	11	$k_1, d_2, d_3, p, N_{max}$ and k_2	d, c, μ, r_1 and r_3
2 state	8	k_1, d_2, d_3 and N_{max}	d, c, μ and r_1

The parameter values estimated by fitting the four versions of the model to NG data of each individual mouse found in Jerse (1999) are summarised in Table A.4.

Table A.4: Estimated parameter values from mice data and the sum of squared errors in fitting shown for each version of the fitted model.

mouse	model	d	c	μ	r_1	r_3	SSE
1	Full model	0.000589	0.000389	7.4×10^{-8}	1.300353	0.122310	1.243
	without B_i	0.000999	0.000783	4.76×10^{-8}	1.141432	0.118238	1.233
	without B_i and B_a	0.000448	0.000647	1.77×10^{-8}	0.126248	0.499961	1.058
	Without B_i, B_a and B_S	0.000010	0.000519	9.48×10^{-7}	0.215005		5.281
2	Full model	0.000011	2.77×10^{-5}	1.12×10^{-7}	0.194523	0.109190	6.190
	without B_i	0.000011	3.13×10^{-5}	4.32×10^{-8}	0.106107	0.106508	6.217
	without B_i and B_a	0.000016	3.14×10^{-5}	2.41×10^{-8}	0.109817	0.106315	6.387
	Without B_i, B_a and B_S	0.000010	2.828×10^{-5}	9.86×10^{-5}	0.345297		11.426
3	Full model	0.000036	6.21×10^{-5}	1.89×10^{-8}	0.146693	0.113997	1.110
	without B_i	0.000155	1.43×10^{-5}	5.66×10^{-10}	0.000100	0.118625	0.781
	without B_i and B_a	0.000140	1.81×10^{-7}	6.22×10^{-10}	0.102697	4.48×10^{-5}	1.727
	Without B_i, B_a and B_S	0.000238	1.00×10^{-3}	9.99×10^{-7}	0.220000		27.068
4	Full model	0.000261	0.000439	5.03×10^{-10}	0.000999	0.053849	0.706
	without B_i	0.000001	1.08×10^{-6}	1.59×10^{-7}	0.000304	0.040650	0.003
	without B_i and B_a	0.000002	1.95×10^{-7}	1.89×10^{-7}	0.039590	0.050262	0.012
	Without B_i, B_a and B_S	0.083397	1.65×10^{-2}	9.93×10^{-6}	4.999848		17.312
5	Full model	1.12×10^{-07}	2.86×10^{-7}	3×10^{-7}	2.64×10^{-5}	0.070755	1.060
	without B_i	1×10^{-07}	1.61×10^{-7}	3.72×10^{-7}	5.14×10^{-6}	0.060913	0.435
	without B_i and B_a	1.4×10^{-07}	3.09×10^{-7}	2.6×10^{-7}	3.52×10^{-5}	0.083613	0.776

	Without B_i , B_a and B_S	0.000100	1.00×10^{-03}	4.19×10^{-10}	0.001000		5.545
6	Full model	0.000264	4.37×10^{-4}	4.99×10^{-10}	0.000999	0.053489	0.760
	without B_i	0.100000	1×10^{-5}	1.29×10^{-12}	5.39×10^{-7}	0.040671	0.006
	without B_i and B_a	0.000002	1.95×10^{-7}	1.81×10^{-7}	0.039011	0.050262	0.023
	Without B_i , B_a and B_S	0.045377	6.52×10^{-1}	9.91×10^{-6}	0.000999		18.068
7	Full model	0.000125	0.000214	4.93×10^{-8}	0.469333	0.044996	0.118
	without B_i	0.000225	0.000532	1.03×10^{-8}	0.291911	0.049358	0.171
	without B_i and B_a	0.000362	0.000999	3.19×10^{-9}	0.062297	0.210559	0.161
	Without B_i , B_a and B_S	0.000392	0.000978	6.63×10^{-9}	0.295279		0.828
8	Full model	0.000336	0.000758	1.94×10^{-9}	0.190611	0.101992	1.682
	without B_i	0.000390	0.000745	1.09×10^{-9}	0.151754	0.099212	0.922
	without B_i and B_a	0.000076	1×10^{-5}	3.59×10^{-9}	0.108747	0.129983	0.809
	Without B_i , B_a and B_S	0.000188	4.438×10^{-4}	2.56×10^{-8}	0.369283	0.004282	2.172
median	Full model	0.000193	0.000302	3.41×10^{-8}	0.168652	0.086373	
	without B_i	0.000190	2.28×10^{-5}	2.67×10^{-8}	0.053205	0.080063	
	without B_i and B_a	0.000046	5.15×10^{-6}	2.09×10^{-8}	0.082497	0.094964	
	Without B_i , B_a and B_S	0.000213	9.89×10^{-4}	9.74×10^{-7}	0.257640		

Appendix A2

Additional details on Chapter 3

A2.1 Further clarifications to figure captions in Chapter 3.

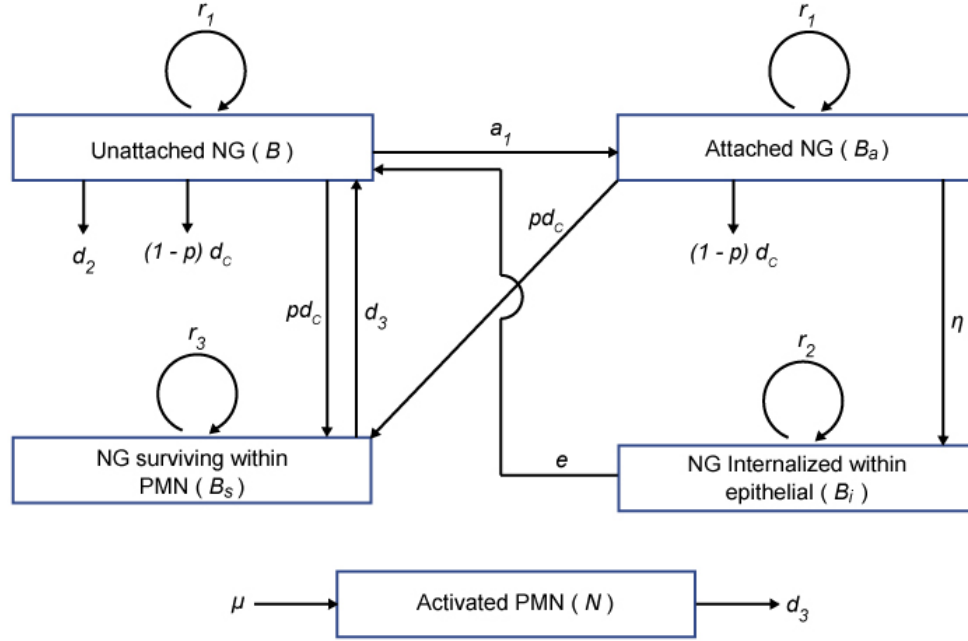


Figure 3.1: Schematic illustration of the within-host model of NG infection. The arrows indicate transitions between model states: unattached NG (B), attached NG (B_a), bacteria internalized within epithelial cells (B_i), NG surviving within PMN (B_s) and activated PMN (N). Model parameters and their assigned values are given in Table 3.2 ($d_c = \frac{dB N}{cN+B}$ refers to the engulfment rate of NG by PMN subject to the ratio dependent constant. When N is relatively low, $d_c \rightarrow d$ while when N is relatively high $d_c \rightarrow \frac{d}{c}$). Here, $(1-p) d_c$ is the rate of NG killing by PMN.

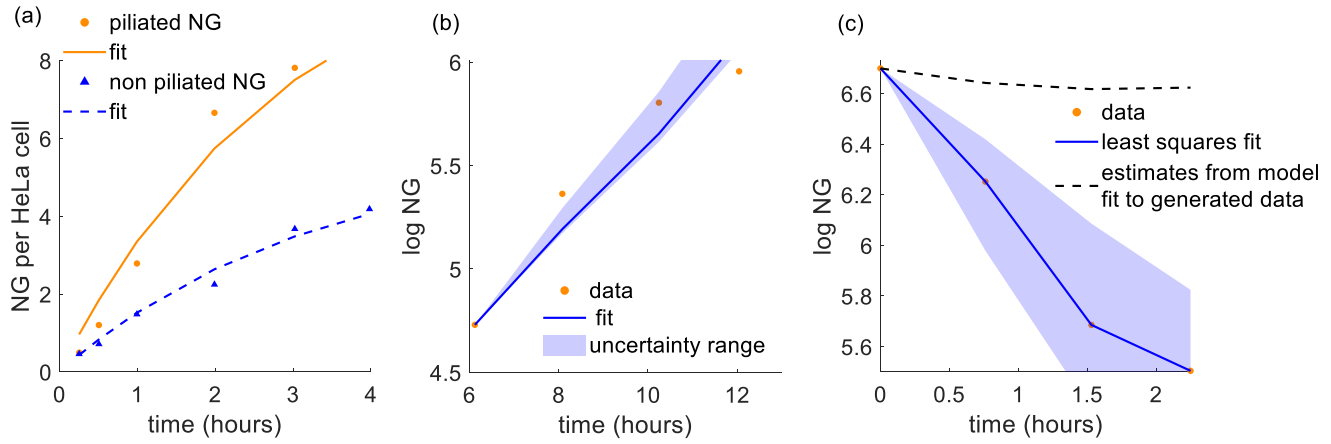


Figure 3.3: Model fit to *in vitro* studies to estimate parameters. (a) The *in vitro* data on

NG attachment to HeLa cells by two types of NG (piliated and non-piliated) from the study by Gubish, et al. (1979) is shown (on linear scale) with the fitted function described in Appendix A, Section A.1.2.1. (b) Data on NG internalization over the period of 6-12 hours as observed in the study by Shaw and Falkow (1988) is shown with the best fit curve obtained by fitting the sub-model on NG internalization to these data (sub-model explained in Appendix A, Section A.1.2.2). The optimal fit is shown by the solid line and the credible intervals obtained around the *in vitro* point estimates are shown by the shaded region. (c) NG killing by PMN as measured by the study by Rest, et al. (1982). The solid line represents the curve obtained from least squares minimization by fitting to the sub model explained in Appendix A, Section A.1.2.3, while the dashed line is the equivalent curve for the base-case parameters, determined through fitting the full model to simulated data based on the qualitative features of the time course of infection. The 95% uncertainty intervals around the *in vitro* point estimates are shown by the shaded region.

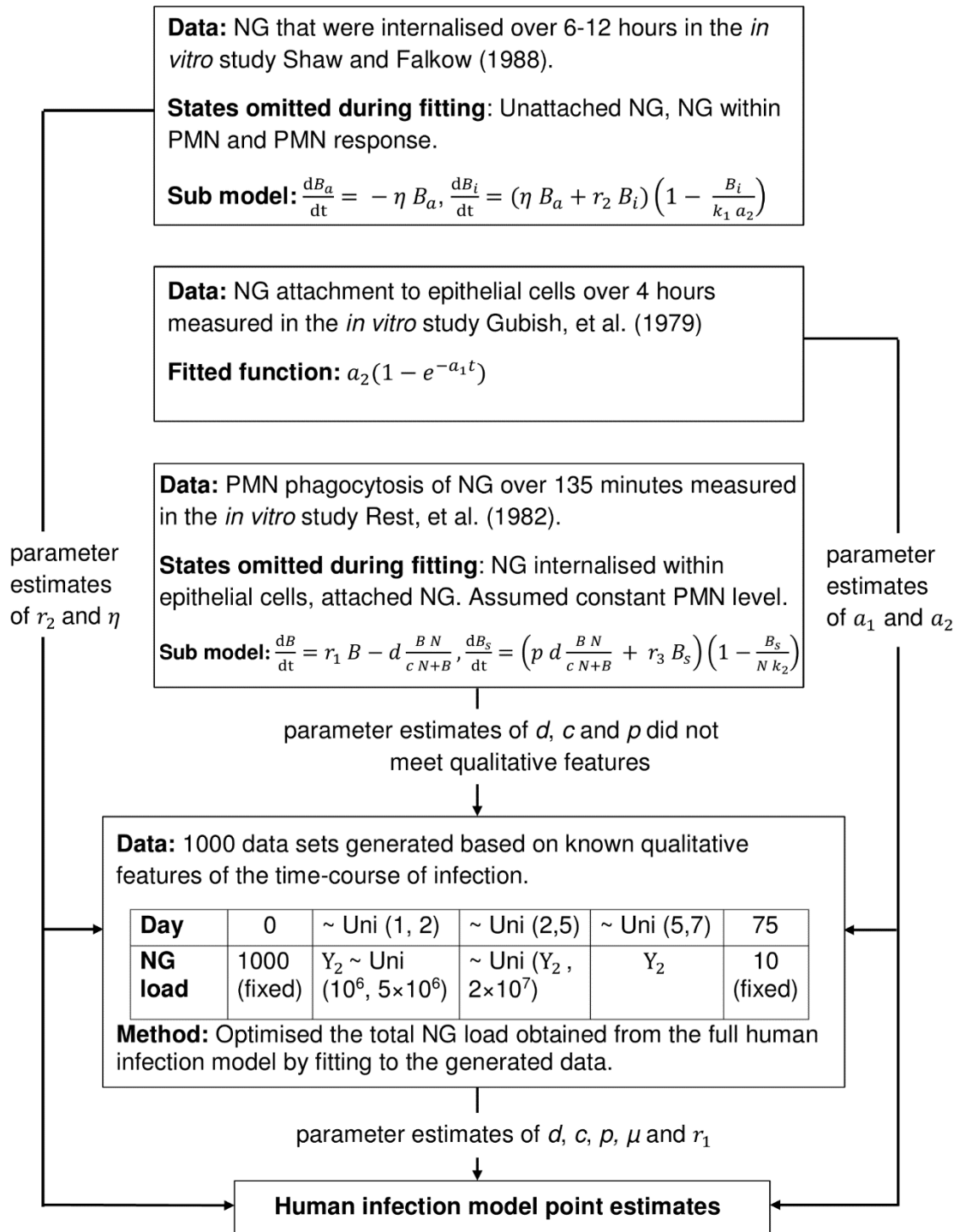


Figure 3.2: Flow diagram summarising the sub-models and data used to estimate the human infection model point-estimate parameters, and illustrating how the estimates feed into the final model. Here, Y_2 is the randomly generated total bacterial load ($B + B_a + B_s + B_i$) observed in the time-course of infection during days 1-2.

A2.2 Simplifying model assumptions

Due to the limitations in data availability and existing knowledge of these within-host processes the following pragmatic assumptions were made during model development:

- In the model unattached and attached NG were assumed to have the same growth rate (r_1). However, it is possible for the growth rates of NG in these two states to be different. Due to the lack of data availability to inform NG growth rates at different extracellular states, we had to make this parsimonious choice and we assume NG growth rates to be only different between the intracellular and extracellular environments. We also do not consider whether attached NG can also live in the interior lumen, as to the best of my knowledge there was no evidence to suggest this in the literature.
- When modelling the replication of attached NG, we assume for simplicity the progeny to also be generated attached to the epithelial cells, in the absence of evidence to the contrary. However, it is possible that in reality some daughter cells remain unattached to the epithelial cells.
- In order to further understand the impact of wash-out rate on model dynamics and to analyse the impact of constant but more rapid wash-out rates, we conducted a univariate sensitivity analysis over the wider range of $10^{-4} - 10^{-1} h^{-1}$. In Fig A2.1, we show that even with much faster wash out rates, infection dynamics with other parameters at based-case remain consistent with qualitative time-course features derived from the literature. As the parameter value of d_2 is varied in the chosen range, the simulated model clearance times vary from 55-79 days which are well within the reported duration of natural infection (1-6 months). The resulting peak

NG load ($3.7 \times 10^6 - 4.3 \times 10^6$) is also consistent with the observations of human experimental studies ($10^6 - 10^8$) (Ramsey, *et al.* 1995; Schmidt, *et al.* 2001; Schneider, *et al.* 1995; Schneider, *et al.* 1991; Schneider, *et al.* 1996). Furthermore, the resulting proportion of NG residing within PMN aligns with the literature observations on cellular NG proportions reported by Veale, *et al.* (1979) and are within the cellular proportions currently estimated from the model simulations.

- As we are not aware of estimates for the density at which the bacteria can colonise the urethral surface, we assumed that the carrying capacity was limited by the ratio of the surface areas of the urethra and NG. Observed values of these surface areas indicate that k_1 cannot exceed $5 \times 10^9 \mu\text{m}^2$. Here, we assume that only a fraction of urethral surface area is available for bacteria to infect, with the base case assumption being $k_1 = 10^7 \mu\text{m}^2$. In order to test sensitivity of model outcomes to this assumption, we conducted a univariate sensitivity analysis by varying k_1 , in the range of $10^6 - 10^9 \mu\text{m}^2$.
- The data on NG attachment to HeLa cells reported in the *in vitro* study by Gubish, *et al.* (1979) suggest that the number of attached NG reach a maximum after a certain time point and remain constant at that level. Therefore, a function of the form $a_2(1 - e^{-a_1 t})$ was chosen as it is the simplest choice that features a constant rate of attachment as well as constant maximum attachment level. This chosen function was fitted to data in Gubish, *et al.* (1979) to estimate the bacterial attachment rate (a_1) and maximal NG attachment capacity of an epithelial cell (a_2).
- In this study, I also assume that the NG load measured in urethral exudates is representative of the natural infection. However, to validate this assumption we are

not aware of studies that assess the representativeness of NG load measured in urethral exudates in comparison to *in vivo* infection

A2.3 Additional model limitations

In the model, the NG attachment to epithelial cells was limited in terms of the urethral carrying capacity as $(1 - \frac{B_a}{k_1 a_2})$. Here, k_1 is the urethral carrying capacity, a_2 is the maximal NG attachment capacity per epithelial cell and B_a is the attached bacteria. A more realistic capacity limitation could be achieved if instead of k_1 , this term was based on the total number of accessible epithelial cells in the urethra. However, this would require adding further complexity into the model to capture accessible and inaccessible epithelial cells. Given the already complex model structure with limited data availability to estimate parameters, the bacterial attachment-limiting term was based in terms of the urethral carrying capacity (k_1). This is a reasonable simplification, as attached NG only reside in this state for a short period before transitioning to intracellular (NG within PMN and NG within epithelial cells) states.

To further analyse the impact of choosing k_1 as the attachment capacity constraint, we performed a univariate sensitivity analysis by varying the parameter value of k_1 in the range of $10^6 - 10^9$. For changes in the parameter value of k_1 , the simulated infection clearance times only varied from 60-112 days, which were well within the duration of natural infection (1-6 months) informed from literature (Ramsey, *et al.* 1995; Schmidt, *et al.* 2001; Schneider, *et al.* 1995; Schneider, *et al.* 1991; Schneider, *et al.* 1996). However, only k_1 values in the range of $2 \times 10^6 - 2 \times 10^8$, would result in infection dynamics that are consistent with the literature in terms of the peak NG load ($10^6 - 10^8$) (Ramsey, *et al.* 1995; Schmidt, *et al.* 2001; Schneider, *et al.* 1995; Schneider, *et al.* 1991; Schneider, *et al.* 1996) (Fig. A2.1). Furthermore, for this wide range of chosen k_1 , the resulting

proportion of NG within PMN (48-65% at 5 days since infection) is consistent with the literature (20-65%) (Veale, *et al.* 1979) (Fig. A2.1).

A2.4 Additional sensitivity analysis.

In order to assess the impact of the parameter values of the washout rate of unattached NG (d_2) and the urethral carrying capacity (k_1), a univariate sensitivity analysis was carried out. All other model parameters are assumed to be at their point estimates and the results are shown in Fig. A2.1 and A2.2. The parameter value of d_2 is varied in the range of $10^{-4} - 10^{-1} h^{-1}$ and k_1 in the range of $10^6 - 10^9$, and the changes in the simulated infection clearance times are assessed.

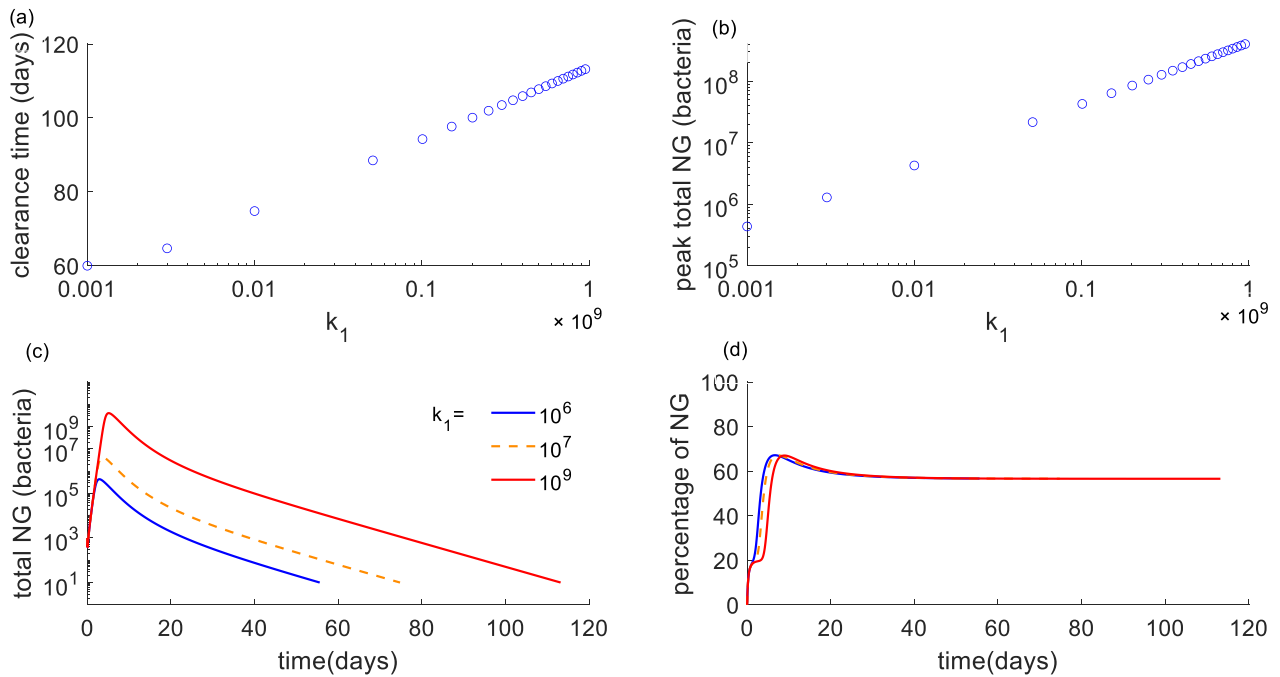


Figure A2.1: Univariate sensitivity analysis results assessing the change in simulated infection clearance times for the changes in parameter value of urethral carrying capacity (k_1). The change in (a) infection clearance times and (b) peak total NG load are shown for the changes in k_1 . For the lower and upper limit of k_1 and the point estimate, the changes in (c) total NG load and (d) percentage of NG within

PMN are shown over time. Panels (a, b) x-axis is in log-scale. Panels (b, c) y-axis is in log-scale. All other parameter values are kept fixed at the point estimates given in Table 3.2.

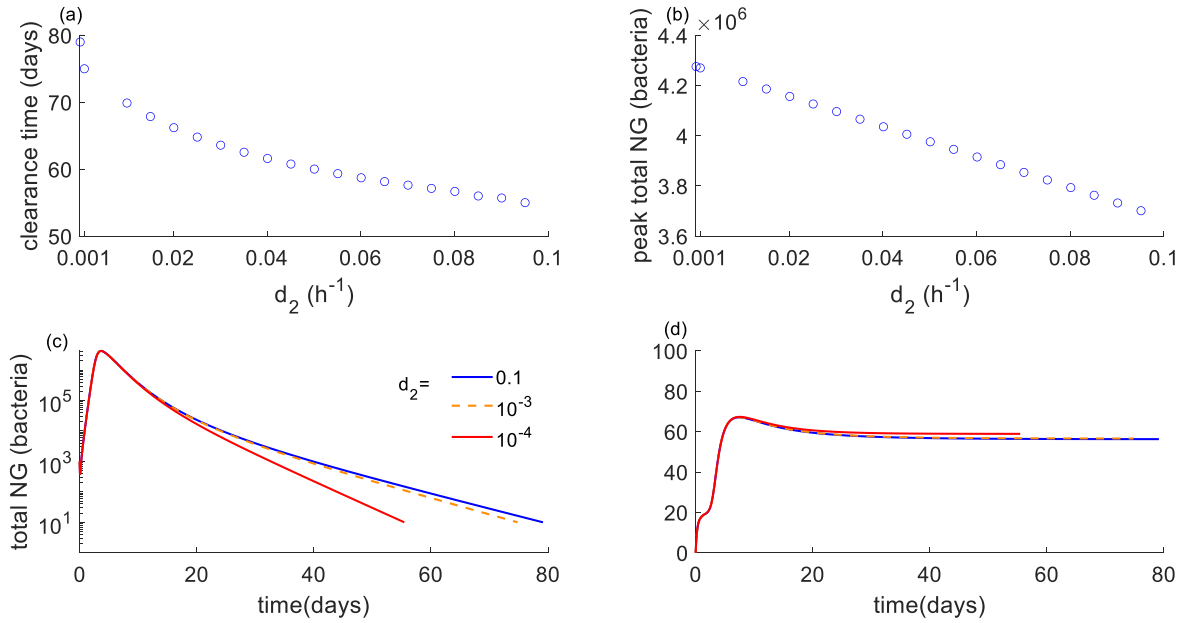


Figure A2.2: Univariate sensitivity analysis results assessing the change in simulated infection clearance times for the changes in parameter value of the washout rate of unattached NG (d_2). The change in (a) infection clearance times and (b) peak total NG load are shown for the changes d_2 . For the lower and upper limit of d_2 and the point estimate, the changes in (c) total NG load and (d) percentage of NG within PMN are shown over time. Panels (a, b) x-axis is in log-scale. Panels (b, c) y-axis is in log-scale. All other parameter values are kept fixed at the point estimates given in Table 3.2.

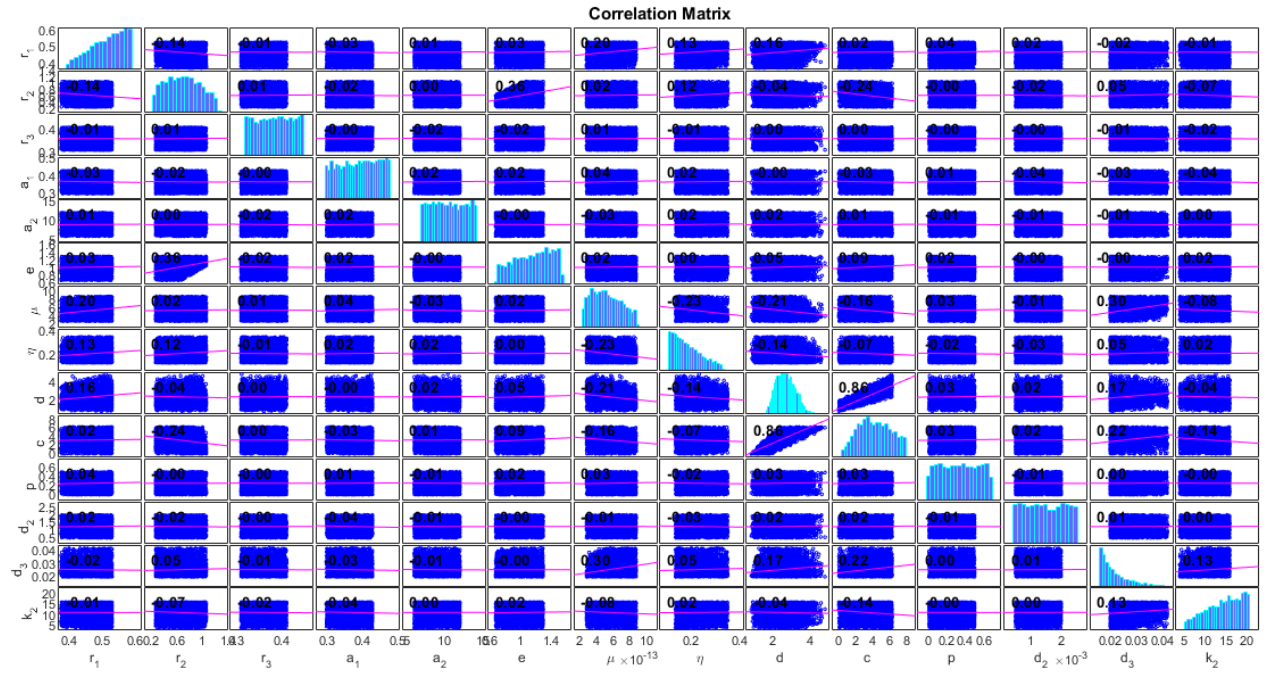


Figure A2.3: Correlation analysis for all model parameters in the natural infection model.

The spearman correlation coefficient is also shown. The parameter notations are as described in Table 3.2.

Appendix B

Supplementary material pertaining to Chapter 4

B.1 Hill function parameter estimation

B.1.1 The Hill function

Drug effects on the bacterial population are modelled using a commonly applied saturating Hill function as in Regoes, *et al.* (2004). The Hill function is determined by four parameters; the maximum bacterial growth rate in the absence of antibiotic (φ_{max}), the minimum bacterial growth rate in the presence of antibiotics (φ_{min}), MIC and the Hill coefficient (k_H). At the value of MIC, the killing effect that is produced from the Hill function is 0. The Hill coefficient reflects how sensitive the change in net bacterial growth rate is for the changes in the antibiotic concentration. As k_H increases it can result in faster bacterial clearance (Figure B.1 (a)). As NG killing through antibiotics suppresses/reduces the bacterial growth φ_{min} is usually <0 and can be used to differentiate between bactericidal vs bacteriostatic antibiotics. Bactericidal antibiotics are associated with low φ_{min} values (due to their high bacterial killing abilities), while bacteriostatic antibiotics which only inhibit bacterial growth are associated with high φ_{min} values. Lower the φ_{min} , faster the bacterial clearance (Figure B.1 (b)).

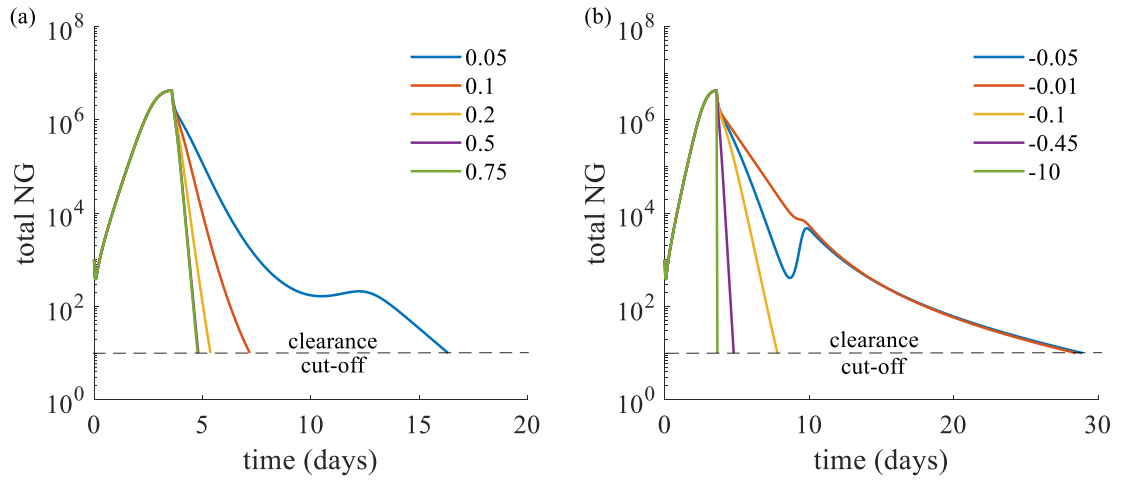


Figure B.1: Change in the bacterial load over time as the Hill function parameter values (a) k_H (from 0.05 to 0.75) and (b) ϕ_{min} (-0.05 to -10) are varied. Only one parameter is varied at a time and all other parameters are kept fixed at the ceftriaxone point estimate values in Table 4.1 in Chapter 4.

B.1.2 Data used to estimate Hill function parameter estimates.

The Hill function parameters of ceftriaxone, cefixime, gentamicin and azithromycin are estimated using NG growth data found in the time-kill experiments by Foerster, *et al.* (2016) and the parameters of gepotidacin are estimated using the time-kill experiment by Farrell, *et al.* (2017). Foerster, *et al.* (2016) reports drug concentrations in the range of $0.016 \times \text{MIC}$ to $16 \times \text{MIC}$ while the study Farrell, *et al.* (2017) reports drug concentrations ranging from $0.25 \times \text{MIC}$ to $10 \times \text{MIC}$. Foerster, *et al.* (2016) have conducted two identical experiments on NG growth and we consider both these experiments when estimating the parameter values. In Foerster, *et al.* (2016) NG count below 100 CFU/mL could not be measured, so only the concentrations with at least three data points are used for the optimisation. For gentamicin, the number of antibiotic concentrations that are used in the optimisation (n) is 8 in each experiment while for azithromycin n is 11 in each experiment and for ceftriaxone, n is 8 and 11 in the two

experiments. In Foerster, *et al.* (2016), NG growth is measured hourly for 6 hours (0, 1, 2, 3, 4, 5, 6 hour time points) and in the study Farrell, *et al.* (2017) it is measured at 0, 2, 4, 8 and 24 hour time points. As in Foerster, *et al.* (2016), the geometric mean of NG data at 0 hours is used as the initial bacterial load (at 0 hours).

B.1.3 Fitting procedure

B.1.3.1 Estimating Hill function parameter values.

The basic fitting approach is described in Chapter 4, Section 4.2.2. In Foerster, *et al.* (2016) NG growth data are presented for two separate experiments. Therefore, in order to obtain the point estimate model parameter values an additional step is taken. First, the Hill function parameters are estimated by fitting separately to the two experimental data sets. This results in two sets of Hill function parameter values. Using these estimated individual sets of parameter values the net growth rates are evaluated using which we then evaluate the mean net growth rate. The Hill function is then fitted to this obtained mean net growth to estimate point estimate parameter values. These individual net growth rates and the fit to mean net growth rate are shown in Figure B.2 for all the nine antibiotics studied in Foerster, *et al.* (2016). The estimated individual parameter values are summarised in Table B.1 along with the sum of squared errors obtained using our approach and using the estimates in Foerster, *et al.* (2016).

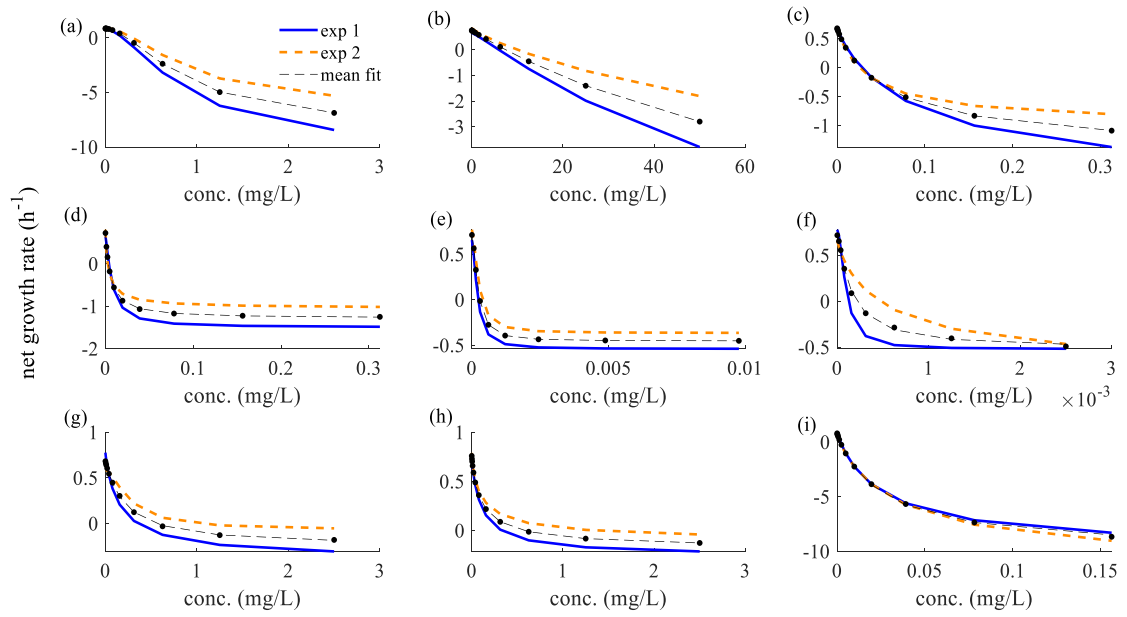


Figure B.2: The net growth rates obtained using the individual parameter values obtained by fitting to the two experimental data sets in Foerster, *et al.* (2016) and the fit to the mean of the individual net growth rates (filled circles indicate data points for mean net growth rate and the dashed line represents the fit) for (a) gentamicin, (b) spectinomycin, (c) azithromycin, (d) penicillin, (e) ceftriaxone, (f) cefixime, (g) chloramphenicol, (h) tetracycline and (i) ciprofloxacin.

Table B.1: Hill function parameter values obtained by fitting to individual experiments and comparison of SSE using our estimates and Foerster, *et al.* (2016) estimates.

Drug ^a	Exp	φ_{max} (h^{-1})	φ_{min} (h^{-1})	MIC (mg/L)	k_H	Sum of squared errors (SSE)	SSE using estimates in Foerster, <i>et al.</i> (2016)
GEN	1	0.82	-10	0.19	1.67	3.11	5.82
	2	0.91	-6.35	0.3	1.76	4.86	10.59
SPT	1	0.66	-10	5.96	1.12	5.76	9.66
	2	0.85	-10	10	0.83	3.99	13.95
AZM	1	0.61	-0.99	0.02	0.97	10.47	45.6
	2	0.69	-2.06	0.03	0.91	5.29	26.02
PEN	1	0.67	-1.48	4.20×10^{-3}	1.35	11.27	16.16
	2	0.92	-1.05	2.80×10^{-3}	0.86	19.05	21.39
CFO	1	0.68	-0.52	2.42×10^{-4}	1.74	6.08	9.40
	2	0.77	-0.36	3.84×10^{-4}	1.76	6.94	7.50
CFM	1	0.78	-0.52	1.23×10^{-4}	1.82	9.95	12.30
	2	0.67	-0.76	4.63×10^{-4}	0.87	8.77	13.81
CHL	1	0.77	-0.04	0.35	0.89	5.32	7.58
	2	0.59	-0.07	1.00	1.64	2.04	2.36
TET	1	0.73	-0.26	0.33	0.94	2.69	2.84
	2	0.80	-0.12	1.37	0.77	2.01	2.34
CIP	1	0.90	-6.62	1.9×10^{-3}	0.95	2.45	5.30
	2	0.73	-5.5	2.0×10^{-3}	1.21	17.12	22.42

^aGEN – gentamicin, SPT – spectinomycin, AZM – azithromycin, PEN – penicillin, CFO – ceftriaxone, CFM – cefixime, CHL – chloramphenicol, TET – tetracycline, CIP – ciprofloxacin.

B.1.3.2 Parameter ranges around the Hill function estimates of ceftriaxone, cefixime, azithromycin and gentamicin for the LHS samples.

Assuming that the resulting net growth rates can show any behaviour between the two individual net growth rates, in order to obtain parameter ranges around the point estimate Hill function parameters, a similar approach as fitting to the mean of the net growth rates as described in Section B.1.3.1 is used. For this, for a particular antibiotic, at each concentration, 5402 uniform random numbers are generated between the two individual net growth rates ($\sim \text{Uniform}(\varphi_1(C), \varphi_2(C))$), where $\varphi_i(C)$ are the respective individual net growth rates of the two experiments at concentration C , where $i=1, 2$. To each of these generated net growth rate curves, the Hill function (Chapter 4, Eq. 4.1) is fitted to obtain 5402 sets of parameter values of φ_{max} , φ_{min} , MIC and k_H for ceftriaxone, cefixime, azithromycin and gentamicin (Figure B.3).

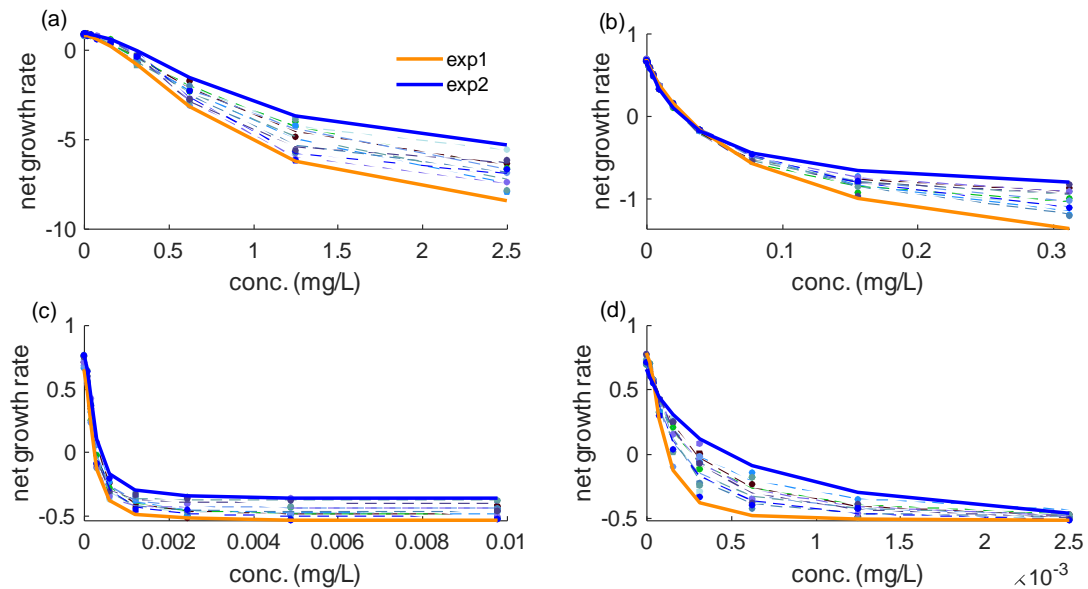


Figure B.3: Fits to generated net growth rates to estimate parameter ranges around the point estimate Hill function parameter values for (a) gentamicin (b) azithromycin (c) ceftriaxone and (d) cefixime. Only 10 samples of generated net growth rates

(filled circles) and the fit of the Hill function to these data points (dotted lines) are shown. The solid lines indicate the individual net growth rates obtained using the two experimental NG load data in Foerster, *et al.* (2016).

B.2 PK/PD parameter calibration

Using the parameter values obtained from published literature (Appendix B, Table B.2 and Chapter 4, Table 4.1), we determine a model-derived susceptibility breakpoint such that for MIC below and above the breakpoint, the infection clears in ≤ 7 days and >7 days, respectively. For some simulations that are generated using the LHS samples, the model-derived susceptibility breakpoints result in values below the Clinical and Laboratory Standards Institute (CLSI) or European Committee on Antimicrobial Susceptibility Testing (EUCAST) defined susceptibility breakpoints (referred as ‘empirical susceptibility breakpoints’). We, therefore refine the original parameter values which are based on literature reports by calibrating the model to these empirical susceptibility breakpoints.

In this parameter refinement process, we first analyse the importance of each parameter's uncertainty in contributing to the variability of the model-derived susceptibility breakpoints (influential parameters) through partial rank correlation coefficients (Fig. B.4). In these influential parameters, parameter ranges are analysed of the simulations that achieve empirical susceptibility breakpoints and these show skewed parameter distributions (Figs B.5- B.8). For gepotidacin, as there is no defined empirical susceptibility breakpoint, the model-derived breakpoint of 0.6mg/L using the point estimates is used as the cut-off for the calibration process. Then, in these influential parameters, the parameter ranges that consist of 90% of the simulations that meet empirical susceptibility breakpoints are selected as the refined range that is used for the

subsequent model simulations. A comparison between the original parameter values (before model calibration) and the refined parameter ranges (after calibration) is shown in Table B.2. In this refinement process, as no simulations using the original parameter ranges met empirical susceptibility breakpoints for cefixime, parameter values for this drug are set at the same values that are indicated as influential for ceftriaxone.

Table B.2: Comparison of the parameter values prior to calibration and after calibration for the five antibiotics ceftriaxone (CFO), cefixime (CFM), gepotidacin (GEP), gentamicin (GEN) and azithromycin (AZM).

Drug	Parameter	Parameter range (prior to calibration)	Reference for parameter values prior to calibration	Parameter range (after calibration)
GEP	φ_{min} (h^{-1})	-0.64, -0.43	Fitting to time-kill data in Farrell, <i>et al.</i> (2017)	-0.64, -0.46
	k_H	1.3 – 3.64	Fitting to time-kill data in Farrell, <i>et al.</i> (2017)	1.78 – 3.64
GEN	V_e (L)	0.28 – 1.29	(Schentag, <i>et al.</i> 1977)	0.6 – 1.29
	k_{12} (h^{-1})	0.01 – 0.04	(Schentag, <i>et al.</i> 1977)	0.03 – 0.04
AZM	V_e (L)	358 – 779	(Ripa, <i>et al.</i> 1996)	485 – 779
	V_i (L)	981 – 2577	(Ripa, <i>et al.</i> 1996)	981 – 1916
	k_{12} (h^{-1})	0.07 – 0.18	(Ripa, <i>et al.</i> 1996)	0.1 – 0.18
	k_{21} (h^{-1})	0.02 – 0.06	(Ripa, <i>et al.</i> 1996)	0.03 – 0.06
CFO	α	0.15 – 0.61	(Jacobs, <i>et al.</i> 1986)	0.49 – 0.61
	V_d (L)	7.8 – 11.9	(Patel, <i>et al.</i> 1982)	7.8 – 9.5
CFM	α	0.15 – 0.61	(Jacobs, <i>et al.</i> 1986)	0.49 – 0.61

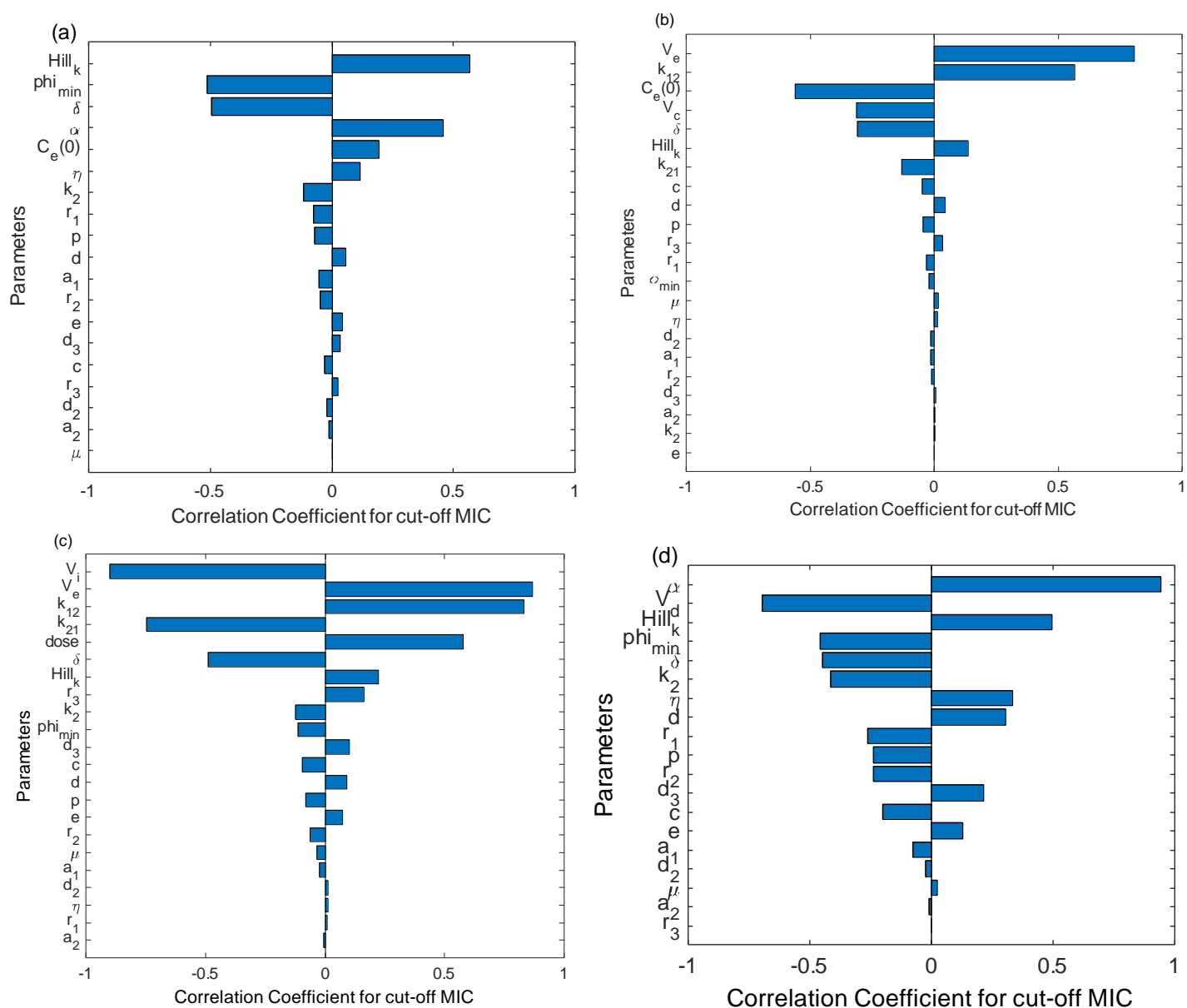


Figure B.4: Tornado plots of partial rank correlation coefficients, indicating the importance of each parameter's uncertainty in contributing to the variability in the model-derived susceptibility breakpoint obtained from the simulations of LHS samples shown for (a) gepotidacin, (b) gentamicin, (c) azithromycin and (d) ceftriaxone.

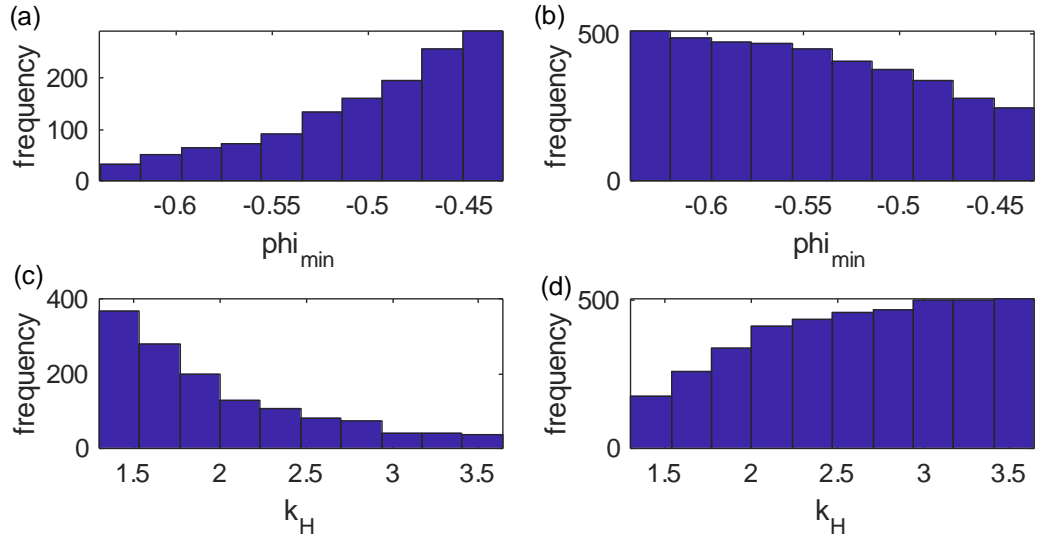


Figure B.5: Parameter distributions of the simulations from LHS samples that resulted in a model-derived susceptibility breakpoint $< 0.64\text{mg/L}$ (left column) and $\geq 0.64\text{mg/L}$ (right panel) shown for the parameters that were indicated as influential for the variability of gepotidacin susceptibility breakpoint (φ_{min} , k_H).

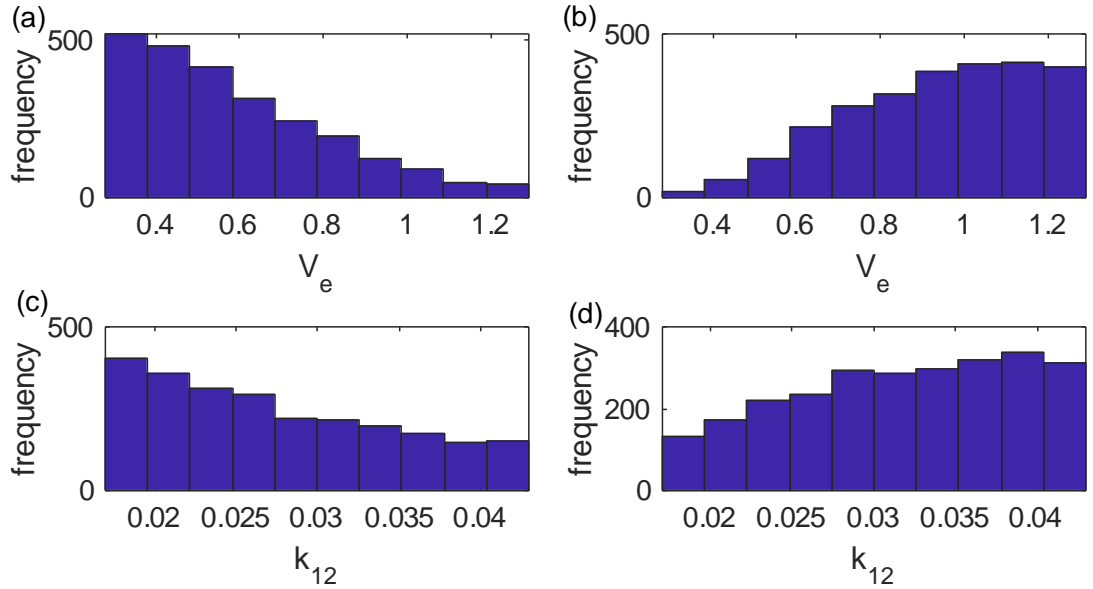


Figure B.6: Parameter distributions of the simulations from the LHS samples that resulted in a model-derived susceptibility breakpoint $< 4\text{mg/L}$ (left column) and $\geq 4\text{mg/L}$ (right column).

(right panel) shown for the parameters that were indicated as influential for the variability of gentamicin susceptibility breakpoint level (V_e, k_{12}).

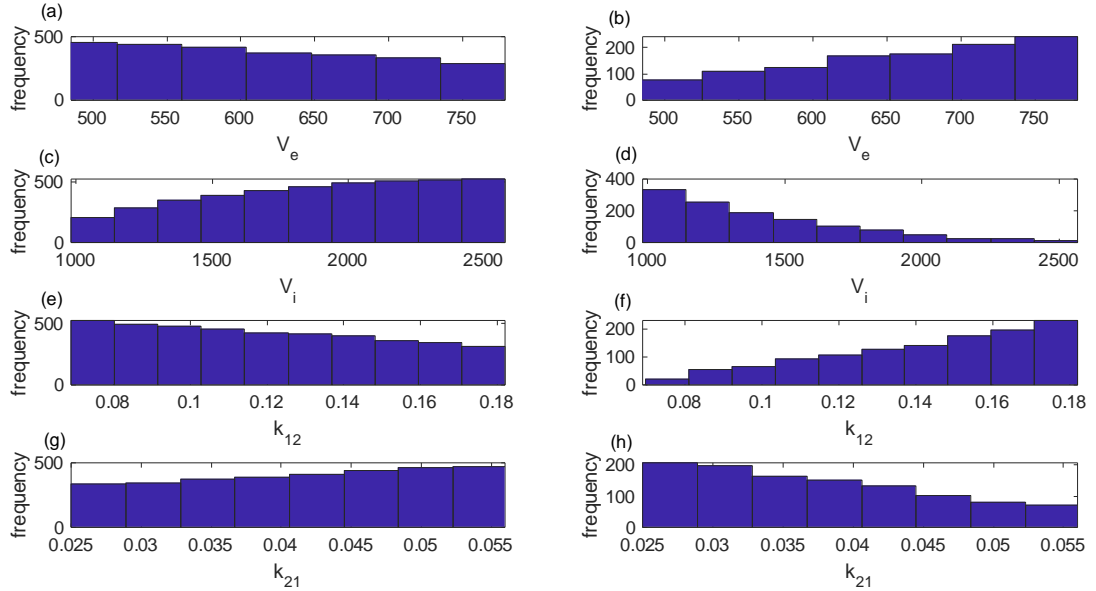


Figure B.7: Parameter distributions of the simulations from the LHS samples that resulted in a model-derived susceptibility breakpoint $< 1\text{mg/L}$ (left column) and $\geq 1\text{mg/L}$ (right panel) shown for the parameters that were indicated as influential for the variability of azithromycin susceptibility breakpoint (V_e, V_i, k_{12}, k_{21}).

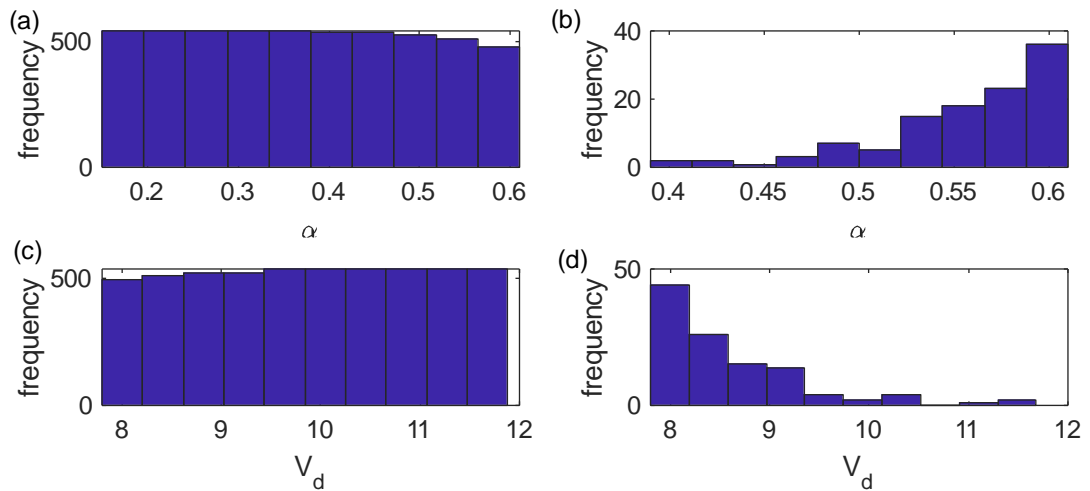


Figure B.8: Parameter distributions of the simulations from the LHS samples that resulted in a model-derived susceptibility breakpoint $<0.125\text{mg/L}$ (left column) and $\geq 0.125\text{mg/L}$ (right panel) shown for the parameters that were indicated as influential for the variability of model-derived susceptibility breakpoint of ceftriaxone (α, V_d). Only 2% of simulations from the LHS samples had model-derived susceptibility breakpoint $\geq 0.125\text{mg/L}$.

B.3 Model equations

Model equations when treatment is included to the four NG states (unattached NG (B), attached NG (B_a) to epithelial cells, NG internalised within epithelial cells (B_i) and NG surviving within PMN (B_s)) are described in this section. The innate immune response through PMN (N) is the considered immune response in the model. Treatment is included based on the drug pharmacokinetics as described in the main file. For parameter values and notations refer Table 4.1, in Chapter 4.

B.3.1 Antibiotic concentration modelled as a one-compartment (ceftriaxone, cefixime and gepotidacin)

$$\begin{aligned} \frac{dB}{dt} = & \left(1 - \frac{B + B_a}{k_1}\right) (r_1 B + d_3 B_s + e B_i) - d \frac{B N}{c N + B} - d_2 B - a_1 B \left(1 - \frac{B_a}{k_1 a_2}\right) \\ & - \frac{(r_1 - \varphi_{min}) \left(\frac{C_e}{MIC}\right)^{k_H}}{\left(\frac{C_e}{MIC}\right)^{k_H} - \frac{\varphi_{min}}{r_1}} B \left(1 - \frac{B + B_a}{k_1}\right) \\ \frac{dB_a}{dt} = & r_1 B_a \left(1 - \frac{B + B_a}{k_1}\right) + a_1 B \left(1 - \frac{B_a}{k_1 a_2}\right) - d \frac{B_a N}{c N + B_a} - \eta B_a \\ & - \frac{(r_1 - \varphi_{min}) \left(\frac{C_e}{MIC}\right)^{k_H}}{\left(\frac{C_e}{MIC}\right)^{k_H} - \frac{\varphi_{min}}{r_1}} B_a \left(1 - \frac{B + B_a}{k_1}\right) \end{aligned}$$

$$\frac{dB_i}{dt} = \left(1 - \frac{B_i}{k_1 a_2}\right) (\eta B_a + r_2 B_i) - e B_i - \frac{(r_2 - \varphi_{min}) \left(\alpha \frac{C_e}{MIC}\right)^{k_H}}{\left(\alpha \frac{C_e}{MIC}\right)^{k_H} - \frac{\varphi_{min}}{r_2}} B_i \left(1 - \frac{B_i}{k_1 a_2}\right)$$

$$\begin{aligned} \frac{dB_s}{dt} = & \left(1 - \frac{B_s}{N k_2}\right) \left(p d \frac{B N}{c N + B} + p d \frac{B_a N}{c N + B_a} + r_3 B_s\right) - d_3 B_s \\ & - \frac{(r_3 - \varphi_{min}) \left(\alpha \frac{C_e}{MIC}\right)^{k_H}}{\left(\alpha \frac{C_e}{MIC}\right)^{k_H} - \frac{\varphi_{min}}{r_3}} B_s \left(1 - \frac{B_s}{N k_2}\right) \end{aligned}$$

$$\frac{dN}{dt} = \mu (N_{max} - N) (B + B_a) - d_3 N$$

$$\frac{dC_e}{dt} = -\delta C_e$$

C_e is the extracellular drug concentration.

B.3.2 Model equations when antibiotic concentration modelled as a two-compartment model (azithromycin and gentamicin).

For these drugs extracellular (C_e) and intracellular (C_i) drug concentrations are modelled separately.

$$\begin{aligned} \frac{dB}{dt} = & \left(1 - \frac{B + B_a}{k_1}\right) (r_1 B + d_3 B_s + e B_i) - d \frac{B N}{c N + B} - d_2 B - a_1 B \left(1 - \frac{B_a}{k_1 a_2}\right) \\ & - \frac{(r_1 - \varphi_{min}) \left(\frac{C_e}{MIC}\right)^{k_H}}{\left(\frac{C_e}{MIC}\right)^{k_H} - \frac{\varphi_{min}}{r_1}} B \left(1 - \frac{B + B_a}{k_1}\right) \end{aligned}$$

$$\begin{aligned} \frac{dB_a}{dt} = & r_1 B_a \left(1 - \frac{B + B_a}{k_1}\right) + a_1 B \left(1 - \frac{B_a}{k_1 a_2}\right) - d \frac{B_a N}{c N + B_a} - \eta B_a \\ & - \frac{(r_1 - \varphi_{min}) \left(\frac{C_e}{MIC}\right)^{k_H}}{\left(\frac{C_e}{MIC}\right)^{k_H} - \frac{\varphi_{min}}{r_1}} B_a \left(1 - \frac{B + B_a}{k_1}\right) \end{aligned}$$

$$\frac{dB_i}{dt} = \left(1 - \frac{B_i}{k_1 a_2}\right) (\eta B_a + r_2 B_i) - e B_i - \frac{(r_2 - \varphi_{min}) \left(\frac{C_i}{MIC}\right)^{k_H}}{\left(\frac{C_i}{MIC}\right)^{k_H} - \frac{\varphi_{min}}{r_2}} B_i \left(1 - \frac{B_i}{k_1 a_2}\right)$$

$$\begin{aligned} \frac{dB_s}{dt} = & \left(1 - \frac{B_s}{N k_2}\right) \left(p d \frac{B N}{c N + B} + p d \frac{B_a N}{c N + B_a} + r_3 B_s\right) - d_3 B_s \\ & - \frac{(r_3 - \varphi_{min}) \left(\frac{C_i}{MIC}\right)^{k_H}}{\left(\frac{C_i}{MIC}\right)^{k_H} - \frac{\varphi_{min}}{r_3}} B_s \left(1 - \frac{B_s}{N k_2}\right) \end{aligned}$$

$$\frac{dN}{dt} = \mu (N_{max} - N) (B + B_a) - d_3 N$$

$$\frac{dC_e}{dt} = -\delta C_e - k_{12} C_e + k_{21} C_i \frac{V_i}{V_e}$$

$$\frac{dC_i}{dt} = k_{12} C_e \frac{V_e}{V_i} - k_{21} C_i$$

B.4 Drug concentration profiles

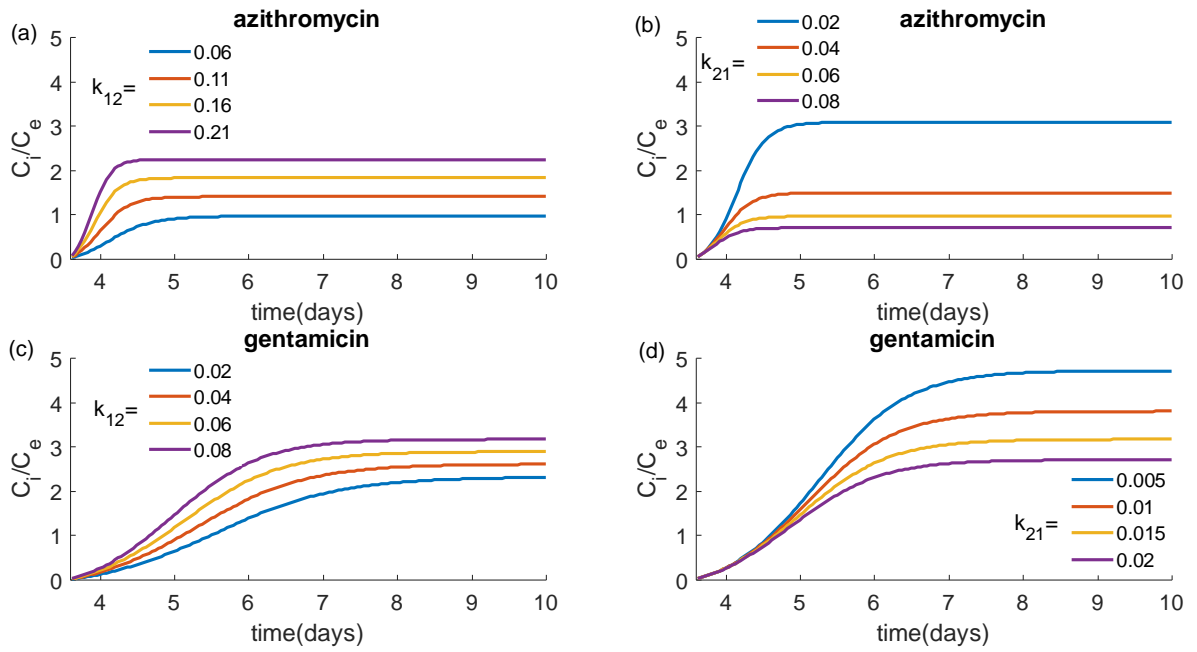


Figure B.9: Change in the ratio of intracellular to extracellular drug concentration C_i/C_e

and the time taken to reach the plateau of C_i/C_e when the parameter values of the rates of drug transfer from (k_{12}) and to (k_{12}) the intracellular compartment are varied. Results are shown for azithromycin (a, b) and gentamicin (c, d). Parameter values are varied over a 2-fold range around the point estimates given in Chapter 4, Table 4.1. Only one parameter is varied at a time.

B.5 NG load behaviour around cut-off MIC

Around the cut-off MIC, the simulations that clear infection result in clearance times < 2 days while samples that fail to successfully clear infection result in infection clearance times > 26 days. The reasons for this dichotomous behaviour in transition from clearance to non-clearance is analysed and the results are shown in Fig. B.10. We observe this dichotomous behaviour is a result of the strict infection clearance cut-off that we have selected. In the simulations that fail to clear infection, although the total NG load falls closer to the clearance cut-off of 10 NG (in some instances to around 11 NG), with NG re-growth, these simulations are classified as uncleared and the time point in which these simulations actually reach 10 NG are taken as the infection clearance times. The impact of this strict threshold is described in detail in Chapter 7.

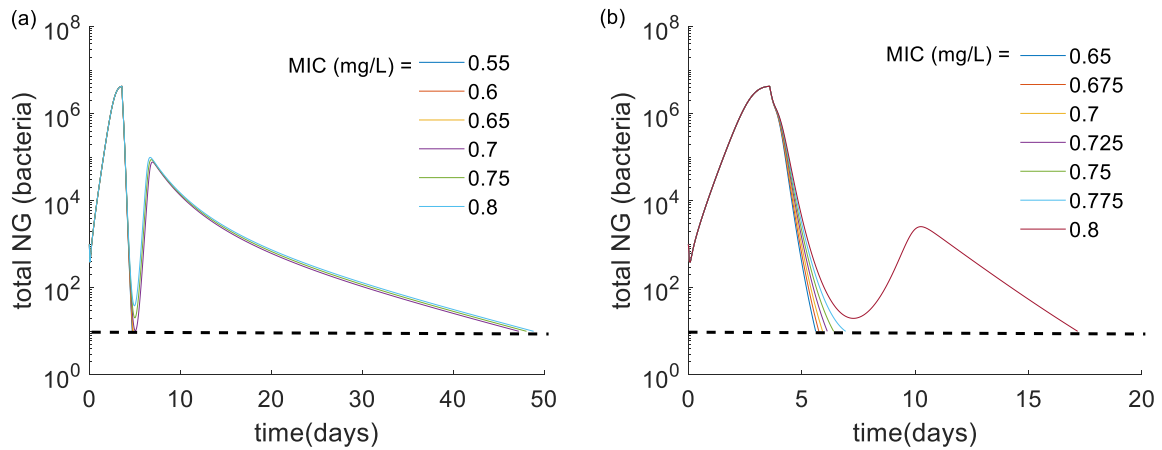


Figure B.10: The change in the total NG load for different values of MIC for (a) gepotidacin and (b) azithromycin. The parameter values are the point estimates.

B.6 Extracellular vs intracellular susceptibility breakpoints.

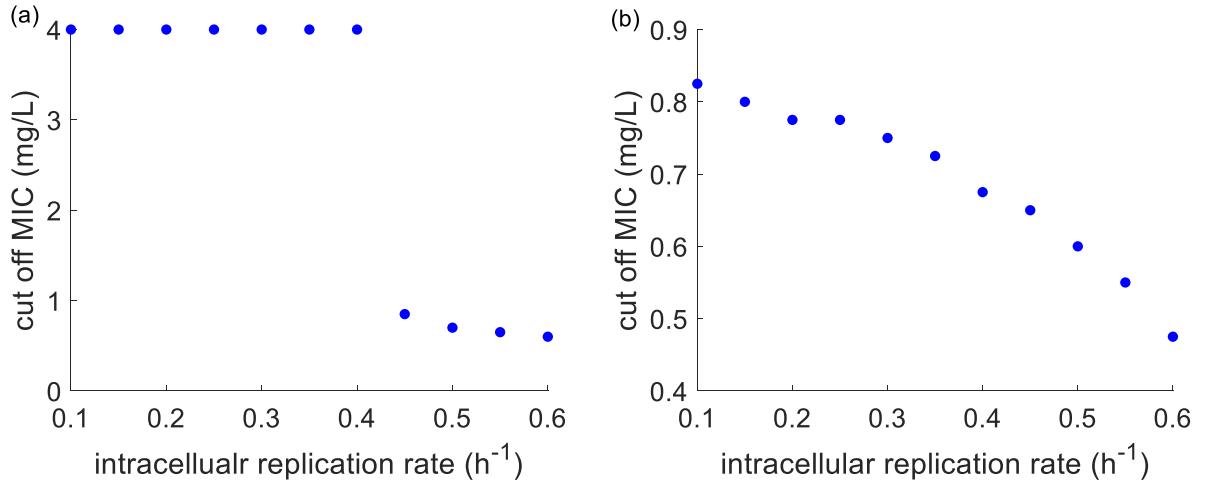


Figure B.11: The impact of the intracellular NG replication rates (r_2 and r_3) on the model derived cut-off MIC for (a) gepotidacin and (b) azithromycin. The parameter values of r_2 and r_3 are varied over the range of $0.1 - 0.6h^{-1}$. All other parameter values are fixed at the point estimates.

Appendix C

Supplementary material pertaining to Chapter 5

C.1 Dual treatment

Drug mechanisms of actions differ between different drug classes. Macrolides (e.g. azithromycin) and aminoglycosides (e.g. gentamicin) disrupt bacterial protein synthesis by inhibiting ribosome functionality (Brooks, *et al.* 2013). As gentamicin and azithromycin have the same mechanisms of action drug interaction between gentamicin and azithromycin are modelled using Loewe additivity (Loewe 1928).

When drugs interact, they can show additive, synergistic or antagonistic effects. An additive effect is observed when the combined effect is similar to the effect obtained when the two drugs are administered individually. Additivity is taken as the reference level and if the observed combined effect is higher than the additive effect it is referred to as being synergistic while if the combined effect is lesser than the additive effect it is referred to as antagonistic. *In vitro* studies have tested drug synergism for treatment of NG strains and for the gentamicin + azithromycin combination no antagonistic or synergistic effects are observed (Furuya, *et al.* 2006; Pereira, *et al.* 2012; Singh, *et al.* 2018). Therefore, in the model, dual combination is tested under additive effect.

C.1.1 Loewe additivity

To model under Loewe additivity, first, the concentration-drug effect relationship

(obtained through $\frac{(\varphi_{max}-\varphi_{min})(\frac{C}{MIC})^{k_H}}{(\frac{C}{MIC})^{k_H} - \frac{\varphi_{min}}{\varphi_{max}}}$) need to be analysed for gentamicin and

azithromycin. Through this, the most dominant drug among the two can be identified.

Once the dominant drug is identified, the additive effect with the combination of azithromycin and gentamicin (E_{ga}) under Loewe additivity is given by equation C.1

(Dini, *et al.* 2018),

$$E_{ga} = \frac{(\varphi_{max, hp} - \varphi_{min, hp}) \left(\frac{C_{ag}}{MIC_{hp}} \right)^{k_{H, hp}}}{\left(\frac{C_{ag}}{MIC_{hp}} \right)^{k_{H, hp}} - \frac{\varphi_{min, hp}}{\varphi_{max, hp}}} \quad (C. 1)$$

where $C_{ag} = C_{hp} + C_{eq}$ and $\varphi_{max, hp}$, $\varphi_{min, hp}$, $k_{H, hp}$ are the Hill function parameter values for the most potent drug out of gentamicin and azithromycin. C_{hp} is the drug concentration of the more potent drug. C_{eq} is the concentration of the more potent drug that is equally effective as the less potent drug at the concentration C_{lp} . This is obtained through,

$$C_{eq} = E^{-1}(E(C_{lp})) \quad (C. 2)$$

where E^{-1} is the inverse function of E given by,

$$E^{-1}(x) = MIC_{hp} \left(\frac{\varphi_{min, hp} x}{\varphi_{max, hp} (x - (\varphi_{max, hp} - \varphi_{min, hp}))} \right)^{\frac{1}{k_{H, hp}}} \quad (C. 3)$$

and $E(C_{lp})$ is the Hill function effect obtained under the less potent drug at concentration C_{lp} .

The model equations under Loewe additivity are as follows for the zero-interaction (additive effect) case:

$$\begin{aligned} \frac{dB}{dt} = & \left(1 - \frac{B + B_a}{k_1}\right) (r_1 B + d_3 B_s + e B_i) - d \frac{B N}{c N + B} - d_2 B - a_1 B \left(1 - \frac{B_a}{k_1 a_2}\right) \\ & - E_{ga} \left(1 - \frac{B + B_a}{k_1}\right) B \end{aligned}$$

$$\begin{aligned} \frac{dB_a}{dt} = & r_1 B_a \left(1 - \frac{B + B_a}{k_1}\right) + a_1 B \left(1 - \frac{B_a}{k_1 a_2}\right) - d \frac{B_a N}{c N + B_a} - \eta B_a \\ & - E_{ga} \left(1 - \frac{B + B_a}{k_1}\right) B_a \end{aligned}$$

$$\frac{dB_i}{dt} = \left(1 - \frac{B_i}{k_1 a_2}\right) (\eta B_a + r_2 B_i) - e B_i - E_{ga} \left(1 - \frac{B_i}{k_1 a_2}\right) B_i$$

$$\begin{aligned} \frac{dB_s}{dt} = & \left(1 - \frac{B_s}{N k_2}\right) \left(p d \frac{B N}{c N + B} + p d \frac{B_a N}{c N + B_a} + r_3 B_s\right) - d_3 B_s \\ & - E_{ga} \left(1 - \frac{B_s}{N k_2}\right) B_s \end{aligned}$$

$$\frac{dN}{dt} = \mu (N_{max} - N) (B + B_a) - d_3 N$$

C.2 Gepotidacin monotreatment

C.2.1 Association between model-derived breakpoint MIC and drug dose.

The following system given in Eq. C.4 and C.5 are non-dimensionalised to analyse whether the model-derived breakpoint MIC increases linearly with drug dose.

$$\frac{dB}{dt} = \left(1 - \frac{B}{k_1}\right) r_1 B - \frac{(r_1 - \varphi_{min}) \left(\frac{C_e}{MIC}\right)^{k_H}}{\left(\frac{C_e}{MIC}\right)^{k_H} - \frac{\varphi_{min}}{r_1}} B \left(1 - \frac{B}{k_1}\right) \quad (C.4)$$

$$\frac{dC_e}{dt} = -\delta C_e \quad (C.5)$$

$$B(0) = B_0 \text{ and } C_e(0) = C_0$$

Let $B = B^* \hat{B}$, $C_e = C_e^* \widehat{C_e}$ and $t = t^* \hat{t}$ such that the new variables B^* , C_e^* and t^* are non-dimensionalised versions of the original variables B , C_e and t respectively. The values of the constants \hat{B} , $\widehat{C_e}$ and \hat{t} are determined later.

Writing the system in terms of the non-dimensionalised variables.

$$\frac{dB^* \hat{B}}{dt^* \hat{t}} = \left(1 - \frac{B^* \hat{B}}{k_1}\right) r_1 B^* \hat{B} - \frac{(r_1 - \varphi_{min}) \left(\frac{C_e^* \widehat{C_e}}{MIC}\right)^{k_H}}{\left(\frac{C_e^* \widehat{C_e}}{MIC}\right)^{k_H} - \frac{\varphi_{min}}{r_1}} B^* \hat{B} \left(1 - \frac{B^* \hat{B}}{k_1}\right) \quad (C.6)$$

$$\frac{dC_e^* \widehat{C_e}}{dt^* \hat{t}} = -\delta C_e^* \widehat{C_e} \quad (C.7)$$

Simplifying Eq. C.6 and C.7 yields,

$$\frac{dB^*}{dt^*} = \hat{t} \left(1 - \frac{B^* \hat{B}}{k_1}\right) r_1 B^* - \hat{t} \frac{(r_1 - \varphi_{min}) \left(\frac{C_e^* \widehat{C_e}}{MIC}\right)^{k_H}}{\left(\frac{C_e^* \widehat{C_e}}{MIC}\right)^{k_H} - \frac{\varphi_{min}}{r_1}} B^* \left(1 - \frac{B^* \hat{B}}{k_1}\right) \quad (C.8)$$

$$\frac{dC_e^*}{dt^*} = -\hat{t} \delta C_e^* \quad (C.9)$$

Choose \hat{B} , $\widehat{C_e}$ and \hat{t} such that,

$$\hat{B} = k_1, \widehat{C_e} = MIC \text{ and } \hat{t} = \frac{1}{\delta}$$

Then Eq. C.8 and C.9 simplifies as,

$$\frac{dB^*}{dt^*} = (1 - B^*) \frac{r_1}{\delta} B^* - \frac{1}{\delta} \left[\frac{(r_1 - \varphi_{min})(C_e^*)^{k_H}}{(C_e^*)^{k_H} - \frac{\varphi_{min}}{r_1}} \right] B^* (1 - B^*) \quad (C.10)$$

$$\frac{dC_e^*}{dt^*} = -C_e^* \quad (C.11)$$

$$B^*(0) = \frac{B_0}{k_1} \text{ and}$$

$$C_e^*(0) = \frac{C_0}{MIC}$$

C.2.2 PK indices to explain effectiveness of different treatment strategies

The higher effectiveness of multiple dose strategies than single dose regimens is explored using the PK indices, $t_{\text{MIC}_{\text{in}}}$, and $\text{AUC}/\text{MIC}_{\text{in}}$ (Fig.C.1).

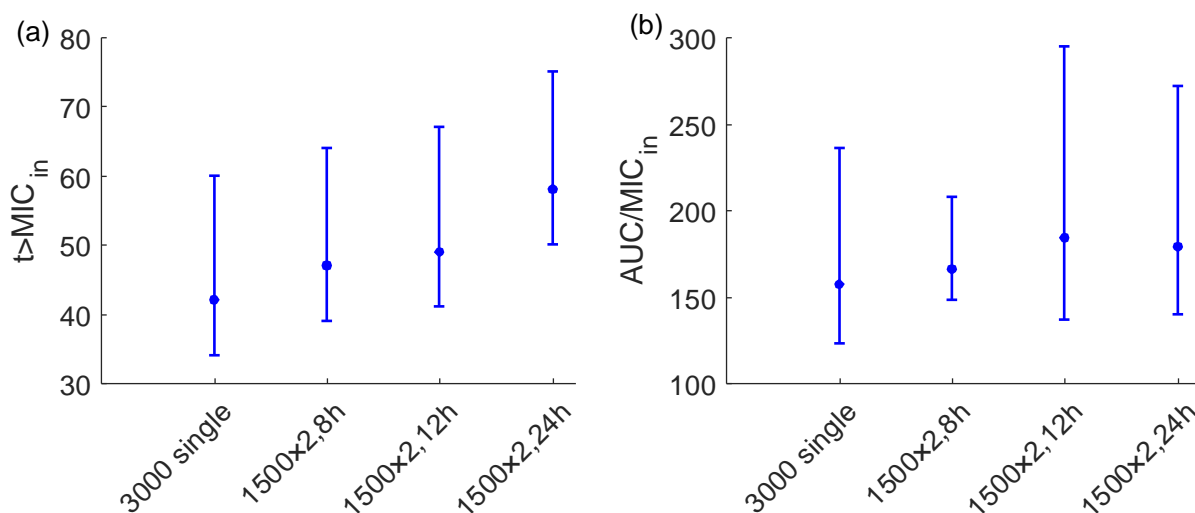


Figure C.1: PK/PD indices evaluated for the 3000mg single dose and multiple dose strategies using 1500mg multiples (with a total accumulation of 3000mg) with dosing intervals of 8, 12 and 24h. (a) time above the MIC ($t_{\text{MIC}_{\text{in}}}$) and (b) area under the total drug concentration ($\text{AUC}/\text{MIC}_{\text{in}}$) calculated using the intracellular concentration. The data points represent the median and the bars represent the 95% range of the PK indices evaluated for the 5402 concentration profiles of the LHS samples for MIC for gepotidacin of 1mg/L.

C.2.3 Threshold gepotidacin concentration required for treatment success

For multiple dose regimens we calculate the time above the MIC using our default method of total time the drug concentration remains above the MIC. We also calculate time above the MIC according to three alternative methods, 1) Total time above the MIC – Total time below the MIC (up till the last threshold crossing); 2) maximal continuous-time above the MIC (the longest period in which the drug concentration is always above

the MIC); and 3) time above the MIC without considering the periods in which it is below the MIC (last time point the concentration is above MIC – first time point the concentration is above MIC). A comparison of these four index calculations is shown in Fig. C.2.

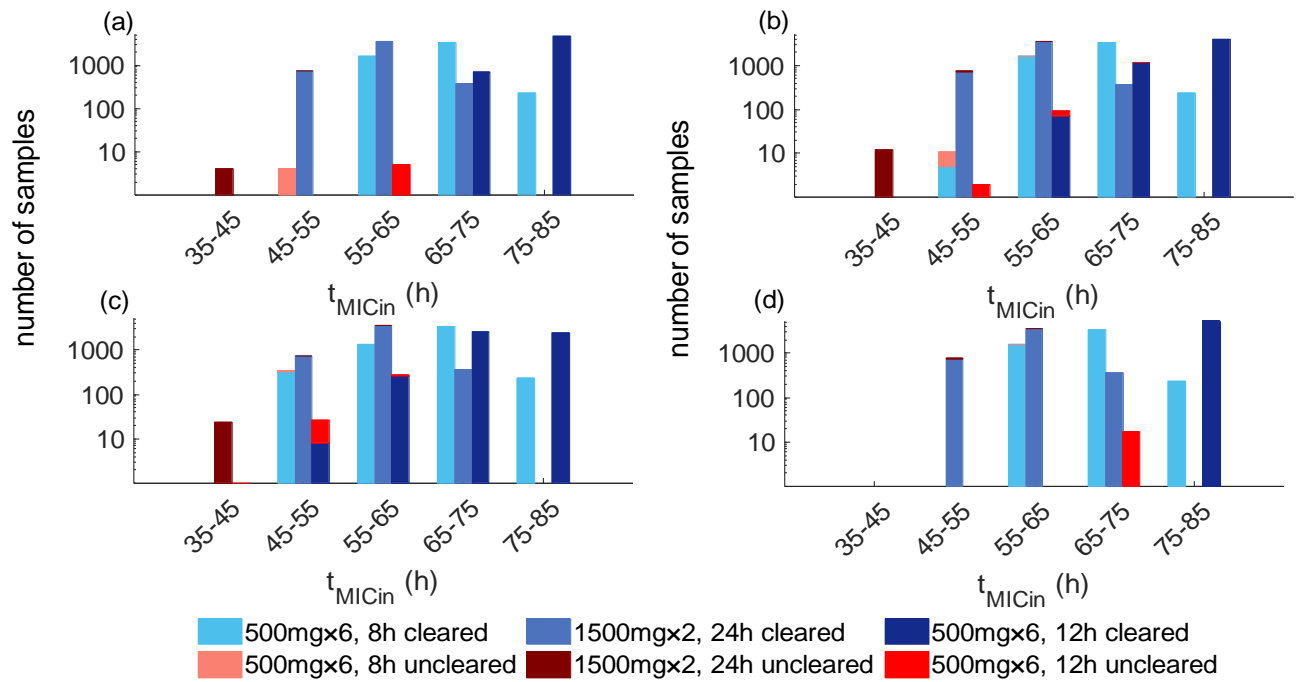


Figure C.2: Comparison of t_{MICin} calculations to differentiate treatment success and failure using intracellular drug concentration. (a) Total time above the MIC, removing periods where it is below; (b) total time above the MIC – total time below the MIC (up till the last threshold crossing); (c) maximal continuous-time above the MIC (the longest period in which the drug concentration is always above the MIC); and (d) time above the MIC without considering the periods in which it is below the MIC (last time point the concentration is above MIC – first time point the concentration is above MIC).

The area under the curve above the MIC (removing the area below the MIC from the total area under the curve) and AUC over a fixed time period of 7 days (AUC_{0-7}/MIC) are calculated as alternative indices and the results are shown in Fig. C.3.

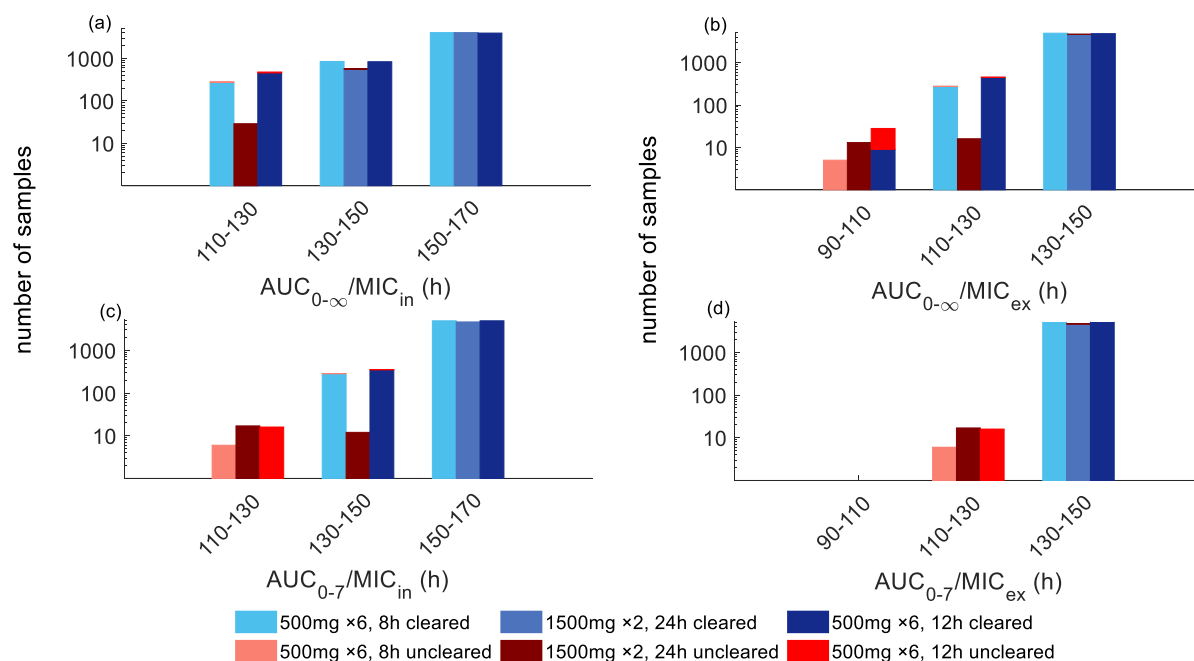


Figure C.3: The area under the curve above the MIC (removing the area below the MIC from the total area under the curve) (a, b) and AUC over a fixed time period of 7 days (AUC_{0-7}/MIC) (c, d) calculated as alternative indices using intracellular drug concentration (first column) and (b) extracellular drug concentration (second column).

The behaviour of the bacterial load of the LHS samples that achieve AUC_{in}/MIC in the range of 147-150h but fail to clear the infection is shown in Fig. C.4.

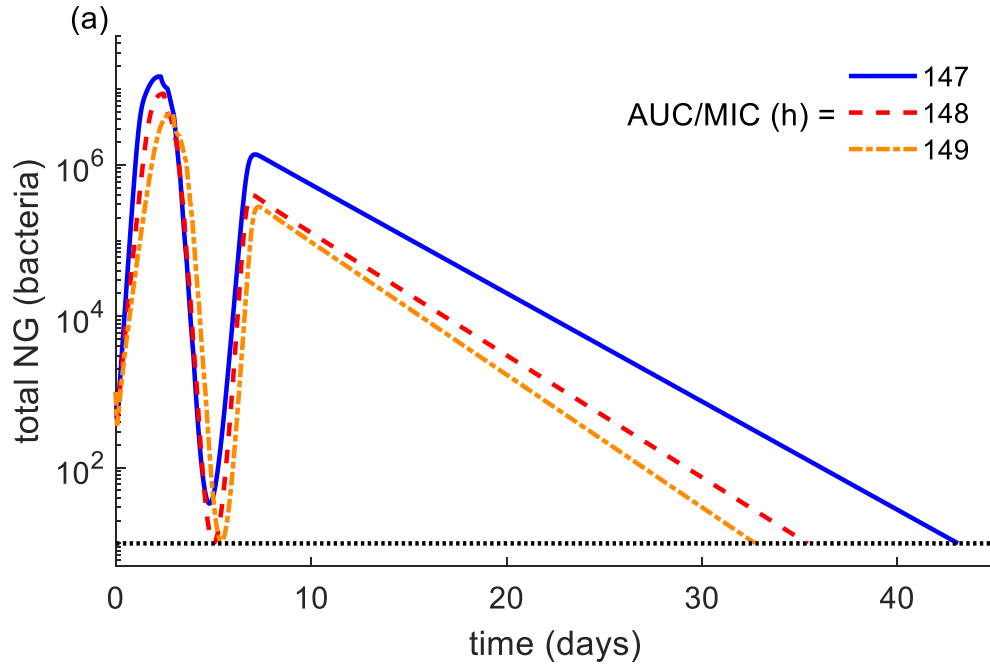


Figure C.4: Change in the total bacterial load over time of the samples that do not clear infection and have PK index $AUC/MIC_{in} < 150h$. The shown bacterial load curves are associated with drug concentration levels that achieve AUC/MIC_{in} in the range of 147-150h. Only three instances are shown for better visualisation.

C.2.4 Testing higher doses of gepotidacin monotreatment

The *in vitro* study by VanScoy, *et al.* (2020) tested higher doses of 4.5 and 6g gepotidacin doses which have not been tested in clinical trials. The effectiveness of these higher doses is summarised in Table C.1.

Table C.1: Percentage of LHS samples (out of 5402) that clear the infection in ≤ 7 days when using single and multiple dose gepotidacin treatment strategies that accumulate to a 4.5 or 6g gepotidacin dose.

Strategy	MIC (mg/L)			
	1	1.5	2	2.5
4500mg single dose	99.96	95.41	90.45	46.65
6000mg single dose	100.00	99.74	95.41	81.89
1500mg $\times 3$, 8h apart	100.00	98.93	89.14	42.21
1500mg $\times 3$, 12h apart	100.00	99.24	90.76	67.42
1500mg $\times 3$, 24h apart	100.00	99.70	93.67	71.71
3000mg $\times 2$, 8h apart	100.00	99.81	96.87	87.23
3000mg $\times 2$, 12h apart	100.00	99.93	98.52	92.02
3000mg $\times 2$, 24h apart	100.00	99.98	99.35	93.29
2000mg $\times 3$, 8h apart	100.00	99.10	98.93	87.75
2000mg $\times 3$, 24h apart	100.00	99.84	99.24	91.13
4500mg on the first day and 1500mg on the second day	100.00	99.98	98.93	92.65

C.3 Gentamicin treatment.

C.3.1 Impact on patient non-compliance on multiple-dose strategies of gentamicin

We analyse the impact of patient non-compliance for the extended gentamicin dosing strategy of $240\text{mg} \times 3$ doses, given 24h apart in combination with a 2g single dose of azithromycin. It is assumed the second dose will not be taken at the appropriate dosing interval. Treatment efficacy is analysed when 15%, 25% 50%, 75% and 100% of the LHS samples are assumed to be subject to non-adherence (Table C.2).

Table C.2: Treatment effectiveness with non-compliance for the dual treatment combination 240mg \times 3 gentamicin, given 24h apart in combination with 2g azithromycin.

Compliance level	(Gentamicin/ azithromycin) MIC (mg/L)					
	4/0.5	4/1	8/0.5	8/1	16/0.5	16/1
Full compliance	100.00	99.91	99.96	98.96	99.76	95.45
15% non-compliance	100.00	99.91	99.89	98.78	99.44	95.15
25% non-compliance	100.00	99.91	99.91	98.78	99.44	94.75
50% non-compliance	100.00	99.89	99.89	98.80	99.44	94.30
75% non-compliance	100.00	99.89	99.87	98.76	99.43	94.13
100% non-compliance	100.00	99.85	99.85	98.74	99.41	94.13

C.4 The Difference in bacterial killing rates elicited by the monotreatment and dual treatment options.

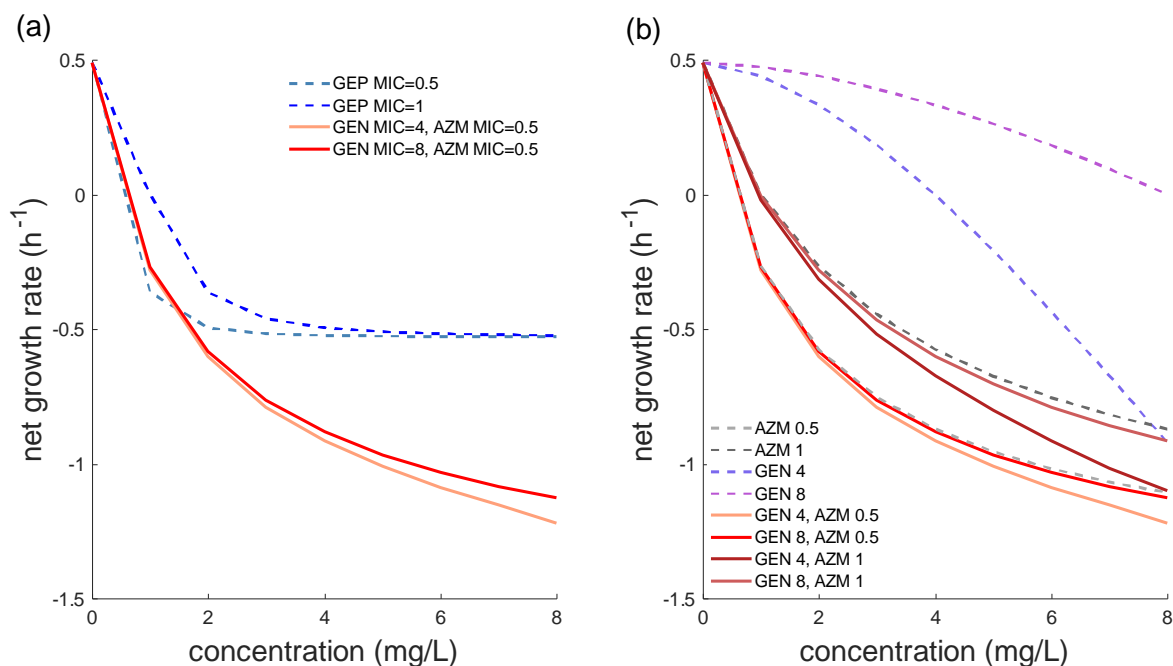


Figure C.5: Comparison of the net bacterial growth rate when treated with monotreatment and dual treatment regimens. (a) monotreatment with gepotidacin and dual treatment and (b) monotreatment with gentamicin and azithromycin compared with dual treatment with gentamicin + azithromycin at doubling MIC values. The dashed lines indicate monotreatment options and solid lines dual treatment. The results are shown using the point estimates. The figure legend represents the drug and the MIC for that drug.

Appendix D

Supplementary material pertaining to Chapter 6

D.1 Model equations

The model equations that describe drug interaction with NG are given below. The associated parameter values are described in detail in main text and summarised in Tables 6.1 and 6.2. The natural infection related parameter values are summarised in Table 3.2, Chapter 3.

$$\begin{aligned} \frac{dB}{dt} = & \left(1 - \frac{B + B_a + B' + B'_a}{k_1}\right) (r_1 B + d_3 B_s + e B_i) - d_c(B) - d_2 B \\ & - a_1 B \left(1 - \frac{B_a + B'_a}{k_1 a_2}\right) - k_{dormant} H(f_{bound_e} - f_c) B \end{aligned}$$

$$\begin{aligned} \frac{dB'}{dt} = & k_{dormant} H(f_{bound_e} - f_c) B - d_a(f_{bound_e})B' - d_c(B') + (d_3 B'_s \\ & + e B'_i) \left(1 - \frac{B + B_a + B' + B'_a}{k_1}\right) \end{aligned}$$

$$\begin{aligned} \frac{dB_a}{dt} = & r_1 B_a \left(1 - \frac{B + B_a + B' + B'_a}{k_1}\right) + a_1 B \left(1 - \frac{B_a + B'_a}{k_1 a_2}\right) - d_c(B_a) \\ & - k_{dormant} H(f_{bound_e} - f_c) B_a - \eta B_a \end{aligned}$$

$$\frac{dB'_a}{dt} = k_{dormant} H(f_{bound_e} - f_c) B_a - d_a(f_{bound_e})B'_a - d_c(B'_a)$$

$$\frac{dB_i}{dt} = \left(1 - \frac{B_i + B'_i}{k_1 a_2}\right) (\eta B_a + r_2 B_i) - e B_i - k_{dormant} H(f_{bound_i} - f_c) B_i$$

$$\frac{dB_i'}{dt} = k_{dormant} H(f_{bound_i} - f_c) B_i - eB_i' - d_a(f_{bound_i})B_i'$$

$$\begin{aligned} \frac{dB_s}{dt} = & \left(1 - \frac{B_s + B_s'}{N k_2}\right) [p d_c(B) + p d_c(B_a) + r_3 B_s] - d_3 B_s - k_{dormant} H(f_{bound_i} \\ & - f_c) B_s \end{aligned}$$

$$\frac{dB_s'}{dt} = k_{dormant} H(f_{bound_i} - f_c) B_s - d_a(f_{bound_i})B_s' - d_3 B_s'$$

$$\frac{dN}{dt} = \mu (N_{max} - N) (B + B_a + B' + B_a') - d_3 N$$

$$\frac{dA_e}{dt} = -k_{el}A_e - k_f A_e + k_r A_i - \frac{k_{PBP}}{n_A V_u} A_e T_e$$

$$\frac{dA_i}{dt} = k_f A_e - k_r A_i - \frac{k_{PBP}}{n_A V_u} A_i T_i$$

$$\begin{aligned} \frac{dT_{be}}{dt} = & \frac{k_{PBP}}{n_A V_u} A_e T_e \\ & - (y \times f_{bound_e}) [d_c(B_a') + d_c(B') + d_c(B_a) + d_c(B) \\ & + d_a(f_{bound_e})(B' + B_a') + d_2 B + \eta B_a] \\ & + \left(1 - \frac{B + B_a + B' + B_a'}{k_1}\right) \{[d_3(B_s' + B_s) + e(B_i' + B_i)](y \times f_{bound_i})\} \end{aligned}$$

$$\begin{aligned} \frac{dT_{bi}}{dt} = & \frac{k_{PBP}}{n_A V_u} A_i T_i \\ & - (y \times f_{bound_i}) \{d_a(f_{bound_i})(B_s' + B_i') + [d_3(B_s' + B_s) + e(B_i' + B_i)]\} \\ & + \left(1 - \frac{B_i + B_i'}{k_1 a_2}\right) \eta B_a (y \times f_{bound_e}) \\ & + \left(1 - \frac{B_s + B_s'}{N k_2}\right) [p d_c(B) + p d_c(B_a)](y \times f_{bound_e}) \end{aligned}$$

$$\begin{aligned}
\frac{dT_e}{dt} = & -\frac{k_{PBP}}{n_A V_u} A_e T_e \\
& - \left(y \times (1 - f_{bound_e}) \right) [d_c(B'_a) + d_c(B') + d_c(B_a) + d_c(B) \\
& + d_a(f_{bound_e})(B' + B'_a) + d_2 B + \eta B_a] \\
& + \left(1 - \frac{B + B_a + B' + B'_a}{k_1} \right) \{ [d_3(B'_s + B_s) + e(B'_i + B_i)] (y \times (1 - f_{bound_i})) \\
& + (r_1 B + r_1 B_a) y \}
\end{aligned}$$

$$\begin{aligned}
\frac{dT_i}{dt} = & -\frac{k_{PBP}}{n_A V_u} A_i T_i \\
& - (y \times (1 - f_{bound_i})) \{ d_a(f_{bound_i})(B'_s + B'_i) \\
& + [d_3(B'_s + B_s) + e(B'_i + B_i)] \} + r_3 B_s \left(1 - \frac{B_s + B'_s}{N k_2} \right) y \\
& + \left(1 - \frac{B_i + B'_i}{k_1 a_2} \right) [\eta B_a (y \times (1 - f_{bound_e})) + r_2 B_i y] \\
& + \left(1 - \frac{B_s + B'_s}{N k_2} \right) [p d_c(B) + p d_c(B_a)] (y \times (1 - f_{bound_e}))
\end{aligned}$$

$H(f_{bound_e} - f_c)$ and $H(f_{bound_i} - f_c)$ are Heaviside step functions that trigger the movement of non-dormant NG to dormant NG states in respectively, extracellular and intracellular environments.

$$f_{bound_e} = \frac{T_{be}}{T_e + T_{be}}$$

$$f_{bound_i} = \frac{T_{bi}}{T_i + T_{bi}}$$

Bacterial killing through drug as a function of the fraction of bound PBP: $d_a(f) = E_{max} \frac{f^m}{EC_{50}^m + f^m}$

Bacterial killing through PMN as a function of the bacterial state: $d_c(g) = d \frac{g N}{c N + g}$

D.2 Concentration-dependent protein binding of ceftriaxone

Here, we investigate the impact of change in ceftriaxone free (unbound to albumin) fraction (f_u) on the infection clearance time simulated from the model. The model produced clearance times are assessed for different MIC parameter values of the Hill function (referred hereafter as ‘MIC’) at different free fractions (Fig. D.1). It could be observed that for $f_u \leq 0.1$, the model-derived susceptibility breakpoint (defined in Chapter 4, Section 4.2.5) of 0.25mg/L remains unchanged. With $f_u > 0.1$, the model-derived susceptibility breakpoint shifts to 0.5mg/L.

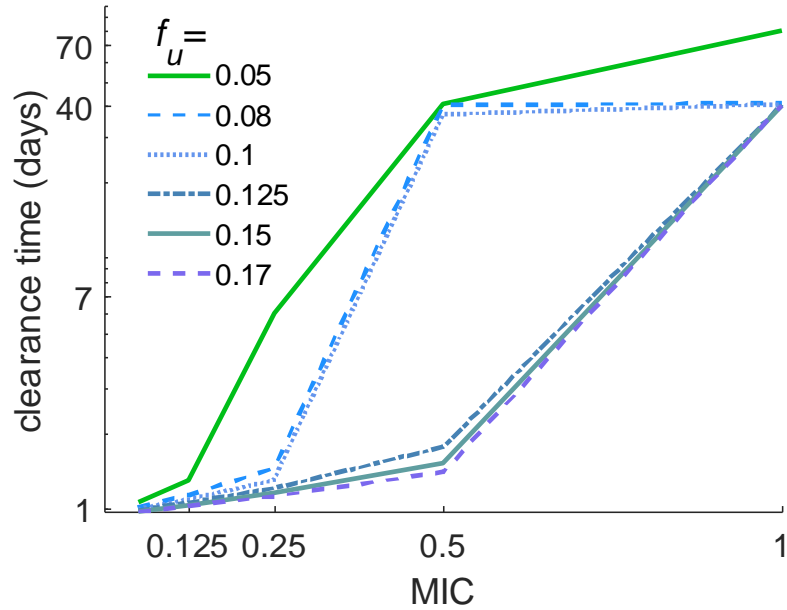


Figure D.1: The model produced infection clearance times assessed at varying MIC levels using different free fraction levels. The figure legend shows different free fraction levels (f_u) between 0.05- 0.17.

D.3 Estimating parameter values related to drug-mediated killing and dormancy

Out of the five cephalosporins used in Dougherty, *et al.* (1981), only three are third-generation cephalosporins. As the drugs that we are interested in (ceftriaxone and cefixime) are third-generation cephalosporins, only these three drugs are selected. However, out of these three, one drug, ceftiofur has bound fractions measured in concentrations that are higher than what is used in Foerster, *et al.* (2016) and therefore, it is not used in the analysis. As the bound PBP fractions relating to the drug cefoperazone produce better fits with NG data in Foerster, *et al.* (2016) than with the bound PBP fractions of cefotaxime (sum of squared errors 3.94 (cefoperazone) vs 7.54 (cefotaxime) shown in Fig. D.2), cefoperazone is used to estimate the Hill function (E_{max} , EC_{50} and m) and rate constant of dormancy ($k_{dormant}$) parameter values. For parameter estimation, the bound fractions reported for binding to PBP2 are used as PBP2 is considered to be the most important binding site relating to NG. The model fits to estimate model parameter values are shown in Fig. D.3.

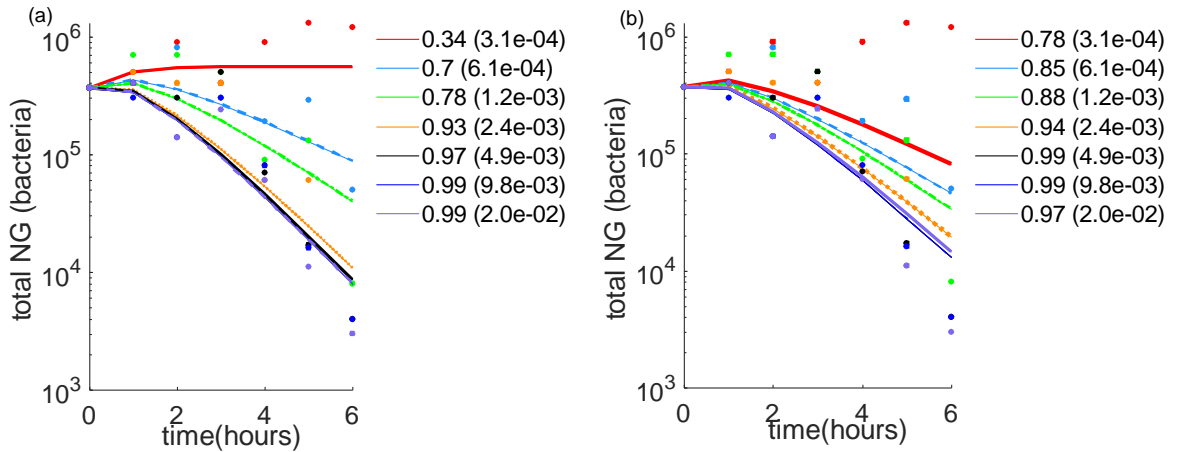


Figure D.2: Fit to NG load data over time with bound PBP fractions of (a) cefoperazone and (b) cefotaxime. The first column in the legend represents the bound PBP fractions reported in Dougherty, *et al.* (1981) and the second column represents the measured drug concentrations in Foerster, *et al.* (2016).

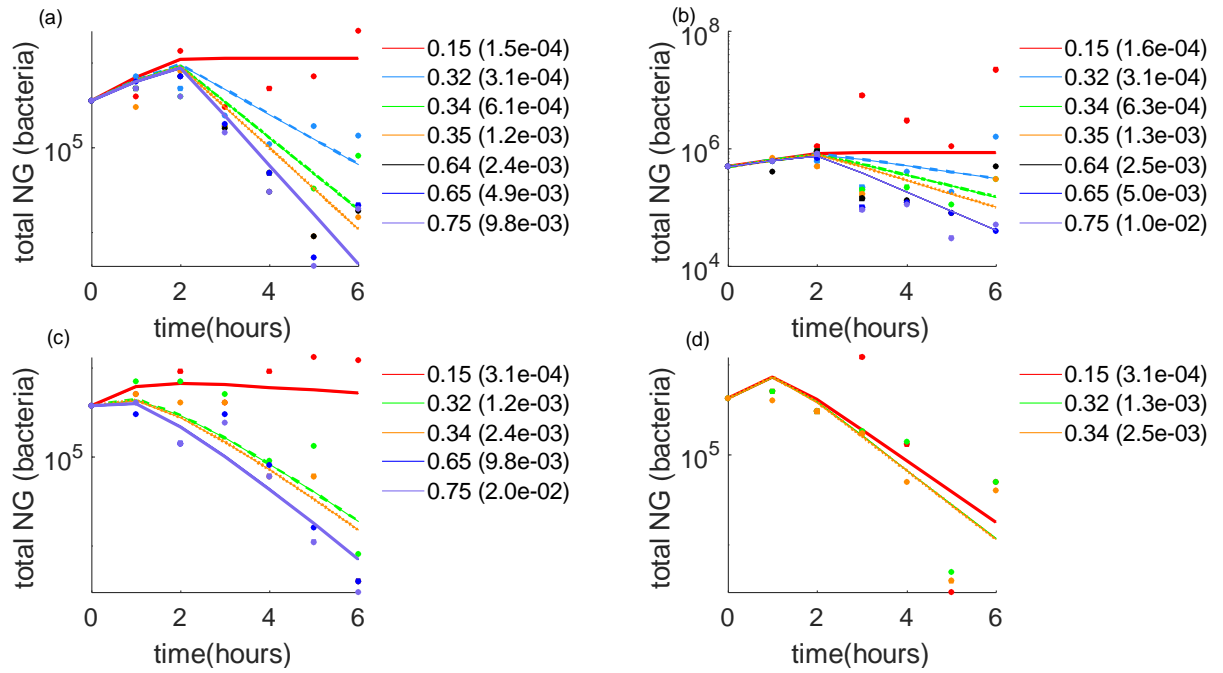


Figure D.3: Estimating the Hill function parameters (E_{max} , EC_{50} and m) and the rate constant of NG moving to dormant states ($k_{dormant}$) when treated with ceftriaxone and cefixime. Fits to the NG data in the two experiments in Foerster, *et al.* (2016) for (a-b) ceftriaxone and (c-d) cefixime. The first column in the legend represents the bound PBP fractions and the second column represents the drug concentration that result in the relevant bound PBP fractions.

D.3.1 Estimating the point estimates of the Hill function parameters

When estimating the Hill function parameter values using Foerster, *et al.* (2016), as there are two separate experiments on NG growth, an additional step is taken to find the point estimate parameters and then to generate parameter ranges around the point estimates. This process is described in detail in Chapter 4, Section 4.2.2.1 and only a brief description is given here. First, two sets of parameter estimates are obtained by fitting separately to the two individual experimental data, using Eq.6.1 and 6.2 in Chapter 6. Then, using these estimated individual parameter sets, the antibiotic mediated killing

effect is calculated using $d_a(f_{bound_e}) = E_{max} \frac{(f_{bound_e})^m}{EC_{50}^m + (f_{bound_e})^m}$, where $d_a(f_{bound_e})$ is the Hill effect that determines the drug-mediated killing rate of the bacterial population when the drug bound PBP fraction is f_{bound_e} . Parameters are described in Table 6.2, Chapter 6.

Then, to obtain the point estimate model parameter values, the mean Hill effect is evaluated using the individual Hill effects ($d_a(f_{bound_e})$). The Hill function is then fitted to this obtained mean killing effect to estimate the point estimates similar to the approach taken in Chapter 4, Section 4.2.2.1.

D.4 PK parameter estimation

Parameter ranges around the rate of drug absorption (k_a), the rate of drug moving from the extracellular compartment to the intracellular compartment (k_f), the rate of drug moving from the intracellular compartment to the extracellular compartment (k_r) are obtained using the method described in Chapter 6, Section 6.2.2.2. The model fits to these generated data is shown in Fig. D.4.

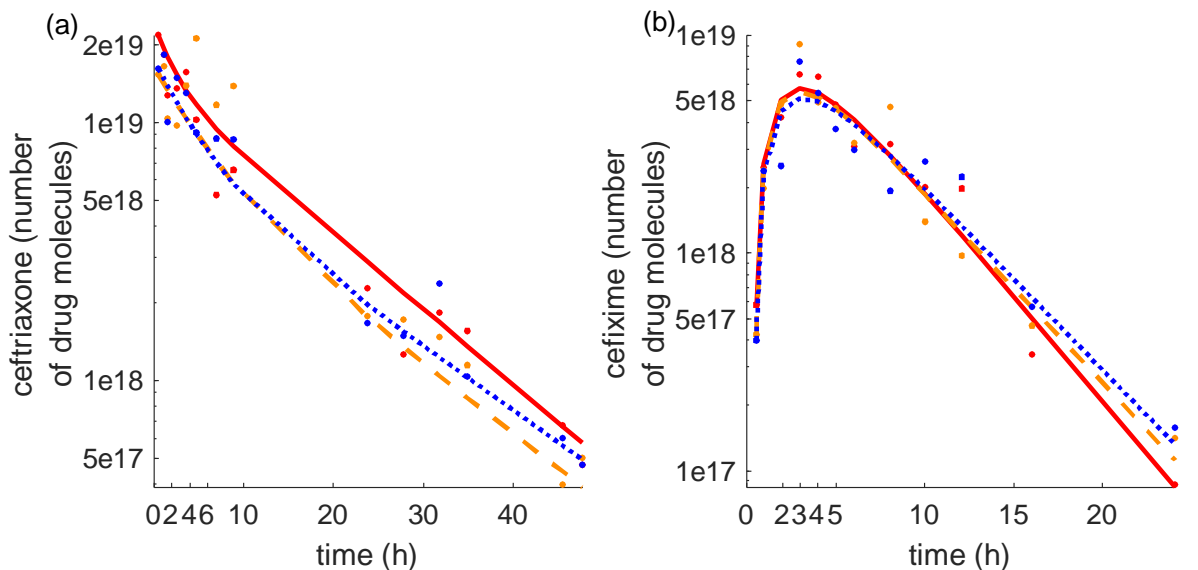


Figure D.4: Model fits to generated data to estimate k_a , k_f and k_r shown for three of the generated data sets (for better visualisation only three examples are shown). (a) Model fit to ceftriaxone data. (b) Model fit to cefixime data. The scatters show the data points and the lines represent the model fits.

We also note that when generating these data for parameter estimation alternative assumptions with larger variance make only negligible differences to model outcomes. To test this, we generated data points through a log-normal distribution with the log number of drug molecules reported in studies being the mean and standard deviation/mean=0.2. Using these generated data, the parameter values are estimated using the same approach described in Chapter 6, Section 6.2.2.2. The parameter values obtained from the data generated through a log-normal distribution ($k_a = 0.46 - 0.87$, $k_f = 0.32 - 0.89$ and $k_r = 2.84 - 5.13$) overlapped with the estimates obtained from data generated through a Poisson distribution ($k_a = 0.61 - 0.90$, $k_f = 0.17 - 0.57$ and $k_r = 3.14 - 4.70$). A comparison of the resulting treatment effectiveness using the parameter estimates obtained from data generated through log-normal and Poisson distribution are shown in Table D.1.

Table D.1: Comparison of the percentage of simulations that clear the infection in ≤ 7 days at MIC for cefixime of 0.5mg/L when data are generated using Poisson and log-normal distributions.

Treatment Strategy	Treatment efficacy	
	Data from Poisson distribution	Data from log-normal distribution
400mg Single	30.27 %	30.85 %
400mg×3, 8h	89.95 %	90.15 %
800mg×3, 8h	99.70 %	99.74 %

D.5 Estimation of the fraction of administered drug molecules that reaches the urethra (f_s)

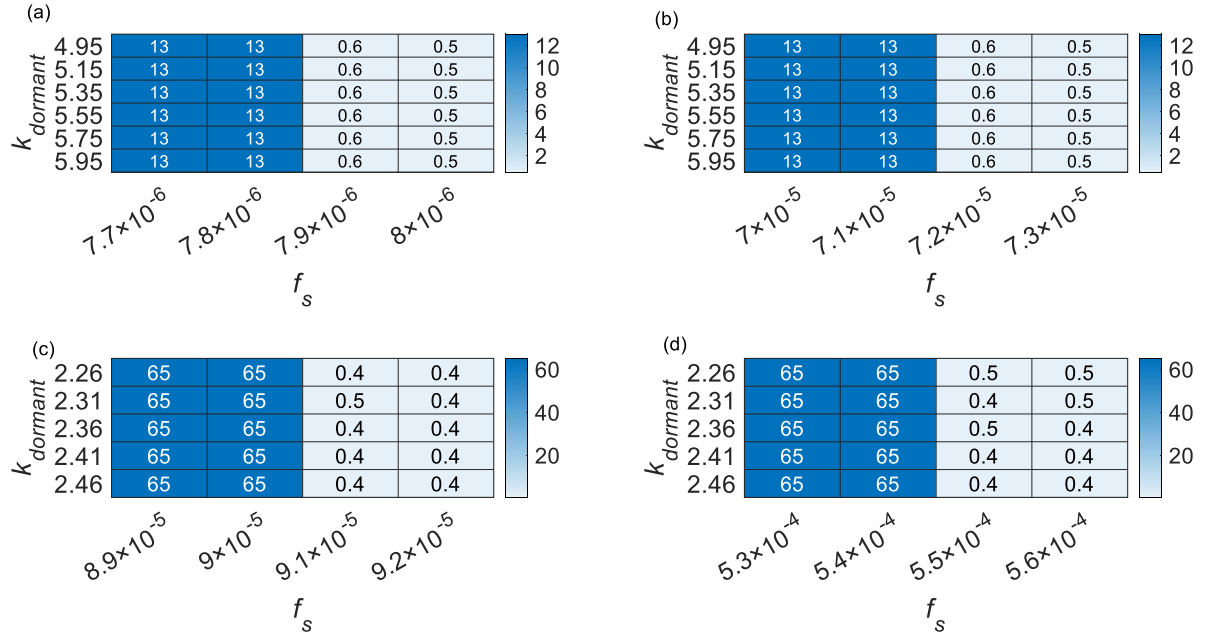


Figure D.5: Model produced infection clearance times (days) for different scaling factor (f_s) values. (a- b) analysed over the ceftriaxone $k_{dormant}$ parameter range of 4.95 – 6.05 (based on estimates obtained in Table 6.2, Chapter 6). (c - d) analysed over the cefixime $k_{dormant}$ parameter range of 2.26 – 2.5 (based on estimates obtained in Table 6.2, Chapter 6). (a, c) Infection clearance times related to a susceptible strain. (b, d) Infection clearance times related to a resistant strain.

D.6 PK/PD parameter calibration

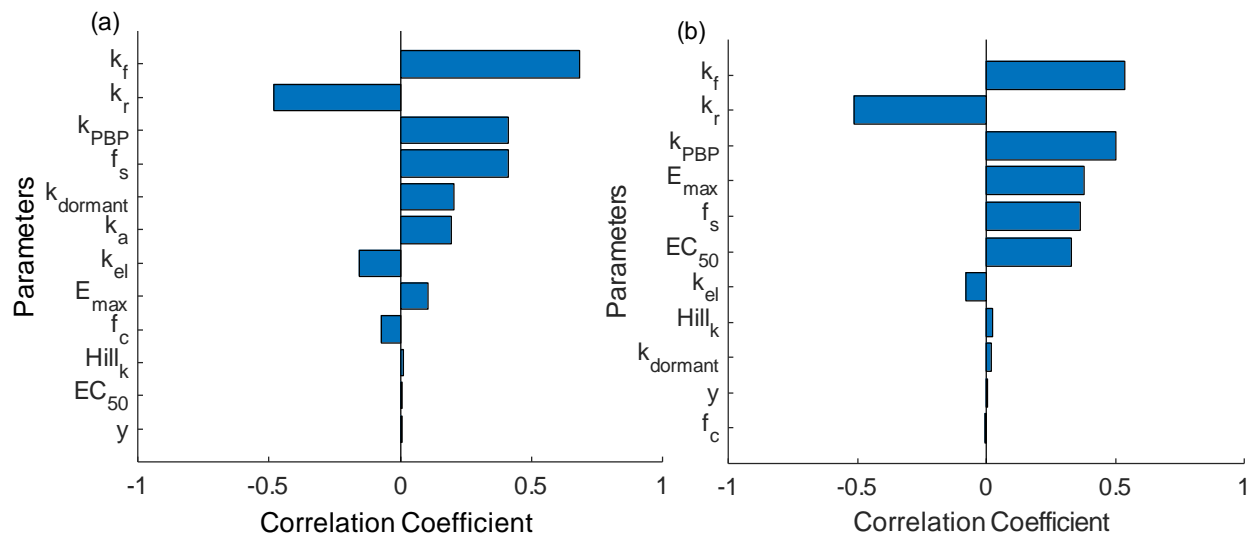


Figure D.6: Tornado plots of partial rank correlation coefficients, indicating the importance of each parameter's uncertainty in contributing to the variability in the model-derived susceptibility breakpoint obtained from the simulations using LHS samples shown for (a) cefixime and (b) ceftriaxone.

Table D.2: Comparison of the parameter values prior to calibration and after calibration
for ceftriaxone (CFO) and cefixime (CFM).

Drug	Parameter	Parameter range (prior to calibration)	Source for parameter values prior to calibration	Parameter range (after calibration)
CFO	k_f	0.38 - 0.85	Method described in Section 6.2.2.2 in the main text	0.41 - 0.85
	k_r	1.35 - 2.78		1.35 - 2.60
CFM	k_f	0.09 - 0.57		0.17 - 0.57
	k_r	3.14 - 5.31		3.14 - 4.7

D.7 MIC expression

An expression to define minimum inhibitory concentration (MIC) is derived using a sub-system that reflects an *in vitro* system with no epithelial cells and immune response.

$$\frac{dB}{dt} = \left(1 - \frac{B + B'}{k_1}\right) r_1 B - k_{dormant} H(f_{bound_e} - f_c) B$$

$$\frac{dB'}{dt} = k_{dormant} H(f_{bound_e} - f_c) B - E_{max} \frac{(f_{bound_e})^m}{EC_{50}^m + (f_{bound_e})^m} B'$$

$$\frac{dT_{be}}{dt} = \frac{k_{PBP}}{n_A V_u} AT_e - E_{max} \frac{(f_{bound_e})^m}{EC_{50}^m + (f_{bound_e})^m} B' y f_{bound_e}$$

Using the above system, an expression for MIC is derived as follows.

At MIC, the corresponding number of drug molecules are given by, $A_{MIC} = MIC \times V_u \times \left(\frac{1}{M_w}\right) \times n_A$, where M_w is the molecular weight of the drug, V_u is the urethral volume and n_A is the Avogadro constant.

If f_c is the fraction of drug bound PBP targets at which the net growth of the bacterial population is zero, at A_{MIC} the drug bound PBP fraction is:

$$\frac{(T_{be})_{MIC}}{(T_{be})_{MIC} + (T_e)_{MIC}} = f_c \quad (D.1)$$

$(T_{be})_{MIC}$ and $(T_e)_{MIC}$ are respectively drug bound and free PBP molecules at MIC.

Since,

$$(T_e)_{MIC} = (B^* + B'^*)y - (T_{be})_{MIC} \quad (D.2)$$

where B^* and B'^* are respectively the steady-state unattached and dormant NG and y is the fixed number of PBP targets per bacterium.

From D.1 and D.2:

$$\frac{(T_{be})_{MIC}}{(B^* + B'^*)y} = f_c \quad (D.3)$$

Since at MIC, the system is at equilibrium,

$$\frac{k_{PBP}}{n_A V_u} A_{MIC} (T_e)_{MIC} = k_{dormant} B^* y f_c \quad (D.4)$$

Substituting Eq. D.3 into the above expression (D.4):

$$\frac{k_{PBP}}{M_w} MIC \times (B^* + B'^*) y (1 - f_c) = k_{dormant} B^* y f_c \quad (D.5)$$

$$MIC = \frac{k_{dormant} f_c M_w}{k_{PBP} (1 - f_c)} \left(\frac{B^*}{B^* + B'^*} \right) \quad (D.6)$$

Since MIC is independent of the drug being present, assuming that $B'^* = 0$,

$$MIC = \frac{k_{dormant} f_c M_w}{k_{PBP} (1 - f_c)} \quad (D.7)$$

D.8 Different cefixime treatment strategies

The extracellular drug concentration profiles converted from the number of molecules simulated from the model are shown in Fig. D.7. Single and multiple dose strategies that accumulate to a total drug dose of 400, 800, 1200 and 2400mg are shown.

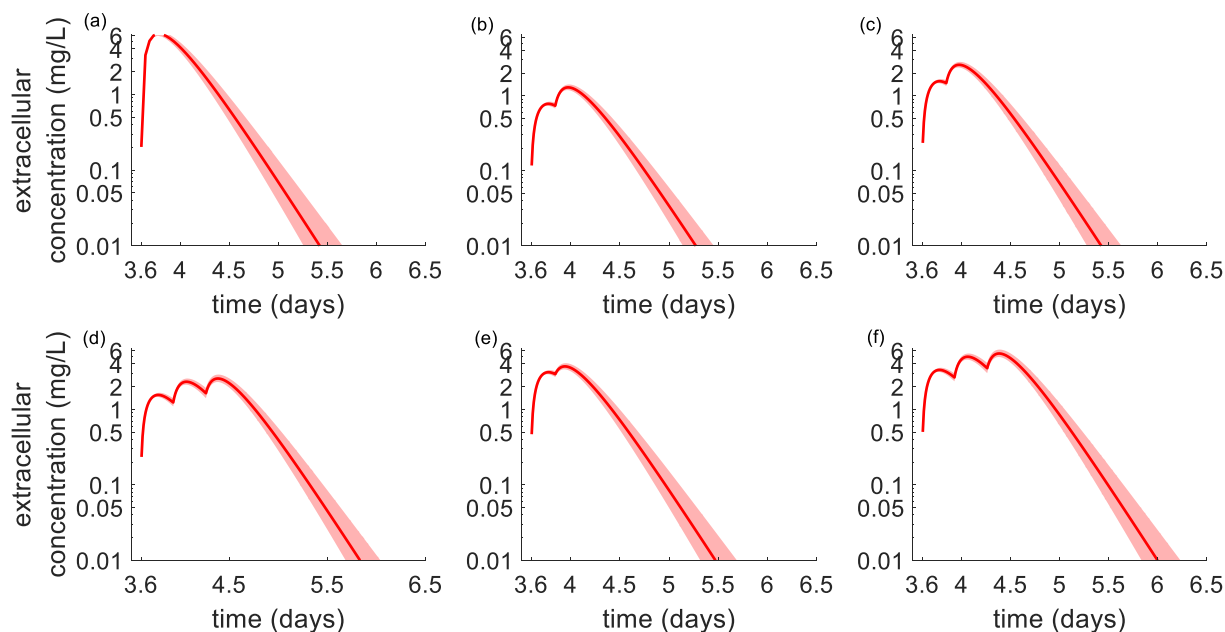


Figure D.7: Change in the extracellular drug concentration profiles for tested cefixime strategies. (a) 1200mg single dose (b) 200mg \times 2, 6h apart (c) 400mg \times 2, 6h apart (d) 400mg \times 3, 8h apart (e) 800mg and 400mg 6h apart and (f) 800mg \times 3, 8h apart. The solid line is the median drug concentration and the shaded area is the 95% range.

D.8.1 Effectiveness of different multiple dose strategies of cefixime

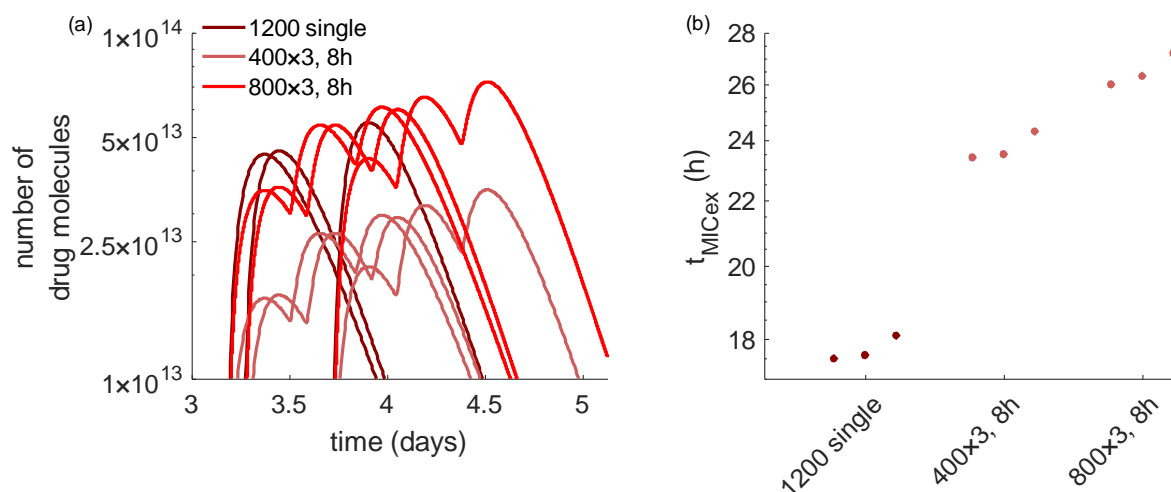


Figure D.8: Behaviour of (a) the intracellular number of drug molecules and (b) the time the extracellular drug concentration remains above the MIC shown for the simulations that cleared infection through multiple dose strategy but failed with the single dose regimen. Results are shown using 1200mg single dose, 400mg×3, 8h and 800mg×3, 8h strategies for MIC for cefixime of 0.5mg/L.

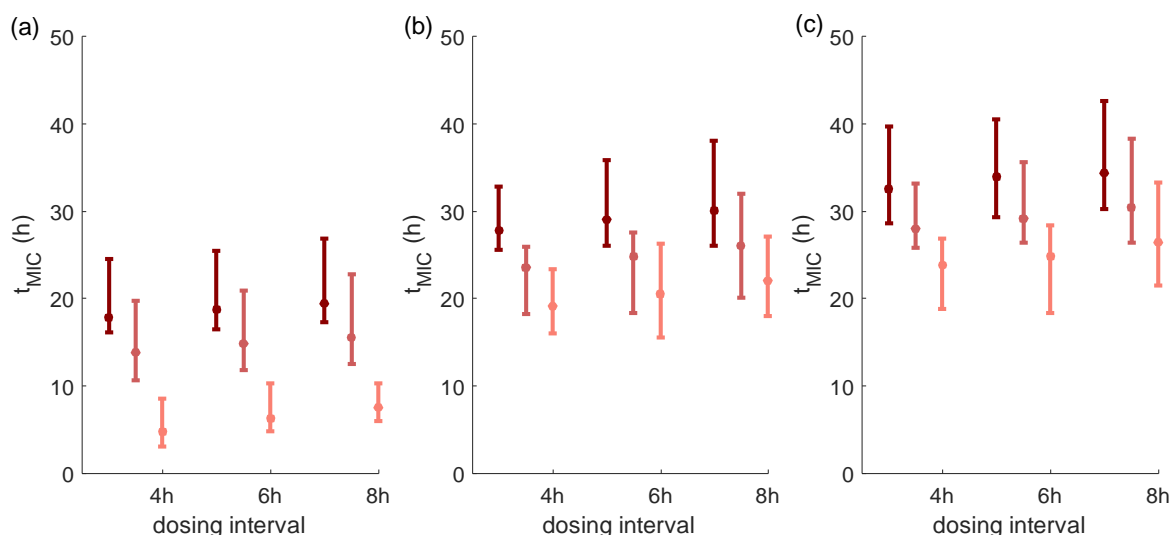


Figure D.9: The time above the MIC (t_{MIC}) obtained for different dose amounts and dosing intervals of cefixime. The t_{MIC} obtained for MIC of 0.25, 0.5 and 1mg/L

shown for the treatment strategies of (a) 2×200mg (b) 400mg ×3 and (c) 800mg ×3 evaluated at 4, 6 and 8h dosing frequencies. The scatter point represents the median and the bars represent the 95% range.

D.8.2 Patient non-adherence with multiple dose strategies

The effectiveness of multiple dose strategies under patient non-adherence is evaluated using the strategy 400mg × 3, 8h apart (Table D.3). When testing non-adherence, it is assumed that the second dose is not taken at the correct dosing interval. Specifically, we consider a uniformly distributed delay of between 0 and 8h to the 2nd dose in comparison to the recommended schedule, with subsequent doses then taken at the correct spacing from the previous dose. Treatment efficacy is analysed when 15%, 25% 50%, 75% and 100% of the simulations using LHS samples are assumed to be subject to non-adherence.

Table D.3: The percentage of simulations that clear infection using 400mg \times 3, 8h cefixime strategy under patient non-adherence.

Method	MIC (mg/L)				
	0.06	0.125	0.25	0.5	1
Full compliance -1200mg single dose	100.00	100.00	99.72	89.72	60.64
Full compliance - 400mg \times 3, 8h	100.00	100.00	99.72	89.95	60.76
20% non-compliance	100.00	100.00	99.68	89.78	60.63
25% non-compliance	100.00	100.00	99.44	87.41	55.29
50% non-compliance	100.00	100.00	99.24	86.15	52.59
75% non-compliance	100.00	100.00	98.87	83.20	49.10
100% non-compliance	100.00	100.00	98.30	80.31	46.24

References

- Aarons L. Physiologically based pharmacokinetic modelling: a sound mechanistic basis is needed. *Br J Clin Pharmacol* 2005;**60**: 581-3.
- Abel zur Wiesch P, Abel S, Gkotzis S *et al*. Classic reaction kinetics can explain complex patterns of antibiotic action. 2015;**7**: 287ra73-ra73.
- Abel zur Wiesch P, Clarelli F, Cohen T. Using chemical reaction kinetics to predict optimal antibiotic treatment strategies. *Plos Comput Biol* 2017;**13**: e1005321.
- Al-Lanqawi Y, Capps P, Abudlmalek K *et al*. Clinical pharmacokinetics of gentamicin. Estimation of initial dosing parameters in hospitalized patients at Al-Amiri Hospital Kuwait. *Med Princ Pract* 2009;**18**: 209-16.
- Alahmadi A, Belet S, Black A *et al*. Influencing public health policy with data-informed mathematical models of infectious diseases: Recent developments and new challenges. *Epidemics* 2020, DOI <https://doi.org/10.1016/j.epidem.2020.100393>: 100393.
- Alcorn TM, Cohen MS. Gonococcal Pathogenesis - Adaptation and Immune Evasion in the Human Host. *Curr Opin Infect Dis* 1994;**7**: 310-6.
- Allen VG, Mitterni L, Seah C *et al*. Neisseria gonorrhoeae treatment failure and susceptibility to cefixime in Toronto, Canada. *JAMA* 2013;**309**: 163-70.
- Amsden GW. Advanced-generation macrolides: tissue-directed antibiotics. *Int J Antimicrob Agents* 2001;**18 Suppl 1**: S11-5.
- Andes D, Craig WA. Pharmacodynamics of the new fluoroquinolone gatifloxacin in murine thigh and lung infection models. *Antimicrob Agents Chemother* 2002;**46**: 1665-70.
- Ankomah P, Levin BR. Two-drug antimicrobial chemotherapy: a mathematical model and experiments with Mycobacterium marinum. *PLoS Pathog* 2012;**8**: e1002487.
- Ankomah P, Levin BR. Exploring the collaboration between antibiotics and the immune response in the treatment of acute, self-limiting infections. *P Natl Acad Sci USA* 2014;**111**: 8331-8.
- Apicella MA, Ketterer M, Lee FK *et al*. The pathogenesis of gonococcal urethritis in men: confocal and immunoelectron microscopic analysis of urethral exudates from men infected with Neisseria gonorrhoeae. *J Infect Dis* 1996;**173**: 636-46.
- Arditi R, Ginzburg LR. Coupling in predator-prey dynamics: Ratio-Dependence. *Journal of Theoretical Biology* 1989;**139**: 311-26.
- Arko RJ. Animal models for pathogenic Neisseria species. *Clin Microbiol Rev* 1989;**2 Suppl**: S56-9.

- Austin DJ, Bonten MJ, Weinstein RA *et al.* Vancomycin-resistant enterococci in intensive-care hospital settings: transmission dynamics, persistence, and the impact of infection control programs. *Proc Natl Acad Sci U S A* 1999;**96**: 6908-13.
- Austin DJ, White NJ, Anderson RM. The dynamics of drug action on the within-host population growth of infectious agents: melding pharmacokinetics with pathogen population dynamics. *J Theor Biol* 1998;**194**: 313-39.
- Ayinde O, Ross JDC. Time to resolution of genital symptoms for uncomplicated gonorrhoea: a prospective cohort study. *Sex Transm Infect* 2020, DOI 10.1136/sextrans-2020-054626: sextrans-2020-054626.
- Baeder DY, Yu G, Hoze N *et al.* Antimicrobial combinations: Bliss independence and Loewe additivity derived from mechanistic multi-hit models. *Philos Trans R Soc Lond B Biol Sci* 2016;**371**.
- Bailey DN, Briggs JR. Gentamicin and tobramycin binding to human serum in vitro. *J Anal Toxicol* 2004;**28**: 187-9.
- Barbee LA. Preparing for an era of untreatable gonorrhea. *Curr Opin Infect Dis* 2014;**27**: 282-7.
- Barbee LA, Nayak SU, Blumer JL *et al.* A phase 1 pharmacokinetic and safety study of extended-duration, high-dose cefixime for cephalosporin-resistant *Neisseria gonorrhoeae* in the Pharynx. *Sex Transm Dis* 2018;**45**: 677-83.
- Barbee LA, Soge OO, Khosropour CM *et al.* The Duration of Pharyngeal Gonorrhea: A Natural History Study. *Clin Infect Dis* 2021, DOI 10.1093/cid/ciab071.
- Barbee LA, Soge OO, Morgan J *et al.* Gentamicin Alone Inadequate to Eradicate *Neisseria Gonorrhoeae* from the Pharynx. *Clin Infect Dis* 2019, DOI 10.1093/cid/ciz1109.
- Barbour AG. Properties of penicillin-binding proteins in *Neisseria gonorrhoeae*. 1981;**19**: 316-22.
- Barcia-Macay M, Seral C, Mingeot-Leclercq MP *et al.* Pharmacodynamic evaluation of the intracellular activities of antibiotics against *Staphylococcus aureus* in a model of THP-1 macrophages. *Antimicrob Agents Chemother* 2006;**50**: 841-51.
- Benet LZ, Hoener BA. Changes in plasma protein binding have little clinical relevance. *Clin Pharmacol Ther* 2002;**71**: 115-21.
- Berenbaum MC. Synergy, additivism and antagonism in immunosuppression. A critical review. *Clin Exp Immunol* 1977;**28**: 1-18.
- Bergan T, Engeset A, Olszewski W. Does Serum Protein Binding Inhibit Tissue Penetration of Antibiotics? *Reviews of Infectious Diseases* 1987;**9**: 713-8.

- Bernoulli D, Blower S. An attempt at a new analysis of the mortality caused by smallpox and of the advantages of inoculation to prevent it. *Reviews in Medical Virology* 2004;**14**: 275-88.
- Biedenbach DJ, Bouchillon SK, Hackel M *et al.* *In vitro* activity of gepotidacin, a novel triazaacenaphthylene bacterial topoisomerase inhibitor, against a broad spectrum of bacterial pathogens. *Antimicrob Agents Chemother* 2016;**60**: 1918-23.
- Bignell C, Unemo M. 2012 European guideline on the diagnosis and treatment of gonorrhoea in adults. *Int J STD AIDS* 2013;**24**: 85-92.
- Binnicker MJ, Williams RD, Apicella MA. Infection of human urethral epithelium with *Neisseria gonorrhoeae* elicits an upregulation of host anti-apoptotic factors and protects cells from staurosporine-induced apoptosis. *Cell Microbiol* 2003;**5**: 549-60.
- Bliss CI. The Toxicity of Poisons Applied Jointly1. *Ann Appl Biol* 1939;**26**: 585-615.
- Blower SM, Dowlatabadi H. Sensitivity and Uncertainty Analysis of Complex Models of Disease Transmission: An HIV Model, as an Example. *International Statistical Review / Revue Internationale de Statistique* 1994;**62**: 229-43.
- Bollenbach T, Quan S, Chait R *et al.* Nonoptimal microbial response to antibiotics underlies suppressive drug interactions. *Cell* 2009;**139**: 707-18.
- Bosnar M, Kelneric Z, Munic V *et al.* Cellular uptake and efflux of azithromycin, erythromycin, clarithromycin, telithromycin, and cethromycin. *Antimicrob Agents Chemother* 2005;**49**: 2372-7.
- Brittain C, Childs M, Duley L *et al.* Gentamicin versus ceftriaxone for the treatment of gonorrhoea (G-TOG trial): study protocol for a randomised trial. *Trials* 2016;**17**: 558-.
- Brittain DC, Scully BE, Hirose T *et al.* The Pharmacokinetic and Bactericidal Characteristics of Oral Cefixime. *Clin Pharmacol Ther* 1985;**38**: 590-4.
- Brooks GF, Carroll KC, Butel JS *et al.* *Jawetz, Melnick & Adelberg's Medical Microbiology*: 26 Edition: McGraw-Hill, 2013.
- Brown LB, Krysiak R, Kamanga G *et al.* *Neisseria gonorrhoeae* antimicrobial susceptibility in Lilongwe, Malawi, 2007. *Sex Transm Dis* 2010;**37**: 169-72.
- Brown SP, Cornell SJ, Sheppard M *et al.* Intracellular demography and the dynamics of *Salmonella enterica* infections. *Plos Biol* 2006;**4**: e349.
- Bulik CC, Okusanya ÓO, Lakota EA *et al.* Pharmacokinetic-pharmacodynamic evaluation of gepotidacin against gram-positive organisms using data from murine infection models. 2017;**61**: e00115-16.
- Bulitta JB, Hope WW, Eakin AE *et al.* Generating robust and informative nonclinical *in vitro* and *in vivo* bacterial infection model efficacy data to support translation to humans. *Antimicrob Agents Chemother* 2019;**63**: e02307-18.

- Burgess JA. Gonococcal Tysonitis without urethritis after prophylactic post-coital urination. *Br J Vener Dis* 1971;**47**: 40-1.
- Buyck JM, Tulkens PM, Van Bambeke F. Pharmacodynamic evaluation of the intracellular activity of antibiotics towards *Pseudomonas aeruginosa* PAO1 in a model of THP-1 human monocytes. *Antimicrob Agents Chemother* 2013;**57**: 2310-8.
- Camara J, Serra J, Ayats J *et al*. Molecular characterization of two high-level ceftriaxone-resistant *Neisseria gonorrhoeae* isolates detected in Catalonia, Spain. *J Antimicrob Chemother* 2012;**67**: 1858-60.
- Carryn S, Van Bambeke F, Mingeot-Leclercq M-P *et al*. Comparative Intracellular (THP-1 Macrophage) and Extracellular Activities of β -Lactams, Azithromycin, Gentamicin, and Fluoroquinolones against *Listeria monocytogenes* at Clinically Relevant Concentrations. *Antimicrobial Agents and Chemotherapy* 2002;**46**: 2095-103.
- Cascone S, Lamberti G, Titomanlio G *et al*. Pharmacokinetics of Remifentanyl: a three-compartmental modeling approach. *Transl Med UniSa* 2013;**7**: 18-22.
- Casey SG, Veale DR, Smith H. Intracellular survival of *Neisseria gonorrhoeae* in human urethral exudate. *Fems Microbiol Lett* 1980;**8**: 97-100.
- Centers for Disease Control and Prevention. Update to CDC's sexually transmitted diseases treatment guidelines, 2010: Oral cephalosporins no longer a recommended treatment for gonococcal infections. *Morbidity and Mortality Weekly Report* 2012;**61**: 590-4.
- Centers for Disease Control and Prevention. 2015 Sexually Transmitted Diseases Treatment Guidelines, 2015.
- Centers for Disease Control and Prevention. Sexually Transmitted Disease Surveillance 2016. Atlanta, 2017.
- Centers for Disease Control and Prevention. Sexually Transmitted Disease Surveillance 2017. Atlanta: U.S. Department of Health and Human Services, 2018.
- Centers for Disease Control and Prevention. Antibiotic resistance threats in the United States, 2019 Atlanta, GA: U.S. Department of Health and Human Services, CDC, 2019a.
- Centers for Disease Control and Prevention. Sexually Transmitted Disease Surveillance 2018. Atlanta: U.S. Department of Health and Human Services, 2019b.
- Chan CH, McCabe CJ, Fisman DN. Core groups, antimicrobial resistance and rebound in gonorrhoea in North America. *Sex Transm Infect* 2012;**88**: 200-4.
- Chanteux H, Mingeot-Leclercq MP, Sonveaux E *et al*. Intracellular accumulation and activity of ampicillin used as free drug and as its phthalimidomethyl or

- pivaloyloxymethyl ester (pivampicillin) against *Listeria monocytogenes* in J774 macrophages. *J Antimicrob Chemother* 2003;**52**: 610-5.
- Chaplin DD. Overview of the immune response. *The Journal of allergy and clinical immunology* 2010;**125**: S3-23.
- Chateau A, Seifert HS. *Neisseria gonorrhoeae* survives within and modulates apoptosis and inflammatory cytokine production of human macrophages. *Cell Microbiol* 2016;**18**: 546-60.
- Château A, Seifert HS. *Neisseria gonorrhoeae* survives within and modulates apoptosis and inflammatory cytokine production of human macrophages. *Cell Microbiol* 2016;**18**: 546-60.
- Chen MY, McNulty A, Avery A *et al.* Solithromycin versus ceftriaxone plus azithromycin for the treatment of uncomplicated genital gonorrhoea (SOLITAIRE-U): a randomised phase 3 non-inferiority trial. *The Lancet Infectious Diseases* 2019;**19**: 833-42.
- Chen SC, Yuan LF, Zhu XY *et al.* Sustained transmission of the ceftriaxone-resistant *Neisseria gonorrhoeae* FC428 clone in China. *J Antimicrob Chemother* 2020;**75**: 2499-502.
- Chisholm SA, Dave J, Ison CA. High-level azithromycin resistance occurs in *Neisseria gonorrhoeae* as a result of a single point mutation in the 23S rRNA genes. *Antimicrob Agents Chemother* 2010a;**54**: 3812-6.
- Chisholm SA, Mouton JW, Lewis DA *et al.* Cephalosporin MIC creep among gonococci: time for a pharmacodynamic rethink? *J Antimicrob Chemother* 2010b;**65**: 2141-8.
- Chisholm SA, Quaye N, Cole MJ *et al.* An evaluation of gentamicin susceptibility of *Neisseria gonorrhoeae* isolates in Europe. *J Antimicrob Chemother* 2011;**66**: 592-5.
- Chow EPF, Tabrizi SN, Phillips S *et al.* *Neisseria gonorrhoeae* bacterial DNA load in the pharynx and saliva of men who have sex with men. *Journal of clinical microbiology* 2016;**54**: 2485-90.
- Ciupe SM, Heffernan JM. In-host modeling. *Infectious Disease Modelling* 2017;**2**: 188-202.
- Clapham HE, Quyen TH, Kien DT *et al.* Modelling Virus and Antibody Dynamics during Dengue Virus Infection Suggests a Role for Antibody in Virus Clearance. *Plos Comput Biol* 2016;**12**: e1004951.
- Clarelli F, Liang J, Martinecz A *et al.* Multi-scale modeling of drug binding kinetics to predict drug efficacy. *Cellular and Molecular Life Sciences* 2020a;**77**: 381-94.
- Clarelli F, Palmer A, Singh B *et al.* Drug-target binding quantitatively predicts optimal antibiotic dose levels in quinolones. *Plos Comput Biol* 2020b;**16**: e1008106.

- Clark AJ. The antagonism of acetylcholine by atropine. *Journal of Physiology (London)* 1926;**61**: 547-56.
- Clinical and Laboratory Standards Institute. *Performance standards for antimicrobial susceptibility testing*— CLSI supplement M100: 28 Edition. CLSI, Wayne, PA, USA, 2018.
- Cohen MS, Cannon JG, Jerse AE *et al.* Human experimentation with *Neisseria gonorrhoeae*: rationale, methods, and implications for the biology of infection and vaccine development. *J Infect Dis* 1994;**169**: 532-7.
- Cole MJ, Tan W, Fifer H *et al.* Gentamicin, azithromycin and ceftriaxone in the treatment of gonorrhoea: the relationship between antibiotic MIC and clinical outcome. *J Antimicrob Chemother* 2019, DOI 10.1093/jac/dkz436.
- Colijn C, Cohen T. How competition governs whether moderate or aggressive treatment minimizes antibiotic resistance. *Elife* 2015;**4**.
- Colijn C, Cohen T, Ganesh A *et al.* Spontaneous emergence of multiple drug resistance in tuberculosis before and during therapy. *PLoS One* 2011;**6**: e18327.
- Connolly KL, Eakin AE, Gomez C *et al.* Pharmacokinetic Data Are Predictive of in vivo Efficacy for Cefixime and Ceftriaxone against Susceptible and Resistant *Neisseria gonorrhoeae* Strains in the Gonorrhea Mouse Model. *Antimicrob Agents Chemother* 2019, DOI 10.1128/AAC.01644-18.
- Craig AP, Gray RT, Edwards JL *et al.* The potential impact of vaccination on the prevalence of gonorrhea. *Vaccine* 2015;**33**: 4520-5.
- Craig WA. Interrelationship between pharmacokinetics and pharmacodynamics in determining dosage regimens for broad-spectrum cephalosporins. *Diagn Microbiol Infect Dis* 1995;**22**: 89-96.
- Craig WA. Pharmacokinetics of antibiotics with special emphasis on cephalosporins. *Clinical Microbiology and Infection* 2000;**6**: 46-9.
- Craig WA, Redington J, Ebert SC. Pharmacodynamics of amikacin in vitro and in mouse thigh and lung infections. *J Antimicrob Chemother* 1991;**27 Suppl C**: 29-40.
- Criss AK, Seifert HS. Gonococci exit apically and basally from polarized epithelial cells and exhibit dynamic changes in type IV pili. *Cell Microbiol* 2006;**8**: 1430-43.
- Criss AK, Seifert HS. A bacterial siren song: intimate interactions between *Neisseria* and neutrophils. *Nat Rev Microbiol* 2012;**10**: 178-90.
- Daly CC, Hoffman I, Hobbs M *et al.* Development of an antimicrobial susceptibility surveillance system for *Neisseria gonorrhoeae* in Malawi: comparison of methods. *Journal of clinical microbiology* 1997;**35**: 2985-8.

- Davies NG, Flasche S, Jit M *et al.* Within-host dynamics shape antibiotic resistance in commensal bacteria. *Nature Ecology & Evolution* 2019;**3**: 440-9.
- De Angelis D, Presanis AM, Birrell PJ *et al.* Four key challenges in infectious disease modelling using data from multiple sources. *Epidemics* 2015;**10**: 83-7.
- Deguchi T, Yasuda M, Hatazaki K *et al.* New Clinical Strain of *Neisseria gonorrhoeae* with Decreased Susceptibility to Ceftriaxone, Japan. *Emerging infectious diseases* 2016;**22**: 142-4.
- Dehio C, Gray-Owen SD, Meyer TF. The role of neisserial Opa proteins in interactions with host cells. *Trends Microbiol* 1998;**6**: 489-95.
- Delgado G, Jr., Neuhauser MM, Bearden DT *et al.* Quinupristin-dalfopristin: an overview. *Pharmacotherapy* 2000;**20**: 1469-85.
- Diekmann O, Heesterbeek JAP, Metz JAJ. On the definition and the computation of the basic reproduction ratio R_0 in models for infectious diseases in heterogeneous populations. *Journal of Mathematical Biology* 1990;**28**: 365-82.
- Dini S, Zaloumis S, Cao P *et al.* Investigating the Efficacy of Triple Artemisinin-Based Combination Therapies for Treating *Plasmodium falciparum* Malaria Patients Using Mathematical Modeling. 2018;**62**: e01068-18.
- Döhrmann S, Cole JN, Nizet V. Conquering Neutrophils. *PLOS Pathogens* 2016;**12**: e1005682.
- Dorfman MS, Wagner RS, Jamison T *et al.* The pharmacodynamic properties of azithromycin in a kinetics-of-kill model and implications for bacterial conjunctivitis treatment. *Advances in therapy* 2008;**25**: 208-17.
- Dougherty TJ, Kennedy K, Kessler RE *et al.* Direct quantitation of the number of individual penicillin-binding proteins per cell in *Escherichia coli*. *J Bacteriol* 1996;**178**: 6110-5.
- Dougherty TJ, Koller AE, Tomasz A. Penicillin-binding proteins of penicillin-susceptible and intrinsically resistant *Neisseria gonorrhoeae*. 1980;**18**: 730-7.
- Dougherty TJ, Koller AE, Tomasz A. Competition of beta-lactam antibiotics for the penicillin-binding proteins of *Neisseria gonorrhoeae*. 1981;**20**: 109-14.
- Dowell D, Kirkcaldy RD. Effectiveness of gentamicin for gonorrhoea treatment: systematic review and meta-analysis. *Postgraduate Medical Journal* 2013;**89**: 142-7.
- Drusano GL. Antimicrobial pharmacodynamics: critical interactions of 'bug and drug'. *Nature Reviews Microbiology* 2004;**2**: 289-300.
- Drusano GL, Ambrose PG, Bhavnani SM *et al.* Back to the future: using aminoglycosides again and how to dose them optimally. *Clin Infect Dis* 2007;**45**: 753-60.

- Duverne C, Bouten A, Deslandes A *et al.* Modification of cefixime bioavailability by nifedipine in humans: involvement of the dipeptide carrier system. *Antimicrob Agents Chemother* 1992;**36**: 2462-7.
- Eagle H, Fleischman R, Levy M. "Continuous" vs. "discontinuous" therapy with penicillin; the effect of the interval between injections on therapeutic efficacy. *N Engl J Med* 1953;**248**: 481-8.
- Edwards JL. The role of complement in gonococcal infection of cervical epithelia. *Vaccine* 2008;**26**: I56-I61.
- Edwards JL, Apicella MA. The molecular mechanisms used by *Neisseria gonorrhoeae* to initiate infection differ between men and women. *Clin Microbiol Rev* 2004;**17**: 965-81, table of contents.
- Edwards JL, Jennings MP, Apicella MA *et al.* Is gonococcal disease preventable? The importance of understanding immunity and pathogenesis in vaccine development. *Crit Rev Microbiol* 2016;**42**: 928-41.
- Elkashif A, Seleem MN. Investigation of auranofin and gold-containing analogues antibacterial activity against multidrug-resistant *Neisseria gonorrhoeae*. *Sci Rep-Uk* 2020;**10**: 5602.
- Escobar A, Rodas PI, Acuña-Castillo C. Macrophage–*Neisseria gonorrhoeae* Interactions: A Better Understanding of Pathogen Mechanisms of Immunomodulation. *Frontiers in Immunology* 2018;**9**.
- European Committee on Antimicrobial Susceptibility Testing. Breakpoint tables for interpretation of MICs and zone diameters 2018 volume 2019, 2018.
- European Committee on Antimicrobial Susceptibility Testing. Breakpoint tables for interpretation of MICs and zone diameters 2019 volume 2019: Version 9.0 Edition, 2019.
- Evans MD, Sammelson R, McDowell S. Differential effects of cotreatment of the antibiotic rifampin with host-directed therapeutics in reducing intracellular *Staphylococcus aureus* infection. *PeerJ* 2020;**8**: e10330.
- Eyre DW, Sanderson ND, Lord E *et al.* Gonorrhoea treatment failure caused by a *Neisseria gonorrhoeae* strain with combined ceftriaxone and high-level azithromycin resistance, England, February 2018. *Euro Surveill* 2018;**23**.
- Eyre DW, Town K, Street T *et al.* Detection in the United Kingdom of the *Neisseria gonorrhoeae* FC428 clone, with ceftriaxone resistance and intermediate resistance to azithromycin, October to December 2018. *Euro surveillance : bulletin European sur les maladies transmissibles = European communicable disease bulletin* 2019;**24**: 1900147.
- Fairley CK, Cornelisse VJ, Hocking JS *et al.* Models of gonorrhoea transmission from the mouth and saliva. *The Lancet Infectious Diseases* 2019;**19**: e360-e6.

- Fairley CK, Hocking JS, Zhang L *et al.* Frequent Transmission of Gonorrhea in Men Who Have Sex with Men. *Emerging infectious diseases* 2017;**23**: 102-4.
- Farrell DJ, Sader HS, Rhomberg PR *et al.* In Vitro Activity of Gepotidacin (GSK2140944) against *Neisseria gonorrhoeae*. *Antimicrob Agents Chemother* 2017;**61**.
- Faulkner RD, Fernandez P, Lawrence G *et al.* Absolute bioavailability of cefixime in man. *Journal of clinical pharmacology* 1988;**28**: 700-6.
- Faulkner RD, Wendy B, Desjardins RE *et al.* Pharmacokinetics of Cefixime After Once-a-Day and Twice-a-Day Dosing to Steady State. *The Journal of Clinical Pharmacology* 1987a;**27**: 807-12.
- Faulkner RD, Yacobi A, Barone JS *et al.* Pharmacokinetic profile of cefixime in man. *Pediatr Infect Dis J* 1987b;**6**: 963-70.
- Feher J. 5.13 - Regulation of Arterial Pressure. In: Feher J (ed.) *Quantitative Human Physiology (Second Edition)*, DOI <https://doi.org/10.1016/B978-0-12-800883-6.00058-6>. Boston: Academic Press, 2012, 608-18.
- Fifer H, Saunders J, Soni S *et al.* British Association for Sexual Health and HIV national guideline for the management of infection with *Neisseria gonorrhoeae*: British Association for Sexual Health and HIV, 2019.
- Fingerhuth. Population dynamics of antibiotic-resistant *Neisseria gonorrhoeae*. PhD thesis, Chapter 4: ETH Zurich, 2017.
- Fingerhuth SM, Bonhoeffer S, Low N *et al.* Antibiotic-Resistant *Neisseria gonorrhoeae* Spread Faster with More Treatment, Not More Sexual Partners. *PLoS Pathog* 2016;**12**: e1005611.
- Flückiger U, Segessenmann C, Gerber AU. Integration of pharmacokinetics and pharmacodynamics of imipenem in a human-adapted mouse model. *Antimicrob Agents Chemother* 1991;**35**: 1905-10.
- Foerster S, Unemo M, Hathaway LJ *et al.* Time-kill curve analysis and pharmacodynamic modelling for in vitro evaluation of antimicrobials against *Neisseria gonorrhoeae*. *BMC Microbiol* 2016;**16**: 216.
- Follows SA, Murlidharan J, Massari P *et al.* *Neisseria gonorrhoeae* infection protects human endocervical epithelial cells from apoptosis via expression of host antiapoptotic proteins. *Infect Immun* 2009;**77**: 3602-10.
- Forrest A, Nix DE, Ballow CH *et al.* Pharmacodynamics of intravenous ciprofloxacin in seriously ill patients. *Antimicrob Agents Chemother* 1993;**37**: 1073-81.
- Foulds G, Johnson RB. Selection of dose regimens of azithromycin. *J Antimicrob Chemother* 1993;**31 Suppl E**: 39-50.
- Foulds G, Shepard RM, Johnson RB. The pharmacokinetics of azithromycin in human serum and tissues. *J Antimicrob Chemother* 1990;**25 Suppl A**: 73-82.

- Francis IP, Islam EA, Gower AC *et al.* Murine host response to *Neisseria gonorrhoeae* upper genital tract infection reveals a common transcriptional signature, plus distinct inflammatory responses that vary between reproductive cycle phases. *Bmc Genomics* 2018;**19**: 627.
- Frère JM. Beta-lactamases and bacterial resistance to antibiotics. *Mol Microbiol* 1995;**16**: 385-95.
- Furuya R, Tanaka M, Nakayama H *et al.* In vitro synergistic effects of double combinations of β -lactams and azithromycin against clinical isolates of *Neisseria gonorrhoeae*. *Journal of Infection and Chemotherapy* 2006;**12**: 172-6.
- Getz WM. Population-Dynamics - a Per-Capita Resource Approach. *Journal of Theoretical Biology* 1984;**108**: 623-43.
- Getz WM. An introspection on the art of modeling in population ecology. *Bioscience* 1998;**48**: 540-52.
- Ghani AC, Aral SO. Patterns of sex worker - Client contacts and their implications for the persistence of sexually transmitted infections. *Journal of Infectious Diseases* 2005;**191**: S34-S41.
- Gog JR, Pellis L, Wood JL *et al.* Seven challenges in modeling pathogen dynamics within-host and across scales. *Epidemics* 2015;**10**: 45-8.
- Golparian D, Rose L, Lynam A *et al.* Multidrug-resistant *Neisseria gonorrhoeae* isolate, belonging to the internationally spreading Japanese FC428 clone, with ceftriaxone resistance and intermediate resistance to azithromycin, Ireland, August 2018. *Euro surveillance : bulletin Europeen sur les maladies transmissibles = European communicable disease bulletin* 2018;**23**: 1800617.
- Gordi T, Xie R, Jusko WJ. Semi-mechanistic pharmacokinetic/pharmacodynamic modelling of the antimalarial effect of artemisinin. *Br J Clin Pharmacol* 2005;**60**: 594-604.
- Gottlieb SL, Ndowa F, Hook EW *et al.* Gonococcal vaccines: Public health value and preferred product characteristics; report of a WHO global stakeholder consultation, January 2019. *Vaccine* 2020;**38**: 4362-73.
- Goutelle S, Maurin M, Rougier F *et al.* The Hill equation: a review of its capabilities in pharmacological modelling. *Fundam Clin Pharmacol* 2008;**22**: 633-48.
- Grassly NC, Fraser C. Mathematical models of infectious disease transmission. *Nature Reviews Microbiology* 2008;**6**: 477-87.
- Grayo S, Join-Lambert O, Desroches MC *et al.* Comparison of the In Vitro Efficacies of Moxifloxacin and Amoxicillin against *Listeria monocytogenes*. *Antimicrob Agents Chemother* 2008;**52**: 1697-702.
- Greco WR, Bravo G, Parsons JC. The search for synergy: a critical review from a response surface perspective. *Pharmacol Rev* 1995;**47**: 331-85.

- Greco WR, Park HS, Rustum YM. Application of a new approach for the quantitation of drug synergism to the combination of cis-diamminedichloroplatinum and 1-beta-D-arabinofuranosylcytosine. *Cancer Res* 1990;**50**: 5318-27.
- Gubish ER, Jr., Mace ML, Jr., Steiner SM *et al.* Assessment of attachment of *Neisseria gonorrhoeae* to HeLa cells by double radiolabeling. *Infect Immun* 1979;**25**: 1043-50.
- Gunderson CW, Seifert HS. *Neisseria gonorrhoeae* elicits extracellular traps in primary neutrophil culture while suppressing the oxidative burst. *MBio* 2015;**6**.
- Guvenc F, Kaul R, Gray-Owen SD. Intimate Relations: Molecular and Immunologic Interactions Between *Neisseria gonorrhoeae* and HIV-1. *Frontiers in Microbiology* 2020;**11**.
- Hanberger H, Nilsson LE, Kihlström E *et al.* Postantibiotic effect of beta-lactam antibiotics on *Escherichia coli* evaluated by bioluminescence assay of bacterial ATP. *Antimicrob Agents Chemother* 1990;**34**: 102-6.
- Hanberger H, Nilsson LE, Nilsson M *et al.* Post-antibiotic effect of beta-lactam antibiotics on gram-negative bacteria in relation to morphology, initial killing and MIC. *Eur J Clin Microbiol Infect Dis* 1991;**10**: 927-34.
- Handsfield HH, Lipman TO, Harnisch JP *et al.* Asymptomatic gonorrhea in men. Diagnosis, natural course, prevalence and significance. *N Engl J Med* 1974;**290**: 117-23.
- Harvey HA, Ketterer MR, Preston A *et al.* Ultrastructural analysis of primary human urethral epithelial cell cultures infected with *Neisseria gonorrhoeae*. *Infect Immun* 1997;**65**: 2420-7.
- Hashino E, Shero M. Endocytosis of aminoglycoside antibiotics in sensory hair cells. *Brain research* 1995;**704**: 135-40.
- Heckels JE, Blackett B, Everson JS *et al.* The influence of surface charge on the attachment of *Neisseria gonorrhoeae* to human cells. *J Gen Microbiol* 1976;**96**: 359-64.
- Helaine S, Thompson JA, Watson KG *et al.* Dynamics of intracellular bacterial replication at the single cell level. *Proceedings of the National Academy of Sciences* 2010;**107**: 3746-51.
- Herrell WE, Cook EN, Thompson L. Use of penicillin in sulfonamide resistant gonorrheal infections. *Journal of the American Medical Association* 1943;**122**: 289-92.
- Herz AV, Bonhoeffer S, Anderson RM *et al.* Viral dynamics in vivo: limitations on estimates of intracellular delay and virus decay. *Proceedings of the National Academy of Sciences* 1996;**93**: 7247-51.

- Hethcote HW, Yorke JA. *Gonorrhea Transmission Dynamics and Control: Lecture notes in Bio Mathematics* 56, 1984.
- Hill AL. Mathematical Models of HIV Latency. *Curr Top Microbiol Immunol* 2018;**417**: 131-56.
- Hill JH. Experimental infection with *Neisseria gonorrhoeae*. *American Journal of Syphilis, Gonorrhea and Venereal diseases* 1943;**27**: 733-71.
- Hill SA, Masters TL, Wachter J. Gonorrhea - an evolving disease of the new millennium. *Microb Cell* 2016;**3**: 371-89.
- Hira SK, Attili VR, Kamanga J *et al*. Efficacy of gentamicin and kanamycin in the treatment of uncomplicated gonococcal urethritis in Zambia. *Sex Transm Dis* 1985;**12**: 52-4.
- Ho DD, Neumann AU, Perelson AS *et al*. Rapid turnover of plasma virions and CD4 lymphocytes in HIV-1 infection. *Nature* 1995;**373**: 123.
- Hoare A, Regan DG, Wilson DP. Sampling and sensitivity analyses tools (SaSAT) for computational modelling. *Theor Biol Med Model* 2008;**5**: 4.
- Hobbs MM, Sparling PF, Cohen MS *et al*. Experimental gonococcal infection in male volunteers: cumulative experience with *Neisseria gonorrhoeae* strains FA1090 and MS11mkC. *Front Microbiol* 2011;**2**: 123.
- Holford NHG, Sheiner LB. Kinetics of pharmacologic response. *Pharmacology & Therapeutics* 1982;**16**: 143-66.
- Holmes KK, Sparling PF, Mardh P *et al*. *Sexually Transmitted Diseases*: 4th Edition. United States of America: McGraw-Hill, 2008.
- Hook EW, 3rd, Golden MR, Taylor SN *et al*. Efficacy and Safety of Single-Dose Oral Delafloxacin Compared With Intramuscular Ceftriaxone for Uncomplicated Gonorrhea Treatment: An Open-Label, Noninferiority, Phase 3, Multicenter, Randomized Study. *Sex Transm Dis* 2019;**46**: 279-86.
- Hook EW, 3rd, Holmes KK. Gonococcal infections. *Ann Intern Med* 1985;**102**: 229-43.
- Hook EW, Newman L, Drusano G *et al*. Development of new antimicrobials for urogenital gonorrhea therapy: clinical trial design considerations. *Clin Infect Dis* 2020;**70**: 1495-500.
- Horner P, Ingle SM, Garrett F *et al*. Which azithromycin regimen should be used for treating *Mycoplasma genitalium*? A meta-analysis. *Sex Transm Infect* 2018;**94**: 14-20.
- Hossain M, Tiffany CA, McDonald M *et al*. Safety and Pharmacokinetics of Repeat Escalating Oral Doses of GSK2140944, a Novel Bacterial Topoisomerase Inhibitor *Abstr 54th Interscience Conference on Antimicrobial Agents and Chemotherapy*. Washington, D.C, 2014.

- Hui B, Fairley CK, Chen M *et al.* Oral and anal sex are key to sustaining gonorrhoea at endemic levels in MSM populations: a mathematical model. *Sex Transm Infect* 2015;**91**: 365-9.
- Hui BB, Gray RT, Wilson DP *et al.* Population movement can sustain STI prevalence in remote Australian indigenous communities. *BMC Infect Dis* 2013;**13**: 188.
- Humphries RM, Abbott AN, Hindler JA. Understanding and Addressing CLSI Breakpoint Revisions: a Primer for Clinical Laboratories. *Journal of Clinical Microbiology* 2019;**57**: e00203-19.
- Imamura Y, Higashiyama Y, Tomono K *et al.* Azithromycin exhibits bactericidal effects on *Pseudomonas aeruginosa* through interaction with the outer membrane. *Antimicrob Agents Chemother* 2005;**49**: 1377-80.
- Imbuluzqueta E, Lemaire S, Gamazo C *et al.* Cellular pharmacokinetics and intracellular activity against *Listeria monocytogenes* and *Staphylococcus aureus* of chemically modified and nanoencapsulated gentamicin. *J Antimicrob Chemother* 2012;**67**: 2158-64.
- Isbey SF, Alcorn TM, Davis RH *et al.* Characterisation of *Neisseria gonorrhoeae* in semen during urethral infection in men. *Genitourin Med* 1997;**73**: 378-82.
- Ison CA, Hadfield SG, Bellinger CM *et al.* The specificity of serum and local antibodies in female gonorrhoea. *Clin Exp Immunol* 1986;**65**: 198-205.
- Ito M, Deguchi T, Mizutani KS *et al.* Emergence and spread of *Neisseria gonorrhoeae* clinical isolates harboring mosaic-like structure of penicillin-binding protein 2 in Central Japan. *Antimicrob Agents Chemother* 2005;**49**: 137-43.
- Ito S, Yasuda M, Hatazaki K *et al.* Microbiological efficacy and tolerability of a single-dose regimen of 1 g of ceftriaxone in men with gonococcal urethritis. *J Antimicrob Chemother* 2016;**71**: 2559-62.
- Jacobs RF, Thompson JW, Kiel DP *et al.* Cellular uptake and cell-associated activity of third generation cephalosporins. *Pediatr Res* 1986;**20**: 909-12.
- Jacobsson S, Mason C, Khan N *et al.* In vitro activity of the novel oral antimicrobial SMT-571, with a new mechanism of action, against MDR and XDR *Neisseria gonorrhoeae*: future treatment option for gonorrhoea? *J Antimicrob Chemother* 2019;**74**: 1591-4.
- Jacobsson S, Mason C, Khan N *et al.* High in vitro activity of DIS-73285, a novel antimicrobial with a new mechanism of action, against MDR and XDR *Neisseria gonorrhoeae*. *J Antimicrob Chemother* 2020, DOI 10.1093/jac/dkaa322.
- Japanese Society for Sexually Transmitted Diseases. Guidelines for the diagnosis and treatment of sexually transmitted diseases 2004. *Jpn J Sex Transm Dis* 2004;**15**: 8-13.

- Jayasundara P, Regan DG, Seib KL *et al.* Modelling the in-host dynamics of *Neisseria gonorrhoeae* infection. *Pathog Dis* 2019;**77**.
- Jenner AL, Aogo RA, Davis CL *et al.* Leveraging Computational Modeling to Understand Infectious Diseases. *Current Pathobiology Reports* 2020;**8**: 149-61.
- Jerse AE. Experimental gonococcal genital tract infection and opacity protein expression in estradiol-treated mice. *Infect Immun* 1999;**67**: 5699-708.
- Jerse AE, Wu H, Packiam M *et al.* Estradiol-treated female mice as surrogate hosts for *Neisseria gonorrhoeae* genital tract infections. *Front Microbiol* 2011;**2**: 107.
- Jie L, Hongna Z, Dong L *et al.* The coupled within-and between host-dynamics in the evolution of HIV/AIDS in China. *Journal of Applied Analysis & Computation*, 2015;**5**: 731-50.
- Johnson LF, Alkema L, Dorrington RE. A Bayesian approach to uncertainty analysis of sexually transmitted infection models. *Sexually Transmitted Infections* 2010;**86**: 169-74.
- Johnson MB, Criss AK. *Neisseria gonorrhoeae* phagosomes delay fusion with primary granules to enhance bacterial survival inside human neutrophils. *Cell Microbiol* 2013;**15**: 1323-40.
- Kallings LO, Eriksson G, Hoffner S *et al.* Penetration of ampicillin into urethral and cervical secretions after oral administration of bacampicillin. *Infection* 1979;**7**: S478-S82.
- Kamaruzzaman NF, Kendall S, Good L. Targeting the hard to reach: challenges and novel strategies in the treatment of intracellular bacterial infections. *Br J Pharmacol* 2017;**174**: 2225-36.
- Katzung BG. *Basic and Clinical Pharmacology* 14 Edition. United States of America: McGraw-Hill Education, 2018.
- Keeling MJ, Danon L. Mathematical modelling of infectious diseases. *British Medical Bulletin* 2009;**92**: 33-42.
- Kent CK, Chaw JK, Wong W *et al.* Prevalence of rectal, urethral, and pharyngeal chlamydia and gonorrhea detected in 2 clinical settings among men who have sex with men: San Francisco, California, 2003. *Clin Infect Dis* 2005;**41**: 67-74.
- Kermack WO, McKendrick AG, Walker GT. A contribution to the mathematical theory of epidemics. *Proceedings of the Royal Society of London Series A, Containing Papers of a Mathematical and Physical Character* 1927;**115**: 700-21.
- Kidd S, Workowski KA. Management of Gonorrhea in Adolescents and Adults in the United States. *Clin Infect Dis* 2015;**61 Suppl 8**: S785-801.
- Kirkcaldy RD, Weinstock HS, Moore PC *et al.* The efficacy and safety of gentamicin plus azithromycin and gemifloxacin plus azithromycin as treatment of uncomplicated gonorrhea. *Clin Infect Dis* 2014;**59**: 1083-91.

- Kjellander JO, Finland M. Penicillin treatment of gonorrheal urethritis. Effects of penicillin susceptibility of causative organism and concomitant presence of penicillinase- producing bacteria on results. *N Engl J Med* 1963;**269**: 834-6.
- Kobuchi S, Kabata T, Maeda K *et al.* Pharmacokinetics of Macrolide Antibiotics and Transport into the Interstitial Fluid: Comparison among Erythromycin, Clarithromycin, and Azithromycin. *Antibiotics (Basel)* 2020;**9**.
- Koelle K, Farrell AP, Brooke CB *et al.* Within-host infectious disease models accommodating cellular coinfection, with an application to influenza†. *Virus Evolution* 2019;**5**.
- Kong FY, Rupasinghe TW, Simpson JA *et al.* Pharmacokinetics of a single 1g dose of azithromycin in rectal tissue in men. *PLoS One* 2017;**12**: e0174372.
- Korenromp EL, Sudaryo MK, de Vlas SJ *et al.* What proportion of episodes of gonorrhoea and chlamydia becomes symptomatic? *International Journal of Std & Aids* 2002;**13**: 91-101.
- Kuepfer L, Niederalt C, Wendl T *et al.* Applied Concepts in PBPK Modeling: How to Build a PBPK/PD Model. *CPT: pharmacometrics & systems pharmacology* 2016;**5**: 516-31.
- Kurtz TG. Solutions of ordinary differential equations as limits of pure jump markov processes. *Journal of Applied Probability* 1970;**7**: 49-58.
- Kurtz TG. The Relationship between Stochastic and Deterministic Models for Chemical Reactions. *The Journal of Chemical Physics* 1972;**57**: 2976-8.
- Lacy P, Stow JL. Cytokine release from innate immune cells: association with diverse membrane trafficking pathways. *Blood* 2011;**118**: 9-18.
- Lahra MM, Martin I, Demczuk W *et al.* Cooperative Recognition of Internationally Disseminated Ceftriaxone-Resistant Neisseria gonorrhoeae Strain. *Emerging infectious diseases* 2018;**24**: 735-40.
- Lahra MM, Ryder N, Whiley DM. A new multidrug-resistant strain of Neisseria gonorrhoeae in Australia. *N Engl J Med* 2014;**371**: 1850-1.
- Lamb HM, Figgitt DP, Faulds D. Quinupristin/dalfopristin: a review of its use in the management of serious gram-positive infections. *Drugs* 1999;**58**: 1061-97.
- Laufen H, Wildfeuer A, Räder K. Uptake of antimicrobial agents by human polymorphonuclear leucocytes. *Arzneimittel-Forschung* 1985;**35**: 1097-9.
- Leduc I, Connolly KL, Begum A *et al.* The serogroup B meningococcal outer membrane vesicle-based vaccine 4CMenB induces cross-species protection against Neisseria gonorrhoeae. *PLOS Pathogens* 2020;**16**: e1008602.
- Lee JJ, Kong M, Ayers GD *et al.* Interaction index and different methods for determining drug interaction in combination therapy. *Journal of biopharmaceutical statistics* 2007;**17**: 461-80.

- Lee K, Nakayama S-I, Osawa K *et al.* Clonal expansion and spread of the ceftriaxone-resistant *Neisseria gonorrhoeae* strain FC428, identified in Japan in 2015, and closely related isolates. *J Antimicrob Chemother* 2019;**74**: 1812-9.
- Lefebvre B, Martin I, Demczuk W *et al.* Ceftriaxone-Resistant *Neisseria gonorrhoeae*, Canada, 2017. *Emerg Infect Dis* 2018;**24**.
- Legros M, Bonhoeffer S. A combined within-host and between-hosts modelling framework for the evolution of resistance to antimalarial drugs. *J R Soc Interface* 2016;**13**.
- Levison ME. Pharmacodynamics of antimicrobial agents. Bactericidal and postantibiotic effects. *Infect Dis Clin North Am* 1995;**9**: 483-95.
- Levison ME, Levison JH. Pharmacokinetics and pharmacodynamics of antibacterial agents. *Infect Dis Clin North Am* 2009;**23**: 791-815, vii.
- Li G, Jiao H, Yan H *et al.* Establishment of a human CEACAM1 transgenic mouse model for the study of gonococcal infections. *J Microbiol Methods* 2011;**87**: 350-4.
- Liu Y, Liu W, Russell MW. Suppression of host adaptive immune responses by *Neisseria gonorrhoeae*: role of interleukin 10 and type 1 regulatory T cells. *Mucosal Immunol* 2014;**7**: 165-76.
- Liu Y, Russell MW. Diversion of the immune response to *Neisseria gonorrhoeae* from Th17 to Th1/Th2 by treatment with anti-transforming growth factor beta antibody generates immunological memory and protective immunity. *MBio* 2011;**2**: e00095-11.
- Loewe S. Die quantitativen Probleme der Pharmakologie. *Ergebnisse der Physiologie* 1928;**27**: 47-187.
- Lohani S, Nazir S, Tachamo N *et al.* Disseminated gonococcal infection: an unusual presentation. *Journal of Community Hospital Internal Medicine Perspectives* 2016;**6**: 31841.
- Lovett A, Duncan JA. Human Immune Responses and the Natural History of *Neisseria gonorrhoeae* Infection. *Front Immunol* 2019;**9**: 3187-.
- Macdonald G. The analysis of equilibrium in malaria. *Tropical diseases bulletin* 1952;**49**: 813-29.
- Mao J, Lu T. Population-Dynamic Modeling of Bacterial Horizontal Gene Transfer by Natural Transformation. *Biophys J* 2016;**110**: 258-68.
- Martcheva M, Li XZ. Linking immunological and epidemiological dynamics of HIV: the case of super-infection. *Journal of biological dynamics* 2013;**7**: 161-82.
- Martin JE, Jr., Lester A, Price EV *et al.* Comparative study of gonococcal susceptibility to penicillin in the United States, 1955-1969. *J Infect Dis* 1970;**122**: 459-61.

- McGee ZA, Johnson AP, Taylor-Robinson D. Pathogenic mechanisms of *Neisseria gonorrhoeae*: observations on damage to human fallopian tubes in organ culture by gonococci of colony type 1 or type 4. *J Infect Dis* 1981;**143**: 413-22.
- McGee ZA, Stephens DS, Hoffman LH *et al*. Mechanisms of mucosal invasion by pathogenic *Neisseria*. *Rev Infect Dis* 1983;**5 Suppl 4**: S708-14.
- McLean AR. Mathematical Modelling of the Immunisation of Populations. *Medical Virology* 1992;**2**: 141-52.
- Mensforth S, Ross J. Assessing the frequency of spontaneous clearance of gonococcal infection in the absence of antibiotic therapy: a review of the literature *The International Union Against Sexually Transmitted Infections Asia Pacific Conference 2018*. New Zealand: Available: [https:// az659834. vo. msecnd. net/ events/raueprod/ production- ashmpublic/9858 72a7 3ea6 4df1 9677 2b80 254c093f](https://az659834.vo.msecnd.net/events/raueprod/production-ashmpublic/985872a73ea64df196772b80254c093f), 2018.
- Mensforth S, Ross JDC. Should we still use azithromycin for gonorrhoea treatment? *Sexual Health* 2019;**16**: 442-8.
- Mercer DK, Torres MDT, Duay SS *et al*. Antimicrobial Susceptibility Testing of Antimicrobial Peptides to Better Predict Efficacy. *Frontiers in Cellular and Infection Microbiology* 2020;**10**.
- Merz AJ, So M. Interactions of pathogenic *neisseriae* with epithelial cell membranes. *Annu Rev Cell Dev Biol* 2000;**16**: 423-57.
- Meyer T, Buder S. The Laboratory Diagnosis of *Neisseria gonorrhoeae*: Current Testing and Future Demands. *Pathogens (Basel, Switzerland)* 2020;**9**.
- Meyers BR, Srulovitch ES, Jacobson J *et al*. Crossover study of the pharmacokinetics of ceftriaxone administered intravenously or intramuscularly to healthy volunteers. *Antimicrob Agents Chemother* 1983;**24**: 812-4.
- Michel J-B, Yeh PJ, Chait R *et al*. Drug interactions modulate the potential for evolution of resistance. *Proceedings of the National Academy of Sciences* 2008;**105**: 14918-23.
- Mideo N, Alizon S, Day T. Linking within- and between-host dynamics in the evolutionary epidemiology of infectious diseases. *Trends Ecol Evol* 2008;**23**: 511-7.
- Miller KE. Diagnosis and treatment of *Neisseria gonorrhoeae* infections. *Am Fam Physician* 2006;**73**: 1779-84.
- Moore K. *Clinically oriented anatomy*: 5 Edition. Philadelphia: Lippincott Williams & Wilkins, 2006.
- Moran JS. Treating Uncomplicated *Neisseria-Gonorrhoeae* Infections - Is the Anatomic Site of Infection Important. *Sexually transmitted diseases* 1995;**22**: 39-47.

- Moran JS, Levine WC. Drugs of choice for the treatment of uncomplicated gonococcal infections. *Clin Infect Dis* 1995;**20 Suppl 1**: S47-65.
- Morris RS, Klausner JD, Buchbinder SP *et al.* Prevalence and Incidence of Pharyngeal Gonorrhea in a Longitudinal Sample of Men Who Have Sex with Men: The EXPLORE Study. *Clinical Infectious Diseases* 2006;**43**: 1284-9.
- Mosleh IM, Boxberger HJ, Sessler MJ *et al.* Experimental infection of native human ureteral tissue with *Neisseria gonorrhoeae*: adhesion, invasion, intracellular fate, exocytosis, and passage through a stratified epithelium. *Infect Immun* 1997;**65**: 3391-8.
- Nakayama S-i, Shimuta K, Furubayashi K-i *et al.* New Ceftriaxone- and Multidrug-Resistant *Neisseria gonorrhoeae* Strain with a Novel Mosaic *penA* Gene Isolated in Japan. *Antimicrobial Agents and Chemotherapy* 2016;**60**: 4339-41.
- National Center for Biotechnology Information. Cefixime, CID=5362065, volume 2020. PubChem Database., 2020a.
- National Center for Biotechnology Information. Ceftriaxone, CID=5479530, volume 2020: PubChem Database., 2020b.
- Negash K, Andonian C, Felgate C *et al.* The metabolism and disposition of GSK2140944 in healthy human subjects. *Xenobiotica* 2016;**46**: 683-702.
- Newman L, Rowley J, Vander Hoorn S *et al.* Global Estimates of the Prevalence and Incidence of Four Curable Sexually Transmitted Infections in 2012 Based on Systematic Review and Global Reporting. *PLoS One* 2015;**10**: e0143304.
- Nguyet MN, Duong TH, Trung VT *et al.* Host and viral features of human dengue cases shape the population of infected and infectious *Aedes aegypti* mosquitoes. *Proc Natl Acad Sci U S A* 2013;**110**: 9072-7.
- Nowak MA, Bangham CR. Population dynamics of immune responses to persistent viruses. *Science* 1996;**272**: 74-9.
- Nowak MA, Bonhoeffer S, Hill AM *et al.* Viral dynamics in hepatitis B virus infection. *P Natl Acad Sci USA* 1996;**93**: 4398-402.
- Nowak MA, May RM, Anderson RM. The evolutionary dynamics of HIV-1 quasispecies and the development of immunodeficiency disease. *AIDS* 1990;**4**: 1095-103.
- Nowak MA, May RMC. *Virus Dynamics: Mathematical Principles of Immunology and Virology*: Oxford University Press, 2000.
- Ober WB. Boswell's clap. *JAMA* 1970;**212**: 91-5.
- Ohnishi M, Golparian D, Shimuta K *et al.* Is *Neisseria gonorrhoeae* initiating a future era of untreatable gonorrhea?: detailed characterization of the first strain with high-level resistance to ceftriaxone. *Antimicrob Agents Chemother* 2011;**55**: 3538-45.

- Packiam M, Veit SJ, Anderson DJ *et al.* Mouse Strain-Dependent Differences in Susceptibility to *Neisseria gonorrhoeae* Infection and Induction of Innate Immune Responses. *Infect Immun* 2010;**78**: 433-40.
- Pankey GA, Sabath LD. Clinical relevance of bacteriostatic versus bactericidal mechanisms of action in the treatment of gram-positive bacterial infections. *Clinical Infectious Diseases* 2004;**38**: 864-70.
- Parsons NJ, Kwaasi AA, Patel PV *et al.* Association of resistance of *Neisseria gonorrhoeae* to killing by human phagocytes with outer-membrane proteins of about 20 kilodaltons. *J Gen Microbiol* 1985;**131**: 601-10.
- Parsons NJ, Kwaasi AA, Patel PV *et al.* A determinant of resistance of *Neisseria gonorrhoeae* to killing by human phagocytes: an outer membrane lipoprotein of about 20 kDa with a high content of glutamic acid. *J Gen Microbiol* 1986;**132**: 3277-87.
- Patel IH, Chen S, Parsonnet M *et al.* Pharmacokinetics of Ceftriaxone in Humans. *Antimicrobial Agents and Chemotherapy* 1981;**20**: 634-41.
- Patel IH, Weinfeld RE, Konikoff J *et al.* Pharmacokinetics and tolerance of ceftriaxone in humans after single-dose intramuscular administration in water and lidocaine diluents. *Antimicrob Agents Chemother* 1982;**21**: 957-62.
- Pelouze PS. *Gonorrhea in the male and female; A book for practitioners*: 3 Edition. Philadelphia: W.B. Saunders, 1939.
- Pene Dumitrescu T, Anic-Milic T, Oreskovic K *et al.* Development of a population pharmacokinetic model to describe azithromycin whole-blood and plasma concentrations over time in healthy subjects. *Antimicrobial agents and chemotherapy* 2013;**57**: 3194-201.
- Pereira R, Cole MJ, Ison CA. Combination therapy for gonorrhoea: in vitro synergy testing. *J Antimicrob Chemother* 2012;**68**: 640-3.
- Perelson AS, Ribeiro RM. Modeling the within-host dynamics of HIV infection. *BMC Biol* 2013;**11**: 96.
- Petousis-Harris H, Paynter J, Morgan J *et al.* Effectiveness of a group B outer membrane vesicle meningococcal vaccine against gonorrhoea in New Zealand: a retrospective case-control study. *Lancet* 2017;**390**: 1603-10.
- Peyrusson F, Tulkens PM, Van Bambeke F. Cellular Pharmacokinetics and Intracellular Activity of Gepotidacin against *Staphylococcus aureus* Isolates with Different Resistance Phenotypes in Models of Cultured Phagocytic Cells. *Antimicrob Agents Chemother* 2018;**62**.
- Phanucharas JP, Gorby GL. Differential intracellular efficacies of ciprofloxacin and cefixime against *Neisseria gonorrhoeae* in human fallopian tube organ culture. *Antimicrob Agents Chemother* 1997;**41**: 1547-51.

- Pomaroli A, Schlogel R. [The male urethra: capacity determination and its significance for urology (author's transl)]. *Urologe A* 1978;**17**: 238-41.
- Poncin T, Fouere S, Braille A *et al.* Multidrug-resistant *Neisseria gonorrhoeae* failing treatment with ceftriaxone and doxycycline in France, November 2017. *Euro Surveillance* 2018;**23**.
- Poole J, Day CJ, Haselhorst T *et al.* Repurposed Drugs That Block the Gonococcus-Complement Receptor 3 Interaction Can Prevent and Cure Gonococcal Infection of Primary Human Cervical Epithelial Cells. *mBio* 2020;**11**: e03046-19.
- Popick AC, Crouthamel WG, Bekersky I. Plasma protein binding of ceftriaxone. *Xenobiotica* 1987;**17**: 1139-45.
- Powell AJ, Tomberg J, Deacon AM *et al.* Crystal structures of penicillin-binding protein 2 from penicillin-susceptible and -resistant strains of *Neisseria gonorrhoeae* reveal an unexpectedly subtle mechanism for antibiotic resistance. *The Journal of biological chemistry* 2009;**284**: 1202-12.
- Prats R, de Pedro MA. Normal growth and division of *Escherichia coli* with a reduced amount of murein. *Journal of bacteriology* 1989;**171**: 3740-5.
- Prokesch RC, Hand WL. Antibiotic entry into human polymorphonuclear leukocytes. *Antimicrob Agents Chemother* 1982;**21**: 373-80.
- Public Health England. Surveillance of antimicrobial resistance in *Neisseria gonorrhoeae* in England and Wales Key findings from the Gonococcal Resistance to Antimicrobials Surveillance Programme (GRASP). 2018.
- Public Health England. Antimicrobial resistance in *Neisseria gonorrhoeae* in England and Wales. Key findings from the Gonococcal Resistance to Antimicrobials Surveillance Programme (GRASP 2018). Public Health England, Wellington House, London, 2019.
- Queensland Health. Aminoglycoside Dosing in Adults 2018.
- Quillin SJ, Seifert HS. *Neisseria gonorrhoeae* host adaptation and pathogenesis. *Nat Rev Microbiol* 2018;**16**: 226-40.
- Ramsey KH, Schneider H, Cross AS *et al.* Inflammatory cytokines produced in response to experimental human gonorrhea. *J Infect Dis* 1995;**172**: 186-91.
- Ramsey KH, Schneider H, Kushner RA *et al.* Inflammatory cytokine response to experimental human infection with *Neisseria gonorrhoeae*. *Ann N Y Acad Sci* 1994;**730**: 322-5.
- Rao GG, Li J, Garonzik SM *et al.* Assessment and modelling of antibacterial combination regimens. *Clin Microbiol Infect* 2018;**24**: 689-96.
- Read TR, Fairley CK, Tabrizi SN *et al.* Azithromycin 1.5g Over 5 Days Compared to 1g Single Dose in Urethral *Mycoplasma genitalium*: Impact on Treatment Outcome and Resistance. *Clin Infect Dis* 2017;**64**: 250-6.

- Regan DG, Hui BB, Wood JG *et al.* Treatment for pharyngeal gonorrhoea under threat. *The Lancet Infectious diseases* 2018;**18**: 1175-7.
- Regoes RR, Wiuff C, Zappala RM *et al.* Pharmacodynamic functions: a multiparameter approach to the design of antibiotic treatment regimens. *Antimicrob Agents Chemother* 2004;**48**: 3670-6.
- Renard C, Vanderhaeghe HJ, Claes PJ *et al.* Influence of conversion of penicillin G into a basic derivative on its accumulation and subcellular localization in cultured macrophages. *Antimicrobial agents and chemotherapy* 1987;**31**: 410-6.
- Rest RF, Fischer SH, Ingham ZZ *et al.* Interactions of *Neisseria gonorrhoeae* with human neutrophils: effects of serum and gonococcal opacity on phagocyte killing and chemiluminescence. *Infect Immun* 1982;**36**: 737-44.
- Rice PA, Shafer WM, Ram S *et al.* *Neisseria gonorrhoeae*: Drug Resistance, Mouse Models, and Vaccine Development. *Annu Rev Microbiol* 2017;**71**: 665-86.
- Ripa S, Ferrante L, Prenna M. A linear model for the pharmacokinetics of azithromycin in healthy volunteers. *Chemotherapy* 1996;**42**: 402-9.
- Rob F, Klubalová B, Nyčová E *et al.* Gentamicin 240 mg plus azithromycin 2 g vs. ceftriaxone 500 mg plus azithromycin 2 g for treatment of rectal and pharyngeal gonorrhoea: a randomized controlled trial. *Clin Microbiol Infect* 2020;**26**: 207-12.
- Rohatgi A. WebPlotDigitalizer: HTML5 based online tool to extract numerical data from plot images Version 4.1 volume 2018. Austin, Texas, USA, 2018.
- Ropp PA, Hu M, Olesky M *et al.* Mutations in *ponA*, the gene encoding penicillin-binding protein 1, and a novel locus, *penC*, are required for high-level chromosomally mediated penicillin resistance in *Neisseria gonorrhoeae*. *Antimicrob Agents Chemother* 2002;**46**: 769-77.
- Rosales C. Neutrophil: A Cell with Many Roles in Inflammation or Several Cell Types? *Front Physiol* 2018;**9**: 113-.
- Ross JDC, Brittain C, Cole M *et al.* Gentamicin compared with ceftriaxone for the treatment of gonorrhoea (G-ToG): a randomised non-inferiority trial. *Lancet* 2019, DOI 10.1016/S0140-6736(18)32817-4.
- Rowland M, Tozer TN. *Clinical Pharmacokinetics Concepts and Applications*: Williams and Wilkins, 1995.
- Rowley J, Vander Hoorn S, Korenromp E *et al.* Chlamydia, gonorrhoea, trichomoniasis and syphilis: global prevalence and incidence estimates, 2016. *Bull World Health Organ* 2019;**97**: 548-62P.
- Rudel T, van Putten JP, Gibbs CP *et al.* Interaction of two variable proteins (PilE and PilC) required for pilus-mediated adherence of *Neisseria gonorrhoeae* to human epithelial cells. *Mol Microbiol* 1992;**6**: 3439-50.

- Sadarangani M, Pollard AJ, Gray-Owen SD. Opa proteins and CEACAMs: pathways of immune engagement for pathogenic *Neisseria*. *FEMS Microbiol Rev* 2011;**35**: 498-514.
- Scangarella-Oman NE, Hossain M, Dixon PB *et al*. Microbiological Analysis from a Phase 2 Randomized Study in Adults Evaluating Single Oral Doses of Gepotidacin in the Treatment of Uncomplicated Urogenital Gonorrhea Caused by *Neisseria gonorrhoeae*. *Antimicrob Agents Chemother* 2018;**62**.
- Schentag JJ, Jusko WJ, Vance JW *et al*. Gentamicin disposition and tissue accumulation on multiple dosing. *J Pharmacokinet Biopharm* 1977;**5**: 559-77.
- Schmidt KA, Deal CD, Kwan M *et al*. *Neisseria gonorrhoeae* MS11mkC opacity protein expression in vitro and during human volunteer infectivity studies. *Sex Transm Dis* 2000;**27**: 278-83.
- Schmidt KA, Schneider H, Lindstrom JA *et al*. Experimental gonococcal urethritis and reinfection with homologous gonococci in male volunteers. *Sex Transm Dis* 2001;**28**: 555-64.
- Schneider H, Cross AS, Kuschner RA *et al*. Experimental human gonococcal urethritis: 250 *Neisseria gonorrhoeae* MS11mkC are infective. *J Infect Dis* 1995;**172**: 180-5.
- Schneider H, Griffiss JM, Boslego JW *et al*. Expression of paragloboside-like lipooligosaccharides may be a necessary component of gonococcal pathogenesis in men. *J Exp Med* 1991;**174**: 1601-5.
- Schneider H, Schmidt KA, Skillman DR *et al*. Sialylation lessens the infectivity of *Neisseria gonorrhoeae* MS11mkC. *J Infect Dis* 1996;**173**: 1422-7.
- Scully BE, Fu KP, Neu HC. Pharmacokinetics of ceftriaxone after intravenous infusion and intramuscular injection. *Am J Med* 1984;**77**: 112-6.
- Seib KL. Gonorrhoea vaccines: a step in the right direction. *The Lancet* 2017;**390**: 1567-9.
- Seifert HS, Wright CJ, Jerse AE *et al*. Multiple gonococcal pilin antigenic variants are produced during experimental human infections. *J Clin Invest* 1994;**93**: 2744-9.
- Seike K, Yasuda M, Hatazaki K *et al*. Novel penA mutations identified in *Neisseria gonorrhoeae* with decreased susceptibility to ceftriaxone isolated between 2000 and 2014 in Japan. *J Antimicrob Chemother* 2016;**71**: 2466-70.
- Semchenko EA, Tan A, Borrow R *et al*. The Serogroup B Meningococcal Vaccine Bexsero Elicits Antibodies to *Neisseria gonorrhoeae*. *Clin Infect Dis* 2019;**69**: 1101-11.
- Sena AC, Bachmann L, Johnston C *et al*. Optimising treatments for sexually transmitted infections: surveillance, pharmacokinetics and pharmacodynamics, therapeutic

- strategies, and molecular resistance prediction. *Lancet Infect Dis* 2020, DOI 10.1016/S1473-3099(20)30171-7.
- Shafer WM, Rest RF. Interactions of gonococci with phagocytic cells. *Annu Rev Microbiol* 1989;**43**: 121-45.
- Shaw JH, Falkow S. Model for invasion of human tissue culture cells by *Neisseria gonorrhoeae*. *Infect Immun* 1988;**56**: 1625-32.
- Simons MP, Nauseef WM, Apicella MA. Interactions of *Neisseria gonorrhoeae* with adherent polymorphonuclear leukocytes. *Infect Immun* 2005;**73**: 1971-7.
- Simons MP, Nauseef WM, Griffith TS *et al.* *Neisseria gonorrhoeae* delays the onset of apoptosis in polymorphonuclear leukocytes. *Cell Microbiol* 2006;**8**: 1780-90.
- Singh AP, Guo L, Verma A *et al.* A Cell-Level Systems PK-PD Model to Characterize In Vivo Efficacy of ADCs. *Pharmaceutics* 2019;**11**.
- Singh R, Dwivedi SP, Gaharwar US *et al.* Recent updates on drug resistance in *Mycobacterium tuberculosis*. *Journal of Applied Microbiology* 2020;**128**: 1547-67.
- Singh V, Bala M, Bhargava A *et al.* In vitro efficacy of 21 dual antimicrobial combinations comprising novel and currently recommended combinations for treatment of drug resistant gonorrhoea in future era. *PloS one* 2018;**13**: e0193678-e.
- Singlas E. [Clinical pharmacokinetics of azithromycin]. *Pathologie-biologie* 1995;**43**: 505-11.
- Smith AM, McCullers JA, Adler FR. Mathematical model of a three-stage innate immune response to a pneumococcal lung infection. *J Theor Biol* 2011;**276**: 106-16.
- Smith DA, Beaumont K, Maurer TS *et al.* Volume of Distribution in Drug Design. *Journal of Medicinal Chemistry* 2015;**58**: 5691-8.
- Smith T, Wolff KA, Nguyen L. Molecular biology of drug resistance in *Mycobacterium tuberculosis*. *Current topics in microbiology and immunology* 2013;**374**: 53-80.
- So W, Crandon JL, Nicolau DP. Pharmacodynamic Profile of GSK2140944 against Methicillin-Resistant *Staphylococcus aureus* in a Murine Lung Infection Model. *Antimicrob Agents Chemother* 2015;**59**: 4956-61.
- Soler-Garcia AA, Jerse AE. *Neisseria gonorrhoeae* catalase is not required for experimental genital tract infection despite the induction of a localized neutrophil response. *Infect Immun* 2007;**75**: 2225-33.
- Song W, Condrón S, Mocca BT *et al.* Local and humoral immune responses against primary and repeat *Neisseria gonorrhoeae* genital tract infections of 17 β -estradiol-treated mice. *Vaccine* 2008;**26**: 5741-51.

- St. Cyr S, Barbee L, Workowski K *et al.* Update to CDC's treatment guidelines for gonococcal infection, 2020. *MMWR Morbidity and mortality weekly report* 2020;**69**: 1911–6.
- Stefanova ME, Tomberg J, Davies C *et al.* Overexpression and enzymatic characterization of *Neisseria gonorrhoeae* penicillin-binding protein 4. *European journal of biochemistry* 2004;**271**: 23-32.
- Stevens JS, Criss AK. Pathogenesis of *Neisseria gonorrhoeae* in the female reproductive tract: neutrophilic host response, sustained infection, and clinical sequelae. *Curr Opin Hematol* 2018;**25**: 13-21.
- Stoeckel K, McNamara PJ, Brandt R *et al.* Effects of concentration-dependent plasma protein binding on ceftriaxone kinetics. 1981;**29**: 650-7.
- Stoeckel K, Trueb V, Dubach UC *et al.* Effect of probenecid on the elimination and protein binding of ceftriaxone. *Eur J Clin Pharmacol* 1988;**34**: 151-6.
- Stupiansky NW, Van Der Pol B, Williams JA *et al.* The natural history of incident gonococcal infection in adolescent women. *Sexually Transmitted Diseases* 2011;**38**: 750-4.
- Sultan B, Benn P, Schembri G *et al.* Test of cure study: a feasibility study to estimate the time to test of cure (TOC) for *Neisseria gonorrhoeae* and Chlamydia trachomatis infections. *Sex Transm Infect* 2020, DOI 10.1136/sextrans-2019-054302.
- Swanson J. Studies on gonococcus infection. IV. Pili: their role in attachment of gonococci to tissue culture cells. *J Exp Med* 1973;**137**: 571-89.
- Swanson J, Barrera O, Sola J *et al.* Expression of outer membrane protein II by gonococci in experimental gonorrhea. *J Exp Med* 1988;**168**: 2121-9.
- Swanson J, Robbins K, Barrera O *et al.* Gonococcal pilin variants in experimental gonorrhea. *J Exp Med* 1987;**165**: 1344-57.
- Talati J. Urethral dilatation. *JPMA The Journal of the Pakistan Medical Association* 1989;**39**: 79-83.
- Tallarida RJ. An overview of drug combination analysis with isobolograms. *J Pharmacol Exp Ther* 2006;**319**: 1-7.
- Tan Y-M, Worley RR, Leonard JA *et al.* Challenges associated with applying physiologically based pharmacokinetic modeling for public health decision-making. *Toxicol Sci* 2018;**162**: 341-8.
- Tapsall JW, Shultz TR, Limnios EA *et al.* Failure of azithromycin therapy in gonorrhea and discordance with laboratory test parameters. *Sex Transm Dis* 1998;**25**: 505-8.
- Taylor SN, Marrazzo J, Batteiger BE *et al.* Single-Dose Zoliflodacin (ETX0914) for Treatment of Urogenital Gonorrhea. *N Engl J Med* 2018a;**379**: 1835-45.

- Taylor SN, Morris DH, Avery AK *et al.* Gepotidacin for the Treatment of Uncomplicated Urogenital Gonorrhea: A Phase 2, Randomized, Dose-Ranging, Single-Oral Dose Evaluation. *Clin Infect Dis* 2018b;**67**: 504-12.
- Terkelsen D, Tolstrup J, Johnsen CH *et al.* Multidrug-resistant *Neisseria gonorrhoeae* infection with ceftriaxone resistance and intermediate resistance to azithromycin, Denmark, 2017. *Euro Surveill* 2017;**22**.
- Terreni M, Taccani M, Pregnolato M. New Antibiotics for Multidrug-Resistant Bacterial Strains: Latest Research Developments and Future Perspectives. *Molecules* 2021;**26**: 2671.
- The Kirby Institute. HIV, viral hepatitis and sexually transmissible infections in Australia: annual surveillance report 2017. UNSW Sydney: Kirby Institute, 2018.
- Theuretzbacher U, Barbee L, Connolly K *et al.* Pharmacokinetic/pharmacodynamic considerations for new and current therapeutic drugs for uncomplicated gonorrhoea – challenges and opportunities. *Clinical Microbiology and Infection* 2020, DOI <https://doi.org/10.1016/j.cmi.2020.08.006>.
- Tiffany CA, Hossain M, McDonald M *et al.* Safety and Pharmacokinetics of Single Escalating IV Doses of GSK2140944, a Novel Bacterial Topoisomerase Inhibitor *Abstr 54th Interscience Conference on Antimicrobial Agents and Chemotherapy*. Washington, D.C, 2014.
- Tomberg J, Fedarovich A, Vincent LR *et al.* Alanine 501 Mutations in Penicillin-Binding Protein 2 from *Neisseria gonorrhoeae*: Structure, Mechanism, and Effects on Cephalosporin Resistance and Biological Fitness. *Biochemistry* 2017;**56**: 1140-50.
- Tomberg J, Unemo M, Ohnishi M *et al.* Identification of amino acids conferring high-level resistance to expanded-spectrum cephalosporins in the penA gene from *Neisseria gonorrhoeae* strain H041. *Antimicrob Agents Chemother* 2013;**57**: 3029-36.
- Torella JP, Chait R, Kishony R. Optimal Drug Synergy in Antimicrobial Treatments. *Plos Comput Biol* 2010;**6**: e1000796.
- Tulkens P, Trouet A. Uptake and intracellular localization of kanamycin and gentamycin in the lysosomes of cultured fibroblasts. *Arch Int Physiol Biochim* 1974;**82**: 1018-9.
- Tulkens P, Trouet A. The uptake and intracellular accumulation of aminoglycoside antibiotics in lysosomes of cultured rat fibroblasts. *Biochem Pharmacol* 1978;**27**: 415-24.
- Tulkens PM. Intracellular pharmacokinetics and localization of antibiotics as predictors of their efficacy against intraphagocytic infections. *Scand J Infect Dis Suppl* 1990;**74**: 209-17.

- Tulkens PM. Intracellular distribution and activity of antibiotics. *Eur J Clin Microbiol Infect Dis* 1991;**10**: 100-6.
- Turvey SE, Broide DH. Innate immunity. *The Journal of allergy and clinical immunology* 2010;**125**: S24-S32.
- Unemo M, Del Rio C, Shafer WM. Antimicrobial resistance expressed by *Neisseria gonorrhoeae*: A major global public health problem in the 21st century. *Microbiol Spectr* 2016;**4**.
- Unemo M, Golparian D, Nicholas R *et al*. High-level cefixime- and ceftriaxone-resistant *N. gonorrhoeae* in Europe (France): novel penA mosaic allele in a successful international clone causes treatment failure. *Antimicrobial Agents and Chemotherapy* 2011;**in press**.
- Unemo M, Golparian D, Nicholas R *et al*. High-level cefixime- and ceftriaxone-resistant *Neisseria gonorrhoeae* in France: novel penA mosaic allele in a successful international clone causes treatment failure. *Antimicrob Agents Chemother* 2012;**56**: 1273-80.
- Unemo M, Nicholas RA. Emergence of multidrug-resistant, extensively drug-resistant and untreatable gonorrhea. *Future Microbiol* 2012;**7**: 1401-22.
- Unemo M, Seifert HS, Hook EW *et al*. Gonorrhoea. *Nature Reviews Disease Primers* 2019;**5**: 79.
- Unemo M, Shafer WM. Antibiotic resistance in *Neisseria gonorrhoeae*: origin, evolution, and lessons learned for the future. *Annals of the New York Academy of Sciences* 2011;**1230**: E19-E28.
- Unemo M, Shafer WM. Antimicrobial resistance in *Neisseria gonorrhoeae* in the 21st century: past, evolution, and future. *Clin Microbiol Rev* 2014;**27**: 587-613.
- Van Bambeke F, Barcia-Macay M, Lemaire S *et al*. Cellular pharmacodynamics and pharmacokinetics of antibiotics: current views and perspectives. *Curr Opin Drug Discov Devel* 2006;**9**: 218-30.
- VanScoy BD, Scangarella-Oman NE, Fikes S *et al*. Relationship Between Gepotidacin Exposure and Prevention of On-Therapy Resistance Amplification in a *Neisseria gonorrhoeae* Hollow-Fiber *In Vitro* Infection Model. *Antimicrob Agents Chemother* 2020, DOI 10.1128/aac.00521-20: AAC.00521-20.
- Veale DR, Finch H, Smith H *et al*. Penetration of Penicillin into Human Phagocytes Containing *Neisseria gonorrhoeae*: Intracellular Survival and Growth at Optimum Concentrations of Antibiotic. *Microbiology* 1976;**95**: 353-63.
- Veale DR, Goldner M, Penn CW *et al*. The intracellular survival and growth of gonococci in human phagocytes. *J Gen Microbiol* 1979;**113**: 383-93.
- Virji M. Pathogenic neisseriae: surface modulation, pathogenesis and infection control. *Nat Rev Microbiol* 2009;**7**: 274-86.

- Vlazaki M, Huber J, Restif O. Integrating mathematical models with experimental data to investigate the within-host dynamics of bacterial infections. *Pathogens and Disease* 2019;**77**.
- von Vietinghoff S, Ley K. Homeostatic regulation of blood neutrophil counts. *J Immunol* 2008;**181**: 5183-8.
- Walkup GK, You Z, Ross PL *et al*. Translating slow-binding inhibition kinetics into cellular and in vivo effects. *Nature chemical biology* 2015;**11**: 416-23.
- Ward ME, Watt PJ. Adherence of *Neisseria gonorrhoeae* to urethral mucosal cells: an electron-microscopic study of human gonorrhea. *J Infect Dis* 1972;**126**: 601-5.
- Watt PJ. The fate of gonococci in polymorphonuclear leucocytes. *J Med Microbiol* 1970;**3**: 501-9.
- Wei X, Ghosh SK, Taylor ME *et al*. Viral dynamics in human immunodeficiency virus type 1 infection. *Nature* 1995;**373**: 117-22.
- Weinstein MP, Lewis JS. The Clinical and Laboratory Standards Institute Subcommittee on Antimicrobial Susceptibility Testing: Background, Organization, Functions, and Processes. *Journal of clinical microbiology* 2020;**58**: e01864-19.
- Westling-Haggstrom B, Elmros T, Normark S *et al*. Growth pattern and cell division in *Neisseria gonorrhoeae*. *J Bacteriol* 1977;**129**: 333-42.
- Weyand NJ. *Neisseria* models of infection and persistence in the upper respiratory tract. *Pathogens and Disease* 2017;**75**.
- Whiley DM, Jennison A, Pearson J *et al*. Genetic characterisation of *Neisseria gonorrhoeae* resistant to both ceftriaxone and azithromycin. *Lancet Infect Dis* 2018;**18**: 717-8.
- Whittles LK, White PJ, Didelot X. Estimating the fitness cost and benefit of cefixime resistance in *Neisseria gonorrhoeae* to inform prescription policy: A modelling study. *PLoS Med* 2017;**14**: e1002416.
- Whittles LK, White PJ, Didelot X. Assessment of the Potential of Vaccination to Combat Antibiotic Resistance in Gonorrhea: A Modeling Analysis to Determine Preferred Product Characteristics. *Clinical Infectious Diseases* 2020, DOI 10.1093/cid/ciz1241.
- Whittles LK, White PJ, Paul J *et al*. Epidemiological Trends of Antibiotic Resistant Gonorrhoea in the United Kingdom. *Antibiotics (Basel)* 2018;**7**.
- Wildfeuer A, Laufen H, Zimmermann T. Uptake of azithromycin by various cells and its intracellular activity under in vivo conditions. *Antimicrobial agents and chemotherapy* 1996;**40**: 75-9.
- Williamson R, Tomasz A. Inhibition of cell wall synthesis and acylation of the penicillin binding proteins during prolonged exposure of growing *Streptococcus*

- pneumoniae to benzylpenicillin. *European journal of biochemistry* 1985;**151**: 475-83.
- Wilson DP. Mathematical modelling of chlamydia. *ANZIAM* 2004;**45**: C201-C14.
- Wilson DP, Timms P, McElwain DLS. A mathematical model for the investigation of the Th1 immune response to *Chlamydia trachomatis*. *Mathematical biosciences* 2003;**182**: 27-44.
- Wise R. The clinical relevance of protein binding and tissue concentrations in antimicrobial therapy. *Clin Pharmacokinet* 1986;**11**: 470-82.
- Workowski KA, Berman S. Sexually transmitted diseases treatment guidelines, 2010. *MMWR Recommendations and reports : Morbidity and mortality weekly report Recommendations and reports* 2010;**59**: 1-110.
- World Health Organization. Manual for the laboratory identification and antimicrobial susceptibility testing of bacterial pathogens of public health importance in the developing world : *Haemophilus influenzae*, *Neisseria meningitidis*, *Streptococcus pneumoniae*, *Neisseria gonorrhoea*, *Salmonella* serotype Typhi, *Shigella*, and *Vibrio cholerae* / Principal authors: Mindy J. Perilla ... [et al.]. Geneva: World Health Organization, 2003.
- World Health Organization. Global action plan to control the spread and impact of antimicrobial resistance in *Neisseria gonorrhoeae*: World Health Organization (WHO), Department of Reproductive Health and Research, 2012.
- Xiridou M, Soetens LC, Koedijk FD *et al.* Public health measures to control the spread of antimicrobial resistance in *Neisseria gonorrhoeae* in men who have sex with men. *Epidemiol Infect* 2015;**143**: 1575-84.
- Yan J, Chen Y, Yang F *et al.* High percentage of the ceftriaxone-resistant *Neisseria gonorrhoeae* FC428 clone among isolates from a single hospital in Hangzhou, China. *J Antimicrob Chemother* 2021;**76**: 936-9.
- Yates JW. Structural identifiability of physiologically based pharmacokinetic models. *J Pharmacokinet Pharmacodyn* 2006;**33**: 421-39.
- Young KD. The Selective Value of Bacterial Shape. 2006;**70**: 660-703.
- Zhou HH, Chan YP, Arnold K *et al.* Single-dose pharmacokinetics of ceftriaxone in healthy Chinese adults. *Antimicrob Agents Chemother* 1985;**27**: 192-6.